AN INVESTIGATION OF VARYING LASER TRIM PATTERN CHARACTERISTICS ON THE PERFORMANCE AND RELIABILITY OF DISCRETE RESISTIVE COMPONENTS

MARIA ALAFOGIANNI

PhD

2018

AN INVESTIGATION OF VARYING LASER TRIM PATTERN CHARACTERISTICS ON THE PERFORMANCE AND RELIABILITY OF DISCRETE RESISTIVE COMPONENTS

MARIA ALAFOGIANNI

A thesis submitted in partial fulfilment of the requirements of the University of Northumbria at Newcastle for the degree of Doctor of Philosophy

Research undertaken in the Faculty of Engineering and Environment

April 2018

Abstract

This project investigates the effects of varying laser trimming geometries on key performance parameters of bar shape thin film resistors. Previous studies related to the effect of the trim geometry and in-service performance are quite limited. As a result, industries are still relying on basic patterns and this research aims to focus on the development of new trim pattern models in order to study the effect of the geometries on the accuracy and long-term stability of the material. In addition to this, the application of the model to thin and thick film materials improves the performance of the resistors. Laser trimming is an essential process in the manufacture of precision thin film resistors due to the fact that it is impossible to deposit batches of the product with resistance tolerances better than ~10%. However, it is quite an expensive process which significantly increases the production costs of integrated circuits. Several popular trim patterns including the plunge cut, double plunge cut, L-cut and scan cut as well as novel patterns; the curved L-cut, the angled L-cut, semi-circle and elliptical cut were modelled and tested experimentally. The effect of these geometries on target resistance value, heat affected zone (HAZ) sensitivity and temperature coefficient of resistance (TCR) were analysed. The HAZ sensitivity is an important parameter that characterises the aging performance of the film caused by the high energy required to vaporize the material in the cut, while the TCR indicates how the resistors behave under cold and high operating temperatures. The modelling process of the different laser trim patterns included numerical simulations to predict the performance of laser–trimmed resistors taking into account the HAZ around the trim and computer-aided models. Conductive paper and thin films were used for the experiments in order to emulate the resistors and verify the theoretical results from the simulations. It is found that variation in trimming shape and length has a direct effect on the performance of resistors giving significant increases in the TCR of the resistor with values of 17.22 ppm/°C for the curved L-cut and 8.52 ppm/°C for the semi-circle. The resistance gain, the power coefficient of resistance (PCR) and the trimming time needed for the cuts were also investigated for clarification of the characteristics of each pattern and it is shown that the semi-circle pattern offers the larger resistance increase in relation to the other patterns.

Contents

List of figures

List of Tables

Acknowledgements

I would like to express my gratitude to my principal supervisor, Dr Martin Birkett for his constant guidance and his willingness to offer assistance based on his invaluable knowledge and experience on the field.

In addition, I would like to thank my second supervisor, Dr Roger Penlington for his advice, useful feedback based on his knowledge and experience and his constant support throughout the duration of this research.

I would also like to thank all the technical staff of the Mechanical and Construction department for their constant assistance with the laboratory experiments and making the essential equipment available to me whenever needed. Furthermore, many thanks should go to Dr Pietro Maiello for his technical advice with SEM measurements and spectrophotometry.

I also gratefully acknowledge the funding from Northumbria University for the financial support of this project. I would also like to thank the Graduate school for the support during this PhD degree.

Declaration

I declare that the work contained in this thesis has not been submitted for any other award and that it is all my own work. I also confirm that this work fully acknowledges opinions, ideas and contributions from the work of others.

Any ethical clearance for the research presented in this thesis has been approved. Approval has been sought and granted by the Faculty Ethics Committee on 1st of June 2015.

I declare that the Word Count of this Thesis is 36170 words

Name: Maria Alafogianni

Signature:

Date:

1 Introduction

1.1 Overview

There is a variety of trimming methods and processes which can be used to adjust the value of resistive components such as anodization, heat trimming, electrical trimming, mechanical trimming, chemical trimming and laser trimming [1]. However, laser trimming is by far the most effective and popular process in the manufacture of precision thin film resistors with tolerances less than ± 1% being readily achieved [1, 2].

In general, it is thought that depositing batches of product with resistance tolerances better than about ± 10% is impossible [3]. However, the resistor film can be fabricated to a lower resistance value than required and then adjusted by removing or 'trimming' away sections of the film material to increase the resistance to its target value in order for precision of less than 10% to be achieved [1, 4, 5]. The effect of laser trim pattern geometry on the electrical properties of thin and thick film resistors is critical to the overall performance of the device. As a result, this research aims to focus on the trim pattern geometries and their effect on the accuracy and long-term stability of thin and thick film materials.

1.2 Research aims and objectives

The aims of this research are:

1) Develop a new trim pattern model in order to study the effect of the geometries on the accuracy and long-term stability of the material.

2) Apply the trim pattern model to thin and thick film materials to improve their performance and verify the results.

The objectives of this work are:

1) Conduct a comprehensive literature review in order to develop a critical understanding of the patterns and geometries of thin and thick film materials as well as understanding the appropriate analytical procedures including characteristics of the material and experimental design techniques.

2) Optimise the potential patterns for maximum trim speed and in-service performance.

3) Refine the trim pattern in order to improve the overall performance of the resistors in relation to the laser trimming time and power.

1.3 Thesis outline

Chapter 1- Introduction

This chapter gives an overview of the research project and the thesis outline is included. In addition, the aims and objectives of this research and the original contribution to knowledge are presented.

Chapter 2- Literature review

This chapter contains a comprehensive and in-depth literature review of previous research relevant to the trimming techniques used in thin and thick film resistors. It consists of an analysis on already existing trim pattern geometries. There is also a description of trimming techniques used on resistors focusing especially on laser trimming due to the fact that it is the most effective and popular method for trimming thin and thick film resistors.

Chapter 3 - Modelling of geometry

The focus of the work in this chapter is on the design of trim strategies and different trim pattern geometries that are simulated and evaluated in order to get the new model. The model of the geometry was created in order to offer a better design while reducing factors that affect the performance of the resistor, such as the heat-affected zone (HAZ), which is the area of the film adjacent to the kerf and can cause more changes in the resistance than in the areas of film that are not irradiated by the laser beam. The modelling process consists of simulations mainly using CAD software such as ANSYS as well as numerical simulations.

Chapter 4 – Laser trimming process parameters

In this chapter, the laser settings chosen for the experiments are presented. There was a variety of trials and tests in order to clarify the appropriate settings and parameters of the laser equipment so that the experiments could be conducted efficiently and accurately. The main settings of the laser concerned its power, frequency and speed. Several trials were performed so that these are adjusted properly in relation to the type of thin films used.

Chapter 5 - Trimming of conductive paper

Existing and new trim patterns presented in Chapter 3, are investigated using conductive paper in order to emulate the resistors. The resistivity of the conductive paper is approximately 5000 Ω/☐. Prior to the trimming of the resistors to the suggested patterns, each page of the paper is cut to the desired resistor shape (30 x 20 mm) and the trim

patterns are created using the laser to cut 30 mm^2 sections at a time and measuring the resistance value each time using the four-wire measurement.

Chapter 6- Trimming thin and thick films

This chapter focuses on the optimisation of laser trimming of thin film materials in relation to the proposed geometries. At first, trials on thin films of the existing trim pattern such as the L-cut, take place using the CO_2 laser (Epilog). A variety of trim patterns were chosen after the trials on the conductive paper and these were compared in relation to their resistance gain and trimming time.

Chapter 7 - Verification of the model

The purpose of this chapter is to assess the performance of the optimum laser trim pattern of the film concerning stability and accuracy so that the best geometry could be chosen. Dry heat stability testing is used in order to check the level of resistance instability.

Chapter 8 - Conclusions and recommendations

In this chapter, the main conclusions from this study are drawn and recommendations for future work in the area of laser trimming of thin film materials are made.

1.4 Original contribution

Laser trimming of film resistors is an established process which allows manufacturers to very accurately control resistance values and resistor ratios. However, it is an expensive processing step which significantly increases the production costs of integrated circuits from both trimming cost and area overhead view-points [1,5]. There have been previous studies related to the trimming process parameters as well as the basic properties of the trimmed devices. However, the research into the effect of varying the trim pattern geometry and or in-service performance is limited. As a result, component manufacturers are still relying on long established basic patterns which have been investigated thoroughly and new trim patterns can offer a beneficial change in the manufacturing process.

The work in this research constitutes the first attempt to investigate the effect of both established and novel trim pattern geometries on the accuracy and long-term stability of thin film material. Numerical simulations were used for calculations of the resistance value and estimation of the HAZ area around the cut. In addition to this, simulations with computer aided software were also conducted in order to estimate the temperature change when power was applied to the resistors. The theoretical results were verified experimentally with indirect and direct methods. Many trim patterns were investigated, such as the elliptical and

curved L-cut, for maximum trim speed and in-service performance. The new trim pattern of the semi-circle is also introduced and its advantages are presented.

2 Literature review

2.1 Introduction

Nowadays, there is a continuous need for smaller, better performing and less expensive resistive components [5-7]. Thin film technology is often used because it offers greater performance and reliability over that of metal composition and wire wound type resistors and they are used extensively in electronic circuits due to their high accuracy and excellent long term stability [1, 8]. When used to manufacture resistors, thin films should have a suitable sheet resistance and TCR and they must be sufficiently stable so that any changes in resistance during their operating life can be reliably expected not to exceed a pre-specified value [1, 9-11]. It is difficult to fabricate resistors to the required resistance value, so they are often fabricated with a lower value and then trimmed to raise their resistance to the required value [1, 2, 12]. Moreover, the resistor should be manufactured to the specification needed at a realistic cost. For thin film resistors, it is generally impossible to deposit batches of material with resistance tolerances better than about $\pm$ 10% [3, 13] .This is partly due to problems in attaining uniform sheet resistance, but mainly due to dimensional variation of the individual resistor elements in the batch, a problem which is amplified as the resistor size decrease [8, 14].

Therefore, when a precision of <10% is required, it is normal practice to fabricate the resistor film to a lower resistance value than required and then adjust it by removing or trimming away sections of the film material to increase the resistance to its target value [4, 5, 15].

There are several desirable trimming characteristics for thin film resistors [4, 8, 16-18]:

- Getting as close to the target resistance as possible (precision).
- Minimising the risk of trimming too much (If a resistor is ‘over-trimmed’, fixing it is not possible, and the component or even the entire board that it is in may have to be scrapped).
- Minimising the length of each trim (A longer trim takes more time to make and impacts the manufacturing throughput thereby costing more money).

Integrated circuits can be classified into the major subdivisions of monolithic and hybrid circuits. Hybrid circuits consist of two types: thin film and thick film. In physical appearance they are both very similar, but they differ in their manufacturing process, which determines their operating characteristics [19, 20].

2.2 Manufacture of thin film circuits

The manufacture of a thin film circuit consists of five steps and these are [19, 21]:

- Deposition of the film layer consisting of resistive or conductive material.
- Patterning of the layer to form the required components and interconnections.
- Adjustment of the resistor components formed in the film to give the required accuracy.
- Adding on the chip components (resistors) and connecting them into the circuit.
- Packaging the completed film circuit assembly.

2.2.1 Deposition of the film

The major techniques currently in use to deposit thin films are evaporation, sputtering and ion-plating [19, 21, 22]. Evaporation is the most popular method and uses equipment similar to that employed in evaporating metal onto monolithic circuits as shown in Figure 2.1 [22, 23].

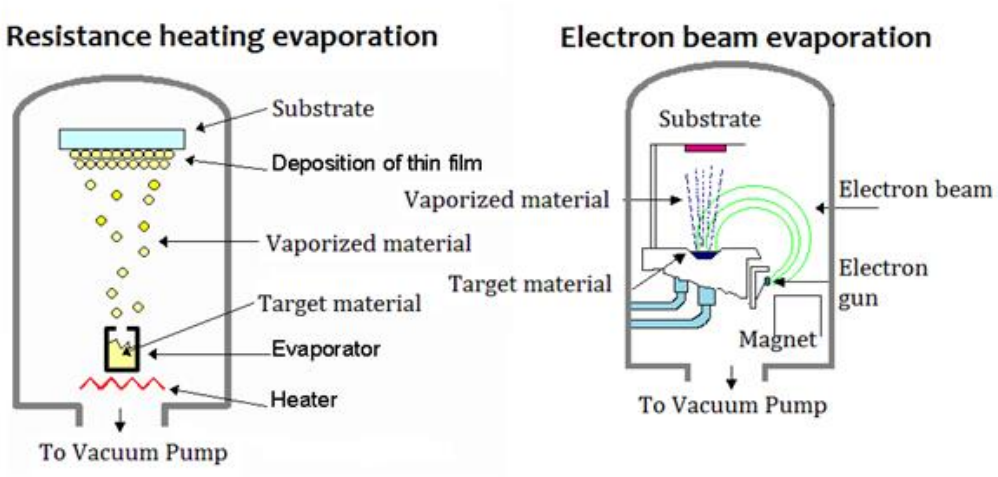

Figure 2.1: Deposition of thin films using evaporation [23].

The substrate is placed around a source which is heated above its vaporisation temperature [19, 24]. A vacuum of between 10^{-5} and 10^{-7} Torr is maintained and under these conditions the free path of the evaporated molecules is much greater than that of the distance between the source and substrate and a thin layer is formed [14, 25]. The substrate is heated by an auxiliary heater so that the adhesion between it and the film is improved [19, 26, 27].

In sputtering, a glow discharge is formed in an atmosphere of argon at between 0.01 and 1 Torr by a high voltage between the source, which forms the cathode, and the anode, which incorporates the substrate [19, 28, 29]. Argon ions are formed by this discharge and are

accelerated to the cathode and a release of the source molecules is caused, which acquires a negative charge. This causes them to be accelerated rapidly to the anode where they impinge onto the substrate and adhere to it, see Figure 2.2 [19, 30]. Sputtering is a cold process since the source does not have to be heated to anywhere near its vaporisation temperature and it is a slower process than evaporation. It can be used to deposit materials with a high vaporisation temperature such as tantalum and its alloys [19, 31-33].

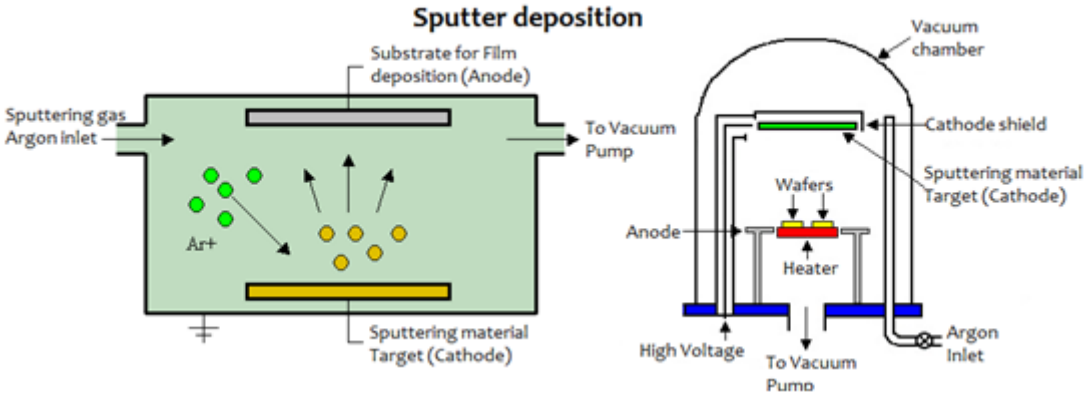

Figure 2.2: Sputter deposition of thin films [23].

The molecules reaching the substrate have considerable energy so that the film density is high [19, 25]. The molecules on striking the substrate also ensure that all residual gas and other impurities are removed prior to and during the film formation. Since negative ions are attracted by a positive substrate the three dimensional coating capability is also much greater than for vaporisation and equal to that of ion-plating [19, 34]. In addition to this, ion-plating can be considered as a mixture of evaporation and sputtering and it is presented in Figure 2.3 [25, 32]. A glow discharge is formed in a low pressure gas as in the sputtering method and the substrate is now the cathode [35, 36].

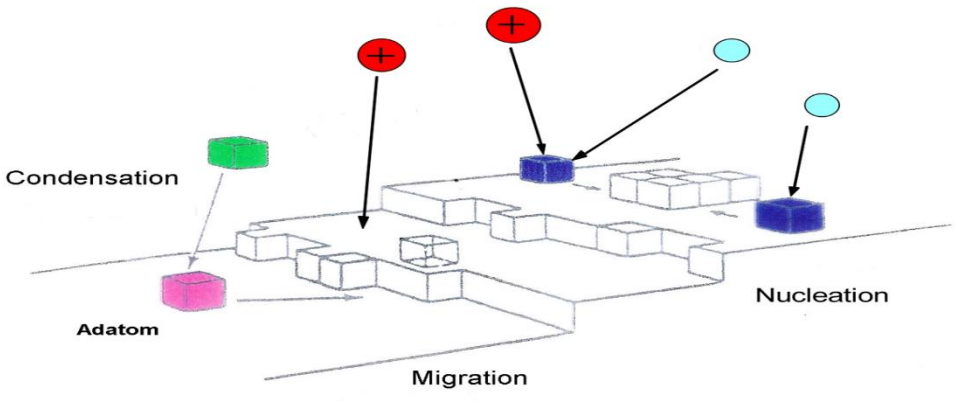

Figure 2.3: Thin film deposition using the ion-plating technique [37].

The film molecules are introduced into the discharge by evaporating the source using resistance, electron beam or flash heated techniques [19]. These molecules are rapidly accelerated to the substrate and impact on it to form a strong bond. Since evaporation is used, film formation is rapid but there is the risk of impurities [19, 38].

2.3 Patterning of films

There are several methods for patterning of films such as photoresist masking, metal masking, inverse photoresist masking and inverse metal masking. Photolithography is probably the most common process in which initially the substrate is completely covered with a film layer, as shown in Figure 2.4 [25, 39]. It is used in microfabrication to pattern parts of a thin film or the bulk of the substrate and it uses light to transfer a geometric pattern from a photomask to a light-sensitive chemical photoresist on the substrate. If positive photoresist is used, the exposed areas become harder and are not removed in the subsequent wash [19]. The surface is then etched to remove the film from the unprotected regions and the remaining photoresist is washed away eventually [19]. If several layers are to be formed then these are both first evaporated on and then followed by photoresist masking and etchants which attack each layer separately [40].

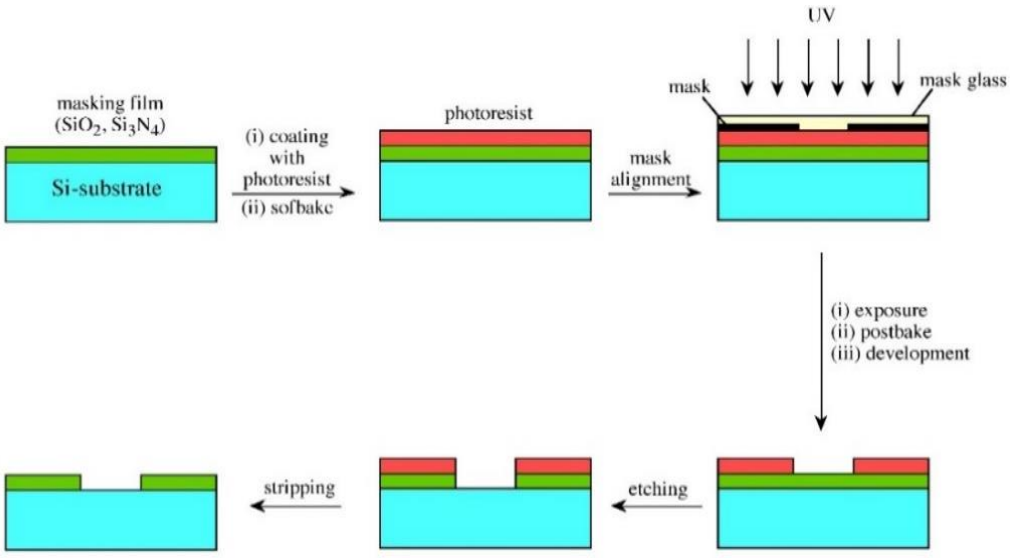

Figure 2.4: Photoresist masking [41].

In general, metal masking is a cheaper process because it does not involve the use of photoresists while in the case of inverse photoresist masking, the bare substrate is first coated with a layer of photoresist [42]. This is then masked and etched to form a pattern in which photoresist is left on the areas which are to have no film and it forms an inverse mask. The film layer is next formed over the whole substrate and it adheres to the bare substrate regions [19, 42]. This method is also used when the evaporated film is difficult to etch without attacking the substrate or the photoresist. As for inverse metal masking, it is very

similar to inverse photoresist masking but uses a metal mask [19]. The bare substrate is initially covered with a metal layer which is then etched to give the inverse metal mask. The required film layer is then deposited over this and finally the original metal mask is dissolved out with a special etchant, taking with it the unwanted film [19, 42].

2.4 Thin film properties

2.4.1 Thin film resistor materials

Thin film materials can be divided into the following categories [1, 14]:

- Metal alloys
- Single metal systems
- Cermets

At first, the most important properties of metals are influenced by their crystal morphology, particle size, surface area and porosity and it is known that due to their periodic crystal structure at low temperature, the electrons can flow [43]. Any change in this periodic nature will also change the flow of electrons and as a consequence the resistivity of the film will be increased. In addition to this, resistance can also be increased due to lattice distortions caused by vibration increases with temperature and that is the reason why TCR is generally positive for all metals [1].

The most widely used metal alloy system in the manufacture of bulk material resistors is Nickel Chromium [44-46]. During the years, nickel chromium was broadly used for the development of thin film resistors due to its high resistivity, low TCR and widespread commercial availability [47]. However, there have been numerous studies focusing on the properties of Ni-chrome thin film resistors and the effects of varying substrate materials and process parameters on their electrical performance and structural properties [48-52]. The most common materials used for thin film resistors on silicon are Silicon-Chromium (SiCr), Nickel-Chromium (NiCr) and Tantalum Nitride (TaN) [8, 53-58]. Thin film resistors generally have more involved manufacturing processes than monolithic resistors but present greater advantages [8, 19]. For instance, the frequency response of a thin film resistor is several times better than that of a monolithic device [8]. This is partly due to the lower parasitic capacitances associated with the resistors and partly due to their higher available sheet resistivity, which reduces the overall size. Thin film resistors can also be made to much tighter tolerances than monolithics since they may be adjusted to the required value after fabrication [19]. The most popular thin film resistor material is an alloy of about 80% nickel and 20% chromium, popularly known as Ni-chrome [19, 59]. It has good adhesion properties and a low temperature coefficient, which is determined by several processing factors such

as the rate of film deposition and the substrate composition. Typical resistor sizes are in the range 20 Ω to 50 kΩ [1]. Nickel is unsuitable on its own for use as a film circuit material since it does not adhere adequately to the substrate [19, 44, 60]. Chromium is sometimes used for resistors. Its principal disadvantage is the tendency to form surface oxides which make it difficult to etch. When high resistance values are required, cermets, which are compounds of a dielectric and a metal are often used. Since cermets are usually available in powder form they are ideally suited to vacuum deposition using flash techniques. It is generally difficult to control the thickness of a cermet film during deposition but it can be subsequently trimmed to give resistor values up to about 1 MΩ with a tolerance better than ± 1% [19]. Tantalum resistors are characterised by excellent stability, a high value of dielectric field strength and high annealing temperature [61, 62]. Tantalum is capable of producing uniform and reproducible film layers which can also be oxidised to form a thin passivating layer. The material has a high melting point and must therefore be deposited by sputtering. Thus, tantalum resistors can be produced with tolerances in the range ± 0.1% with stability in this range over 25 years [1, 19, 63, 64].

The substrate is the starting material for any thin film circuit on which it is formed. This can be made from a variety of materials such as glass or pure glazed alumina. Thin films can also be formed on silicon dioxide which is very useful as it gives a method of combining monolithic and film circuits on a single chip [19, 65]. Since thin films have relatively tight tolerances they place many demands on the requirements of the substrate, which should be clean and free from cracks and scratches [19]. The surface of the substrate should be smooth and there should be no dimensional changes with time which may cause registration of masks and bad line definition and the substrate should be a good electrical insulator. For power handling, it is also important that the substrate is a good thermal conductor and in these applications it is sometimes mounted on a heatsink [19, 66, 67].

2.4.2 Thick film materials

Thick film technology is used to produce electronic devices such as surface mount components, hybrid integrated circuits and sensors [17, 18]. Thick film circuits are widely used in the automotive industry due to their high reliability and their extended temperature range along with massive thermo-cycling of circuits without failure [65, 68]. The use of thick film technology permits the design of resistors with a wide range of Ohmic values [69, 70]. Practical limits are imposed for the minimum area which can be allotted to a specific resistor. In addition, extremely low value resistors, typically 1 to 10 Ω, can be sensitive to screen-printed conductor tracks, where they provide an interconnection pattern to the resistor. The manufacturing of such devices is an additive process involving deposition of several

successive layers of resistors onto an electrically insulating substrate using a screen-printing process [65, 70]. The typical process of the fabrication of thick films consists of the laser scribing of the substrates, ink preparation, screen printing, drying/curing, firing, laser trimming of resistors, mounting of capacitors semiconductors, separation of elements and integration of devices [65].

The most frequently used substrates are made of 96% Alumina (Al_2O_3). Alumina is very hard and not very machinable, therefore lasering of the material is the most efficient way to cut it to the desired shape [71]. With the lasering it is possible to scribe, profile and drill holes. Scribing is a lasering process where a line of laser pulses are fired into the material and 30-50% of the material thickness is removed, this weakens the substrate and after all other process are done to build the thick film circuit, the substrates can easily be divided into single units. The adjustment of thick-film resistor values was first performed by mechanical means such as mechanical abrasion or sand blasting [65]. However, these methods are very slow and not clean enough. The use of laser processing in microelectronics proved to be faster, cleaner, non-contacting and more accurate than previous techniques [72]. Laser trimming can easily be used instead of computer control and automation and it appears to be the preferable method for high-volume manufacturing of thick-film hybrid microcircuits and the YAG laser has become the most important production tool for this operation [13, 73, 74]. The thick-film resistors that may require trimming can either be printed onto a large substrate or can be in the form of trimmable surface-mount technology (SMT) chips mounted onto the substrate [75]. During the manufacturing of film resistors, parameters such as the sheet resistance, temperature coefficient of resistance and resistance stability need to be considered and these are presented in the next sections.

2.4.3 Sheet resistance, R_s

The resistance of a thin film resistor is given by [1, 5]:

$$R = \frac{pl}{dw} \qquad \text{Equation 2-1}$$

Where *p* is the resistivity, *l* is the length of the resistor, *d* is the thickness and *w* is the width of the resistor.

However, the ratio (*l/w)* equals to the number of squares in the film pattern (☐).

So, the sheet resistance of the film, R_s, is usually used to describe thin film resistors and it is defined as *p/d* and it is given by the following equation [1, 8, 70, 76-78]:

$$R_s = \frac{\Omega}{R} = \frac{p}{d} \qquad \text{Equation 2-2}$$

And is expressed in Ω/☐.

2.4.4 Temperature co-efficient of resistance, TCR

Temperature co-efficient of resistance (TCR) of the film is a parameter which describes the change in resistance of the film with change in its temperature *dR(T)/dT* which is a nearly constant value for most metal films and it is commonly used as an average parameter [1, 16, 76]

$$TCR_{av} = \frac{1}{R_i}\frac{R_e - R_i}{T_e - T_i} \times 10^6 \quad ppm/°C \qquad \text{Equation 2-3}$$

where, R_i is the initial resistance at temperature T_i and R_e is the end resistance at temperature T_e. Typical values of T_i and T_e are 20 °C and 70 °C respectively. However, using the above approach and assuming the resistance changes linearly as a function of temperature is not strictly valid for thin film resistors. Errors can arise from the composite TCR effect of conductor materials which are measured in series with the resistor element [1, 8]. For this reason, a more accurate method of defining the TCR of the resistor is to measure its change in resistance over the extremes of its operating range, typically -55 to +125 ppm/°C for surface mount devices and -55 to +155 ppm/°C for axial leaded components. This parameter is generally referred to as extended TCR and denoted as TCR_{ex} [1, 16, 76].

2.4.5 Resistance stability, ΔΩ/Ω

Resistance stability or reliability is basically a measure of the change in resistance of the film against a certain specification over a period of time. There are a number of conditions under which the reliability of the component can be tested such as DC load, dry heat or humidity [1, 8, 79].

The severity of the effects of a test condition on the resistor depends greatly upon film thickness. For thicker films, the resistance value is lower and the load voltage that can be applied is lower, as well. Moreover, humidity is also likely to have less effect on a more robust thicker film [1, 8, 80, 81].

The most convenient and universal test condition is that of dry heat (temperature) as the test can be performed by simply storing the film in an oven [1, 8, 70]. Dry heat stability tests generally entail measuring the change in the resistance value of the film *ΔΩ*, following storage at the upper category temperature, usually 155 °C for axial resistors and 125 °C for surface mount resistors for a period of 1000 hours [1]

$$\Delta\Omega/\Omega = \frac{R_e - R_i}{R_i} \times 100\% \qquad \text{Equation 2-4}$$

where R_i is the initial resistance and R_e is the end resistance following storage [1].

2.5 Resistor trimming methods

There are a number of different trimming methods which can be used to adjust the value of the resistor, including anodisation, heat trimming, electrical trimming, mechanical trimming, chemical trimming and laser trimming [1]. However, of these techniques laser trimming is by far the most effective and popular method and is still a subject of continuing theoretical and experimental analysis and optimisation [1, 4, 5, 15, 16].

2.5.1 Anodisation

Anodisation is an electrolytic passivation process used to increase the thickness of the natural oxide layer on the surface of metal parts [82]. The process is called anodising because the part to be treated forms the anode electrode of an electrical circuit [83]. Anodising increases resistance to corrosion and wear, and provides better adhesion for paint primers and glues than does bare metal. Anodic films can also be used for a number of cosmetic effects, either with thick porous coatings that can absorb dyes or with thin transparent coatings that add interference effects to reflected light [83].

Metal film resistors can be formed by depositing upon dielectric substrates thin layers of film-forming metal and electrolytically anodising the same to form oxide layers which, by reducing the resistor film thickness, produces the desired resistance value. Such techniques have involved simultaneously anodising the resistor and measuring its value, until the desired value is successfully attained and anodising is terminated after this point [84]. Thus, anodising and measuring should be carried out simultaneously but this might cause inaccurate measurements. It has thus been proposed alternately to connect the resistor to an anodising current source and then to a bridge measuring circuit for measuring the resistance value. This process is continued until the resistor reaches the expected value. However, there are a few basic problems with such operations such as the fact that significant time is needed in order to determine the resistance value accurately in view of the speed limitations of automatic bridges. Furthermore, adjusting a resistor accurately requires that the adjustment between measurement cycles should be small, meaning that many measurements are required to be made. In addition to this, high speed switching of the resistor from the anodising current source to the bridge measuring circuit can cause problems of thermal generation, contact resistance and reliability [84]. Moreover, the large capacitance formed by the electrolyte gel on the resistor separated by, for example, the Ta_2O_5 dielectric layer in the case of tantalum resistors, requires a long discharge time, around 40 minutes, after each anodising cycle before accurate measurements can be made [56, 57, 85].

In Figure 2.5, a method of trim anodising a thin film resistor to a predetermined value is presented. It can be alternately achieved by applying anodising current to the resistor and measuring whether the value of the resistor is greater or less than the predetermined value in a relatively rapid trimming cyclical manner [86]. In each cycle, which is principally anodising and to a minor extent settling and measuring, the resistor value is approaching the predetermined value. Modifying such a cycle can provide a relatively slow trim with the cycle being principally settling and measuring and to a minor extent anodising and it can help to avoid overshooting the resistance value [87].

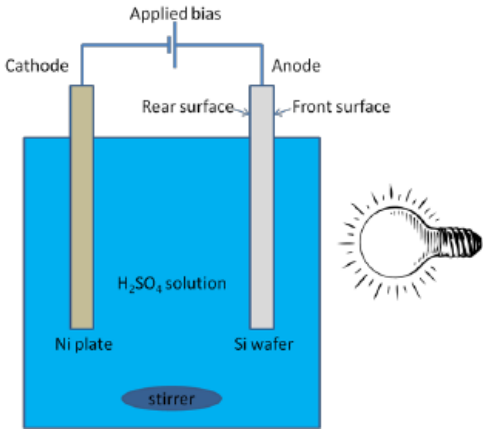

Figure 2.5: Anodisation process [88].

A method for controlling the trimming of metal resistors is by anodisation and it is practically applicable for adjusting the value of thin film resistors during manufacture. Thin film resistors may be produced by selective etching of a thin layer of metallic material which has been deposited upon an insulated substrate [88]. As a practical matter, the accuracy of such a process yields resistors with a tolerance of approximately 10%. To improve upon this, and provide resistors having a tolerance of better than 1%, the metal film resistors have been subjected to an anodisation process [89].This involves initially constructing the resistor to have a value lower than the desired value. The resistor is then anodized in an electrolytic cell thus forming an insulating oxide on the surface thereof. This process can be thought complicated because the flow of current from the anodisation should be taken into consideration when determining the actual resistance value to avoid inaccurate values [89].

2.5.2 Heat and electrical trimming

Heat or electrical trimming are often used in preparing thin film resistors, both for stabilising the resistivity and for tailoring to required values. Localized high temperatures are achieved by direct resistance heating, thus providing a means for the individual tailoring of selected resistors in a thin film network [90]. Each resistor is probed at its terminations and direct

current is applied to initiate heating. Surface oxidation essentially decreases the thickness of the conducting film, thus increasing resistance. The other reaction or reactions occurring are not as readily apparent but usually have the overall effect of decreasing film resistivity. The nature of this change is metallurgical and includes such things as stress relief, vacancy condensation and other structural realignment processes [90]. The rate at which the resistance change occurs is dependent upon many variables, especially deposition parameters which affect the initial film structure. The difficulty in correlating rate of change with a particular film thickness, substrate material etc., necessitates a direct monitoring method for obtaining precision values. This may be achieved by accurate measurement of the voltage-current values during trimming with appropriate temperature coefficient compensation [91].

Electrical trimming of resistors is accomplished by forcing large current-density pulses through the resistor body, generating sufficient Joule heating to cause a decrease in the resistor value [92]. Resistance reductions of over 50% of the as-processed value can be easily achieved with remarkable accuracy. Once trimmed, a portion of the resistance can be “recovered” by applying current pulses above the trim threshold current [93-98]. Pulse current trimming is an efficient method of accurately trimming individual resistors after packaging. Trimming resistors after the element is packaged, as opposed to wafer-level trimming, compensates for any resistance changes introduced during the packaging process, and thus results in the most accurate final resistor values. Insufficient pulse width will result in an incomplete trim at a fixed pulse amplitude [99-102]. The resistor’s initial value is measured and compared with the desired target. If trimming is required, a trim current pulse of sufficient amplitude is applied. The resistance is measured during and after each applied trim current pulse. Joule heating causes the resistor’s value to rapidly increase to an “instantaneous” resistance value, during which time the resistor element is self-annealed. Upon removal of the trim current pulse, the resistor quickly cools to its “ambient” resistance which is the value measured after the film has returned to room temperature (25 °C) [48, 63, 98, 99, 103-105]. After removal of the first trim current pulse, the resistance is less than the initial resistor value. This represents the amount of resistance trimmed during the pulse and is proportional to the trim current pulse amplitude [103-105]. Larger increments in trim current result in greater steps in resistance reduction. The trim current pulse amplitude is incremented until the target resistance is obtained [48, 68].

2.5.3 Mechanical trimming

Mechanical trimming concerns grinding away part of the film layer. The resistance adjustment is done by removing a part of the resistor material by a narrow jet of abrasive

particles (air abrasive trimming) using the scribe method, which can theoretically give similar results to the ones from laser trimming. For instance, in a top hat shape resistor, a sharp line cut into the resistive element increases the effective length of the resistor and it leads to the increase of the resistance. However, this sharp line can also cause instabilities on the resistor due to local damage on the film and the underlying substrate [106, 107]. Manufacturing tolerances of ±1% can actually be achieved by the air abrasive trimming. For the case of the fluid abrasive method, distilled water is sucked into an air brush where it mixes with streaming nitrogen, dispersing into fine droplets and emerging from a nozzle as a high velocity jet. It is worth adding that the fluid abrasive method is not expensive to implement and can provide very high trim values and trimmed resistors stable enough to handle high power densities. Mechanical abrasion is believed to be the predominant trimming mechanism, the micrometer-sized water droplets providing the necessary energy [108].

Thus, abrasive trimming can increase the resistor value in one of two ways [108]:

- Removing material to form a kerf, as with laser trimming. This increases the number of resistor squares, thus increasing the value.
- Reducing the thickness of the resistor film area. In that way, the sheet resistivity is increased and as a consequence the resistance value also increases.

2.5.4 Chemical trimming

Chemical trimming or industrial etching is the subtractive manufacturing process of using baths of temperature-regulated etching chemicals to remove material to create an object with the desired shape. It is mostly used on metals, though its use with other materials is becoming increasingly important [3, 14, 84, 109]. It was developed from armor-decorating and printing etching processes developed during the renaissance as alternatives to engraving on metal. The process essentially involves bathing the cutting areas in a corrosive chemical known as an etchant, which reacts with the material in the area to be cut and causes the solid material to be dissolved; inert substances known as maskants are used to protect specific areas of the material as resists [109].

In general, etching has applications in the printed circuit board and semiconductor fabrication industries since it can offer resistor tolerance at the value of ±2% [84]. It is also used in the aerospace industry to remove shallow layers of material from large aircraft components, missile skin panels and extruded parts for airframes. Etching is used widely to manufacture integrated circuits and micro-electrochemical systems. In addition to the standard, liquid-based techniques, the semiconductor industry commonly uses plasma

etching which involves a high-speed stream of glow discharge (plasma) of an appropriate gas mixture given in pulses at a sample [109].

2.5.5 Laser trimming process

As previously mentioned, laser trimming is by far the most popular method for trimming of thin and thick film resistors due to the fact that it allows manufacturers to control resistance values and resistor ratios with accuracy of ±0.2 mm [1, 2, 7, 11, 12, 110]. Laser trimming requirements have not changed that much in the past few years. However, the applications such as circuit feature geometry and device complexity have changed dramatically. Even though older systems might be able to be effective, the constant development of laser control and beam positioning and the availability of new technologies like diode-pumped lasers, machine vision, automated parts handling and dual high-speed processors make the new systems much better production tools for the modern factory and the trim speed range is from 1 mm/s to 300 mm/s [15, 16, 111]. The trimming operation can be characterised as passive or active [112]. Passive trimming refers to the trimming of the resistors to a specific predetermined value. The resistance is monitored during the trimming, and when the desired resistance is reached, the laser pulsing stops. In functional trimming, the circuit is operating as in reality while it is being trimmed. The performance of the circuit is measured during trimming and the trimming is terminated when the circuit is operating properly and within specification. Functional trimming improves the performance of the device and increases yield. It often requires fully automatic, complicated test algorithms [112].

In laser trimming, the laser uses a light beam of a few micro-meter in diameter to remove the resistive film from the ceramic substrate in a very short time period of less than 1 ms, see Figure 2.6 [1]. On impacting the resistor film, the high intensity coherent light pulse is absorbed by the material causing it to heat and vaporise. The process is dependent on several variables such as the intensity of the laser pulse, or the power level, the focus of the pulse and also the properties of the material being ablated [112].

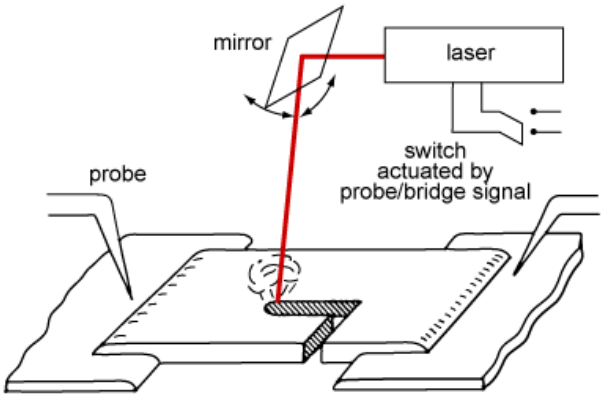

Figure 2.6: Laser trimming process [113].

The laser beam is scanned across the resistor to produce a continuous kerf, changing the resistance value of the film as it progresses. In addition to the properties of the beam itself, the accuracy to which the resistance value can be adjusted depends on both the shape of the cut and also the speed at which the measurement system can switch the laser beam off between pulses once the target resistance value is reached [1, 7, 114-117].

There are two main types of laser commonly used for the adjustment of resistive films, the CO_2 and the Nd:YAG [7, 99, 118]. The pulsed carbon dioxide (CO_2) laser has a long pulse width with high energy per pulse, which causes vaporisation of the film. Even though the long pulse width can cause damage to the substrate and the resistive material at the edge of the kerf, known as the heat affected zone (HAZ), the CO_2 laser can be effectively used for laser trimming of thin films [118].

It is worth mentioning that Nd:YAG lasers pumped by arc lamps and operating at a wavelength of 1064 nm were used in the early years. In the recent years, diode-pumped Nd:YLF lasers operating at a wavelength of 1047 nm have been used successfully for the same purpose. However, functional trimming of thin films on silicon has been difficult because the wavelengths of 1064 and 1047 nm are both absorbed by the silicon and produce free electrons and holes in the silicon. This generates a photoelectric response, causing error signals in the output of the circuit. The photoelectric response should dissipate before a good measurement can be made since time is needed for the device to recover after each laser pulse [7]. In general, the use of a Nd:YAG or Nd:YLF lasers operating at 1319 nm can eliminate this problem. This wavelength is long enough that the corresponding photon energy is smaller than the energy band gap of silicon, so the laser light will not generate free carriers in the silicon. These types of lasers are commercially available and may be incorporated in trimming systems intended for use with silicon devices. The neodymium: yttrium-aluminium-garnet (Nd:YAG) laser uses an acousto-optic Q-switch to give a two-way optical switching of the laser beam. This type of system can produce short

pulses of high peak power at a wavelength of 1064 nm, so the film is quickly vaporised and the heat flow is minimised. However, parts of the material surrounding the kerf can be damaged significantly [2, 110, 116]. In addition to the use of shorter pulses, it is worth mentioning that lasers operating in the green region of the visible spectrum can provide additional reductions in the HAZ due to the decrease in laser spot size resulting from the shorter wavelength of 532 nm which influences the absorption process [119].

2.6 The heat-affected-zone (HAZ)

Laser heating is a thermal-chemical process, combining heating, melting, material removal and sharp solidification or quenching. During this process, when the temperature of the work piece reaches the melting point, a molten layer is created and material removal takes place [2, 12, 120]. After heating, when the laser moves further, the process of solidification initiates grain refinement near the kerf area [16, 116]. The Heat-Affected Zone (HAZ) is the zone of the base material which has not melted but whose microstructure and mechanical properties were affected by the heat generated during laser cutting [7, 121, 122]. The heat generated by the laser cutting process and after cooling causes this change in the region near the cut surface. The HAZ may lead to undesirable effects such as fatigue resistance, surface cracking and distortion. So, it is interesting to select the appropriate laser cutting parameters in order to minimize the HAZ. It is an area of a base metal which, while not melted, still has had its chemical properties altered by high temperature exposure [76].

Changes that can occur at the HAZ tend to cause stresses that reduce the strength of the material. The HAZ can also suffer from a decreased resistance to corrosion or cracking and these changes can also lead to the formation of nitrides at the HAZ, which can affect the performance of the device. In addition, the microstructure at the HAZ can be altered in a way that increases its hardness compared to the surrounding material. Hardness, sensitization, and high local stresses in or near the HAZ may be mitigated by practices such as controlled heat treatment and solution annealing [63, 123-125].

The size of changes in physical properties that can affect the HAZ of the material is dependent on a number of factors, including the base material and the amount and concentration of heat input during the trimming process [13, 101, 126, 127].

On the other hand, the size and effect of the HAZ is determined by other factors. The less time the material is exposed to heat, the less time the heat has to act on it. Thus, during trimming, faster cut speeds tend to lead to a smaller HAZ. Finally, the type and thickness of the material being cut also plays a huge part in the size of an HAZ since different metals react to heat differently [124, 125]. The changes to the material's microstructure can be

reduced by using heat treatment and adjusting the laser parameters such as the type of the laser, laser beam diameter and mode as well as laser power accordingly. Power is the measured power of the laser beam used to trim the resistor material and Q-rate is the frequency at which the Q-switch interrupts the laser beam and hence its peak power and pulse duration. As for the bite size, it is the distance the laser beam is moved across the resistor surface between pulses and hence the amount each pulse overlaps [2]. As a result, smaller HAZ can be achieved so that less material is wasted.

A major cause of post-trim drift in laser trimmed resistors is due to the HAZ bordering the kerf. It would therefore seem beneficial to consider this area in more detail. A Q-switched YAG laser is typically adjusted to operate in single traverse electromagnetic (TEM_{00}) mode, with the energy profile of the beam having a Gaussian distribution [2, 9, 12]. This profile is then translated into a Gaussian temperature profile in the thin film as shown in Figure 2.7 [9, 12].

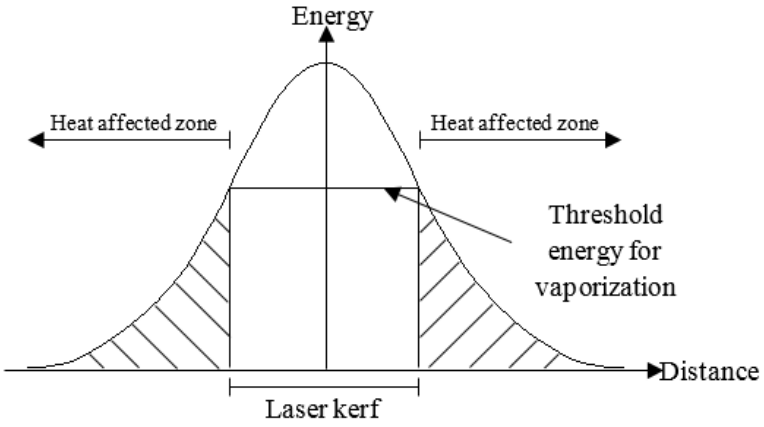

Figure 2.7: The fundamental mode laser beam profile as a Gaussian distribution [2, 12, 16].

Only the central part of the profile is of sufficient intensity to cause vaporisation of the thin film. For the areas of film adjacent to the kerf, the energy absorbed from the laser beam is less than the threshold required for vaporisation. Thus this region of the film becomes a heat affected zone and is known to exhibit considerably more change in resistance with time than areas of film not irradiated by the laser beam (see Figure 2.8) [12]. This aging effect is partly due to the fact that the film which was stabilised and or passivated prior to the adjustment process has now been re-exposed along the edges of the laser kerf [12]. The remainder of the resistance changes are related to changes in the structural properties of the film material because of the rapid heating and cooling during the trimming process such as the sheet resistance and TCR [122, 128].

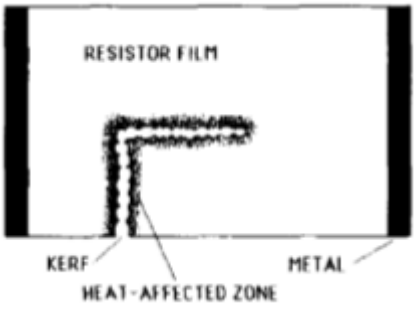

Figure 2.8: The HAZ in laser trimming and is subject to long-term annealing effects [122].

In addition to the length of the kerf and hence the amount of HAZ, the extent to which the HAZ protrudes into the current carrying path of the trimmed resistor is an important parameter in determining the overall stability of the resistor [15, 16, 76]. These parameters can usually be suitably optimised through variation in the shape of the continuous trim and also the properties of the laser beam itself. It is a usual approach to simulate the HAZ by finite element analysis and it is important for the virtual process chain of laser based manufacturing and necessary for the prediction and optimization of the trimming quality [16, 119, 122].

2.7 Spectrophotometry

In general, the basic function of a spectrometer is to take in light, break it into its spectral components, digitize the signal as a function of wavelength, and read it out and display it through a computer [129]. This process is described in this section because of its relation with the wavelength and the reflectance of the material. The first step is to direct light through a fiber-optic cable into the spectrophotometer through a narrow aperture known as an entrance slit. The slit vignettes the light as it enters the spectrometer. In most spectrophotometers, the divergent light is usually collimated by a con-cave mirror and then it is directed onto a grating. The grating then disperses the spectral components of the light at slightly varying angles, which is then focused by a second mirror and imaged onto the detector [129]. Alternatively, a con-cave holographic grating can be used to perform all three of these functions simultaneously and it has various advantages and disadvantages [130]. Once the light is imaged onto the detector the photons are then converted into electrons which are digitized and read out to a computer. The software then interpolates the signal based on the number of pixels in the detector and the linear dispersion of the diffraction grating to create a calibration that enables the data to be plotted as a function of wavelength over the given spectral range. Thus, a spectrometer is an imaging system, which maps a plurality of monochromatic images of the entrance slit onto the detector plane. This slit is critical to the spectrophotometer’s performance and determines the amount of light (photon

flux) that enters the optical bench and is a driving force when determining the spectral resolution. Other factors are grating, groove frequency and detector pixel size. The optical resolution and throughput of a spectrometer will ultimately be determined by the installed slit. Light is entering the optical bench of a spectrometer via a fiber or lens and it is focused onto the pre-mounted and aligned slit which controls the angle of the light which enters the optical bench [129]. For solid samples, the intensity of the measurement light beam, I_o, is measured without the sample set. Then, the sample is set in the path of the measurement light beam, and the intensity of the light beam after it passes through the sample, I_t, is measured.

$$T=I_t/I_o \qquad \text{Equation 2-5}$$

As shown in Figure 2.9, the spectrophotometer consists of a light source, a spectrophotometer, a sample compartment, and a detector. Although it was already mentioned in the previous section that the sample is exposed to monochromatic light, there are instruments in which white light is passed through the sample before being passed into the spectrophotometer. This method is usually employed in high-speed photometry instruments that use array detectors [129].

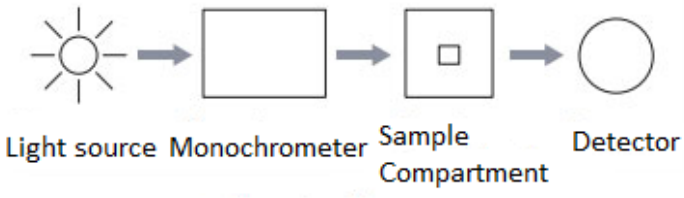

Figure 2.9: Schematic of a spectrophotometer [129].

2.8 Resistor Trimming

2.8.1 Conventional Trimming Geometries

The performance of laser-trimmed resistors depends on both trim path and geometry [4, 5]. There is a variety of trim patterns that can be used for the adjustment of surface-mounted bar-shaped thin film resistors such as the plunge cut, L-cut, shadow cut, double plunge cut, scan cut and serpentine cut [4, 5, 7]. The geometry of the resistor and the resistivity of the film determine the resistance value of the resistor. Thus, identical geometries will achieve the same value if the film resistivity is consistent. Then, the appropriate trim depends on a combination of resistor geometry and the desired precision and speed. Many variables can determine the best cut and its characteristics: resistor-aspect ratio, amount of resistance change required, resistor material, final tolerance, stability and trim throughput rate [1, 2,

12]. Generally, methods to improve the cut selection and its characteristics require further tests and analysis [131].

The plunge cut, as shown in Figure 2.10, is the simplest, fastest and most economical type of cut. It consists of a single kerf orthogonal to the current flow through the resistive material. It generally gives less precision than multiple trims, but a shorter period of time is needed to perform this cut [1, 2, 12].

Figure 2.10: Plunge cut.

However, its tolerance accuracy is quite limited at around 10% and it cannot be used for trimming high-accuracy resistors because of the fast change in the value of resistance as the cut approaches the opposite side of the resistor. If the initial value of the resistor is close to final value, the cut will stop before the point of significant resistance increase and after this point, control and accuracy are difficult to achieve [1, 4].

The L-cut, see Figure 2.11, is the most frequently used of trim pattern due to its precision, stability and tolerance accuracy. The L-cut can overcome the problem of rapid value change inherent in the plunge cut. The resistance increases quickly, in relation to the trim speed, as the laser cuts the kerf perpendicular to the current flow (y-direction) and is called transverse cutting [7, 12, 123, 132].

Figure 2.11: L-cut.

Then, after it turns through 90 °C, it increases slowly until the target value is reached in an area of equal current density and this is called longitudinal cutting (x-direction). In Figure 2.12, a typical plot of the resistance value vs. the trim length is presented. The point which is annotated as “corner” is the point of the cut in which the kerf is changing direction to cut the x-leg [1].

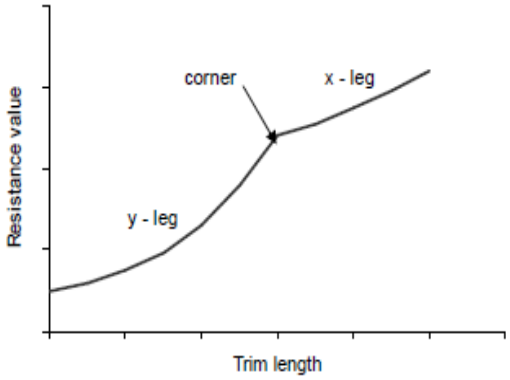

Figure 2.12: Typical plot of the resistance increase for the L-cut [1].

An additional benefit of the L-cut is that it allows a wider adjustment range than the plunge cut for resistors. In Figure 2.13, the resistance increase for the case of the L-cut is depicted. The stability of the resistor can be maximised by varying the ratio of the x and y legs. It is worth noting that the optimum performance is usually achieved when the y leg is as short as possible. However, the drawback of the L-cut is the additional trimming time needed in order to perform this cut and that fact makes it slightly more expensive than other methods.

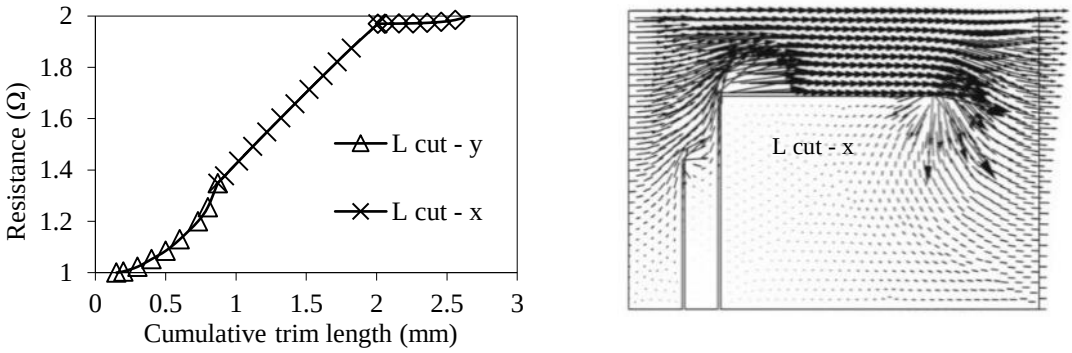

Figure 2.13: Typical plots of resistance increase with kerf length and corresponding model of current density for the L-cut and shadow cut [1].

A shadow cut, as shown in Figure 2.14, is thought to be an expensive type of cut. It consists of an L-cut or plunge cut and an additional plunge to its side. The trim usually starts at approximately 15 to 20% of the total resistor length away from the conductor-resistor junction to avoid junction effects and provide maximum room for the second cut [133]. The shadow trim usually falls close but outside of the L-cut or plunge shadow to provide a slow rate of resistor value change. The shadow trim can fine tune the resistor to the last 1% of the nominal value desired and it does not exceed the main cut length (L-cut or plunge) [7].

Figure 2.14: Shadow cut.

The cut that consists of two plunge cuts is called double plunge, see Figure 2.15. In this cut, the trim is kept within the centre third of the resistor body to maximise value change for a given depth of cut and to allow for shifts in resistance. The first cut of the double plunge brings the resistor to a value that permits the second cut to work in a lower rate-of-change area. The second cut is an additional cut which works in the shadow of the first cut. Current flows down the length of the resistor and since the second cut is made in a location, where little current flow occurs, it has less effect on changing the resistor value [1]. For this reason, the second cut should be shorter than the first cut. The trim speed can be greater than for a plunge cut since precision derives from the second cut, which occurs in a less sensitive trim area than the first. The second trim should always be shorter than the first. It is usually kept within 50 to 75% of the first trim length for better results [1, 2, 12]. At equal trim lengths, the rate of change increases rapidly and may cause overshoot and out-of-tolerance values. By performing this cut, tighter resistance tolerances can be achieved. However, this type of cut is more expensive due to the additional trimming time needed [4, 5].

Figure 2.15: Double plunge cut.

A scan cut, as shown in Figure 2.16, is used to sense the edge of the resistor and to trim resistors to the nominal value desired when the resistance correction is small and precision is needed. The scan cut starts before the resistor edge and a proper kerf width is chosen so that all of the resistor material is removed between scan lines [1, 12]. It is most commonly used when the device is required for high frequency applications to minimise creation of capacitive reactance components of an RC circuit [7]. It can also be used in high voltage situations due to the reduced likelihood of voltage breakdown across the trim kerf. Unfortunately, this type of cut can be three times more consuming to perform and consequently it is not cost-effective for general use [7].

Figure 2.16: Scan cut.

A serpentine cut (see Figure 2.17) can offer improved tolerance accuracy due to the large resistance gain and it can be used when the pre-value resistance is much lower than the target value. Multiple cuts are made in areas of high current density which effectively increase the geometric length of the resistor and consequently its resistance value [7].

Figure 2.17: Serpentine cut.

This cut uses multiple plunge cuts to trim resistors of larger areas to a nominal resistor value that is many times that of the initial value. However, the disadvantage of the long trim length is the increased amount of heat-affected-zone surrounding it, which can lead to stability issues [1, 7]. In some cases, where the resistance gain is very large, increases in the temperature coefficient of resistance can also occur due to the amount of material which has been raised to temperatures in excess of the zero TCR heat treatment temperature without being vaporised.

Previous studies which tried to overcome this problem clarified that it is common practice to employ a two stage serpentine trim when precision thin film resistors are needed [1]. The vast majority of the trimming is performed in the first trim stage and the resistor is adjusted to around -1% from its target value. The device is then stabilised, typically overnight at around 200 ºC to relieve stresses built up in the HAZ. As it is not possible to accurately predict the resistance change that occurs during this stabilisation operation, the second stage of the adjustment process, the fine trim, is required to accurately adjust the resistor to target value and usually consists of one or two plunges in the shadow of the first serpentine, see Figure 2.18 [1, 2, 12].

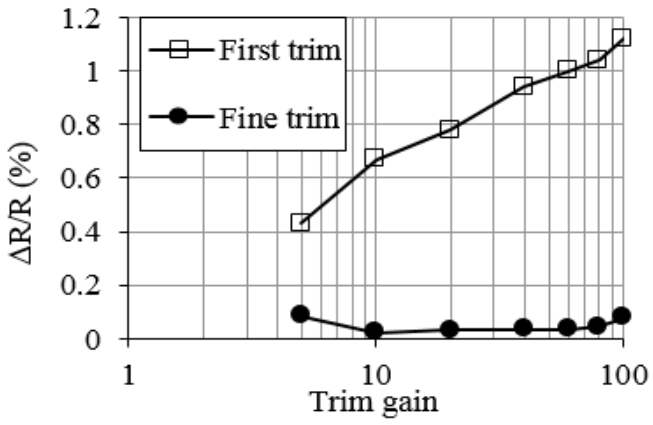

Figure 2.18: Two stage serpentine trim pattern and corresponding variation in resistance stability with increasing trim gain for CuAlMo TFR's trimmed with both first and fine trims [1].

This type of cut can be very time consuming and expensive, although the increasing availability of auto substrate handling equipment can help to reduce the majority of the labour cost involved.

In addition to these common trim patterns, there are others such as the curved L, curved J, curved U and curved U with isolation cuts and their schematic approach is shown in Figure 2.19 [7]. With the curved L and the curved J, their speed, accuracy and stability are adequate and it seems that the hot spots, which are regions with higher intensity caused by the laser beam, in turn can be reduced [7].

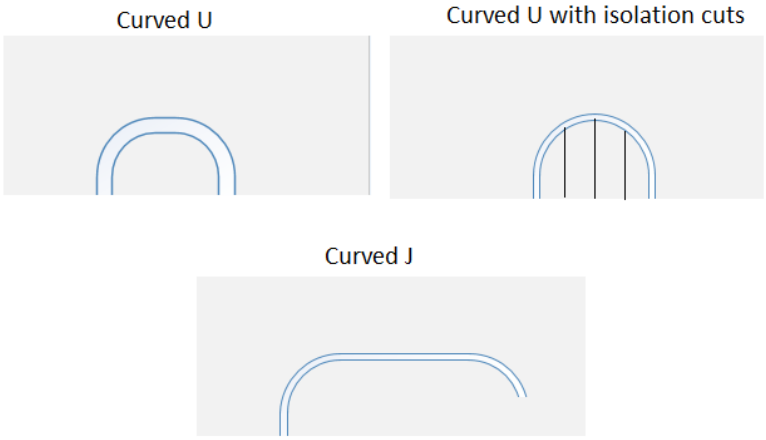

Figure 2.19: Schematic approach of curved U, curved U with isolation cuts and curved J trim patterns.

They can also achieve tolerances less than 1%. As for the curved U with or without isolation cuts, it appears to have stability and tolerance at around 1% but the trim speed is really slow [7].

2.8.2 Alternative trimming geometries and methods

A more direct solution to overcome the issues associated with the HAZ is to trim by link cutting, see Figure 2.20. This process involves sequentially opening up shorting bars in loop and ladder type patterns to increase the resistance in discrete steps. Once the trimming bars are opened, the current is redirected around the new longer path thus eliminating any current crowding in the trimmed area or HAZ. Although this method can improve aging effects, larger chip area is required compared to the conventional bar design, which can lead to less products. Moreover, as the resistance is adjusted in discrete steps a very large number of links may be required to give resolution comparable with the continuous trim approach [122].

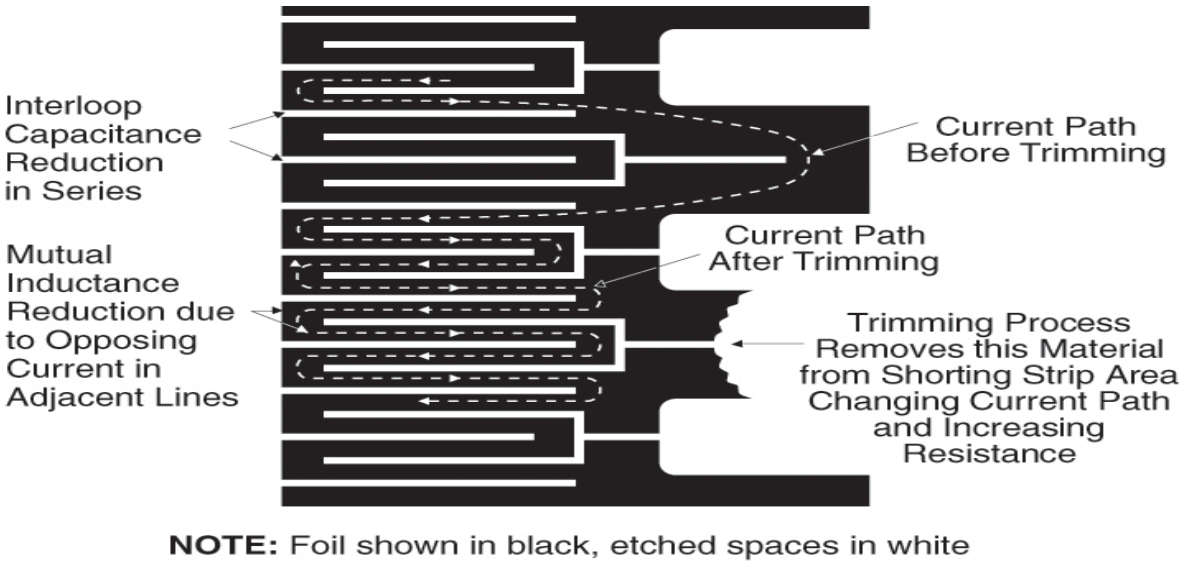

Figure 2.20: Demonstration of link cutting [122].

There have however been methods reported to make the benefits of the link cutting approach applicable to bar resistors. Perhaps the most notable of these involves cutting a Swiss cheese pattern in the resistor, as shown in Figure 2.21, which forces current crowding only in non-heat affected areas [16, 76]. This pattern differs from the typical trim structure since it consists of additional trim targets that are void of material (holes) [16]. To adjust the resistance to the desired target, successive trims to a combination of targets along the trim paths indicated are made [16]. Swiss cheese technique is thought to be simple and repairable. It can be used in a range of substrates and last-minute design changes are easily implemented. Devices are designed for low-thermal resistance and arranged so that all devices have the same distance from cold-plate-type heat sinks [16].

Figure 2.21: Swiss cheese pattern design [16].

Another study proposed a type of laser trimming performing an L-cut in a ‘top hat’ shape thin film resistor, avoiding excessive crowding of the current lines after trimming [123]. The resistor has a rectangular shape but in order to avoid excessive crowding of the current lines after trimming, an extra rectangular part is added on the side opposed to that which will be cut. The laser cut is L-shaped for a precise ending of the trimming process when the

resistance reaches the desired value. So, the laser starts the trimming process vertically and the resistor value rises rapidly. When the desired value is close, the laser beam starts to move horizontally, slowing down the speed of raising the resistor value and a more precise stop moment is possible.

The top-hat structure, shown in Figure 2.22 (a), has as a base a rectangle with 20 x 10 arbitrary units. It has on the upper side an extra space of 10 x 5 units, allowed for displacement of current lines during trimming. It is considered that the laser beam cuts a trimming path of 0.1 units wide.

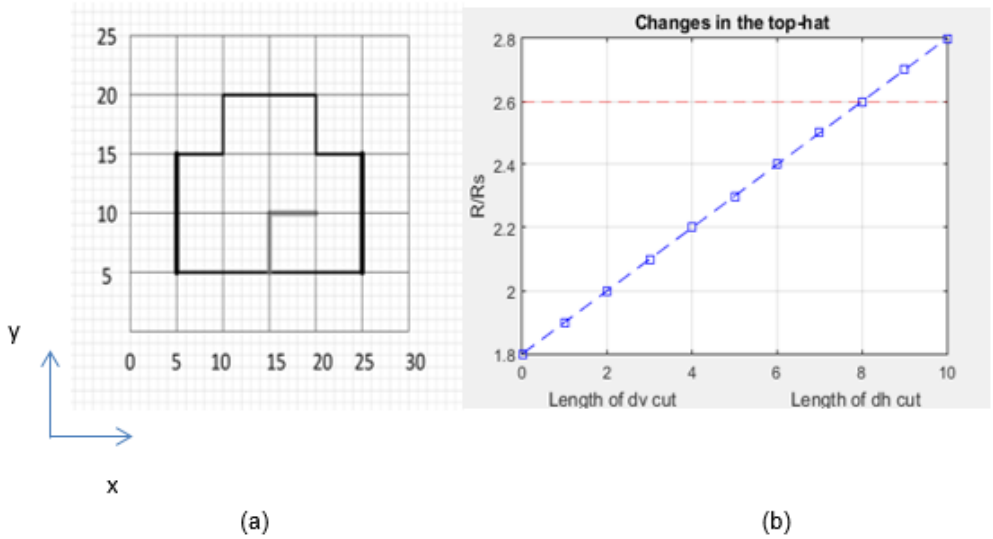

Figure 2.22: (a) Top-hat resistor with L-cut, (b) Rise of the value of the top-hat resistor [123].

In Figure 2.22 (b), the actual value R/R_s (where R_s is the specific resistance of the film) of the top hat resistor is presented as function of the vertical cut d_v (from 0 to 5 units) and further as function of the horizontal cut d_h in order to determine its corresponding length for $R= 2.5\ R_s$ [123].

Trim pattern design has an effect on the resistance distribution and long-term resistance drift performance of thin films such as CuAlMo. The L-cut pattern and the serpentine cut were applied on films with sheet resistance of around 0.75 Ω and the investigation took into account three laser trim parameters during this experiment: power, Q-rate and bite size [2, 12]. The best results of post-trim resistance drift of around 0.12% are achieved with minimum power and maximum bite size. The power of the laser beam needs to be controlled in order to ensure the removal of all the resistive material, otherwise, shallow trimming and dirty kerfs will cause instability. As for the trimmed tolerances, these were less than ± 0.5% [2, 12]. In Figure 2.23, the standard deviation of the resistance with increasing trim gain for L-cut and serpentine cut is shown in order to achieve the target tolerance.

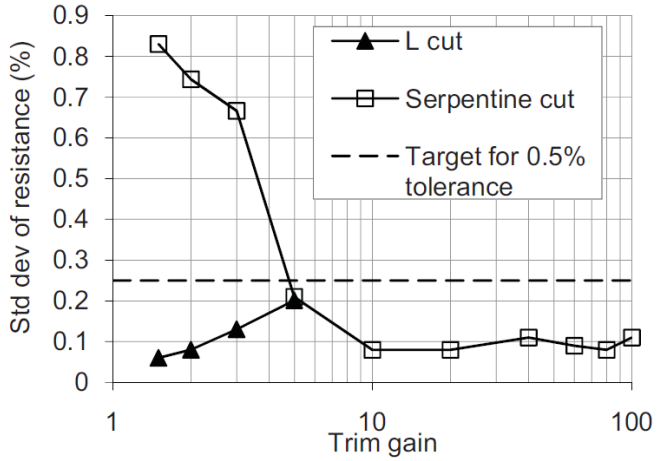

Figure 2.23: Standard deviation of resistance with increasing trim gain for L-cut and serpentine cut [1].

The plunge cut and the L-cut have been shown to be effective when trimming other materials such as Ta_2N material using a YAG laser operating in TEM_{00} mode. On the L-cut, the geometrical position of the turning point results in minimum aging and depends on the initial resistor dimensions and the final value to which it is to be laser trimmed. Moreover, oxidation of the Ta_2N after trimming can reduce conductivity along the kerf leading to a subsequent increase in the final resistor value and depends on both the material and trim configuration [120]. As for the case of the laser adjustment of $Ta_{42}Si_{13}N_{45}$ thin films, precise trimming can be achieved using femtosecond irradiation. Part of the film was removed and the removal rate of the material was down to 20 nm per pulse with the prospect to be further decreased. According to this study, it was proven that infrared laser irradiation by microsecond and nanosecond pulses permits a complete layer removal [63].

An innovative laser trimming method for designing resistors with a resistance value lower than that needed by the application is random trimming. This method is accomplished by cutting holes into conductive paper in order to increase its resistance value. It is performed by cutting a hole in a random point (see Figure 2.24 (a)). Random trimming is a quite long process and that is the reason why it was combined with a plunge cut (see Figure 2.24 (b)). A single-dive offers rough adjustment and wide trim range fast and then the random trim and voids helped to get closer to the target resistance. Thus, the heat-affected zone is decreased and the sensitivity of the trim is minimized [5].

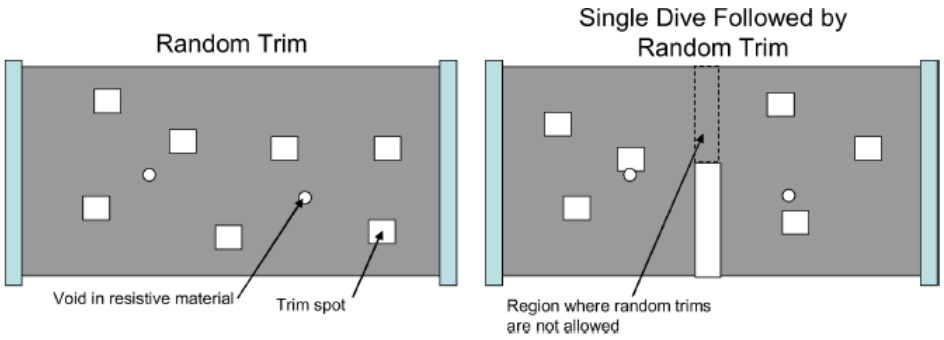

Figure 2.24: (a) Pure random trimming, (b) Single dive first and then random trim to target [5].

Another recent method focuses on the effect of replacing the two contact bar resistor with a three contact distributed structure, trimmed by narrow cuts around the additional contact of various shapes, see Figure 2.25 [5]. With this method, some encouraging results were concluded due to the fact that the design is simplified and the fabrication process can be faster and cheaper [11, 133]. However, the additional trimming time and materials required did not appear to justify the improvements in resistor performance reported.

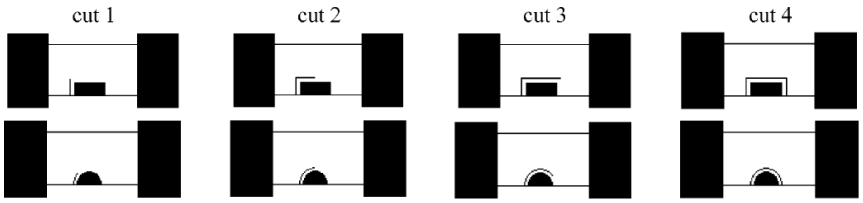

Figure 2.25: Illustration of laser cut length used in three-contact resistors with rectangular and semi-circular additional contact [5].

2.9 Summary

A thorough review research has been conducted on previous studies and projects concerning thin and thick film resistor trimming. A brief description of the film deposition process was presented since it is one of the first steps in the manufacturing of thin film circuits before the trimming process takes place. Various trimming methods were also discussed, highlighting the fact that laser trimming is by far the most appropriate and efficient method for trimming of thin and thick film resistors. The advantages and disadvantages of basic trimming patterns which are widely used in the industry were also introduced and it was shown that the geometry of the patterns can significantly affect the overall performance of the resistors especially in relation to the heat affected zone. It is shown that more recent studies have focused on alternative trimming geometries that would lead to further optimisation of the laser trimming process and would improve the performance of the resistors and this is also the main focus of this research.

3 Modelling of trim geometry

3.1 Introduction

In this research, modelling was conducted using both numerical simulations and computer-aided software in order to investigate the effect of the geometry of trimming patterns. The numerical simulations were mainly focused on calculating the resistance value and TCR for different trim lengths. Also, modelling using computer aided software concerned the temperature change of the resistors while applying power and the current density was also investigated. In general, ANSYS is a software that gives the ability to produce virtual prototypes and it is widely used for simulating the behavior of complete products. Thus, ANSYS workbench 15.0 platform, which is a finite element analysis tool, was used for the simulations of this study. The thermal electric analysis was followed for the thermal distribution and current density for both types of resistors examined, either conductive paper or thin films.

Existing trimming patterns of thin film resistors were modelled as well as more specialized cuts such as the curved L-cut, angled L-cut and semi-circle. Thus, easy comparisons can be made for the different patterns and the stability and tolerance accuracy of the resistor can later be determined. MATLAB R2015 was the version used in this study and it was proven very useful for further calculations related to TCR and HAZ to get an estimated value for these parameters which would be useful for further comparisons between the different pattern geometries.

3.2 Modelling of the resistors

3.2.1 Numerical simulations

Simplified numerical models can be developed easily that can actually match the experimental trimming results [4, 5]. Thus, numerical simulations of the resistors that allow variations in trimming patterns were used in order to model the resistor. In Figure 3.1, the model of the plunge cut is shown for reference of the dimensions of the resistor and other variables that were used for the calculations with MATLAB, based on equations from previous studies [4, 5].

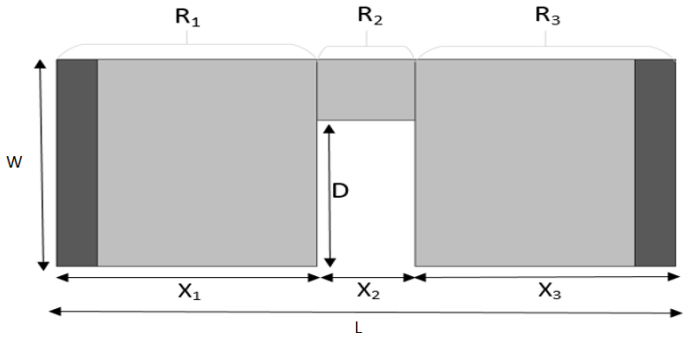

Figure 3.1: Model of plunge cut.

One important factor for this study is the calculation of the resistance value *R* which is given by:

$$R = \frac{\rho L}{A} = \frac{\rho L}{TW} = \frac{\rho}{T}\left(\frac{L}{W}\right) = R_{\square}\left(\frac{L}{W}\right) \qquad \text{Equation 3-1}$$

where ρ is the bulk resistivity, A is the cross-sectional area of the resistor, $R_{\square}$ is the sheet resistance, and L, W and T are the length, width and thickness of the resistor, respectively. The length, the width and the thickness were constant for all the calculations since they referred to the same sample. For the case of the conductive paper, the length L was 30 mm, the width W was 20 mm and the thickness T was 0.1 mm. As for the thin film resistor, the dimensions of the substrate were 6 x 25 mm and the thickness was 1 mm.

In addition to this, the modelling methodology used contains models based on summing resistors in series to enable the plunge cut to be formed, as shown in Figure 3.1 and it was modelled using the following equations [4, 5]:

$$R = R_1 + R_2 + R_3 \qquad \text{Equation 3-2}$$

$$R = R\left(\frac{x_1}{W}\right) + R\left(\frac{x_2}{W-D}\right) + R\left(\frac{x_3}{W}\right) \qquad \text{Equation 3-3}$$

$$R = R\sum_{i=1}^{n}\left[\frac{\frac{x_1}{n}}{W-\left(\frac{D}{n}\right)\left(\frac{2i-1}{2}\right)}\right] + R\left(\frac{x_2}{W-D}\right) + R\sum_{i=1}^{m}\left[\frac{\frac{x_3}{m}}{W-\left(\frac{D}{m}\right)\left(\frac{2i-1}{2}\right)}\right] \qquad \text{Equation 3-4}$$

Where n and m are the number of rectangles on either side of the trim and R is the specified value which depends on the normalised resistance value, L and W.

A similar approach to the one above was used for the double plunge cut and serpentine cut. However, for the L-cut and curved L-cut, the total resistance was calculated as the parallel combination of R_1 and R_2, as per equation:

$$R = \frac{R_1 \times R_2}{R_1 + R_2} + R_3 \qquad \text{Equation 3-5}$$

The area that is the combination of R_1 and R_2 refers to the one which is not affected by the laser trimming, as shown in Figure 3.2.

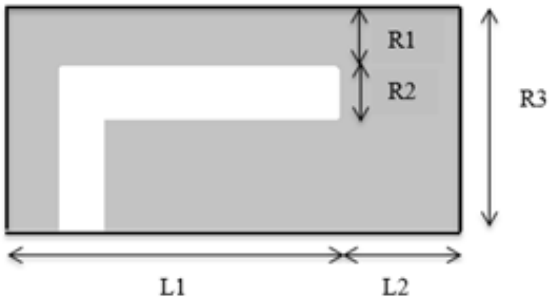

Figure 3.2: Model of L-cut.

3.2.2 HAZ Sensitivity

As previously mentioned, the HAZ is one factor that affects the performance of the resistor since it is the area surrounding the cut affected by the laser. The material around the pattern is affected and the larger the size of this area, the more unstable it can become. The sensitivity of the HAZ is related to the maximum power density, P_{max}, based on previous research [16, 76]. It is defined as the fraction of the total power that is dissipated in the HAZ and it is expressed as

$$S_{HAZ} = \frac{P_{HAZ}}{P_s} \qquad \text{Equation 3-6}$$

where P_s is the power dissipation of the resistor and P_{HAZ} is the total power dissipated in the HAZ. Based on this equation, the sensitivity was calculated for the plunge cut, the double plunge, the L-cut and the serpentine cut and the results are shown in the Table 3.1 below.

Table 3.1: Average of HAZ sensitivity for different trim patterns.

Type of cut	**S_{HAZ}**	**P_{max} (%)**
Plunge cut	0.11	1.29
Double plunge	0.12	2.17
Serpentine cut	0.13	2.25
L-cut	0.10	0.82

It was found that the sensitivity of the HAZ in serpentine cut has the greatest change in the resistance value at an average of 13% due to the fact that the value of P_{max} is also increased. The sensitivity for the plunge and double plunge cut is 11 and 12%, respectively. As for the L-cut it is shown that it has the lower sensitivity to the HAZ at the value of 10%. The

calculation of the sensitivity to the HAZ can offer an estimation of the area of the HAZ and its size surrounding the cut.

3.3 Modelling using conductive paper

Conductive (carbon-based) paper was the material set used for the modelling and it was later verified experimentally. This type of paper was an affordable option and it could offer results in a short period of time and it was used in this research. Thus, the modelling was based on this material so that proper comparisons to be made. In this case, the outline dimensions that were chosen for the model were based on previous studies on trim pattern geometries on conductive paper and the dimensions of the resistor for the experiments used were 280 x 100 mm [4, 5]. Also, in this study, silver contacts were added to the two ends of the resistor using silver paint. Then, it was decided to use alternative dimensions for the resistor of 140 x 100 mm.

However, even though these previously mentioned dimensions were also simulated, the final dimensions chosen were 30 x 20 mm after many trials in order to achieve a proper comparison between the results from simulations and experiments, see Figure 3.3. Silver contacts were simulated for the resistor shape but the final decision was the use of carbon ink (Bare Conductive) in order to have the ability to compare the simulations with experiments once again. The shape of the resistor was first modelled without any type of pattern applied to it and represented the theoretical behaviour of the untrimmed resistor.

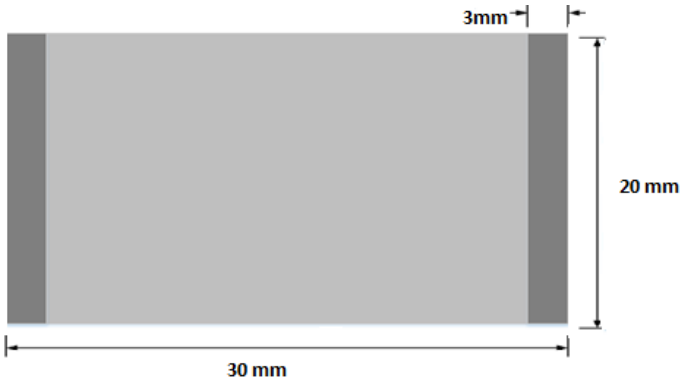

Figure 3.3: Dimensions of the resistor using conductive paper.

As previously mentioned, the simulations were conducted using ANSYS Workbench and the thermal electric approach. The material was determined for the simulations using values from the experimental analysis of the conductive paper and theoretical values obtained from CES Edupack from Granta Design.

The modelling referred to the case of applying a voltage of 15 V which equates to around 0.012 W at the side of the resistor so that an estimate of the temperature distribution for the conductive paper could be expressed. The outputs of the simulation contained the temperature change as well as the current density. In Figure 3.4, the meshing and the temperature change for the conductive paper without carbon ink contacts are shown while power was applied to it. The maximum temperature is shown as 28 °C while the initial temperature was set at 22 °C.

In addition, the temperature change and the current density for the resistor dimensions of 30 x 20 mm with carbon ink contacts is presented in Figure 3.5. After the application of carbon ink the temperature reaches up to 32 °C. The current density is mainly depicted in the area of the carbon ink and it is the area with the higher value of temperature.

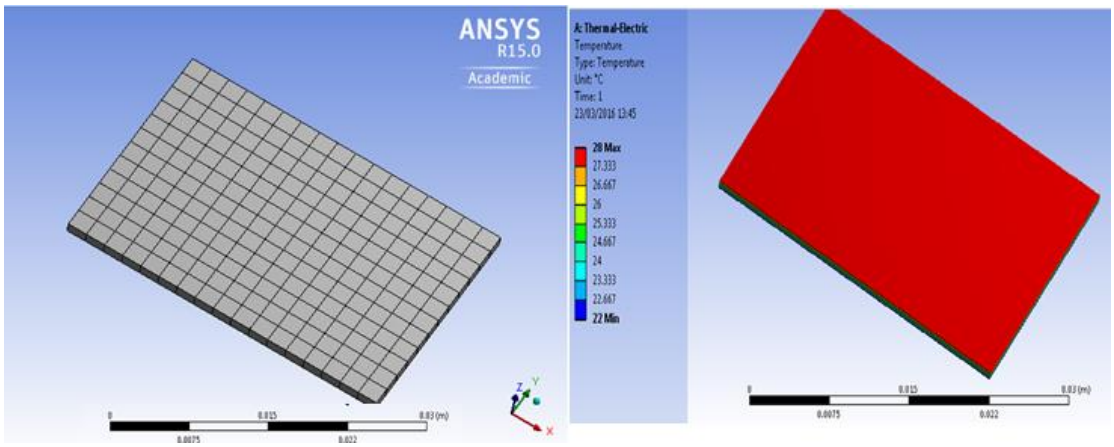

Figure 3.4: Meshing and thermal-electric simulation using ANSYS for conductive paper without carbon ink contacts.

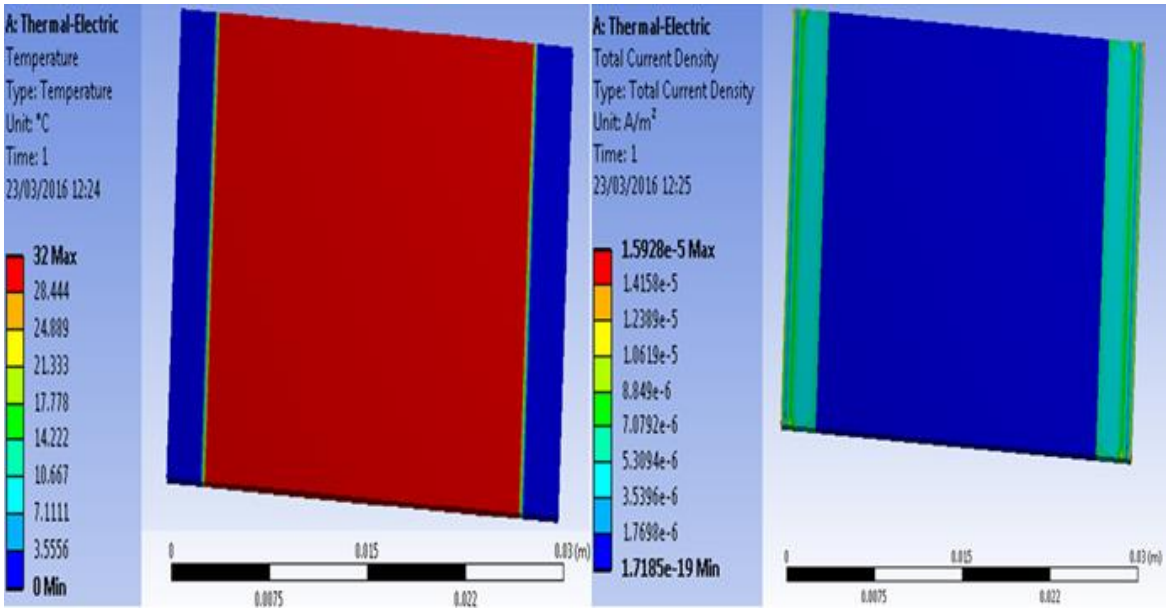

Figure 3.5: Thermal-electric simulation using ANSYS for conductive paper with carbon ink contacts.

It is shown that the temperature is normally distributed throughout the resistor in both the cases either with or without carbon ink contacts. As for the current density, it is worth commenting that once again it is normally distributed but there is a significant variation in the parts of the sides of the resistor that contain the carbon ink contacts. This is mostly due to the fact that the contacts are the ones in which the power was applied to and this was causing the temperature rise and then it was distributed to the rest of the area.

3.3.1 Plunge cut

The plunge cut, as previously mentioned, is a type of cut which gives a large resistance increase. Multiple simulations were conducted for both conductive paper and thin films for the calculation of the resistance value in relation to the trim length. The results for the case of the conductive paper are presented in Figure 3.6. The range of the trim length varies from 0 to 14 mm for the plunge cut. Based on the parameters shown in Figure 3.1, the position of the cut was placed for $X_1 = X_3 = 12.5$ mm and for $X_2 = 5$ mm. The resistance value, as expected, is increased in relation to the trim length. Hence, the longer the trim length the larger the resistance increase. For instance, it is shown that for the trim length of 14 mm the resistance value reached up to 18.5 kΩ from 6.5 kΩ.

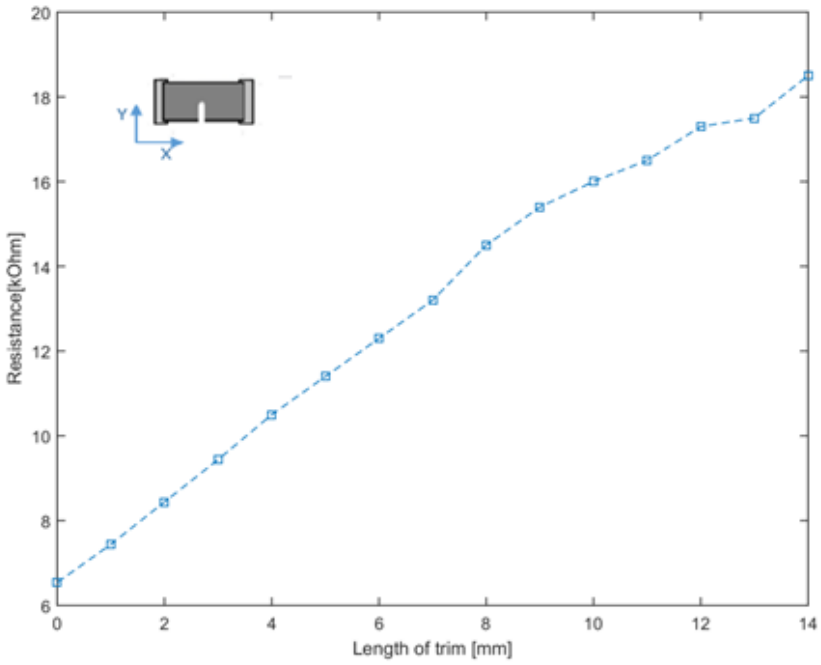

Figure 3.6: Simulation results for the resistance value vs. trim length for the plunge cut using conductive paper.

The temperature in relation to the voltage applied to the sample was also simulated so that a comparison could be made with the experimental results. As shown in Figure 3.7, the temperature vs voltage plot is presented for the plunge cut with trim length of 5 mm, 10 mm

and 15 mm. The plunge cut with trim length of 5 mm appears to have a constant increase in temperature as more power is gradually applied to the sample. The trend is similar with the other two lengths of 10 and 15 mm, respectively. However, for the first case, the temperature rises up to the value of 32 °C, while the other cases, the value increased to 33.9 and 34.2 °C. The temperature value does not seem to follow a constant trend but the temperature of the resistor depends on the voltage and thus power applied to it.

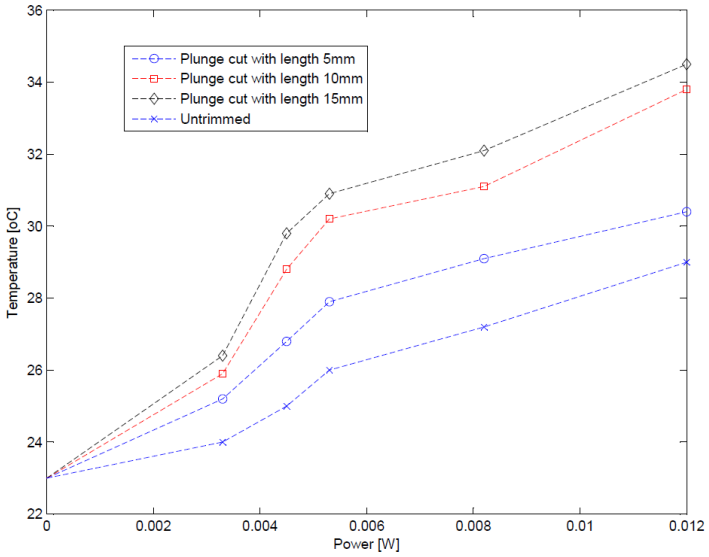

Figure 3.7: Simulation results of temperature vs power for different lengths of the plunge cut.

It is clearly shown that the higher the value of the voltage applied to the resistor, the higher the increase in temperature will be. It can also be thought that the trim length might also have an effect in the temperature change since it affects the resistance value hence the power applied to the resistor. Once the resistor is trimmed and its resistance value is increased, the voltage needed to test the resistor will be higher and that will lead to its temperature to be increased subsequently.

3.3.2 Double plunge

As previously explained in detail in Chapter 2, the double plunge cut consists of a main plunge cut and a shadow plunge next to it. This type of cut obviously offers a large resistance gain. In Figure 3.8, the resistance value vs. trim length is presented for the double plunge cut consisting of two plunge cuts with dimensions 5 mm and 10 mm, respectively. The initial resistance value was 6.5 kΩ and the change in the direction is showing the point in which the shadow cut is starting. The final resistance value when the cut was completed was 17.6 kΩ. Thus, this pattern can offer a resistance gain of 11.1 kΩ for a trim length of 14 mm.

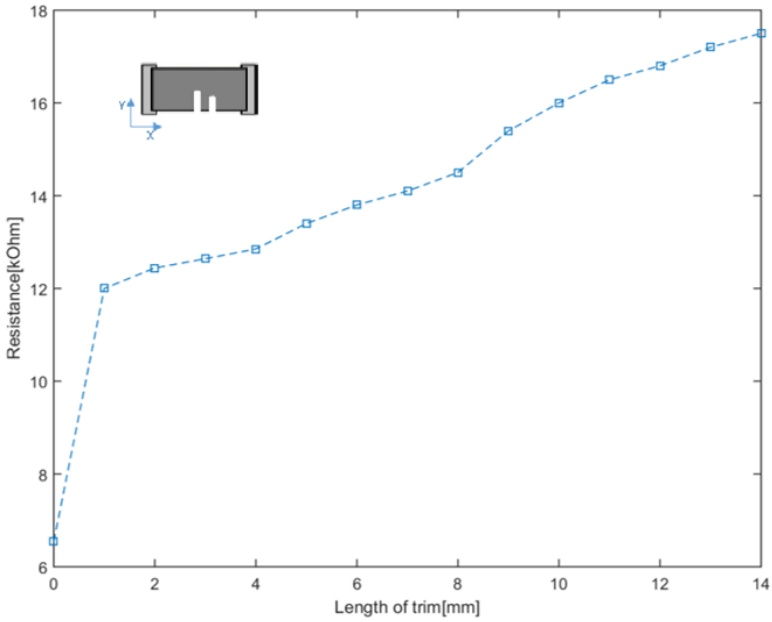

Figure 3.8: Resistance value vs trim length for the double plunge, consisting of 5 and 10 mm.

In Figure 3.9, the results from simulations using ANSYS are shown for the temperature change when voltage was applied to the resistor. Three double plunge cuts with different dimensions are presented, the first cut consists of two plunges of 5 mm and 10 mm, while the others refer to set of trim lengths of 5 and 15 mm and 10 and 15 mm, respectively. As shown, the temperature increases in relation to the voltage for all three different cut dimensions. The initial temperature is set at 23 °C for all three patterns so that there is a common reference point. When voltage of 15 V is applied to the samples, the temperature reaches up to 25.25 °C for the total trim length of 15 mm for the first simulation. After that, for total trim length of 20 mm for the two plunges, the temperature value is 26.25 °C. As for the total trim length of 25 mm, the temperature reaches up to 27 °C. Thus, it is clear that the temperature is higher when higher voltage is applied to the resistor. There might not be a direct correlation with the trim length and the temperature increase but it is shown that for the case of the double plunge cut the temperature rise is higher for the longer trim length. The cause of this might be due to the fact that higher power is needed since the resistance value will be higher.

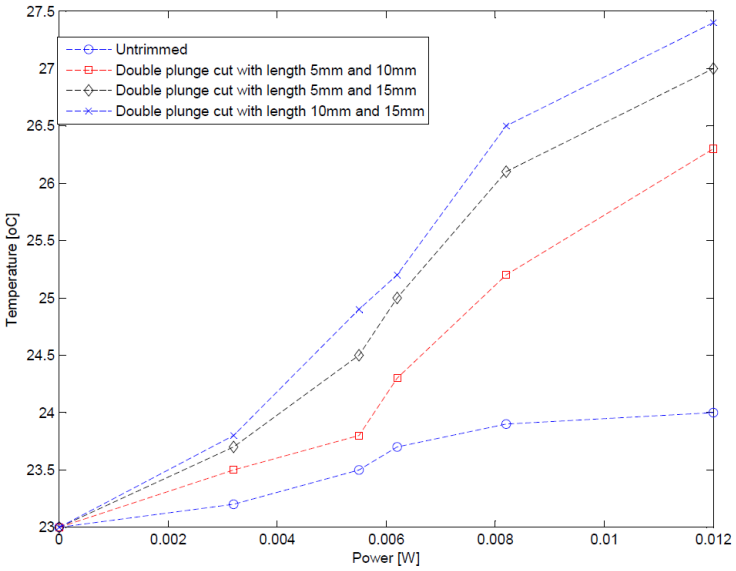

Figure 3.9: Simulation results of temperature vs voltage for the double plunge cut with different lengths.

3.3.3 L-cut

The L-cut, is thought as the most popular and effective trim pattern. In Figure 3.10, two types of L-cut with different dimensions are shown. The increase in their resistance value in relation to the trim length is presented. The starting point is common for both cases and set at 5 kΩ. For the case of the L-cut with dimensions of x = 5 mm and y = 15 mm, the resistance shows a quick increase until the point in which the plunge cut is completed at 5 mm and then the increase continues until the total trim length of 20 mm is achieved. The trend is similar in the case of the L-cut with dimensions of x = 10 mm and y = 10 mm but the difference is that the resistance value is quickly increased until the trim length of 10 mm since the plunge cut is longer for this case. Also, the increased in the resistance in the second case is higher since it reaches up to the value of 12.5 kΩ as opposed to 7.8 kΩ in the first case.

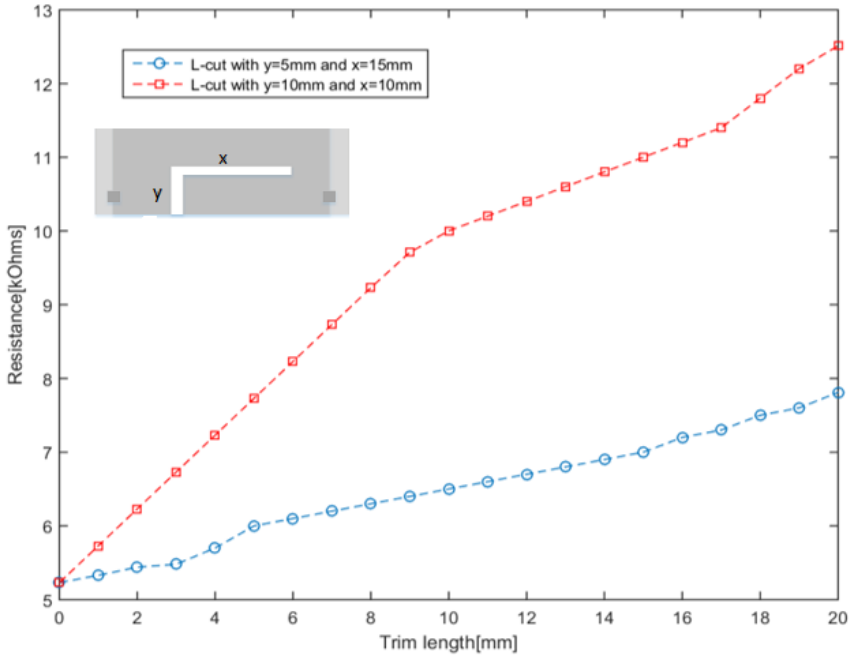

Figure 3.10: Resistance value vs. trim length for the L-cut with different dimensions based on results from simulations.

In Figure 3.11, the graph for the simulation results of temperature in relation to voltage is shown for different trim lengths of the L-cut. The y-leg was set at 5 mm for three model samples and the x-leg with values of 5 mm, 10 mm and 15 mm respectively. The fourth sample displayed had a value of x and y-leg at 10 mm. The initial temperature was set at 23 °C. The temperature is increasing in all the samples but the highest increase is shown with the higher power applied to them. The temperature of the pattern with total trim length of 15 mm reached up to 28 °C while the one with trim length of 20 mm reached up to 27.5 °C. As for the L-cut with length of both legs of 5 mm, the highest value of temperature reached up to 23.5 °C. The temperature for the L-cut with values for both x and y-leg of 10 mm it is shown that it reached 25 °C. Thus, it is shown that the higher temperature value is noted for all the samples for the higher voltage applied to the resistor.

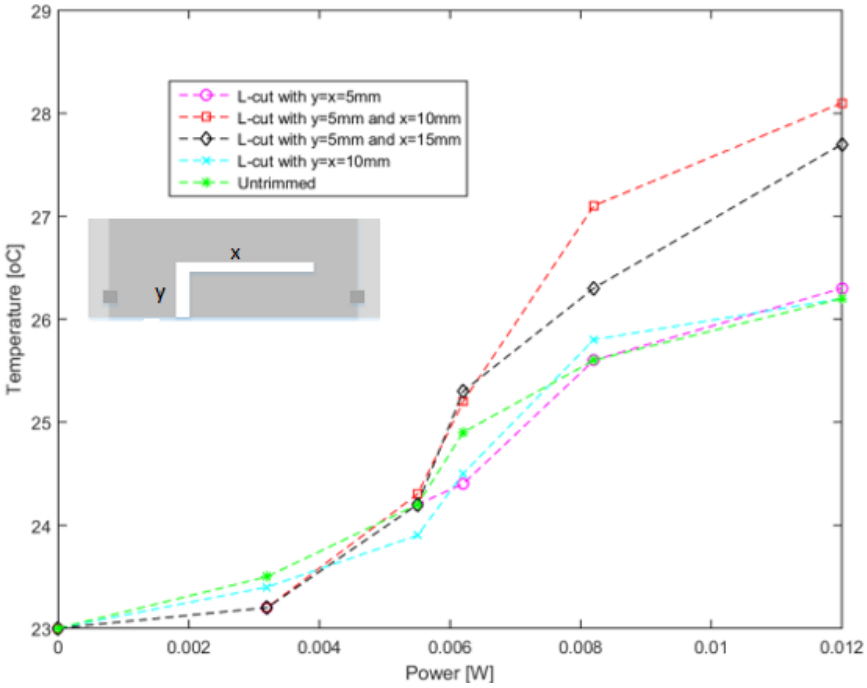

Figure 3.11: Simulation results for temperature vs. voltage for the L-cut with various dimensions.

3.3.4 Angled L-cut

The angled L-cut is not one of the basic trim patterns that is greatly used in manufacturing but previous studies [7] related to this cut were limited and hence it has been chosen for further investigation. The resistance value was calculated for this type of cut in relation to the trim length. The results of the simulation are shown in Figure 3.12 for the angled L-cut with values of *a* = 5 and 10 mm and *x* = 10 and 5 mm, respectively. The resistance value was set at 6 kΩ and the total trim length for both samples was 15 mm. The resistance of the angled L-cut with value *a* of 5 mm was increased up to the value of 10.2 kΩ while for *a* = 10 mm has reached up to 11.7 kΩ.

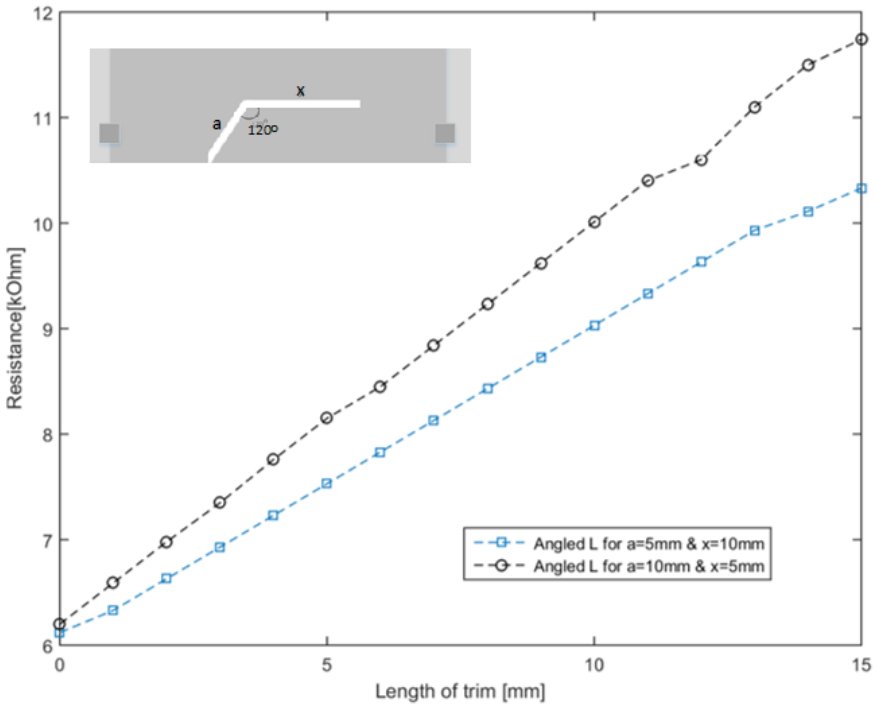

Figure 3.12: Resistance value vs. trim length for the angled L-cut with different dimensions based on simulation results.

The angled L-cut was also modelled so that the increase in temperature to be calculated using ANSYS when voltage was applied to it. The voltage range was once again from 0 to 15 V since this is the allowed range for the conductive paper. Three variations of length for the angled L-cut were modelled in relation to their temperature change with values of *a* for 5 mm and 10 mm and with values for *x* = 5 mm, 10 mm and 15 mm, as shown in Figure 3.13. The trend between the three model samples is the same and the final temperature varies slightly from 28.5 to 28.8 °C for a voltage of 15 V. The angled L-cut does not appear to have the trend of the L-cut but it seems that it has a constant increase in temperature as the cut progresses.

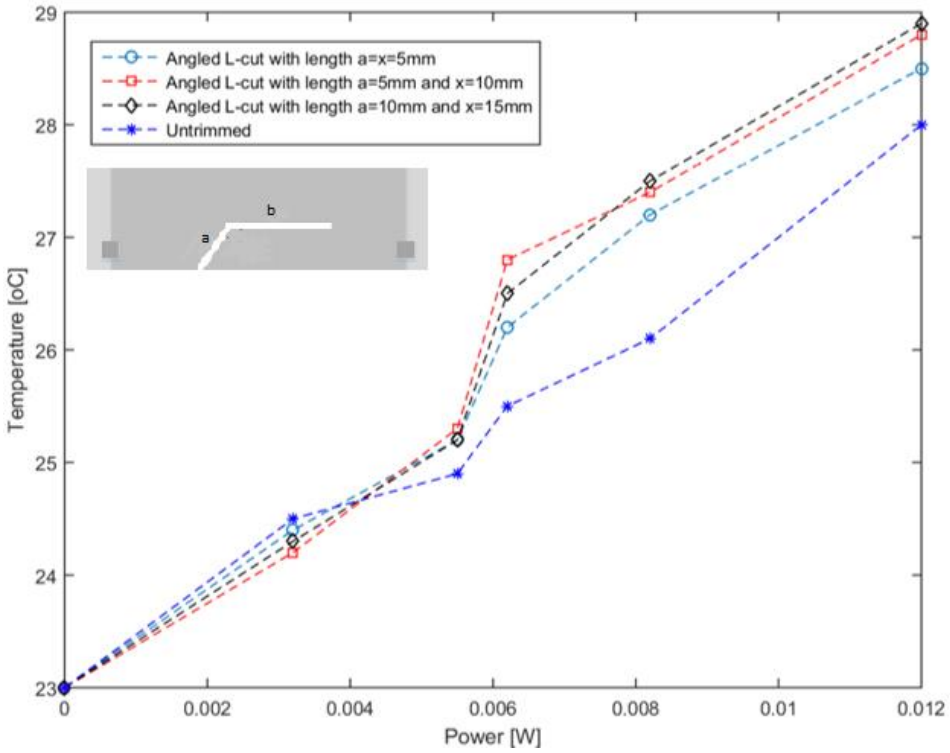

Figure 3.13: Simulations results for temperature vs voltage for different lengths of the angled L-cut.

3.3.5 Curved L-cut

The curved L-cut is once again one of the newer trim patterns [7] since it is thought to be an optimized version of the L-cut, since the corner of the x and y-leg is replaced with a smooth connection using the curve. There has been a variety of trim dimensions modelled for this type of cut and one of them was with dimensions of x = 3 mm and y = 10 mm as shown in Figure 3.14. There is an increasing trend for the resistance value as the cut progresses until the total trim length of 13 mm. The final resistance value reached up to 11.7 kΩ when the cut was completed. In this case, there is no corner shown similar to the L-cut when the cut changes direction. A slight change is noted at the point of the trim length of 3 mm, in which the plunge has been completed and the curve is starting, however this is much less prominent than in the case of the L-cut where it transitions from *y* to *x* leg.

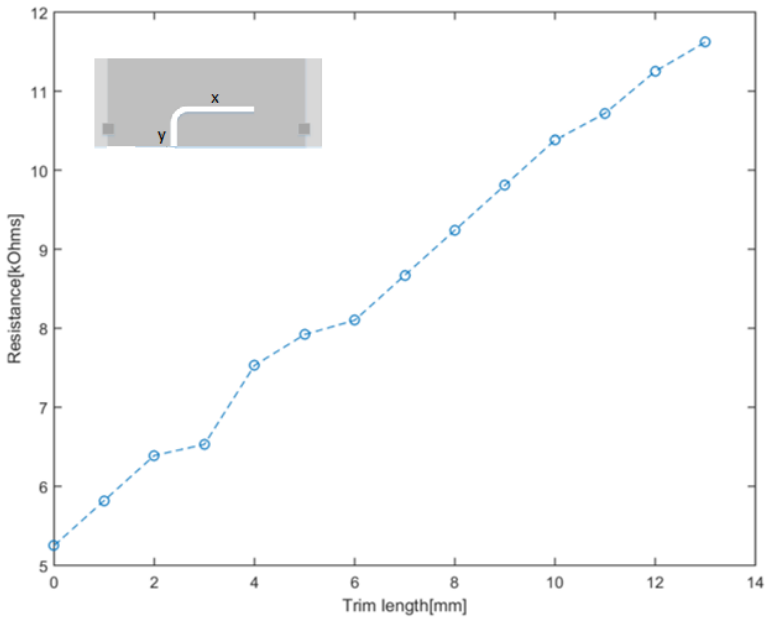

Figure 3.14: Simulation results for resistance value vs trim length for curved L-cut with x = 3 mm and y = 10 mm.

Different values of x and y for the curved L-cut were also investigated in relation to the temperature change of the resistor when voltage was applied to it. In Figure 3.15, the initial temperature set of the resistor was 23 °C. The trend in the increase of the temperature is similar between the samples and the highest value for all three is within the range of 27.5 to 28 °C when a voltage of 15 V was applied. It is clear that the temperature is increased gradually the higher the value of voltage applied to the samples.

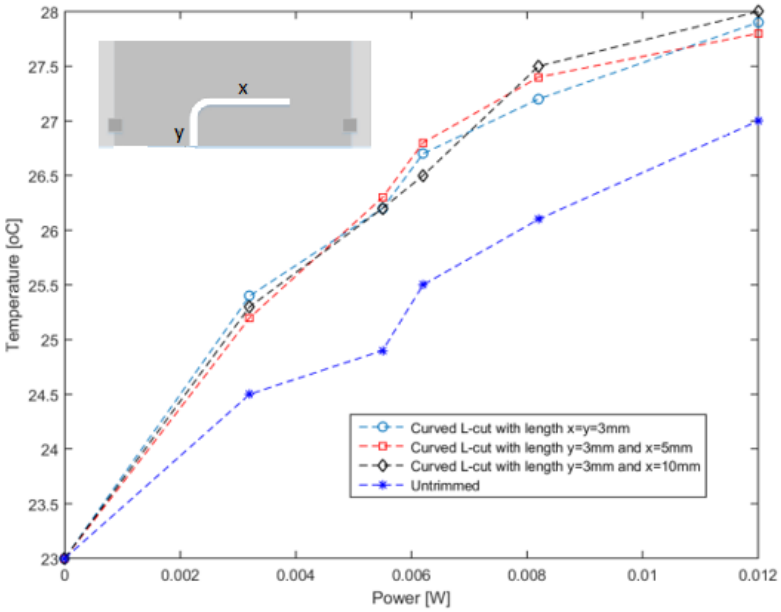

Figure 3.15: Simulation results for temperature vs. voltage for the case of the curved L-cut.

3.3.6 Scan cut

Another common trim pattern, which was modelled using ANSYS, was the scan cut. The dimensions which were investigated were 5 x 10 mm, 5 x 15 mm and 10 x 15 mm, as shown in Figure 3.16. Once again, the increase in temperature has a similar trend for this type of cut with slight variations between the samples with different dimensions. The sample with dimensions 10 x 15 mm had the highest temperature increase with a value of 29.5 °C and at the value of 28.9 °C with dimensions of 5 x 10 mm for the value of 0.012 W.

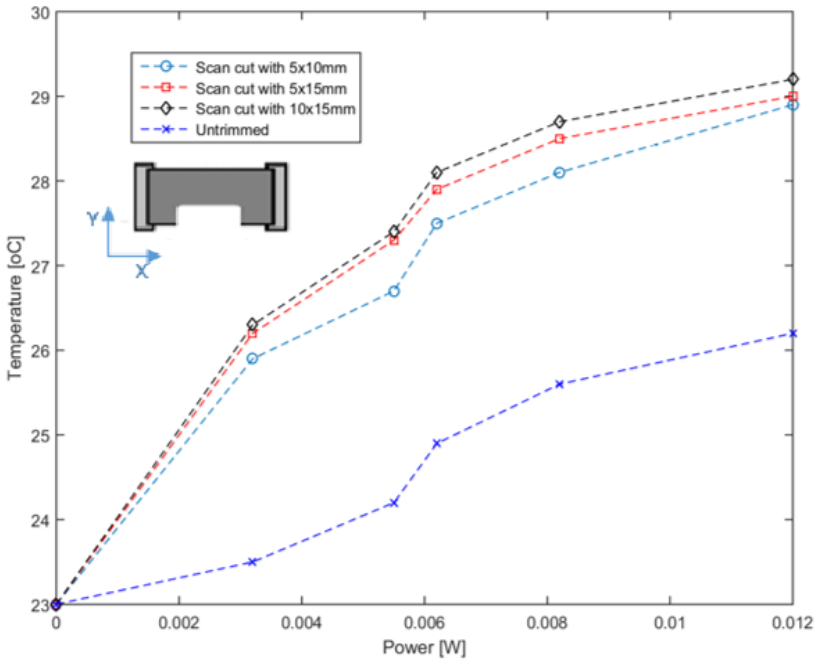

Figure 3.16: Simulation results of temperature vs. voltage for the case of the scan cut.

3.3.7 Semi-circle cut

A novel trim pattern geometry was analysed for its possible use for the production of resistors. The semi-circle cut was not presented in any previous study and it was investigated thoroughly in this research. Its design has supposedly a smaller area affected by the laser kerf since it is a constant cut and it does not contain any corners which would potentially cause damages in the film.

The change in the resistance value for the semi-circle cut with total trim length of 30 mm. The trim length in this case is larger due to the fact that it refers to the circumference of the actual cut. As seen in Figure 3.17, the initial resistance value was 6.5 kΩ and it is gradually increased up to 15 kΩ. Thus, it gives a total resistance gain of 8.5 kΩ, which is a significant gain for a resistor.

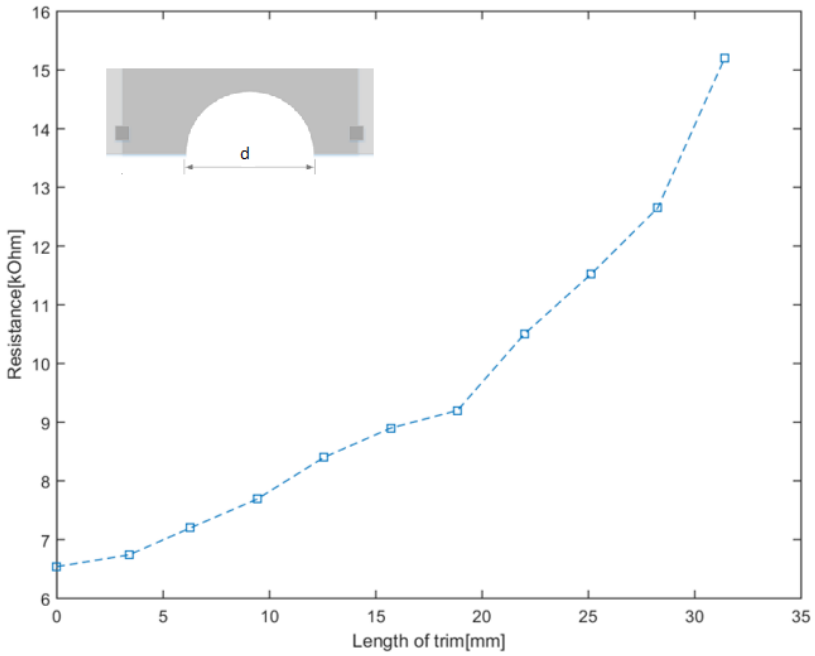

Figure 3.17: Simulation results of resistance value vs. trim length for the case of the semi-circle cut.

Various dimensions were once again modelled for the case of the temperature change of the semi-circle, as shown in Figure 3.18. The dimensions of the semi-circle pattern were for values of *r* set at 5 mm, 8 mm and 10 mm. As expected, the higher the value of *r*, the higher the trim length hence the resistance gain.

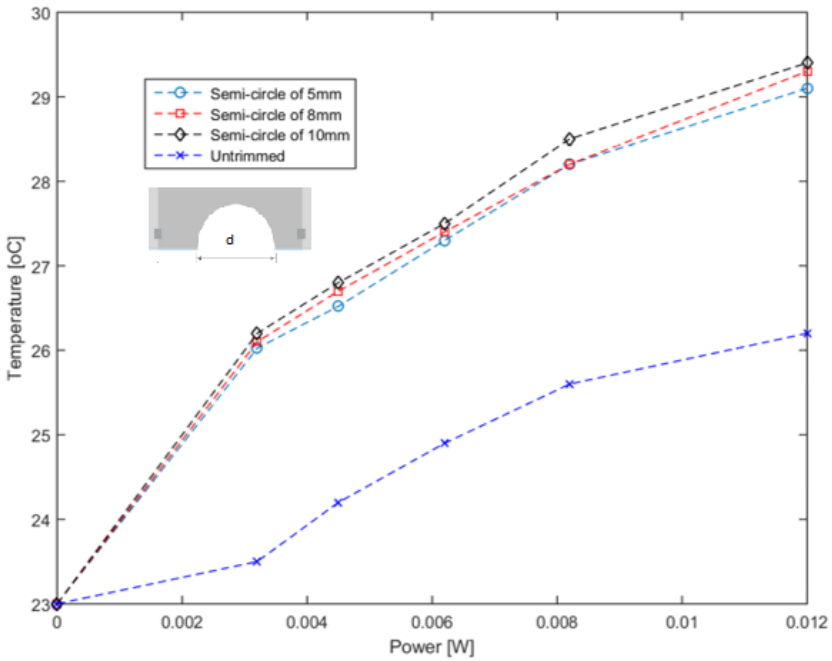

Figure 3.18: Simulation results of temperature vs. voltage for the case of the semi-circle.

3.3.8 Elliptical cut

The elliptical cut was also modelled so that values for resistance and temperature could be obtained. There are two variables that determine the dimensions of this cut and these are the distances *a* and *b*. In Table 3.2, the initial and final resistance values of this pattern with a variety of values of *a* and *b* are presented. The initial resistance value was set at 5.3 kΩ.

Table 3.2: Simulation results for the elliptical cut with dimensions *a* and *b*.

b (mm)	a (mm)	$R_{initial}$ (kΩ)	R_{final} (kΩ)	Gain (kΩ)
2.5	5	5.3	7.3	2
2.5	7.5	5.3	9.8	4.5
5	7.5	5.3	11.45	6.15
5	8	5.3	15.3	10

It is shown that the resistance gain can reach up to 10 kΩ for the values of 5 mm and 8 mm of b and a respectively. This type of cut can offer a large resistance gain which is related to its dimensions.

In Figure 3.19, the graph of the temperature change in relation to the power for three model samples with different values of *a* and *b* are presented. The initial temperature was set at 25 °C. Three different sets of a and b were modelled as shown in Figure 3.18 with *b* taking the values of 2.5 and 5 mm while the value of *a* was 5 and 7.5 mm.

The highest value of temperature is noted at V = 15 V of the graph at 29.5 °C. The temperature increase trend is similar between the different models. The temperature for the

elliptical cut with b = 2.5 mm and a = 7.5 mm reached up to 29.25 °C while for b = 2.5 mm and a = 5 mm the temperature was 29 °C.

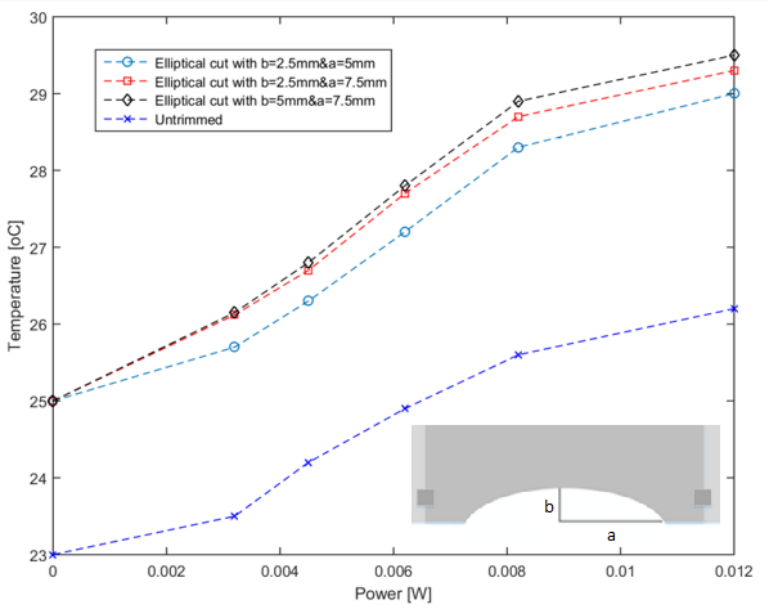

Figure 3.19: Simulation results for temperature vs. voltage for different dimensions of the elliptical cut.

3.4 Modelling of the thin film resistor

A similar approach with the conductive paper was followed for the case of the thin film resistor but with different dimensions of the resistor and width of the cut. The dimensions for the thin film resistor were 21 x 6 mm, so that it matches the dimensions of the thin films used for the experiments. However, for the case of the thin film only the following patterns were modelled for further investigation since the majority of common and novel patterns were already modelled for the case of the conductive paper.

The simulation results for the case of the plunge cut of 5 mm are shown in Figure 3.20. There is a clear increase as the cut progresses and it jumps from the initial value of 55.2 Ω to 82.5 Ω. Thus, the resistance gain was 27.3 Ω which was expected in a way since the plunge cut, based on previous studies and the results of this section, can offer a high resistance gain rate.

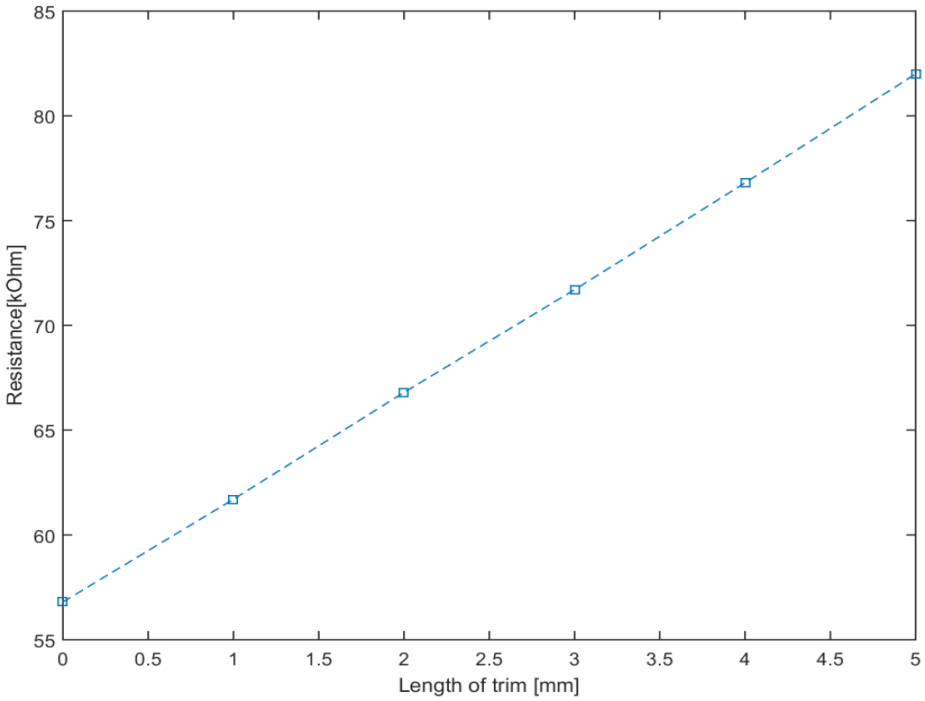

Figure 3.20: Simulation results for resistance value vs. trim length for the case of the plunge cut of 5 mm using thin film.

In Figure 3.20, the graph of temperature change vs. power applied to the thin film resistors is presented. The cuts that were investigated further after the analysis using the conductive paper, were modelled using the thermal electric approach in ANSYS. The cuts presented in the plot are the plunge, the L-cut, the angled-L, the curved-L, the semi-circle and the elliptical cut. All of these samples were trimmed until they reached the target of 70 Ω so that a comparison could be made.

The initial temperature was set at the value of 25 °C. As expected, the temperature increases, as the value of the power increases. For the elliptical cut it is shown that the temperature increases faster when 0.3 W are applied to it in relation to the other types of cuts. However, for all the samples, higher values of temperature are noted at the value of power of 5 W. The highest temperature value for the maximum power is shown in the case of the angled L-cut at 92 °C. The plunge cut and semi-circle cut seems to have a large increase in temperature up to around the value of 82 °C. The curved L-cut appears to have the lowest increase in temperature at 71 °C at the power of 5 W. As for the elliptical cut, the temperature reaches the value of 79 °C for the highest power value.

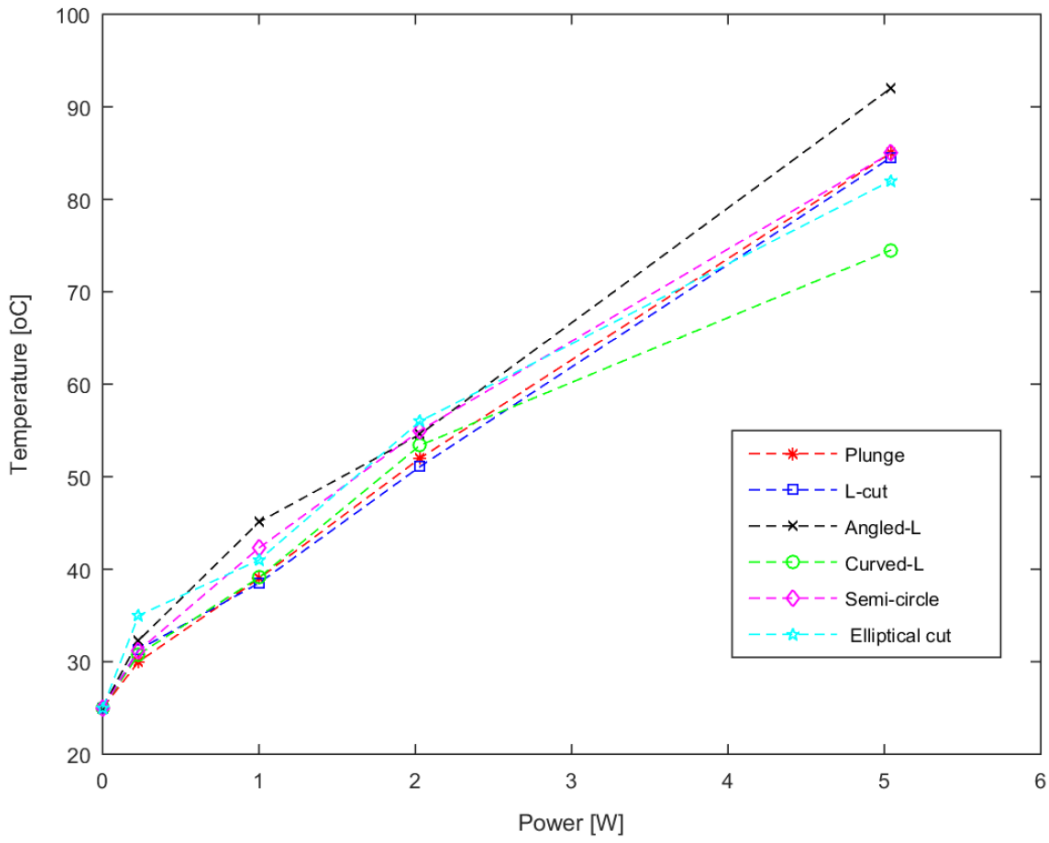

Figure 3.21: Temperature vs. power for different patterns trimmed up to the value of 70 Ω.

In the plot, the values of temperature refer to the points with the higher temperature distribution according to the simulations even though the temperature distribution seemed uniform with exception of the area above the cut in which the current flow is higher.

3.5 Summary

In this chapter, the modelling of the trim patterns was presented using MATLAB and ANSYS. The resistance value and the HAZ sensitivity were calculated using MATLAB while the simulations concerning the temperature distribution were conducted in ANSYS using the thermal electric approach. The modelling referred to the two materials used in this research which were the conductive paper and thin film resistors. The plunge, double plunge, L-cut, angled L-cut, curved L-cut, scan cut, semi-circle and elliptical cut were modelled for the case of the conductive paper with larger dimensions of the resistor. After that point, the trim patterns chosen for modelling with the thin film resistor settings were the L-cut, angled L-cut, curved L-cut, semi-circle and elliptical cut. Many results were presented with various dimensions so that certain factors could be determined first theoretically and then verified experimentally in the following chapters. The simulations provided the theoretical trend of the resistance increase and temperature change so that comparisons to be made.

4 Laser processing parameters

4.1 Introduction

The main properties of laser sources, that are relevant for the applications in material processing, are the wavelength, the intensity distribution in the beam and the total beam power. In general, the wavelength determines the magnitude of absorption by a certain material [134]. As for the intensity distribution, it refers to the ability of the beam to focus and adjust the width of the processed track, which in the case of cutting is the kerf width. In addition to this, the total beam power determines the work piece volume heated, molten or evaporated per unit time and its influence on the processing speed is quite significant [135].

In relation to the laser power, it is worth mentioning the temporal distribution of the beam is important for material processing and there are two options: the continuous wave operation and the pulsed mode. The continuous wave operation is mostly used for processing tasks with high speed while the pulsed mode can be beneficial for processes with reduced speed such as along contours with sharp bends or for considerably enhanced temperature, that allow the material to melt. For cutting certain materials, 'super-pulses' are used which have a very high peak power, but with a reduced length, leaving the average power unchanged as it is fixed by the energy balance. The beam parameter product depends on the wavelength and on the mode order. If the beam parameter product is small, a beam of high quality is obtained. The beam can then be focused to a very small spot size (10 microns) and it can also show a small divergence, that means it can widen only in a low rate with increasing distance from the source. It can also be used to process work pieces that are far away from the laser source without a loss of beam energy. It is therefore essential that the beam mode order is as low as possible which means that the intensity distribution of the beam is close to the Gaussian shape and that the wavelength is quite small.

Thus, it is worthwhile thinking that a wavelength in the mid infrared, as 10 µm is an optimum choice, since it allows the laser treatment of nearly all materials in terms of an acceptable absorption [135]. In any case, a large beam power is helpful in material processing and it can compensate even low absorption or poor ability to focus the beam. So, a mode as close as possible to the Gaussian shape and a beam power as high as possible is a good compromise for general material processing such as laser trimming.

Carbon dioxide lasers have been proven to be effective for general material processing in manufacturing engineering and they are the most commonly used lasers for industrial applications. This type of laser was invented in 1964 and it uses a mixture of carbon dioxide (CO_2), nitrogen (N_2) and helium (He) gases for the conversion of electric energy, that is

usually supplied by DC (direct current) or RF (radio-frequency) currents, to infrared radiation with a wavelength of 10.6 µm [134]. These lasers combine excellent beam mode with nearly unlimited beam power and lasers with a continuous wave power of 45 kW are very common on the market. The reason for this high-power capability of the CO_2 laser is due to the relatively large efficiency of theoretically more than 30% for the conversion of electric energy to radiation power. Furthermore, it offers the possibility of a very efficient cooling by moving the hot CO_2 gas mixture away from the electrode system, where it is heated, cooling it by heat exchangers and recirculating it to the electrode system where it cares for the conversion of electric energy to radiation [135]. CO_2 lasers can be operated in the fundamental mode or in a 'doughnut mode' that can be useful for material processing.

The radiation power output per unit volume of the laser plasma depends on the density of the CO_2 molecules. So, the more CO_2 that is available, the higher is the laser power per unit volume. In addition to this, He and N_2 should be as high as possible and therefore an experimental optimum has been found with around 70 to 80% He and the remainder covers the N_2 and CO_2 content. Energy supply to the CO_2 plasma is, with some minor exceptions usually carried out by electric power, where either DC currents, low frequency currents with 50 Hz or some 1000 Hz or RF currents up to a frequency of about 100 MHz. DC currents are widely used in CO_2 lasers, since they are simple to operate and correspondingly rather cheap [135].

4.2 Theory of the Gaussian beams for CO_2 lasers

The quantities which are required to characterise Gaussian beams are described in this section. The propagation of a Gaussian beam can be fully determined when the position of the beam waist and the beam radius at that position are known. In Figure 4.1, a schematic approach of the profile of the Gaussian beam is presented.

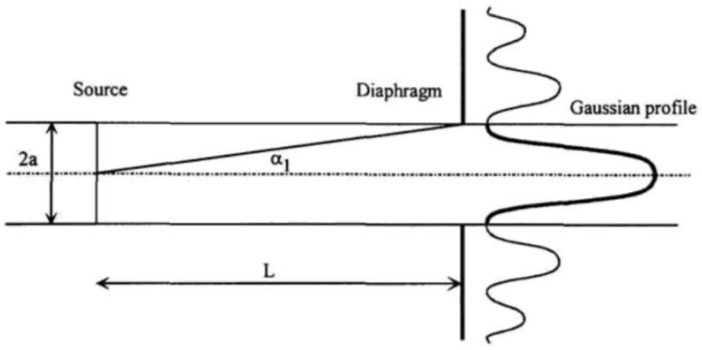

Figure 4.1: Schematic of a Gaussian beam [118].

The beam characterization is usually based upon the transversal intensity distribution I(x,y), as shown in Figure 4.2. Since the intensity distribution I(x,y) of a real laser beam is usually measured as a function of the coordinates perpendicular to the direction of propagation and cannot be given as an analytical function, numerical calculations are needed in order to get numbers for beam characterization [135]. As a first step, the direction of propagation of the beam must be found, which is defined as the straight line containing the centres of the intensity distributions at different distances, *z*, from the source of the beam.

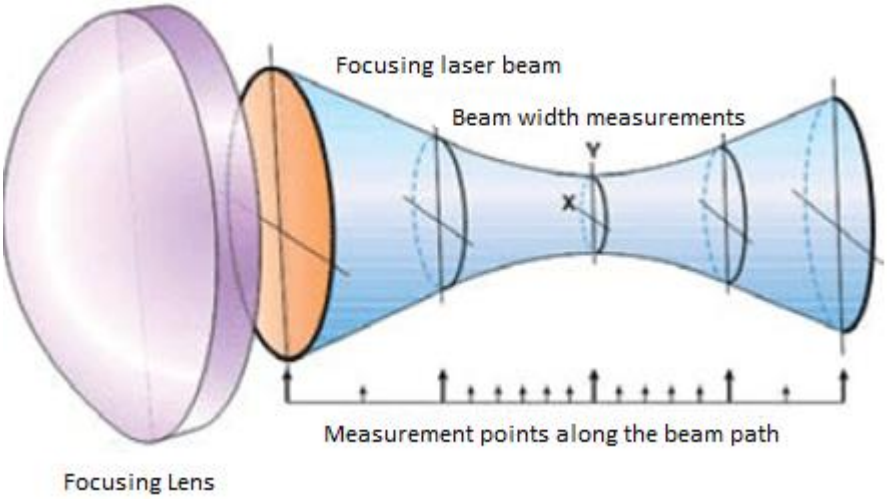

Figure 4.2: Characterisation of the laser beam [118].

This centre of the beam can also be understood as the position of the beam. Afterwards the beam diameters, d_x and d_y, can be derived. In general, real laser beams do not show exact symmetry in the transverse directions and therefore the beam diameters in x-direction, d_x, and in y-direction, d_y, are different. When the beam diameters are known at different distances from the beam source, the divergence angles, Θ_x and Θ_y, can be evaluated, which are also different from each other in the case of missing symmetry properties of the beam under consideration [135].

4.3 Position of the beam

The position of a laser beam can be determined once the centre of the transversal intensity distribution I(x,y) is found. The coordinates x_0, y_0 of this point are obtained by calculating the centre of gravity or the first moments of the intensity distribution function:

$$x_0 = \frac{\iint_A xI(x,y)dxdy}{\iint_A I(x,y)dxdy} \qquad \text{Equation 4-1}$$

$$y_0 = \frac{\iint_A yI(x,y)dxdy}{\iint_A I(x,y)dxdy} \qquad \text{Equation 4-2}$$

The integration area, *A*, must include all regions where a beam intensity greater than zero can be observed. This definition is of course trivial for symmetric distributions, where the centre of gravity and the position of the maximum intensity are identical. For real laser beams, however, it is possible that the beam position deviates from the point of maximum intensity. In this situation, it is important to use the above definition in order to get reliable results for the beam diameter and the beam divergence [118].

4.4 Beam diameter

The beam radius of a Gaussian beam has been introduced as the scaling factor which is responsible for the width of a Gaussian function. Comparing this definition of the beam radius to results from statistics where Gaussian functions are also used, the beam radius can be related to the standard deviation [135]. By generalizing this result to real laser beams, where the intensity distribution is obtained from measurements, the beam radius can be defined on the basis of the standard deviation or the second moment of the intensity distribution, respectively [135]. For arbitrary beams, where no symmetry properties can be found, again two different beam diameters for the x and y direction must be calculated.

$$d_x^2 = 16\frac{\iint_A (x-x_0)^2 I(x,y)dxdy}{\iint_A I(x,y)dxdy} \qquad \text{Equation 4-3}$$

$$d_y^2 = 16\frac{\iint_A (y-y_0)^2 I(x,y)dxdy}{\iint_A I(x,y)dxdy} \qquad \text{Equation 4-4}$$

4.5 Fine structure of the CO_2 laser spectrum due to molecular rotation

The CO_2 laser molecule shows three axes of symmetry, one that connects the centres of the three atoms and two other ones perpendicular to this axis, as shown in Figure 4.3. Therefore, the CO_2 molecule can carry out rotations around these axes.

These three kinds of rotations around the three axes of symmetry are also associated with a certain kinetic energy, whereas the two rotations around the axes perpendicular to the one that connects the centres of the atoms are degenerated, meaning they have the same energy levels. The typical difference of the energy levels is 0.01 E_v and is thus ten times smaller than the energy of the vibrations. So, the combined vibrational-rotational states of the molecule show energy levels roughly given by the vibrations, but having a fine structure due to the rotational levels, that lead to a certain spreading of the main energy levels, thus

yielding laser wavelengths between roughly 9 and 11 µm, that can be utilized by choosing a certain vibrational-rotational state. It should be mentioned that due to the influence of a rising pressure on the line width of the energy levels, a high gas pressure leads to an overlapping of the various vibrational-rotational energy levels, therefore forming a continuous energy band, that extends from 9 to 11 µm and allows a continuous tuning of the laser frequency.

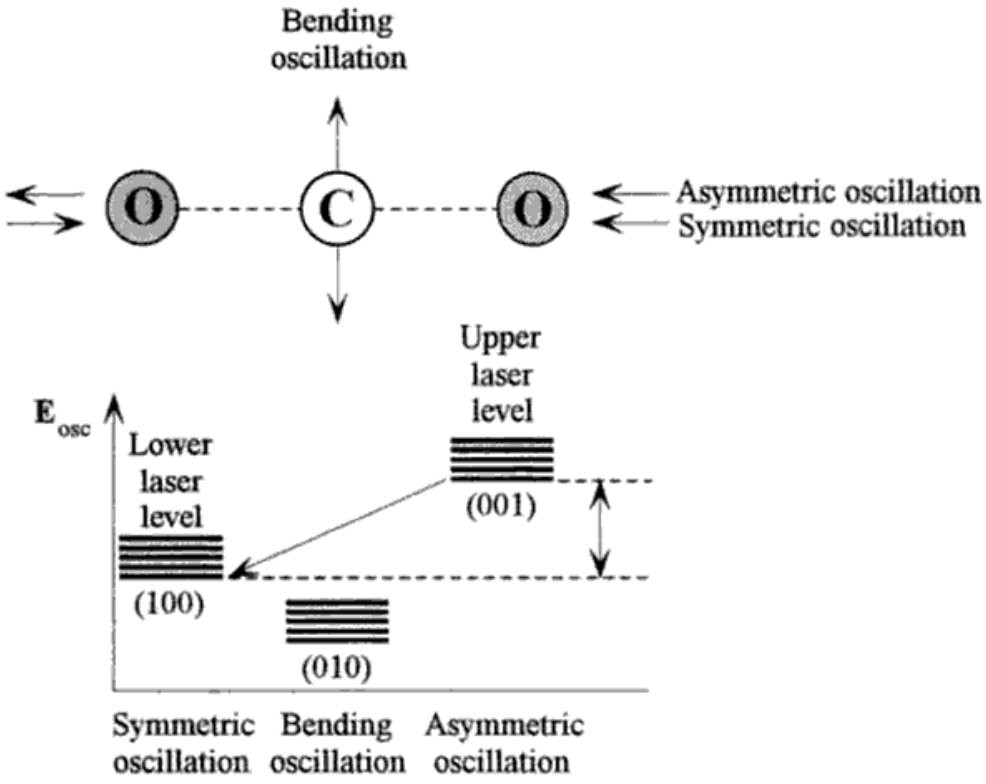

Figure 4.3: Vibrational-rotational states of the CO_2 molecule [113].

4.6 Epilog mini CO_2 laser

The Epilog mini laser cutter (see Figure 4.4) consists of a laser control panel which displays speed, power, frequency and runtime. The operating modes for this equipment are: the raster the vector and the combined mode. The vector mode which refers to cutting was used for the experiments of this study. The laser source consists of digitally controlled air-cooled CO_2 laser tubes which are fully modular and permanently aligned.

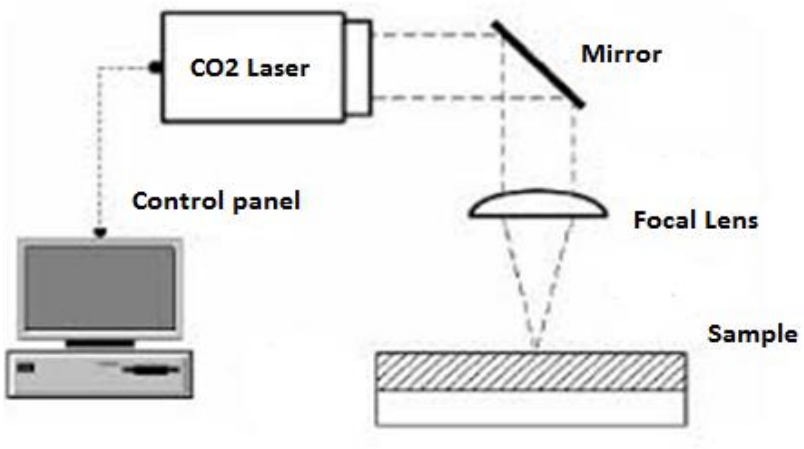

Figure 4.4: Schematic of laser cutter [113].

The CO_2 laser beam itself is invisible and operates at a wavelength of 10.6 μm. The beam is about 1.2 mm and the focus lens gives the beam an hourglass shape. The energy density is concentrated at the centre point, allowing a precise and clean material removal and the centre of the hourglass is the focal point. It is worth noting that the laser beam path is completely enclosed within the cabinet. For cutting, the laser is driven along a path and the laser remains switched on for the duration of the cut. Under this mode, the laser cuts entirely through the material, separating the part from the background.

This laser also has many standard features for engraving and cutting applications. Auto-focus with 2-inch focus lens is one of these features and it works on any solid surface including transparent materials, while focus is determined at the first point of cutting to ensure precise focus even on uneven surfaces. The laser uses a plunger that is attached to the carriage to determine correct focus position. When auto-focus is activated, the engraving table moves up until the work-piece pushes the plunger up. The table then moves down until the work-piece is in precise focal position. When a job starts, the carriage will move to the first point of cutting and the table will then move up towards the focus lens until the plunger is activated. The table will then move down until it is the correct distance from the focus lens. Another feature of the equipment is the air assist which keeps combustible gases away from the cutting surface. It directs a constant stream of compressed air across the material surface at the point of burn. Directing the compressed air both down and back towards the exhaust vent, the air assist removes the heat and combustible gases from the work surface.

4.6.1 Pre-cleaning of the laser cutter

Before using the equipment for the set of the experiments, the optics such as the mirrors and lenses of the laser were cleaned. The two optical components which required most

cleaning were the focus lens and the mirror directly above it. The lens and mirror are a single assembly and they were removed from the machine for cleaning.

Figure 4.5: Representation of cleaning the optics.

A swab made of tissue for lens cleaning, moistened with optics cleaner, was used to clean the optics. Also, rubbing alcohol was used in the case of removing fingerprints. After wetting the swab thoroughly with the solvent and then blotting it against a piece of cotton so that it was no longer soaking wet, the optic was daubed gently, rotating the swab after each daub to expose clean areas to the surface, until the optic was free of visible contamination. At that point, a fresh swab was prepared and the surface was cleaned with a zig-zag motion across it. It was crucial to allow enough time for the optics to dry before operating the laser. In addition to the focus lens and the mirror directly above it, there is also a mirror located on the left side of the head and is mounted to the X beam. This mirror is very well protected and there was no need for regular cleaning. However, from time to time it was accessed with a swab in order to be cleaned, as well.

Another part of the laser that needed proper care was the optical strip and encoder. These are located under the protective cover of the X-beam assembly. The optical encoder helps the precise positioning for the x-axis carriage. If the encoder or encoder strip gets dirty, the X-axis can lose its position. Under normal circumstances, there is not a serious issue, but since precise cuts were needed for this study, it was regularly checked if there was any dust built up on the encoder strip which would prevent the optical encoder from working properly. In the case that the x-axis carriage was losing its position throughout the duration of the experiments, the X-beam protective cover was removed and the optical strip was wiped off using a soft cotton cloth. Furthermore, the bearing system in the laser was cleaned once a week using a soft cloth or cotton swab with some alcohol to clean each of the bearing tracks which the mirror and lens run along. Also, the exhaust blower needed periodically cleaning in order to remove built-up debris.

4.6.2 Laser cutting speed

Speed settings determine the travel speed of the carriage as the laser cuts. Speed is adjustable in the print driver in 1% increments from 1 to 100%. In general, according to the

manufacturer, the slower the speed, the deeper the cut and speed settings are heavily dependent on the hardness and the thickness of the materials being cut. Since the actual values of the speed were not available in order to make proper calculations and estimations, several experiments took place in order to determine these values. Several cuts with different lengths were performed in order to measure the time needed for them to be processed. The laser system consists of a timer that gives the time taken for the cut to be completed and an additional timer was also used to confirm this value. Some of the results of these tests to determine the speed are shown in Figure 4.6 as well as a representation of the different percentages given from the equipment with their actual values. It is worth mentioning that the laser speed was calculated for 10 mm/s for the speed percentage of 15%. In Figure 4.7, the values of the laser speed are presented in relation to the time needed for the cut to be performed. Moreover, the values on percentages were measured in order to clarify their actual value and the results are shown in Table 4.1.

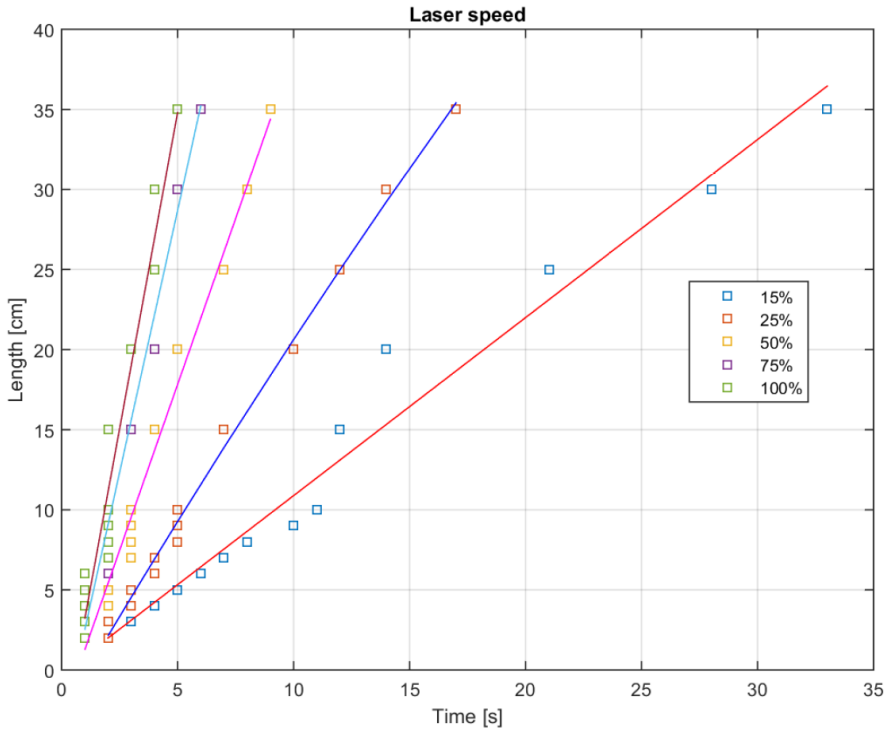

Figure 4.6: Laser speed measured based on trim length (cm) and time (s) and correlation with percentages shown on the control panel display.

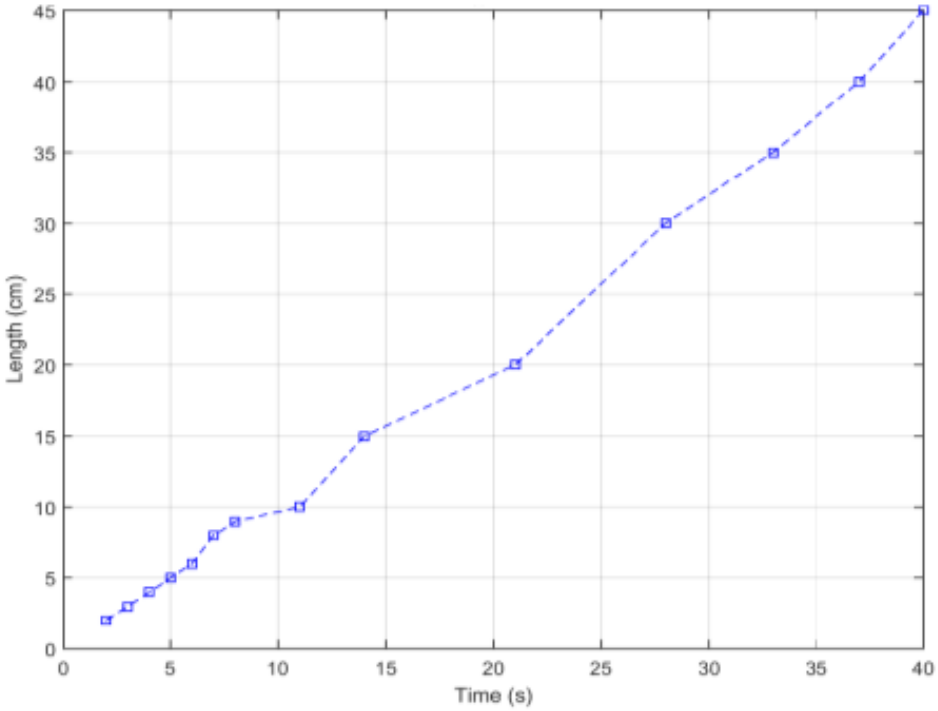

Figure 4.7: Laser speed on the measurements of trim time needed in seconds for cuts with length in cm to be performed.

Table 4.1: Laser speed expressed in mm/s.

Laser speed in %	Laser speed in mm/s
15	1
25	1.66
50	3.34
75	5.01
100	6.67

4.6.3 Laser power

In general, power is a simple way to gain an understanding of the laser and it can give a complete idea of the laser's capabilities. This is the amount of laser power that is applied to the material surface and in this case concerns a 45 W laser. At a given speed, higher power will produce deeper cutting. Adjustable in 1% increments, the power can be controlled from the display control panel. Power can also equate speed in this laser system, according to the manufacturer. Thus, tests were performed using a laser power meter from Laser Instrumentation-Model 5104, which uses a thermal sensor (thermopile based) and it can measure up to 300 W. These measurements were performed in order to determine the actual values of the power that concerned this percentage shown on the display control

panel, see Figure 4.8. The maximum power which is represented in the 100% on the display control panel corresponds to measured power of 45 W.

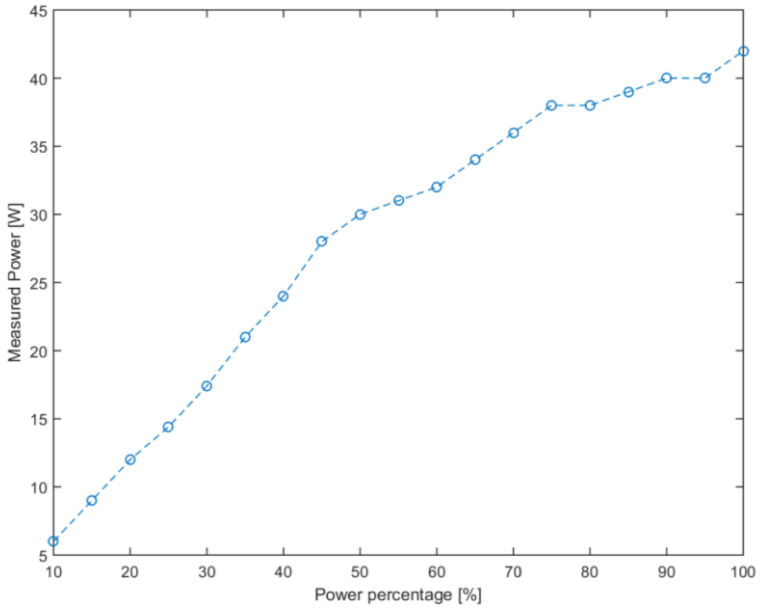

Figure 4.8: Actual values of the laser power in relation to the power percentages of the control panel display of the laser cutter using laser power meter.

4.6.4 Frequency

Frequency is the number of laser pulses that the laser fires per second as shown in Figure 4.9 for a fixed scan speed. A lower frequency number will have the effect of less heat applied to the material being cut. Higher frequencies are useful in this case, since a large amount of heat is desirable to melt and they can offer cuts with higher depth. The laser beam diameter and the dot size are related and the value is 1.2 mm.

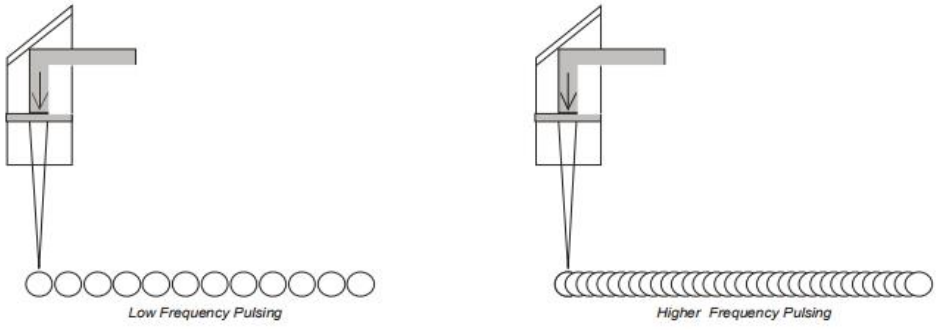

Figure 4.9: Low and high frequency pulsing.

The frequency range is 1 to 5000 Hz and it is worth noting that setting the frequency at a low value (50 to 100 Hz) will produce a perforation. Midrange values are used to reduce over burn when cutting, and high values are often used when more heat is desired to melt

the sides when cutting. In this laser cutter, resolution which is related to frequency, is expressed in dots per inch (DPI) and is determined by the number of dots that are engraved for every inch of movement. The higher the resolution setting, the finer the detail that can be achieved. The following Figure 4.10 shows the concept of lines and dots-per-inch. The arrows show the change in direction of the carriage between the line and the difference in dot density between 300 DPI and 600 DPI.

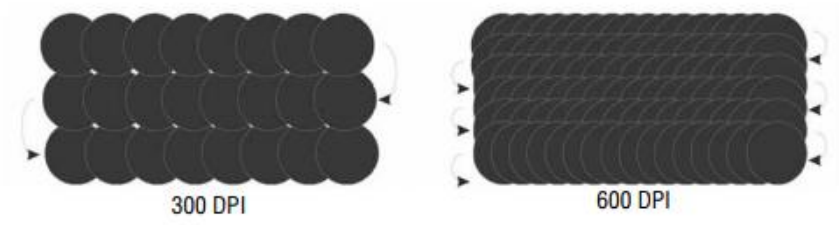

Figure 4.10: Examples of resolution in DPI.

There is a range of resolution settings starting from 75 DPI and reaching until 1200 DPI. It is worth commenting that all these different settings were tested in order to make the choice for this research. Some of these tests are presented in Figure 4.11, measuring the effect of the different resolution settings on the power measurements and as can be seen the DPI does not seem to have an effect on the laser power.

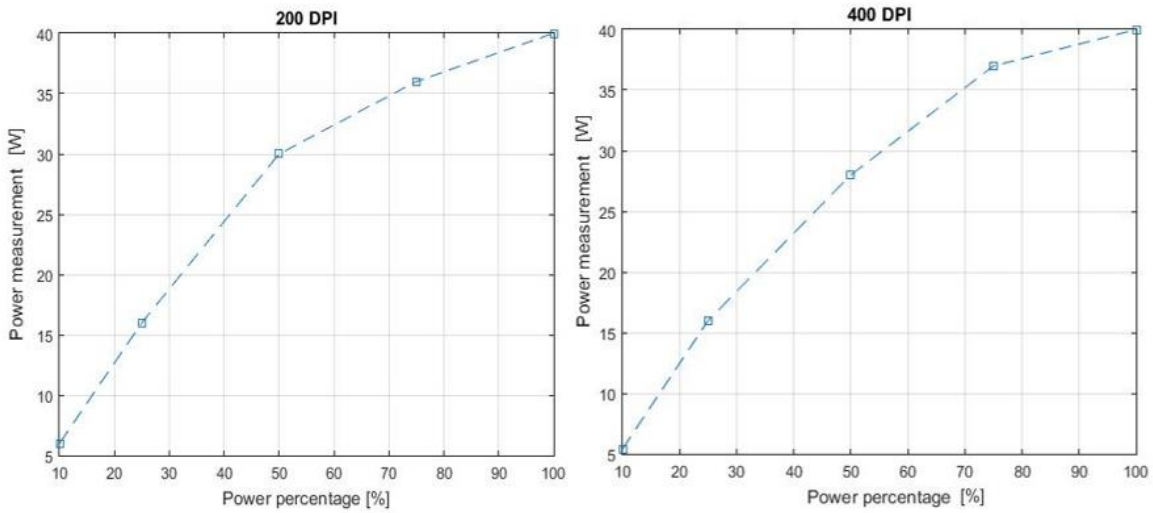

Figure 4.11: Measurements of power with resolution range settings of 200 and 400 DPI in order to check their effect on the laser power.

In Figure 4.12, the depth of the cut in relation to different values of frequency is shown in order to have a clearer image and representation of the frequency so that it can be clarified which value would be used for the experiments in this study. The measurements were obtained using Alicona. The power applied was 16 W and the speed was set at 1 mm/s, since these were the values chosen for most of the tests in order to co-relate. As shown the

higher frequency which is 5 kHz gives the deepest cut while the depth of the cut is significantly less for the lower values of frequency. Thus, the higher value of frequency offers cleaner cuts due to the higher frequency pulsing and better edge definition.

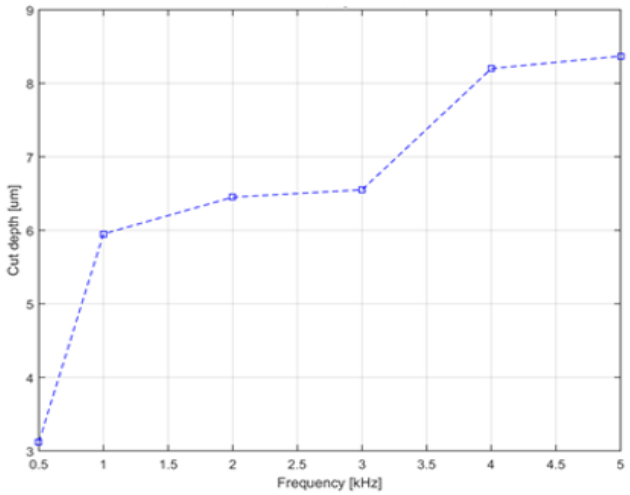

Figure 4.12: Depth of the laser cut in relation to the frequency for laser power set at 16 W and 15% speed based on Alicona measurements.

4.7 Laser settings for trimming of thin films

After all the previously mentioned tests were performed and the equipment was calibrated and adjusted to the needs of this research, constant settings were established and used for all the experiments as shown in Table 4.2.

Table 4.2: Laser processing parameters used for experiments.

Laser settings	
Power (W)	16
Speed (mm/s)	1
Frequency (kHz)	5

The frequency was set at 5 kHz for all the experiments and the speed value of 1 mm/s was proven to be the optimum option for the trimming. The higher value of power for this laser cutter is 45 W which makes it quite high for the materials under study and the power range used was between 16 and 20 W. A detailed representation of the power set points in relation to the power output measured is shown in Figure 4.13 for reference.

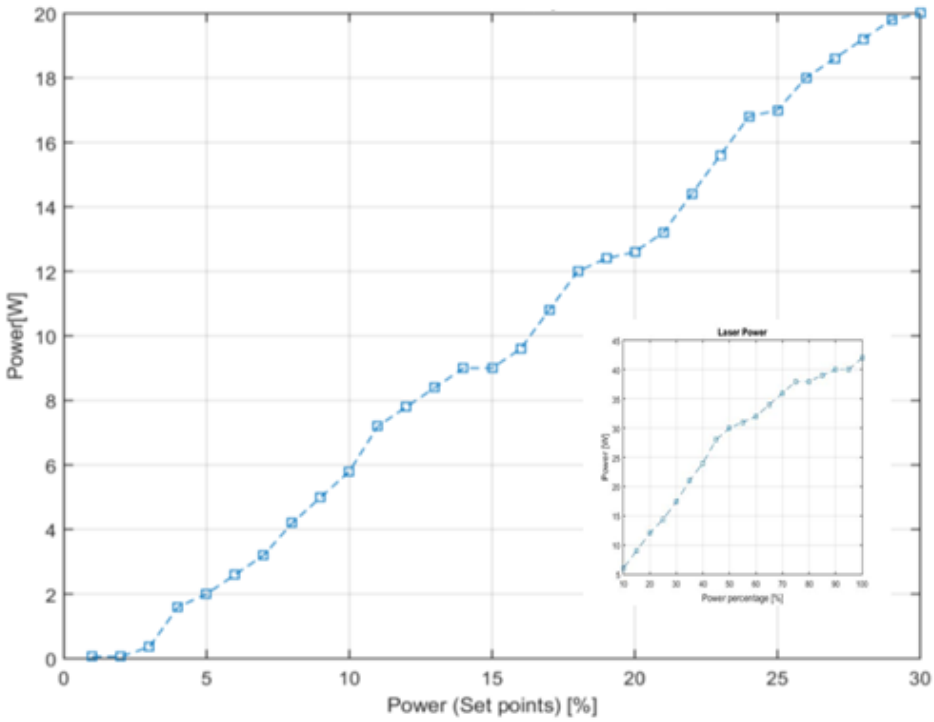

Figure 4.13: Laser power measurements in Watts in correlation with the laser power percentage from the control cabinet of the laser cutter for frequency of 5 kHz and speed of 1 mm/s.

Due to the fact that this research needs really fine detail on the dimensions and geometry of the patterns, the resolution set for all the experiments and tests was 600 DPI. The choices were also based on the visual quality and the depth of the cut. Samples of thin films were trimmed with all these different settings and then using a 3D micro coordinate machine, Alicona Infinite Focus, the depth was measured by the relevant software of the microscope. An example of the depth profile is shown in Figure 4.14. The depth profile provided by the measurement software gives a value of the depth cut and it was proven beneficial in order to clarify the settings of the laser used for this research.

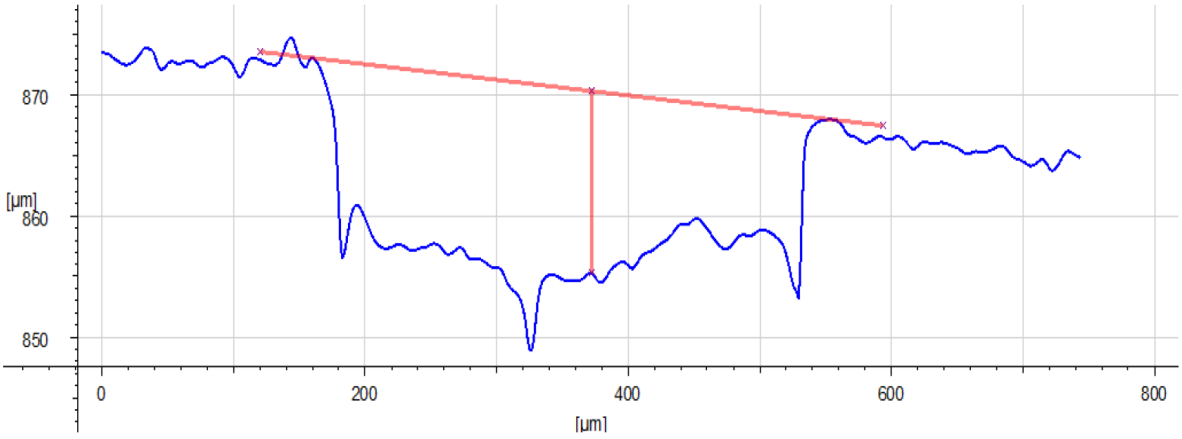

Figure 4.14: Depth profile given by the Alicona Infinite Focus software referring to the measurement of cut depth with aspect ratio 1:7.3.

Also, it was possible to decide how clear the cut was and the differences with various settings from the images obtained by the microscope for cuts under different speed settings (see Figure 4.15). The cut which was performed with a laser speed of 1 mm/s is the cleanest and the film was cut through and it is shown that the higher the speed the worst the cutting result such as in case of 6.67 mm/s.

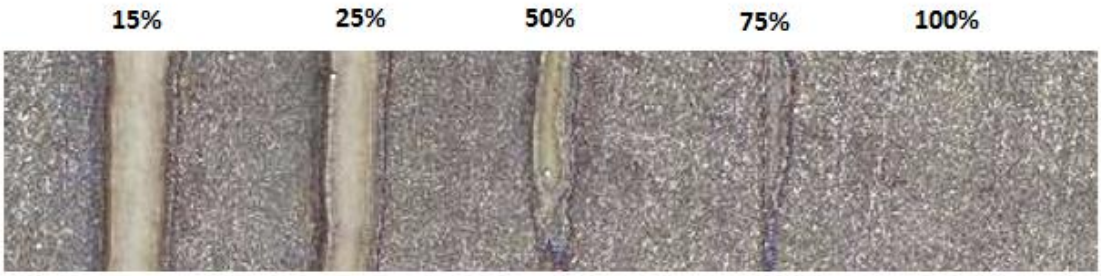

Figure 4.15: Image obtained using Alicona for cuts with speeds 15%, 25%, 50%,75%,100%.

In Figure 4.16, an SEM image is shown with a higher resolution for the cut with speed 15%. The working distance as shown on the image was set at 20 mm and the magnification was 225x. The laser spots from the laser pulse are clearly shown in this image so that the pattern can be created.

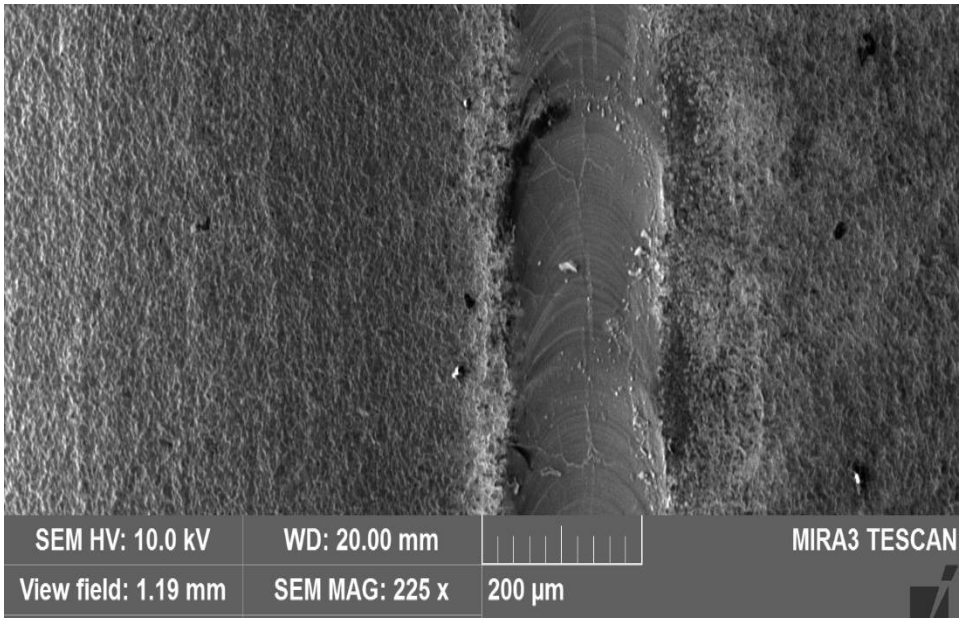

Figure 4.16: SEM image of the cut trimmed with laser speed of 1 mm/s.

4.8 Summary

In this chapter, the theory behind the laser beam and the beam diameter were presented. In addition to this, this research contains experiments using the Epilog CO_2 laser cutter and all the steps of the cleaning process in order to secure reliable cuts were mentioned. Several

tests and measurements took place and settings such as the laser power, speed and frequency took place and the settings for trimming thin films were determined. The laser power was set at 16 W, the laser speed was 1 mm/s and the frequency used was 5 kHz.

5 Trimming of conductive paper

5.1 Introduction

In this chapter, existing trim patterns that were presented in Chapter 2 and novel geometries are verified experimentally using conductive paper. The novel geometries were the curved L-cut, angled L-cut, semi-circle and elliptical cut.

In general, paper, cardboard and other wood-based products are used in communication, packaging and numerous other aspects of modern life and conductive paper is of particular interest owing to its efficiency in electromagnetic interference shielding, potential use in electronic circuits, active matrix displays and static electrical dissipation [4, 5].

Conductive papers are usually prepared by filtration of conductive particles and cellulose fibrous aqueous slurries in a Buchner funnel fitted with a nylon cloth with a filtering threshold of 8-12 μm and 33 μm. Cloths with different filtering thresholds are used in order to optimise the process, reducing the filtering time and to obtain homogenous samples. After the filtration step, wet samples are sandwiched between absorbing paper and pressed and then dried under vacuum [4].

In this project, conductive paper was chosen for the experiments because it was easy to handle, especially for the early stages, in order to examine different geometries. It also offers wide flexibility with an extremely good conductivity; not to mention the fact that its cost is low [4]. In addition to this, it can be easily used for disposable and recyclable device production.

5.2 Characterization of the conductive paper

Conductive paper (Model: PK-9025) from Pasco is designed for plotting equipotential and electric fields and has a resistivity of approximately 5 kΩ/☐ (see Figure 5.1). Electrical contacts to the paper are usually made either with clean, smooth metallic probes, or with the use of a soft graphite pencil. This paper was previously used for experiments with contacts made from a conductive ink pen (silver ink) but it was replaced by the use of conductive carbon ink due to its better stability and ease of application.

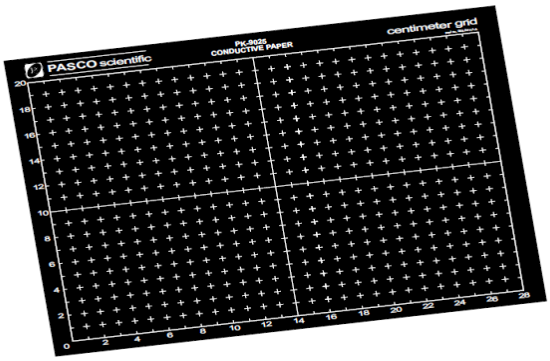

Figure 5.1: Sample of the conductive paper used for the experiments at its original dimensions (A4 paper).

The thickness of the paper was measured using a mechanical gauge and its value is 1.4 x 10^{-5}mm. The surface morphology and topography was imaged using a SEM (Scanning Electron Microscope- Model: Tescan Mira 3) and the chemical composition was analysed using EDS (Energy Dispersive Spectroscopy- Model: Aztec Oxford Instruments).

5.2.1 SEM-EDS Analysis

A sample of the conductive paper used for the experiments described in this section was scanned using the SEM and the image is shown in Figure 5.2. The outcome of the SEM analysis was further analysed using EDS so that the chemical composition could be identified. For the EDS analysis, the magnification used was 450x, the voltage 20 kV and the working distance 15 mm.

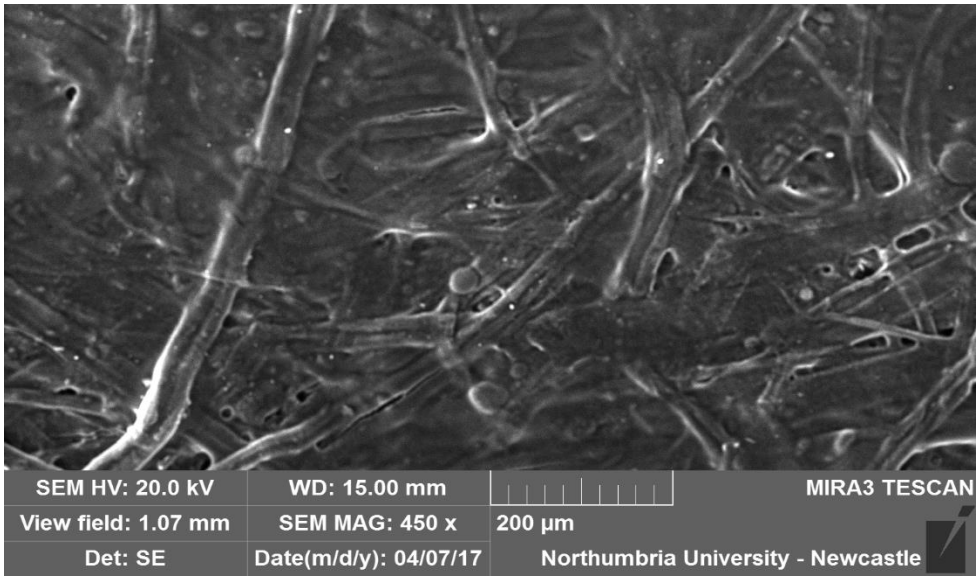

Figure 5.2: SEM image of conductive paper (PASCO).

After that, the EDS software, Aztec Energy from Oxford Instruments, was used to identify the elements of the conductive paper so that this information can be used for the numerical simulations.

The spectrum of the elements detected using the software is presented in Figure 5.3. The peaks in the spectrum are labelled during acquisition of the analysis and the elements that were detected are represented. Carbon was the highest peak which proves that it is the main material of the layer of the conductive paper.

Figure 5.3: Spectrum of the materials detected in the tested sample of conductive paper (Graph counts per second per electron-volt (cps/eV) vs KeV.

In Table 5.1, the measured intensities of the conductive sample analysed are presented. It is shown that the surface of the conductive paper is covered in carbon, as it was expected from the information provided from the manufacturer. However, other elements were also identified from the EDS analysis in smaller percentages such as Sulphur, Calcium, Indium and Silicon. It is reasonable to suppose that this is due to potential impurities of the production of the material.

Table 5.1: Measured intensities of the specimen.

Element	**Weight (%)**
C	98.84
S	0.42
Ca	0.42
In	0.22
Si	0.10
Total	100

5.3 Experimental procedure

The Epilog laser cutter (Model 8000) will be used for the trials and further details about the equipment are presented in Chapter 4. Existing trim patterns such as the plunge cut, the L-

cut, the double plunge cut and the scan cut were investigated. To emulate the resistors, the previously described conductive paper was trimmed to the required geometry using the laser. The power used for the trimming was 12 W, with a speed of 1 mm/s and frequency of 5 kHz. For a constant sheet resistance (Ohms per square), the resistance of a planar resistor does not change with size like length or width as long as the ratio of length to width (aspect ratio) is constant.

5.3.1 Experimental setup

Prior to the trimming of the resistors to the above mentioned patterns, each page of the paper was cut to the resistor desired shape. At first, the chosen dimensions were 100 x 140 mm as shown in Figure 5.4. After the shape of the resistor is set, electrical contact to the paper is made with the use of strips of electric paint (Bare conductive) placed on the ends of the paper (approximately 10 mm wide).

Figure 5.4: Dimensions of the resistor made from conductive paper.

The trim patterns were created using the laser to cut 100 mm^2 at a time and measuring the resistance value each time using the four-wire measurement. However, it was noticed that the resistance of the conductive paper is not uniform and it varies from page to page due to variations in thickness in the resistive material that is used to coat the sheets. Thus, a normalization factor needs to be established in order to achieve the uniformity in the results from the measurements. The normalization process scaled all measurements from each sheet to the average value. To normalize the various sheets based on the average, 10 and 15 initial measurements from each sheet were made prior to trimming, the measurements were averaged, so that a scaling factor could be estimated. Every measurement taken from

the specific sheet thereafter (during trimming) was multiplied by this scaling factor before comparison with data from other sheets. The normalization process was performed for every resistor used in this experimental study. This normalization procedure accounts for variations in the sheet resistance from sheet-to sheet only (variations in series resistance in the measurement path are not taken into consideration, for instance clamp pressure). Thus, the sheet resistance is set as constant. Series resistance variations are reflected in the standard deviation in the measured resistance after normalization.

In addition to this, because of these variations in the resistance value of the conductive paper, it was necessary to take the measurements before applying the carbon ink contacts and apply the normalization factor. After that, another set of measurements were taken which included the resistance value when the carbon ink contacts were added.

Both carbon ink and silver ink were tested as contacts for two different samples presented as sample 1 and 2 and their comparison is shown in Figure 5.5. The deviation of resistance for the different types of ink was calculated by the measurements on the day that the contacts were applied and then the measurements were repeated after 24 hours.

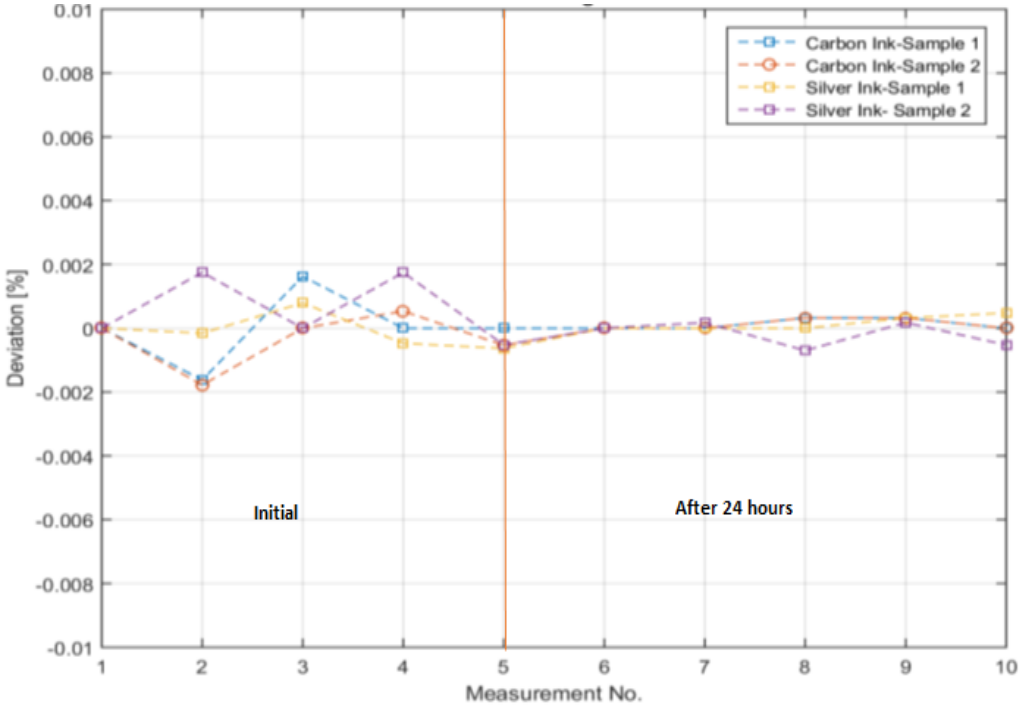

Figure 5.5: Difference in the resistance change and comparison between carbon and silver ink contacts.

This procedure helped to clarify which type of ink will be used due to its stability after 24 hours of the application on the conductive sheet of paper. Once again, ten measurements were taken in total and the first five measurements concerned the initial change in the resistance value (on the day of the application of the ink) and the following five represent the change after 24 hours. Both inks had similar behaviour at the initial stage and after 24

hours. However, it is shown that there are less fluctuations in the deviation of the resistance after 24 hours and they can even be less than 0.001% for the carbon ink and around 0.002% for the silver ink. This change after 24 hours is probably due to the fact that the ink is dry and absorbed properly. Thus, the use of the carbon ink was chosen for the contacts because even though the differences in resistance change are insignificant between these two types of ink, the application of the carbon ink is easier and less time is needed compared to the silver ink.

5.4 Results and Discussion

The change in the resistance value for the trim length with range of 0-14 mm from simulations in comparison with the experiments for different patterns such as the plunge, double plunge, L-cut, scan cut, curved L-cut as well as the semi-circle is presented in this section.

In Figure 5.6, the simulation and experimental results for the case of the plunge cut is presented. The change in the resistance value is faster in the case of the plunge cut and as a consequence less trimming time is needed to perform this cut in comparison with other more complicated ones. The normalised resistance value before trimming is 5.5 kΩ and the highest value for the resistance is 15.2 kΩ and 15.5 kΩ for simulations and experiments accordingly for a trim length of 14 mm.

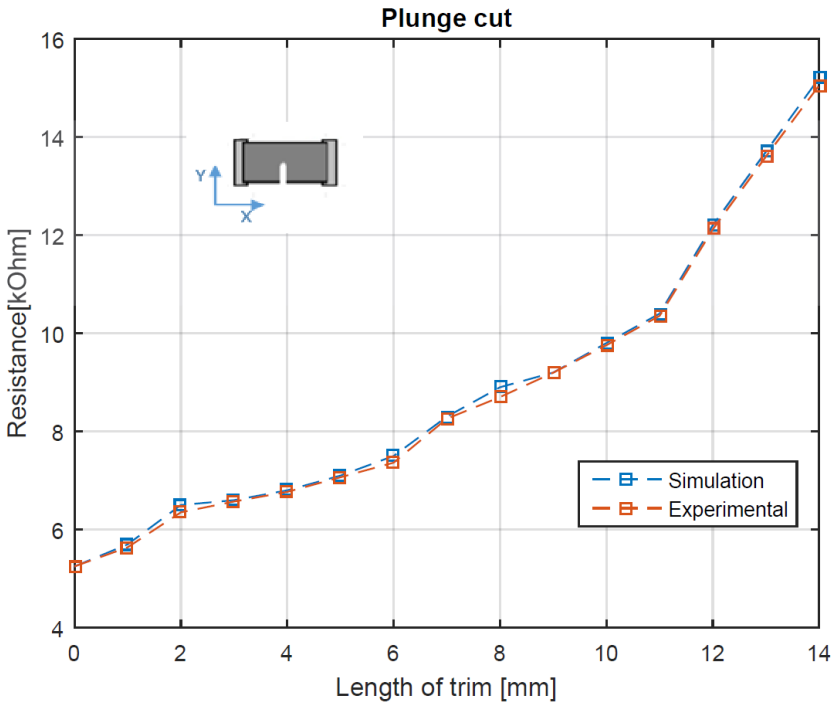

Figure 5.6: Simulation and experimental results for the change in the resistance value for the plunge cut.

Up to the trim length of 5 mm, the results from both simulations and experiments seem to be close to identical but after that point, at the range of 5-14 mm, small fluctuations are depicted. It is worth commenting that the simulation results concern ideal conditions and due to the fact that the difference with the experiments is so small, there is confidence that the results are verified correctly.

In Figure 5.7, the results for the case of the double plunge cut are presented for both simulations and experiments. For this type of cut, it is shown that the resistance value increases fast for the first plunge and it reaches 12 kΩ and then for the second cut (shadow) the increase is slower when it reaches the point of 15.2 kΩ for the trim length of 14 mm. This cut seems to be a good option as for the stable change in the resistance value that can offer but additional trimming time is needed for the shadow cut. Thus, it is worthwhile thinking that the increase in trimming time also increases the production costs.

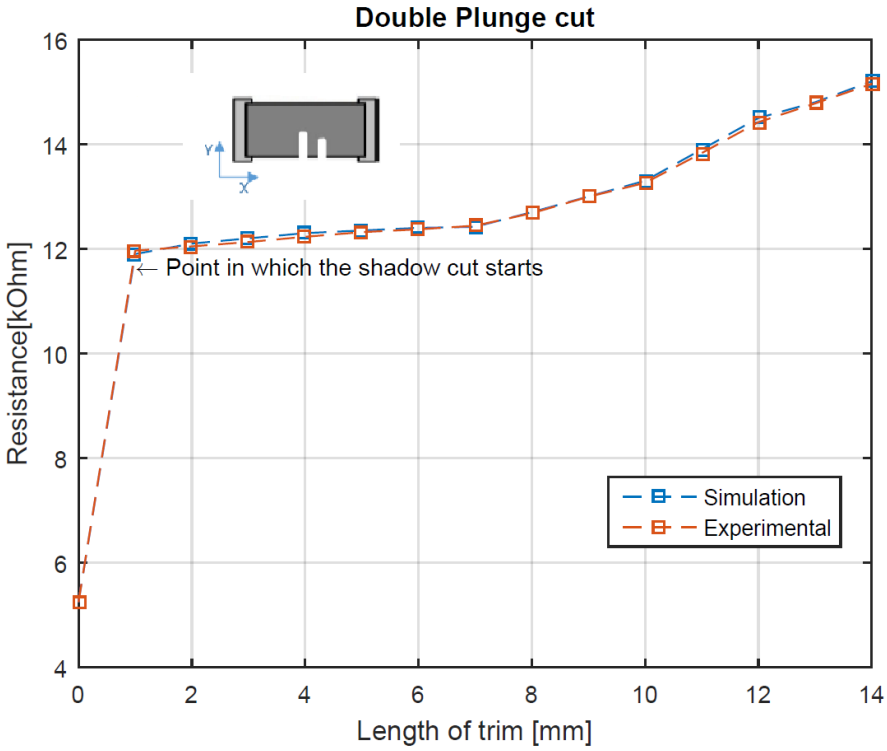

Figure 5.7: Simulation and experimental results for the change in the resistance value for the double plunge cut.

As for the L-cut, shown in Figure 5.8, the resistors were trimmed so that the trim changed direction after 4 mm. The normalised untrimmed value is 6 kΩ and the highest trimmed value for this pattern was 11.5 kΩ for a trim length of 14 mm. It is worth noting that once again the resistance value increases fast until the point in which the cut changes direction after 4 mm. Thus, it is depicted that the simulation and experimental results are close to identical up to the point where the kerf changes direction from y to x. However, a slight fluctuation can be seen after the trim length of 4 mm between the simulation and

experimental results. The resistance value is increased faster in the case of the simulation in relation to the experimental value, even though the final resistance value is close in both cases.

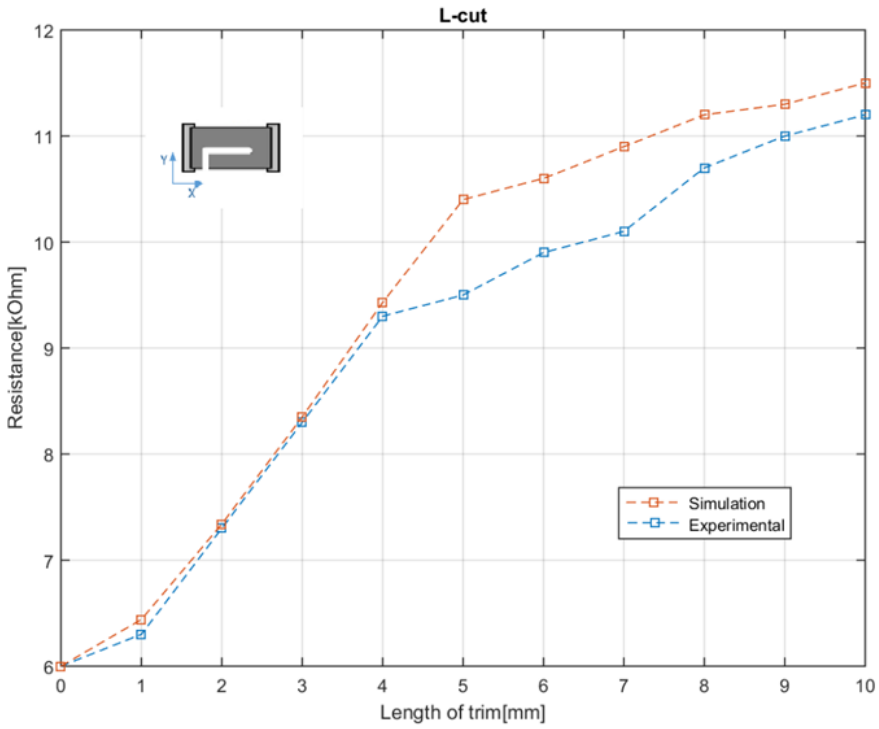

Figure 5.8: Simulation and experimental results for the change in the resistance value for the L-cut.

In Figure 5.9, the curved L-cut is introduced and it can be thought of as an optimised pattern due to the fact that the record from previous research was limited. The resistors were trimmed so that the trim changed direction after 10 mm. In the plot, the change of direction of the cut is shown when the slope of the line changes. As for the highest trimmed value for this pattern was 12.2 kΩ for trim length of 14 mm. It is worth noting that the resistance value increases fast until the point in which the cut changes direction after 10 mm. As a result, this type of cut can be considered to be the most accurate pattern in comparison with the other ones because it combines the reliable and stable characteristics of the L-cut which is the most popular laser trim pattern for thin film resistors but with smoother edges to reduce current crowding.

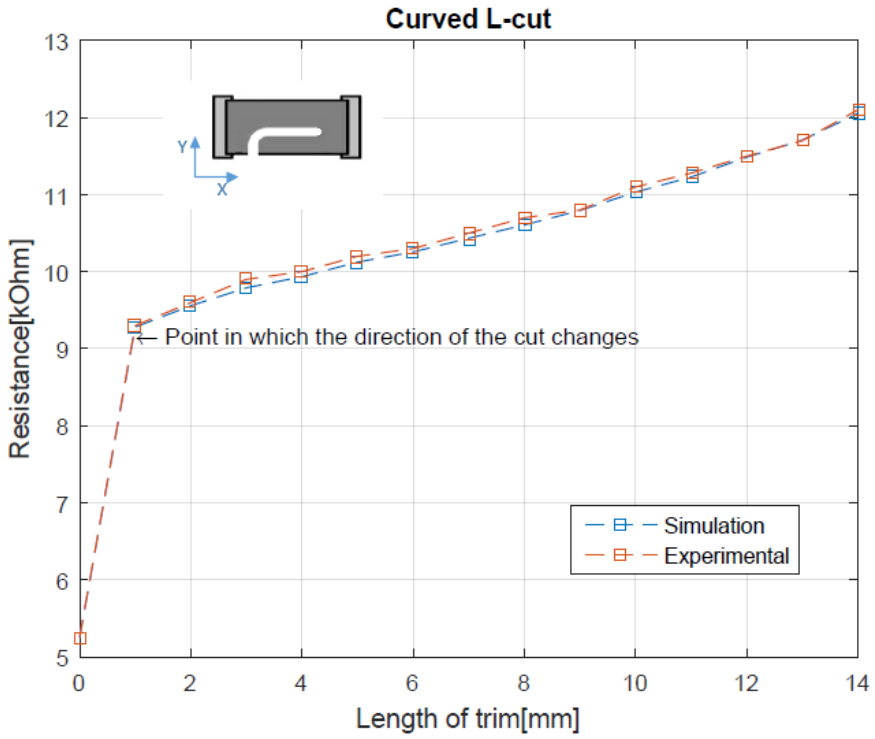

Figure 5.9: Simulation and experimental results for the change in the resistance value for the curved L-cut.

As for the scan cut, shown in Figure 5.10, the resistors were trimmed so that the trim changed direction after 4 mm. The normalised untrimmed value is 6.5 kΩ and the highest trimmed value for this pattern was 8.5 kΩ for trim length of 14 mm. Once again, the resistance value increases fast until the point in which the cut changes direction after 4 mm. However, overall, the rate of change looks fairly linear.

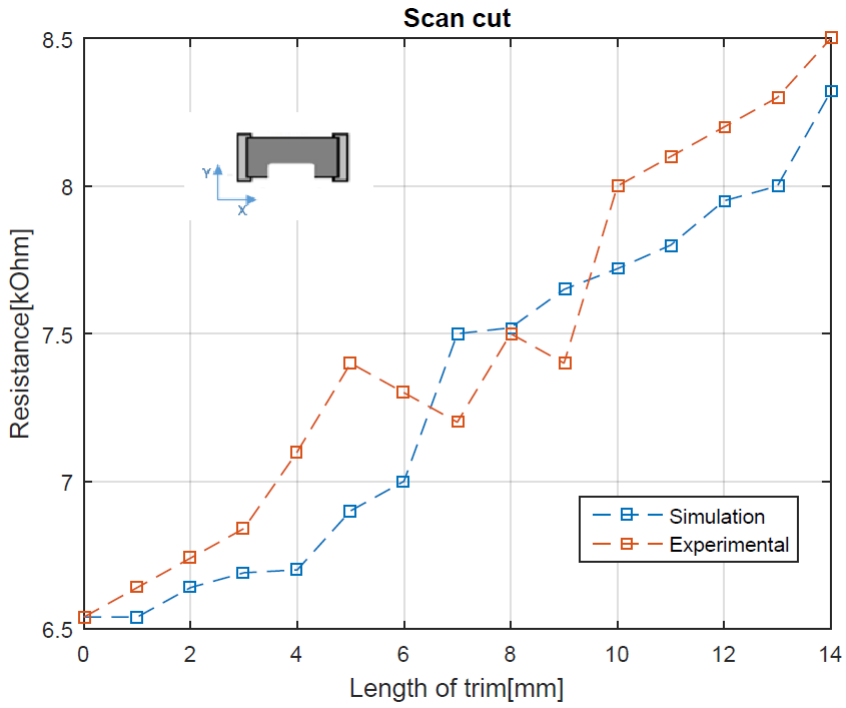

Figure 5.10: Simulation and experimental results for the change in the resistance value for the scan cut.

For the case of the scan cut, fluctuations are shown in the line that represents the experimental results, especially for the trim length range of 5 until 8 mm and the increase in the resistance value is clearly depicted as the trim length increases. However, this increase is relatively low in comparison with the other patterns and that makes the scan cut less effective.

In Figure 5.11, a novel pattern is presented with the shape of semi-circle and the change of the resistance value is shown. The trim length concerns the diameter (d) of the semi-circle for different samples. The normalised resistance value is 6.5 kΩ and the highest value is for the diameter of 32 mm at 15.2 kΩ. Once again, the difference in the resistance value between the experimental and simulation results are around 0.52 kΩ. It is worth commenting that the semi-circle seems to be a pattern that needs further investigation and trials on thin films will follow so that this pattern can be evaluated thoroughly.

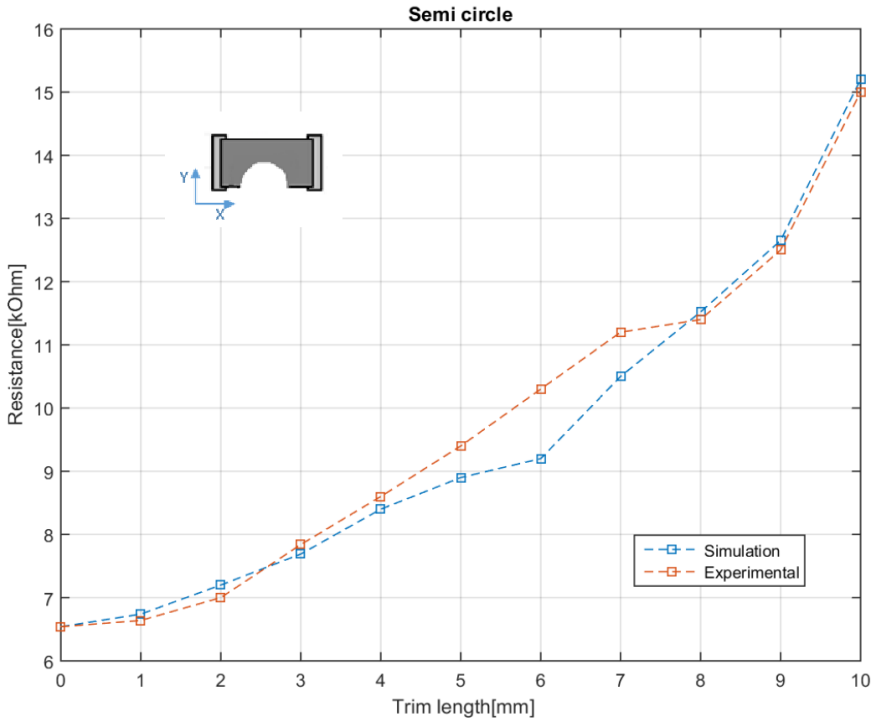

Figure 5.11: Simulation and experimental results for the change in the resistance value for the semi-circle cut.

In addition to this, the samples with different types of cut were tested using a thermal camera so that the change in temperature when voltage was applied could be measured. In Figure 5.12, the measurement using thermal camera (Model: FLIR B620) for the resistor with the plunge cut is presented and the maximum temperature is shown to reach the value of 32.4 °C while the minimum is measured at 23.8 °C. As expected from the theory, the highest temperature is distributed in the centre of the resistor and the minimum on the outer parts of the resistor. In addition to this, the cross in the image of the plunge cut is placed right at the top of the cut so that we are able to have a value for the temperature at the point in which the current is expected to flow when a load is applied to the resistor. As for the case of the plunge cut, the highest temperature is 30.4 °C and it appears at the upper part of the plunge.

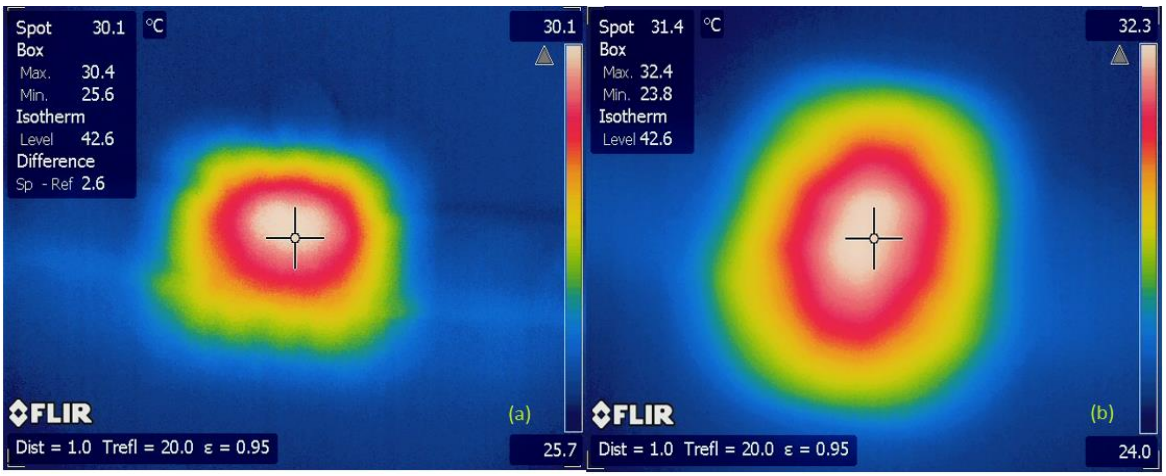

Figure 5.12: Thermal distribution for the untrimmed sample of conductive paper (a) and for the plunge cut of 5 mm (b).

In Table 5.2 below, the experimental results for the change in temperature, the calculation of TCR and the trimming time are presented. The TCR can be used to specify the stability of the resistor and it can depict the resistive element's sensitivity to temperature change due to the temperature variations. The TCR was calculated using the measurements of the resistance value for the different values of temperature. Once again, the same cuts were tested with various trim lengths. For the case of the plunge cut, it is shown that the increase in the resistance is higher for the trim length of 15 mm with the significant gain of 10.11 kΩ.

Table 5.2: Experimental results for temperature change and TCR for the plunge and double plunge.

Type of cut	**Trim length (mm)**		**Temperature (Initial)**	**Temperature (Final)**	**R_i (kΩ)**	**R_f (kΩ)**	**Resistance gain (kΩ)**	**TCR (ppm/°C)**	**Trim time (s)**
Plunge	5		25	30.4	5.25	5.96	0.71	0.68	6
	10		25	33.8	5.25	12.16	6.91	11.58	11
	15		25	34.5	5.25	15.36	10.11	18.29	17
Double plunge	5	10	25	25.3	5.25	8.76	3.51	-0.47	27
	5	15	25	26.3	5.25	15.83	10.58	2.62	22
	10	15	25	27	5.25	16.32	11.07	4.23	25

Furthermore, as expected the increase in the resistance value and TCR is even higher for the case of the double plunge cut in relation to the single plunge. However, additional trimming time is required in order to perform this cut. It is also worth mentioning that the temperature rise also causes an increase in the TCR values, as well.

In addition to this, the L-cut, curved L-cut and scan cut shapes for various trim lengths were also tested experimentally and the temperature change and TCR are shown in Table 5.3.

For the case of the L-cut, the two values of the trim length refers to the y and x leg. As previously mentioned in the literature, the length of the y leg is usually less than the x leg in order to achieve better stability. Thus, in this case, the lengths chosen were either the same for both legs or varying the x leg. The initial temperature is different from the other two cuts due to the fact that the experiments for the L-cut took place on a different date. The TCR for this cut appears to have fluctuations between the different values of the y leg.

As for the curved L-cut it is supposed to be a better version of the L-cut, so the characteristics are expected to be similar. However, the TCR seems to be really low but the main reason for that might be the behaviour of the conductive paper which was used for the experiments. For the scan cut, the TCR values are also low in comparison with the other cuts (plunge, double plunge and L-cut). Thus, it is worthwhile thinking that the scan cut even though it can offer good characteristics, cannot be considered as a pattern that needs further investigation due to the fact that the volume of the material removed is quite significant. The angled L-cut was also investigated and as also shown in Table 5.3, the initial resistance value was higher than the other ones. It can offer a resistance gain up to 1.89%. As for the TCR, it varies from 0.37 to 2.43 ppm/°C and it appears to be closer to the curved L-cut and that is why it was one of the chosen patterns to be investigated further.

Table 5.3: Experimental results for temperature change and TCR for the L-cut, curved L-cut and scan cut.

Type of cut	**Trim length (mm)**		**Temperature (Initial in °C)**	**Temperature (New in °C)**	**R_i (kΩ)**	**R_f (kΩ)**	**Resistance gain (kΩ)**	**TCR (ppm/°C)**	**Trim Time (s)**
L-cut	5	5	18	23.3	6.87	8.75	1.88	11.47	12
	5	10	18	28.1	6.77	8.97	2.20	11.86	16
	5	15	18	27.7	5.23	7.81	2.58	8.96	21
	10	10	18	25.2	5.23	12.51	7.28	14.15	21
Curved L-cut	3	3	25	27.9	5.25	8.36	3.11	1.72	7
	3	5	25	27.8	5.25	8.48	3.23	1.72	8
	3	10	25	28	5.25	11.62	6.37	3.64	13
Scan cut	5	10	25	28	5.25	7.19	1.94	1.11	16
	5	15	25	28.2	5.25	7.81	2.56	1.56	21
	10	15	25	28.06	5.25	8.32	3.07	1.79	26
Angled L-cut	5	5	23	28.6	6.04	9.29	3.25	0.37	12
	5	10	23	28.85	6.12	10.33	4.21	2.43	17
	10	5	23	28.5	6.2	11.74	5.54	1.97	15

The experimental results for the change in temperature and TCR for the newly introduced semi-circle shape are presented in Table 5.4. For this cut, the trim length is linked to the radius of the semi-circle and the values tested were for 3, 5, 8 and 10 mm. The temperature increase is shown to be stable for the various trim lengths while the resistance gain can reach up to 9.95 kΩ for the trim length of 10 mm. The semi-circle shape can be thought as an optimised version of the scan cut as it can offer similar results with less trimming time needed due to its 'smoother' shape without sharp corners and less waste in the material removed.

Table 5.4: Experimental results for temperature change and TCR for the semi-circle.

Type of cut	Trim length (r=mm)	Temperature (Initial in °C)	Temperature (New in °C)	R_i (kΩ)	R_f (kΩ)	Resistance gain (kΩ)	TCR (ppm/°C)	Trim time (s)
Semi-circle	3	25	29.2	5.25	7.1	1.85	1.48	5
	5	25	29.4	5.25	9.6	4.35	3.65	7
	8	25	29.5	5.25	11.42	6.17	5.29	10
	10	25	29.5	5.25	15.2	9.95	8.53	12

As previously mentioned, the plunge cut and the L-cut are fundamental patterns which are commonly used in the industry. The double plunge cut consists of two plunges which means that additional trimming time is added in relation to a single cut and that makes this type of cut unsuitable for further analysis. The curved L-cut is a pattern that gives the accuracy of an L-cut and it gives us confidence that less laser power will be needed to perform the cut especially in the case of thin films. Also, the scan cut will not be analysed further due to the waste of material removed. But, the newer pattern of semi-circle offers promising results and it can be thought as a potential geometry.

Thus, after all this analysis, it was decided which patterns will be further investigated using thin film resistors. The aim was to have as low a TCR as possible and high resistance gains. So, both newer patterns, the curved L-cut and semi-circle seem to be promising patterns for the geometry of the laser trimming and they will be applied to thin films, as well. Furthermore, the plunge cut, and the L-cut will also be tested again in order to have a proper comparison, since these are the most commonly used patterns in industry.

5.5 Summary

In this chapter, the laser trimming trials of the conductive paper were presented. As previously mentioned, conductive paper was used for the experiments of the first stages of this research in order to verify results obtained from simulation in less time and

economically. It is worthwhile thinking that certain consideration was taken for the set-up of the experiments in order to achieve the highest stability of the conductive paper and to be confident that the factors that might affect the results are minimised.

It is shown that the results from the simulations are close to those obtained from the experiments for most of the patterns. The normalised resistance value is 6.54 for all the samples and the highest resistance value for trim length of 14 mm is around 15 kΩ for plunge and double plunge cuts and around 12 kΩ for the curved L-cut.

The progression that the trim length is increased is clearly depicted in the results plots. It was shown that the theoretical results are close to the ones from the experiments and it is reasonable to suppose that the conductive paper has proven to be useful before the trials of the thin films so that a decision could be made on which patterns will be investigated further. In addition to this, conductive paper can also be used as an alternative method to emulate resistors and can give reliable results for laser trim patterns.

6 Trimming thin films

6.1 Introduction

In this chapter, the experimental procedure of laser trimming of thin film materials in various trim geometries is analysed. Multiple trimming patterns, both basic and novel ones, were previously tested using conductive paper as described in Chapter 5 and it was possible to clarify which patterns could be further investigated and applied to the thin films. Thus, the patterns that were chosen to be tested were the L-cut, the curved L-cut, angled L-cut, the semi-circle and elliptical pattern. A variety of trim lengths and dimensions for each type of trim pattern were applied on the thin films so that a proper comparison could be made for each design's capabilities. These thin films were trimmed using the Epilog CO_2 laser system with the specified settings for power, speed and frequency as detailed in Chapter 4.

6.2 Thin film resistor

6.2.1 Thin film materials

The thin film resistor used for the experiments consists of a resistive manganese-based material. However, the exact composition of this material is confidential and it is not possible to disclose details of it in this thesis. The films were grown on 6 x 25 x 1 mm thick, 96% Al_2O_3 substrates. The resistor shape was patterned in a bar configuration using a screen-printable mask, which was applied prior to deposition and was subsequently removed with a light solvent wash (Isopropylic alcohol). Once deposited, the annealing process followed for 4 hours at 428 °C in air. The different batches of thin films used are represented with capital letters and their thickness can be found in Table 6.1.

Table 6.1: Types of batches of thin films and their thickness.

Batch	**Thickness (nm)**
A	488
B	496
C	504
D	614
E	617

In Figure 6.1, an SEM image with high magnification using the resolution mode was taken in order to depict the material morphology before being heat-treated and laser trimmed. As

shown in the figure, the magnification was set at x2.38k, the working distance was 15 mm while the voltage was set at 20 kV and the SE detector was used. As shown, there is a variation in grain shape and size due to the sputtering method used for the manufacturing of the thin film resistor.

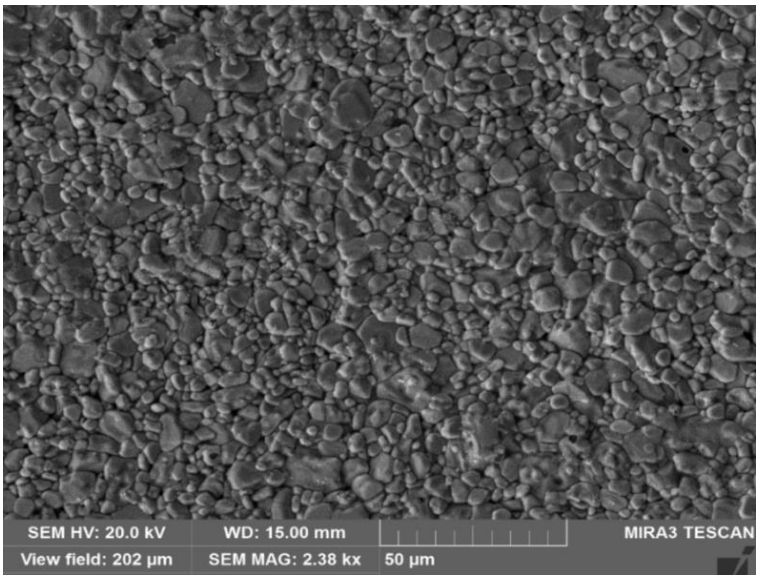

Figure 6.1: SEM Image of the untrimmed sample of the resistor before heat treatment.

Spectrophotometry was also used to relate the reflectance of the thin film material surface with the wavelength of the laser system (700 nm). In Figure 6.2, the reflectance in relation to the wavelength based on the measurements of the spectrophotometer is presented for all different batches A to E.

For the case of batch A, it is shown that the thin film can reflect light at a percentage of 34 and 42.25% for the wavelengths of 700 and 1400 nm, respectively. As presented, there are slight fluctuations in the percentage of the reflectance between the different batches. Batches B and D appears to be more reflective until the wavelength of 500 nm and then the increase is similar for all batches. Another small increase for B and D appears again closer to wavelength of 1400 nm.

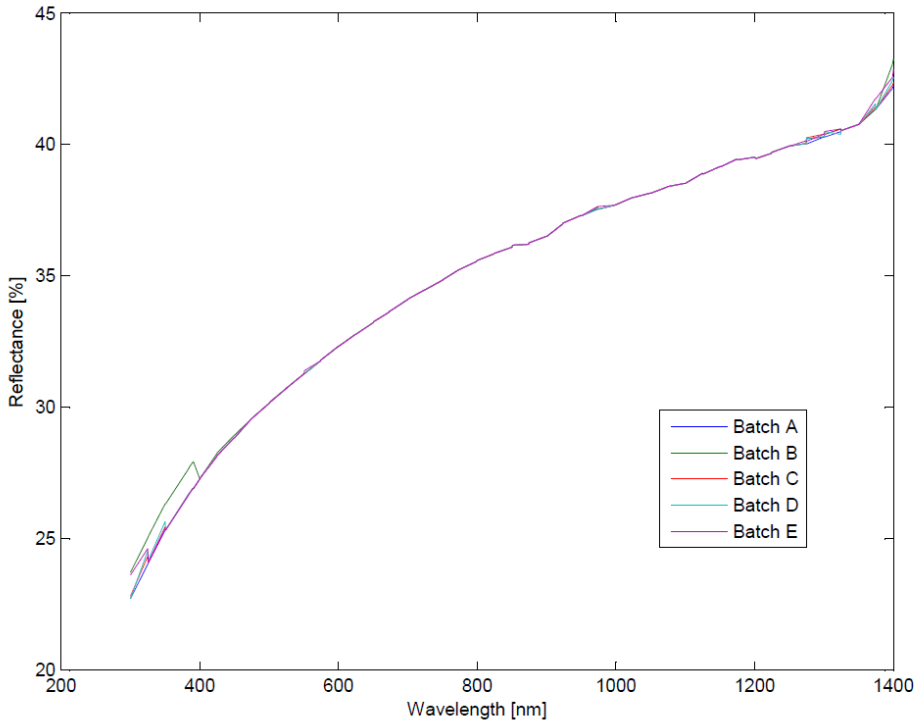

Figure 6.2: Reflectance vs. wavelength for batches A, B, C, D, E.

As for batches C and E, they are following the same trend as the one from batch A. However, overall, these tests give confidence that the reflectance for all the batches investigated in this research are proportional and their characteristics are comparable. In Table 6.2, the value of reflectance for different batches was measured for the wavelengths of 700 and 1400 nm. As previously mentioned the percentage of the reflectance shown in the table can give an indication of the quantity of light reflected from the surface.

Table 6.2: Reflectance measurements for 700 and 1400 nm.

Batch	Wavelength (nm)	Reflectance (%)
A	700	34
	1400	42.25
B	700	34.11
	1400	42.25
C	700	34.2
	1400	43.26
D	700	34.27
	1400	42.35
E	700	34.25
	1400	42.86

It is worth mentioning that the batches of the films seem to have similar reflectance values with slight differences that vary from 34.11 to 34.27% for the wavelength of 700 nm and

from 42.25 to 43.26% for the wavelength of 1400 nm. Batches D and E have the highest percentage of reflectance for both 700 and 1400 nm wavelengths in relation to the other thin film batches. However, overall there seems to be a trend for these specific wavelengths for all five batches. Thus, it was proven that these compositions have similarities and the same laser settings can be used for all of them.

In addition to this, in Figure 6.3, the samples from different batches were trimmed with an L-cut up to a target value so that any differences could be investigated after trimming. The dimensions of the cut were x = 7 mm and y = 3 mm and k was 2 mm. The target set was 70 Ω and as shown, the initial value for the untrimmed resistance was close to 55 Ω for all samples. All the samples seem to have a similar trend for the change of their resistance value. It is clear that their resistance value rapidly increases until the end of the y-leg at a trim length of 3 mm. However, after that point, the resistance increase is slower since the laser changes direction and it starts trimming the x-leg for the next 7 mm, which makes the total trim length of 10 mm.

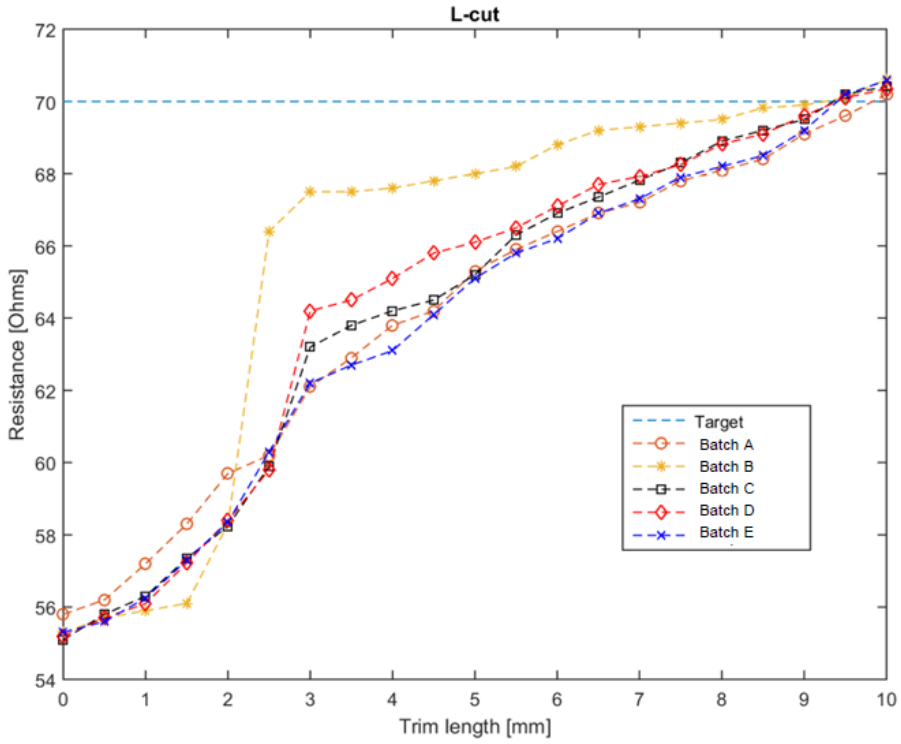

Figure 6.3: Resistance value vs trim length for the case of the L-cut until the target value of 70 Ω.

It is shown that batch B has a difference in relation to the other four batches according to the resistance increase before the kerf starts to change direction and the cut progresses. Thus, the other four batches were actually used for the rest of the experiments in order to achieve repeatability and comparability on the results.

6.2.2 Direct and indirect method of the resistance value measurements

The resistance value was continuously measured using the four-probe method while the laser was performing the cut and it was calculated per mm of the actual trim length. The experimental results were calculated based on the measurements shown and the changes were recorded using video so that the actual timeframe could be captured and calculated accordingly in relation to the laser speed. In this study, the laser speed of the cutter is 1 mm/s, as detailed in Chapter 4, and was constant for the trimming of all the samples. So, the same speed and same power was used for the experiments. However, these results were also verified using the software Labview and a comparison between the two methods for the case of the L-cut is shown in Figure 6.4.

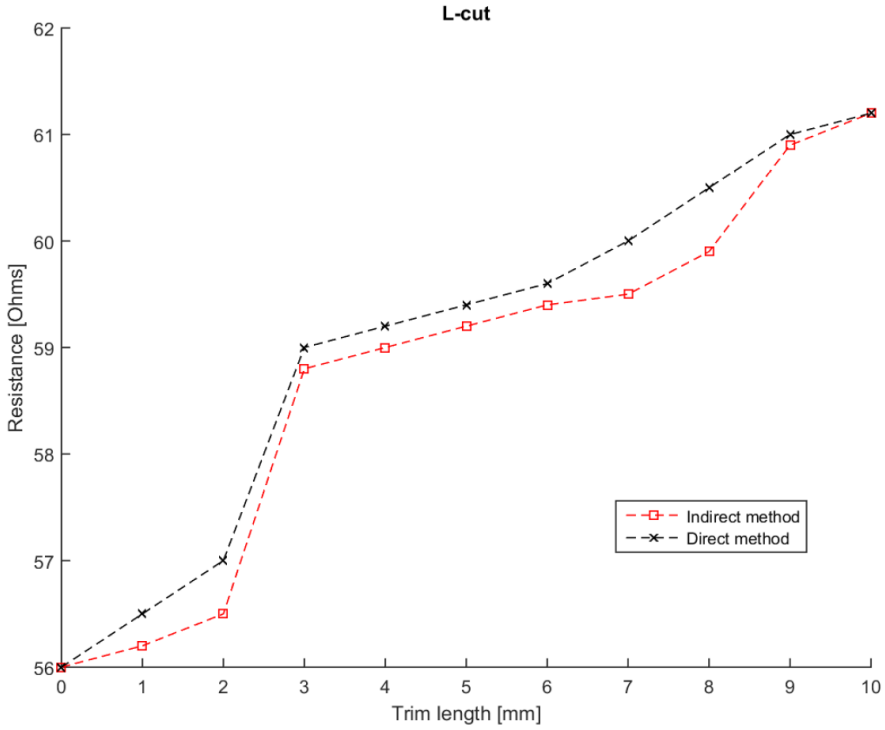

Figure 6.4: Resistance vs. trim length for the L-cut using direct and indirect method.

Labview is a software which offers a platform so that the real data from measurement hardware can be integrated and the results depicted. It can be thought as a direct method since it is synchronised with the measurement system so that accurate results are produced. It is clear that both methods follow the same trend with slight differences and the final value was the same as shown in Figure 6.4. It is worth noting that the results for most of the trimmed patterns were achieved using the indirect method.

6.2.3 Dimensions of sample

After research and trials with different dimensions of film resistors, especially with smaller samples of 10 x 6 mm, that were tested during the first stages of this study, it was finally

decided the size of the resistor should be larger for the experimental procedure. Thus, the dimensions of 25 x 6 x 1 mm were finally chosen for this research. It was proven that this size of resistor allows enough space for the different laser trim patterns to be tested effectively so that reliable conclusions could be made depending on the width of the cut. The dimensions of the thin film resistor are presented in Figure 6.5. The resistor consists of an aluminium oxide substrate and the actual dimensions of the film deposited are 21 x 6 mm. It is also shown that the resistor consists of two square silver contacts of 2 mm each on the left and right sides.

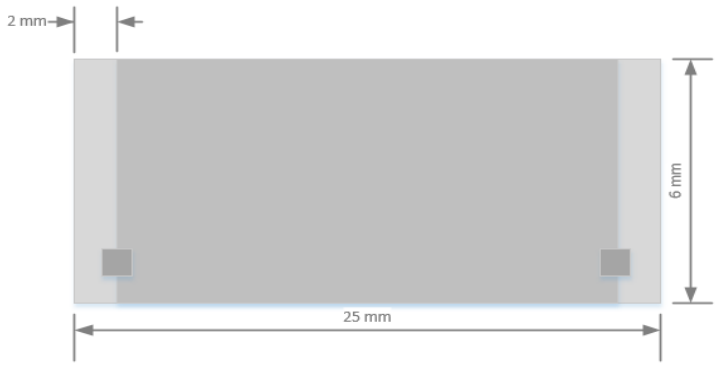

Figure 6.5: Schematic representation of dimensions of the thin film resistor used for the experiments.

6.2.4 Position of the cut

Before trimming the resistors, the position of the cut had to be set. Thus, several samples and a variety of positions were investigated in order to clarify the importance of the starting point of the cut. One of these tests concerned samples with a plunge cut of 5.94 mm, which is 99% of the width (6 mm) performed in different positions. In that way, it was possible to check the effect of the start position on the overall change of the resistance value. A schematic approach of the plunge in relation to the distance from the left contact *k* is shown in Figure 6.6.

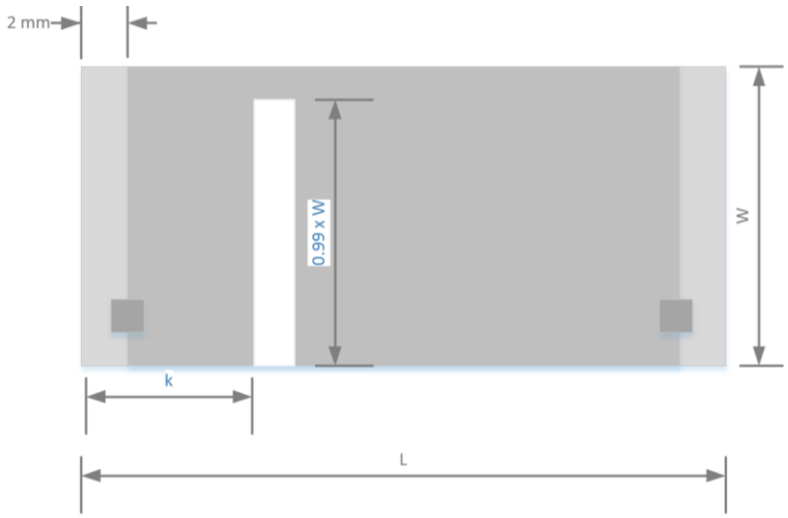

Figure 6.6: Schematic approach of the position of the plunge cut in relation to distance *k*.

In the following Table 6.3, five samples with similar untrimmed resistance values were tested with different values of *k* determining the starting point of the cut. As expected the trimmed value of the resistor and the gain is very high since the trim length of the cut is the highest possible. In that regard, the length of the plunge was kept the same and the value *k* varied. The trimming time for all the samples is the same since the length of the cut was constant. The trimmed resistance value is similar for the samples and the difference between the highest and lowest trimmed value is around 6%.

Table 6.3: Resistance value for samples trimmed with plunge cut of 5.94 mm but different value of *k*.

Sample No.	**k (mm)**	**$R_{initial}$ (kΩ)**	**$R_{trimmed}$ (kΩ)**	**Resistance gain**	**Trimming time (s)**
1	2	0.0596	37.63	630.37	6
2	6	0.0568	36.76	646.18	6
3	11	0.0512	35.44	691.19	6
4	16	0.0555	35.87	645.31	6
5	18	0.0517	36.45	704.03	6

Thus, the position of the cut has a very small effect on the trimmed resistance value of the sample. However, the analysis of the L-cut contains different starting points so that their performance can be assessed taking into account variable *k*.

6.3 Laser trim patterns

6.3.1 The L-cut

According to previous studies that were reviewed in Chapter 2, the L-cut is thought to be the most popular laser trim pattern and it is widely used in manufacturing of thin film resistors because of its stability and tolerance accuracy [2]. Thus, this pattern, even after the trials on the conductive paper, was chosen to be further analysed so that it can be compared with the novel patterns. A schematic diagram of the L-cut is shown in Figure 6.7, where *x* refers to the length of the x-leg while *y* concerns the length of the y-leg. The variable *k* is also depicted and it refers to the distance between the end of the contact and the beginning of the cut. The resistance value was measured before and after trimming using the four-probe method with the Agilent multi-meter.

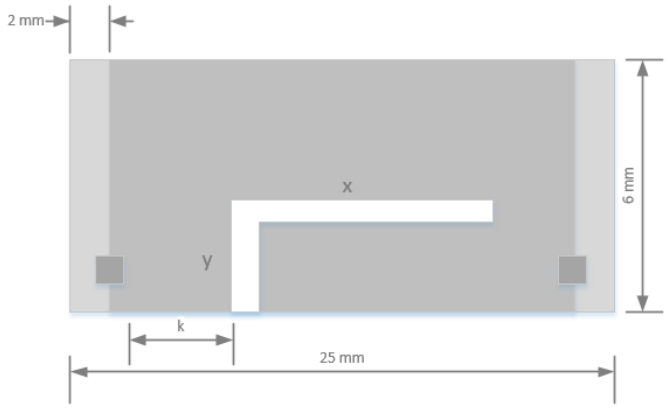

Figure 6.7: Schematic approach of the L-cut for length of x-leg and y-leg.

The samples were also analysed using SEM imaging, as shown in Figure 6.8. In image 6.8 (a), the sample was scanned using an SE detector on the wide field mode and the working distance was set at 20 mm while the voltage was 10 kV. This image depicts the overall pattern hence the magnification was lower in relation to image 6.8 (b) in which the magnification used was higher. From the SEM images, it is shown that the film was cut through and the cut was clean in the greatest proportion of the samples. However, in a few samples, some very small remains of the film were detected in the area of the cut but their effect is proven to be insignificant to the overall performance of the resistor. These are possibly causing the small fluctuations of the resistance value in between the samples of around ± 5%. Furthermore, the area of the film that was affected from the heat of the laser kerf is also found around the cut.

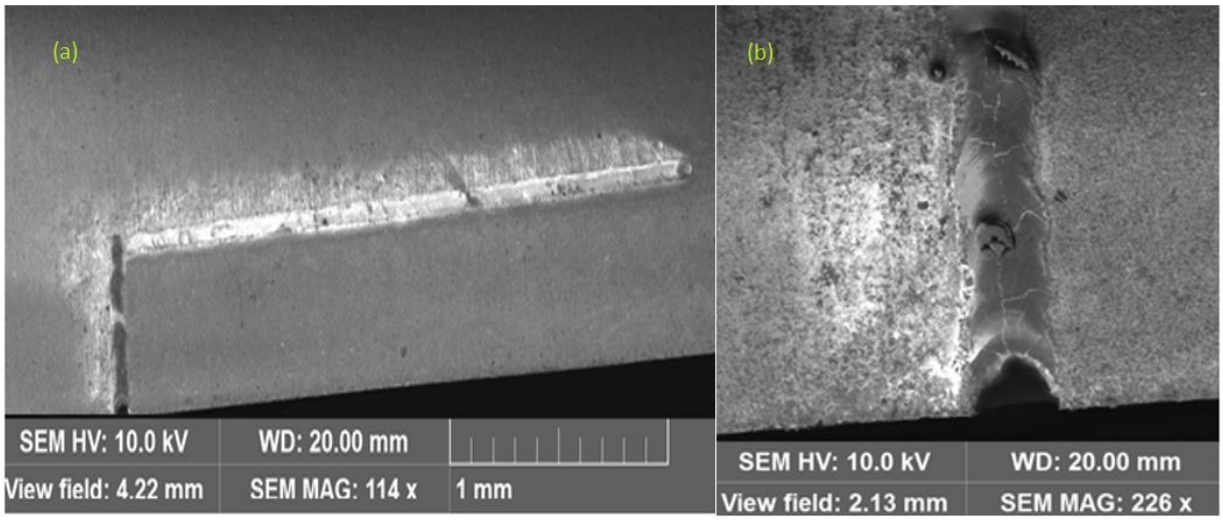

Figure 6.8: (a) SEM image for the L-cut with x = 3 mm and y = 7 mm for (a) at x114 and (b) at x226.

The resistance value was measured before and after the thin film resistor was trimmed using the four-probe method. Table 6.4 shows the resistance values of the untrimmed and trimmed samples, the trim lengths for *x* and *y* legs as well as the value of the parameter *k* with a range of 1 to 5 mm. The resistance gain was also calculated and the trimming time needed to perform the cut was measured. The trimming time is the same as in the previous case and it is proportional to the trim length. As for *k* = 3 mm, the trend is similar, once again, to the one for the previous cases. It is shown that the resistance gain is between 17.06 and 19.65% for the case of y = 2 mm and it is between 74.81 and 78.49% for *y* = 5 mm. The trimming time varies from 8.95 to 15 s. The resistance gain for the case of y = 2 mm and k = 4 mm is between 17.06 and 19.67%, while for *y* = 5 mm it is between 74.84 and 79.68% based on the results. The trend is similar to the previous cases for k = 5 mm, as shown in Table 6.4. The resistance gain is between 17.09 and 20.67% for the length of the y-leg of 2 mm and between 74.83 and 78.85% for y-leg of 5 mm. As expected the longer the y-leg the larger the resistance gain. However, the longer the trim, the more expensive the cut since more laser power and trimming time is needed.

Table 6.4: Resistance gain for L-cut samples trimmed with a variety of trim lengths for *k* from 1 to 5 mm.

	y (mm)	x (mm)	$R_{initial}$ (Ω)	$R_{trimmed}$ (Ω)	Trim gain (%)	Trimming time (s)
k=1 mm	2	6	58.70	68.61	16.88	7.95
		7		69.20	17.88	8.99
		8		69.82	18.94	10
		9		70.02	19.28	11
		10		70.21	19.60	11.99
	3	6	60.60	73.20	20.79	9
		7		75.17	24.04	10
		8		76.14	25.64	11
		9		76.85	26.82	12
		10		76.92	26.93	13
		6		80.10	19.91	10
		7		80.40	20.36	11

	4	8	66.80	81.52	22.04	12
		9		81.75	22.38	13
		10		81.96	22.69	14
	5	6	58.40	102.08	69.01	11
		7		103.40	71.19	12
		8		103.62	71.55	13
		9		103.87	71.97	14
		10		104.21	72.53	15
		15		115.23	80.99	19.6
k=2 mm	2	6	58.20	68.05	16.92	8.2
		7		68.62	17.90	9
		8		69.22	18.93	10
		9		69.50	19.41	11
		10		69.65	19.67	12
	3	6	56.80	68.61	20.79	9
		7		70.45	24.03	10
		8		71.36	25.63	11
		9		72.05	26.84	12
		10		72.09	26.91	13
	4	6	55.80	66.91	19.91	10
		7		67.16	20.36	11
		8		68.09	22.02	12
		9		68.29	22.38	13
		10		68.46	22.69	14.2
	5	6	55.70	97.37	74.81	11
		7		98.74	77.27	12
		8		98.85	77.47	13
		9		99.06	77.84	14.3
		10		99.42	78.49	15.2
k=3 mm	2	6	61.20	71.64	17.06	8.95
		7		72.15	17.81	9
		8		72.80	18.95	10
		9		73.10	19.44	11.2
		10		73.23	19.65	12
	3	6	56.90	68.73	20.79	9
		7		70.58	24.04	10
		8		71.52	25.69	11
		9		72.18	26.85	12
		10		72.22	26.92	13
	4	6	60.70	72.78	19.90	10
		7		73.06	20.36	11
		8		74.08	22.04	12
		9		74.32	22.44	13
		10		74.51	22.75	14
	5	6	59.40	103.85	74.83	11
		7		105.17	77.05	12
		8		105.41	77.46	13
		9		105.65	77.86	14
		10		106.23	78.83	15
k=4 mm	2	6	56.80	66.49	17.06	8.2
		7		66.96	17.89	9.2
		8		67.57	18.96	10
		9		67.85	19.45	11
		10		67.97	19.67	12
	3	6	57.20	69.11	20.82	9
		7		70.95	24.04	10
		8		71.15	24.39	11
		9		72.58	26.89	12.2
		10		72.61	26.94	13
	4	6	60.40	72.42	19.90	10
		7		72.71	20.38	11
		8		73.71	22.03	12
		9		73.95	22.43	13
		10		74.24	22.91	14
	5	6		104.03	74.84	11.2

		7	59.50	105.35	77.06	12
		8		105.58	77.44	13
		9		106.41	78.84	14
		10		106.91	79.68	15
k=5 mm	2	6	61.5	72.01	17.09	8
		7		72.53	17.93	9
		8		73.16	18.96	10
		9		73.45	19.43	11
		10		74.21	20.67	12
	3	6	57.5	69.48	20.83	9
		7		71.32	24.03	10
		8		72.27	25.68	11
		9		72.86	26.71	12
		10		72.98	26.92	13
	4	6	61.2	73.40	19.93	10
		7		73.67	20.37	11
		8		74.71	22.07	12.2
		9		74.93	22.43	13.2
		10		75.12	22.74	14
	5	6	58.1	101.58	74.83	11
		7		102.87	77.05	12
		8		103.11	77.47	13
		9		103.34	77.86	14
		10		103.91	78.85	15

As previously presented, the initial resistance value for the untrimmed samples had to be normalised since the values of the samples were not identical so that we have a common reference point for the rise of the value after the trimming. The samples were carefully chosen beforehand with similar values for each set of trimming with the same *y* leg so that proper comparisons can be made and repeatability achieved. It is clear that the chosen lengths for y were 2, 3, 4 and 5 mm. As for the values of *x*, these were 6, 7, 8, 9 and 10 mm, for *y* from 2 to 4 mm. In this table, there is also an additional case with trim length for x = 15 mm and y = 5 mm for the case of k = 1 mm. These cut dimensions could not be tested for different values of *k* due to the limited size of the resistor.

The samples with a larger *y* leg have the greater resistance gain based on these results. For instance, the case of the L-cut with y = 5 mm and x = 10 mm has a resistance gain of 72.53% while the one with y = 2 mm and x = 10 mm has a resistance gain of 19.60%. This trend was expected since the longer the plunge of the *y* leg the higher the resistance increase, hence the percentage of resistance gain. It is also shown that there is an increase in the resistance with the increase of the length of the x-leg. For the case of y = 2 mm and x = 6 mm the resistance gain was 16.88% while for the sample with the same y-leg and x = 10 mm the resistance gain was 19.60%, meaning that there is a difference in the percentage of 2.72%. Thus, the length of *x* leg is also important depending on the resistance gain requirements for the resistor. Furthermore, the sample with y = 5 mm and x = 15 mm gives a resistance gain of 80.99% which is logical since the longer the trim length the higher the resistance gain. As for the trimming time, it varies from 7.95 to 19.6 s, for total lengths of 8 and 20 mm, respectively. The resistance gain, in both k = 1 mm and k = 2 mm, have a

similar trend with a value of 19.67% for the case of y = 2 mm and x = 10 mm and 78.49% for y = 5 mm and x = 10 mm. It is also shown that the trend is similar for the case of y = 3 mm and x = 4 mm. It is clear that the longer the y-leg the larger the resistance gain.

Overall, several positions for k were investigated for the L-cut, as shown in detail in the previous table. However, as discussed previously, the position of the cut based on the *k* value does not have a significant effect on the case of the L-cut as presented in Figure 6.9, for *x* = 7 mm and *y* = 3 mm. The resistance trim gain is the same for the same dimensions with a very small fluctuation of 0.01%, even though the starting point of the cut is different. In addition to this, the trimming time needed for the cut to be performed was also not affected by the different values of *k* since it remained at 10 seconds. It is shown that the trimming time is mostly affected by the trim length and not the start position.

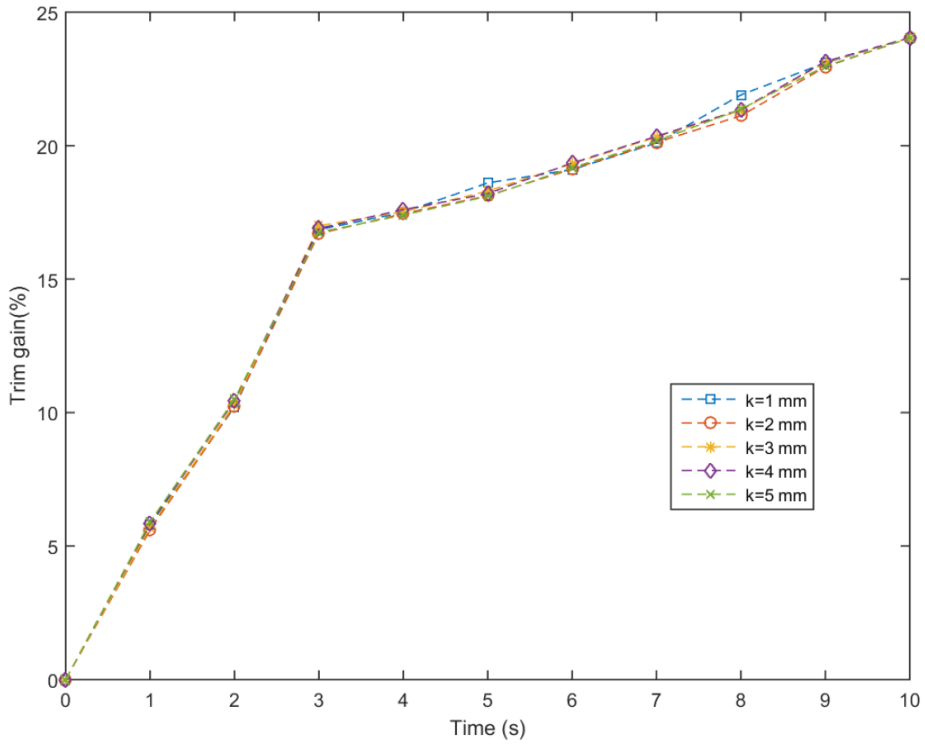

Figure 6.9: Trim gain vs. trimming time for the case of L-cut (x = 3 mm and y = 7 mm) for different values of *k*.

Thus, the trim length plays an important role. As it was expected, based on previous studies, the longer the y-leg, the larger the resistance gain since the y-leg has similar behaviour to a plunge cut and it is not surprising due to the fact that the plunge is a type of cut that can give a large percentage of resistance increase.

Based on these results, Figure 6.10 was plotted to show the resistance change with an error margin of ± 3% in the case of total trim length of 10 mm but with *x* values from 2 to 4 mm and *y* values from 6 to 8 mm. The larger increase in resistance is shown for x = 4 mm and

y = 6 mm, which is more than 21% in comparison with the L-cut of x = 2 mm and y = 8 mm, which had an increase of 15.5%.

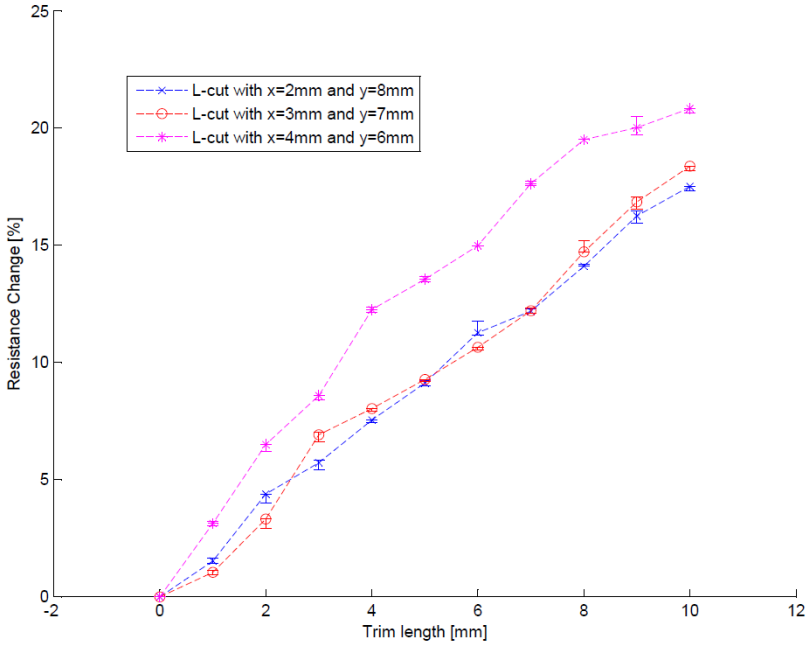

Figure 6.10: Resistance change vs. trim length for L-cut samples with total trim length of 10 mm.

The experimental results for the case of the L-cut with dimensions of x = 10 mm and y = 4 mm for five samples are presented in Figure 6.11. The purpose of these results is to investigate the repeatability of the resistance value increase for the same trim length. The value of the resistance appears to be increased quickly until the length of the trim is 4 mm and then it starts to increase gradually with a slower rate since the laser has changed direction and it is trimming towards the x-axis. It is shown that the initial value of the resistor before trimming is around 6 kΩ and then the final resistance value after trimming is around 11.5 kΩ which means there is a resistance gain of 91.66%. Thus, this type of cut is reliable and as shown even though there are slight changes between the each sample the length of the cut once again plays a more important role.

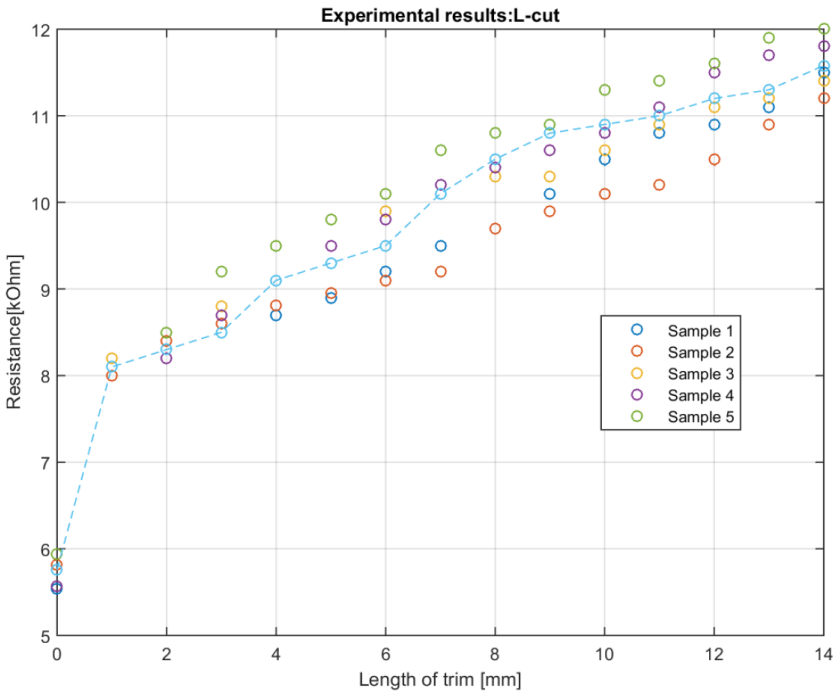

Figure 6.11: Experimental results for the L-cut with x=10 mm and y=4 mm.

To sum up, the L-cut has been proven to be a reliable trim pattern since it offers repeatability and its resistance gain can be managed depending on its trim length, particularly for the y-leg. Thus, it is reasonable that it has been widely used for the manufacturing of thin film resistors all these years.

6.3.2 Curved L-cut

The curved L-cut can be thought as one of the newer design patterns due to the fact that research for this type of cut was limited and it could be investigated further. As previously mentioned in Chapter 4, this cut can be proven quite promising since there is no corner between the *y* and *x* leg and the laser can perform a continuous cut that can decrease the trim time significantly. In Figure 6.12, a schematic diagram of the curved L-cut is shown and *x* is referred to the length of the straight part of x-leg while *y* concerns the length of the straight part of the y leg.

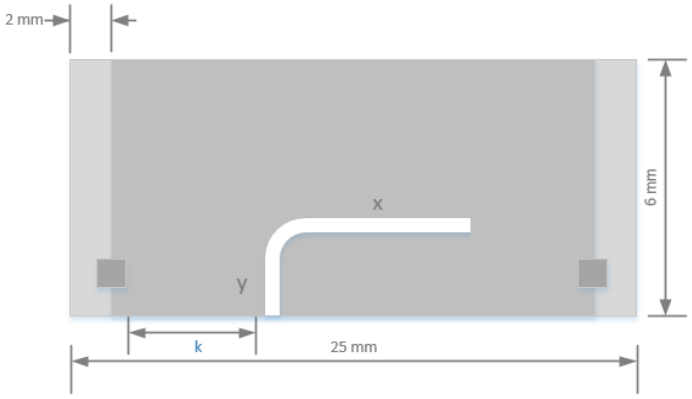

Figure 6.12: Schematic representation of the curved L-cut with trim length variables y and x.

In Figure 6.13 (a) and (b), images using SEM and the SE detector are shown. In image (a), the overall image of the curved L-cut is depicted with dimensions of x = 3 mm and y = 7 mm. In image (b), the focus is on the curve of the cut and a higher magnification of x60 was used. The HAZ around the cut is also clearly visible in both.

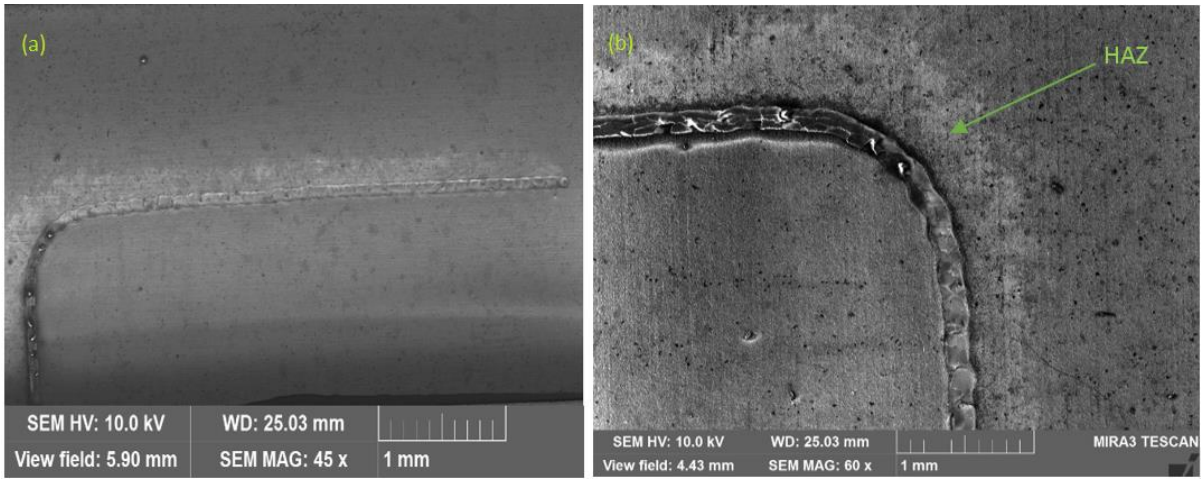

Figure 6.13: SEM image of the curved L-cut with dimensions *x* = 3 mm and *y* = 7 mm for (a) at x45 and (b) at x60.

Similar length variations like the L-cut were chosen for the tests of the curved L-cut and they are presented in Table 6.6. The starting point of the curved L-cut was for the values of *k* of 2 and 3 mm. As explained previously, for the plunge cut and the L-cut, the start position, *k,* of the cut is not causing a large difference to the resistance value and that is the reason why the tests only concerned the two mentioned values above.

Once again, the values for the resistance of the untrimmed samples are presented, which were normalised so that proper comparisons could be made. The resistance gain is significantly lower than that of the L-cut for values of *y* = 2 mm and *x* = 6 mm, since it is only 12.42% in relation to 16.92% for the case of the L-cut. While in general it produces a higher resistance gain of 22.26 and 27.88% for *k* = 2 mm and k = 3 mm, respectively. The trimming time varies from 8.2 to 15 s for this type of cut as well.

Table 6.5: Resistance gain for curved L-cut samples with a variety of trim lengths for values of *k* of 2 and 3 mm.

	y (mm)	x (mm)	$R_{initial}$ (Ω)	$R_{trimmed}$ (Ω)	Resistance gain (%)	Trimming time (s)
k=2 mm	2	6	58.70	65.99	12.42	8.2
		7		66.32	12.98	9
		8		68.10	16.01	10
		9		68.22	16.22	11
		10		68.55	16.78	12
	3	6	61.60	67.52	9.61	9
		7		68.25	10.80	10
		8		68.53	11.25	11
		9		69.23	12.39	12
		10		69.55	12.91	13
	4	6	66.80	70.95	6.21	10
		7		71.61	7.20	11
		8		71.82	7.51	12
		9		72.23	8.13	13
		10		72.65	8.76	14
	5	6	65.80	78.53	19.34	11
		7		78.92	19.94	12
		8		79.12	20.24	13
		9		80.25	21.96	14
		10		80.45	22.26	15
k=3 mm	2	6	58.95	66.22	12.33	8.2
		7		66.54	12.87	9
		8		68.23	15.74	10.2
		9		68.56	16.30	11
		10		68.95	16.96	12
	3	6	60.60	67.36	11.15	9
		7		68.12	12.41	10
		8		68.45	12.95	11
		9		69.42	14.55	12
		10		69.98	15.48	13
	4	6	66.50	71.23	7.11	10
		7		71.56	7.61	11
		8		71.98	8.24	12
		9		72.12	8.45	13
		10		72.56	9.11	14
	5	6	58.40	72.53	24.19	11.2
		7		73.13	25.22	12.3
		8		73.85	26.45	13
		9		74.25	27.14	14
		10		74.68	27.88	15

The experimental results of the trials of the curved L-cut with dimensions of *x* = 10 mm and y = 4 mm are shown in Figure 6.14. Five samples were tested with the exact same trim pattern applied to them so that resistance value variations can be observed between samples of different batches. In that way, the repeatability of the cut was tested and as shown, the difference between the samples was around 15%. Thus, it can be thought that the resistance values are repeatable for the samples that were trimmed with the curved-L cut applied to them. It is shown that a faster increase of resistance value occurs at the point of 1 mm since the plunge cut is performed and then the curve of the cut is starting until the distance of 4 mm and then the laser is slowly changing direction and starts trimming towards the x-axis until the length of x reaches 10 mm.

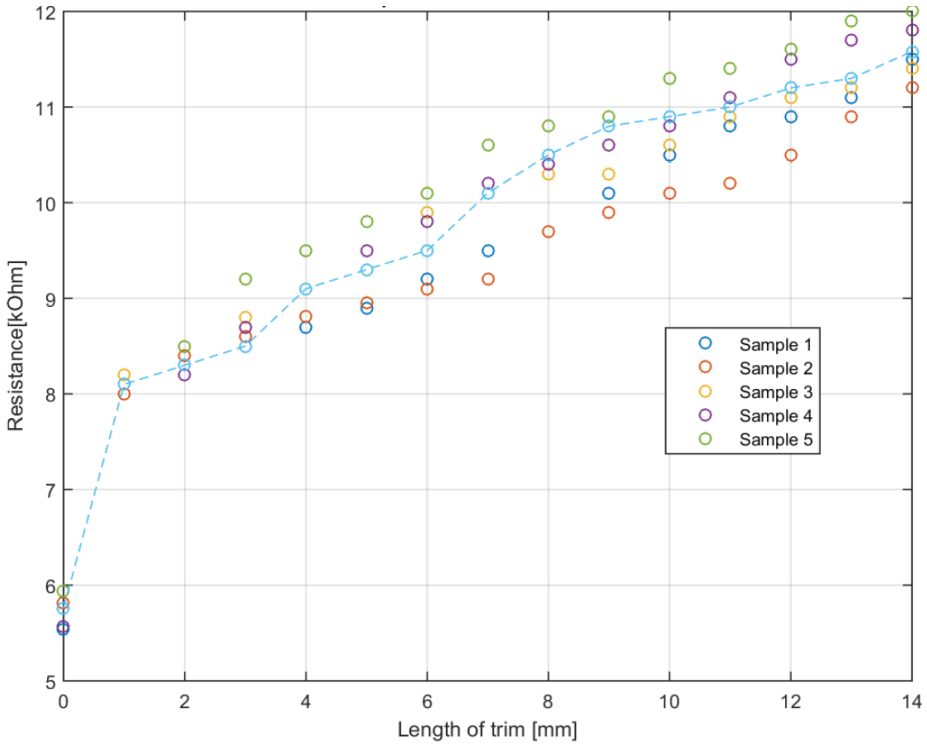

Figure 6.14: Resistance value vs trim length for five curved L-cut samples with x = 10 mm and y = 4 mm.

6.3.3 Angled L-cut

The angled L-cut can be characterised as a type of modified L-cut based on previous studies [116]. The design of this trim pattern is shown in Figure 6.15.

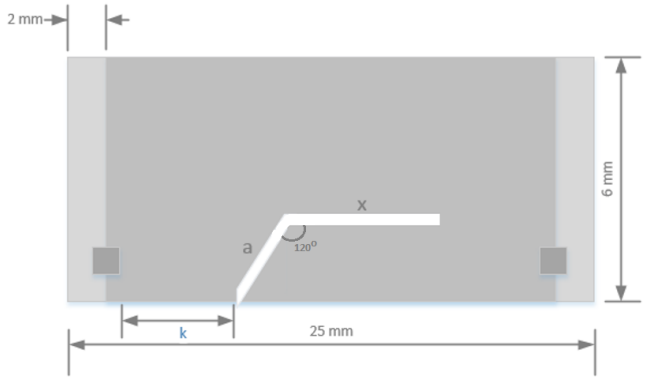

Figure 6.15: Schematic representation of the angled L-cut with trim length variables *a* and *x*.

The difference of this pattern is that the angle of the cut is 120° instead of 90° like in the case of the common L-cut. This pattern was chosen to be investigated since previous research on it is really limited but it has shown that it might be beneficial for the production of thin film resistors and it mostly concerned theoretical results. In Figures 6.16 and 6.17, SEM images of the angled L-cut are shown for reference.

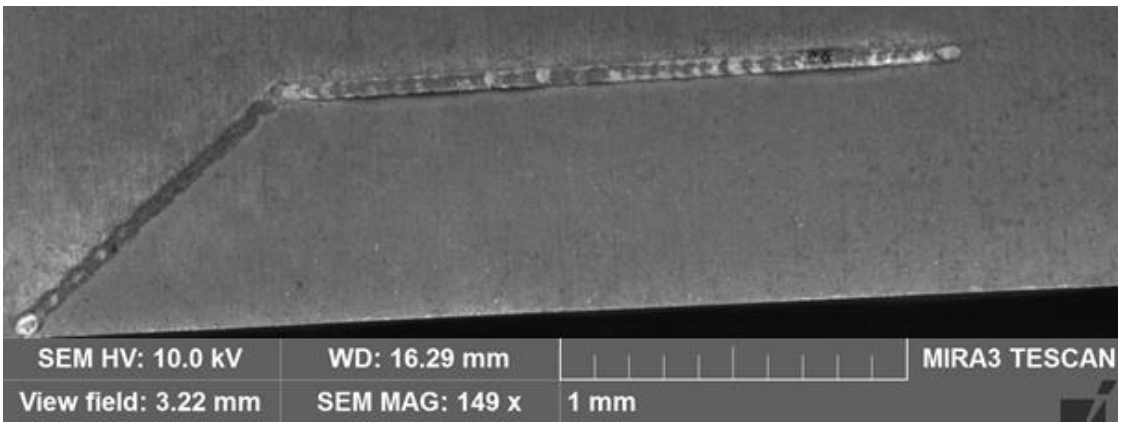

Figure 6.16: SEM image of the angled L-cut for a = 3 mm and x = 7 mm.

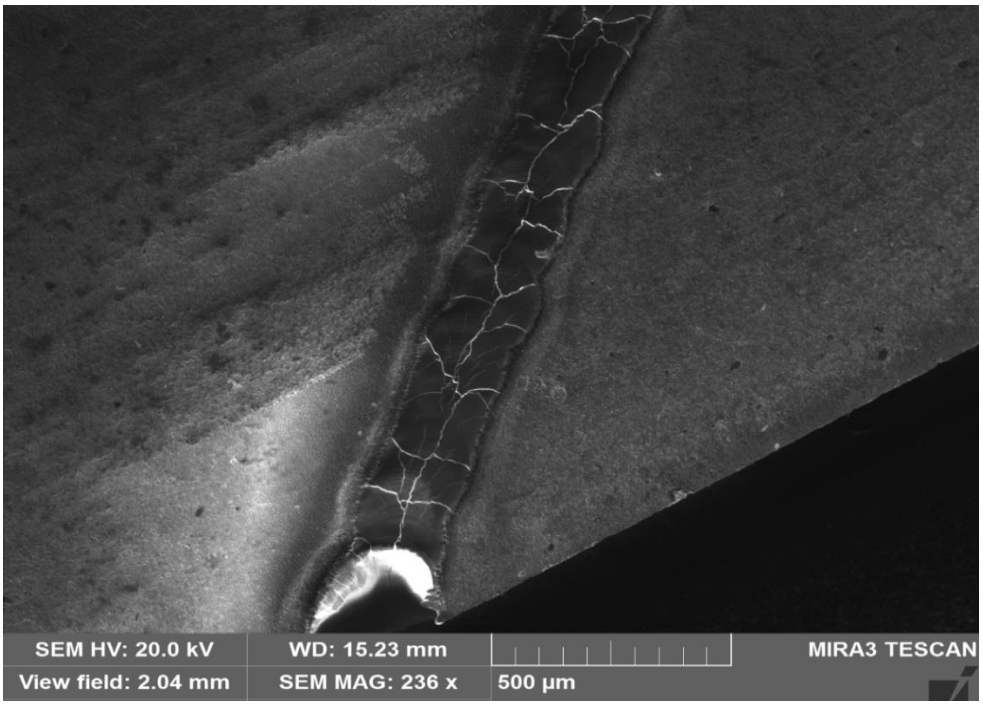

Figure 6.17: SEM image of the a-leg of the angled L-cut.

In Table 6.6, the resistance values of the untrimmed and trimmed samples are shown for different trim lengths. The value of y was between 2 and 5 mm while the value of x was between 6 and 10 mm, like the cases of L-cut and curved L-cut. However, it is clearly shown that the resistance gain for this pattern is quite small in comparison with the two previous geometries. The trimming time for this pattern varies from 7.96 to 14.97 s for trim length of 8 and 15 mm respectively.

For instance, for the trim length of a = 2 mm and x = 6 mm, the resistance gain is only 10.45% in comparison with gain of 12.42 and 17.96% for the curved L-cut and L-cut, respectively. Thus, with the angled L-cut we can achieve a resistance gain of 5.13 to 13.70%. Even though the gain of the resistance value is not as high as the other types of

cuts, this pattern can be used if the value needs to reach a certain target slowly and with reduced current crowding.

Table 6.6: Resistance gain of the angled-cut for value of *k* of 2 and 3 mm.

	a(mm)	x(mm)	$R_{initial}$ (Ω)	$R_{trimmed}$ (Ω)	Resistance gain (%)	Trimming time (s)
k=2 mm	2	6	62.70	69.25	10.45	8.2
		7		69.54	10.91	9
		8		69.23	10.41	10
		9		69.65	11.08	11
		10		69.98	11.61	12
	3	6	61.60	68.37	10.99	9
		7		69.14	12.24	9.95
		8		69.52	12.86	10.95
		9		69.62	13.02	11.95
		10		70.04	13.70	12.95
	4	6	67.30	71.23	5.84	9.92
		7		71.56	6.33	10.98
		8		71.98	6.95	11.95
		9		72.12	7.16	12.89
		10		72.56	7.81	13.78
	5	6	65.90	72.53	10.06	10.85
		7		73.13	10.97	11.92
		8		73.85	12.06	12.96
		9		74.25	12.67	13.79
		10		74.68	13.32	14.97
k=3 mm	2	6	66.70	69.25	3.82	7.96
		7		69.54	4.26	8.95
		8		70.23	5.29	9.89
		9		70.85	6.22	10.99
		10		71.58	7.31	11.95
	3	6	62.60	69.37	10.81	9
		7		70.14	12.04	9.99
		8		70.52	12.65	10.95
		9		70.62	12.81	11.96
		10		71.08	13.54	12.98
	4	6	66.80	70.23	5.13	10.3
		7		70.56	5.63	10.94
		8		70.98	6.26	11.91
		9		71.12	6.47	12.87
		10		71.36	6.83	13.68
	5	6	69.80	73.53	5.34	10.81
		7		74.13	6.20	11.85
		8		74.85	7.23	12.92
		9		75.25	7.81	13.84
		10		76.68	9.85	14.93

In Figure 6.18, the experimental results for the angled L-cut are shown for a trim length of 10 mm for five samples of different batches. The procedure followed for the measurements is the same as previously described. The test samples were chosen to have untrimmed values as close as possible to each other. Thus, the average value of the untrimmed samples is 56.25 Ω. For samples 1 and 2, the trend is similar and the value of the resistance is increased close to 60 Ω following trimming. However, for samples 3, 4 and 5, it is shown that they have a similar trend and the resistance is increased close to 65 Ω but the starting point is slightly higher than that of samples 1 and 2. Thus, the angled L-cut cannot be used

for applications that need a large resistance gain but it can be thought that it optimises the trimming time while reaching a certain target value.

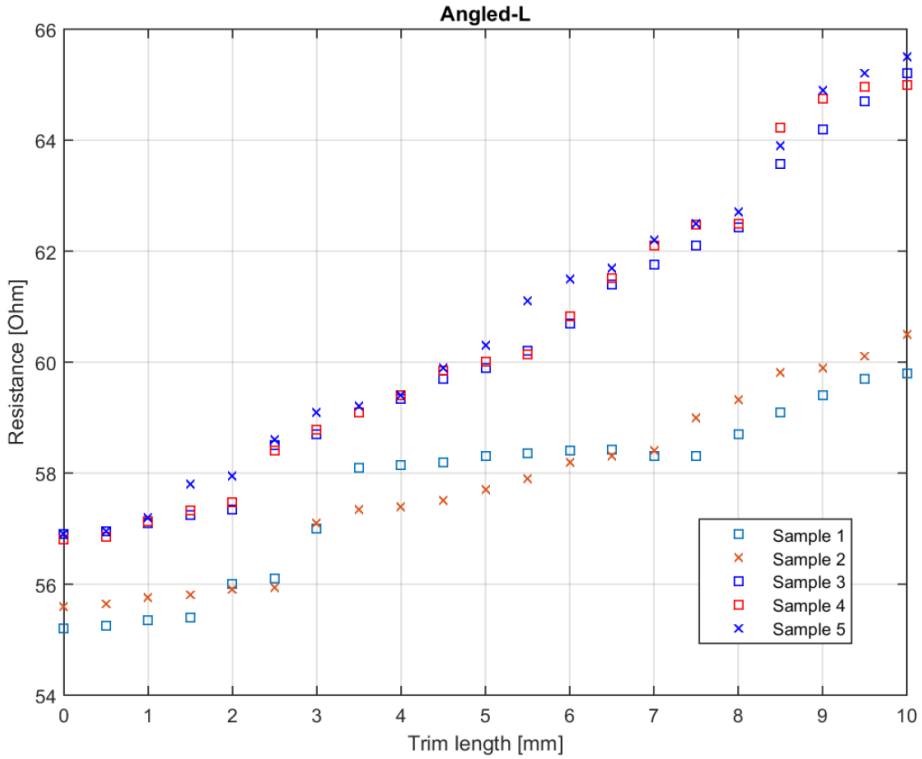

Figure 6.18: Experimental results for the angled L-cut for *x* = 7 mm and *a* = 3 mm.

6.3.4 Semi-circle cut

The semi-circle cut can be characterised as a novel pattern since no previous investigation has been noted. It has a similar design to the one of the scan cut as described in Chapters 2 and 5, while avoiding the sharp corners that add additional trimming time and increase current crowding. The design of the trim pattern is presented in Figure 6.19. The cut consists of a semi-circle and different values of the diameter *d* were tested in this study.

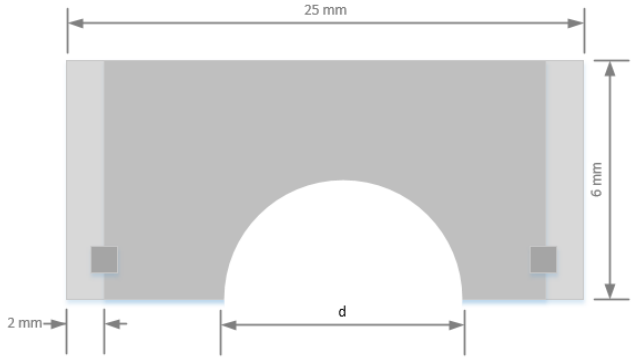

Figure 6.19: Schematic approach for the semi-circle pattern for diameter d.

In Figure 6.20, the SEM image is shown for the semi-circle pattern with magnification of x313.

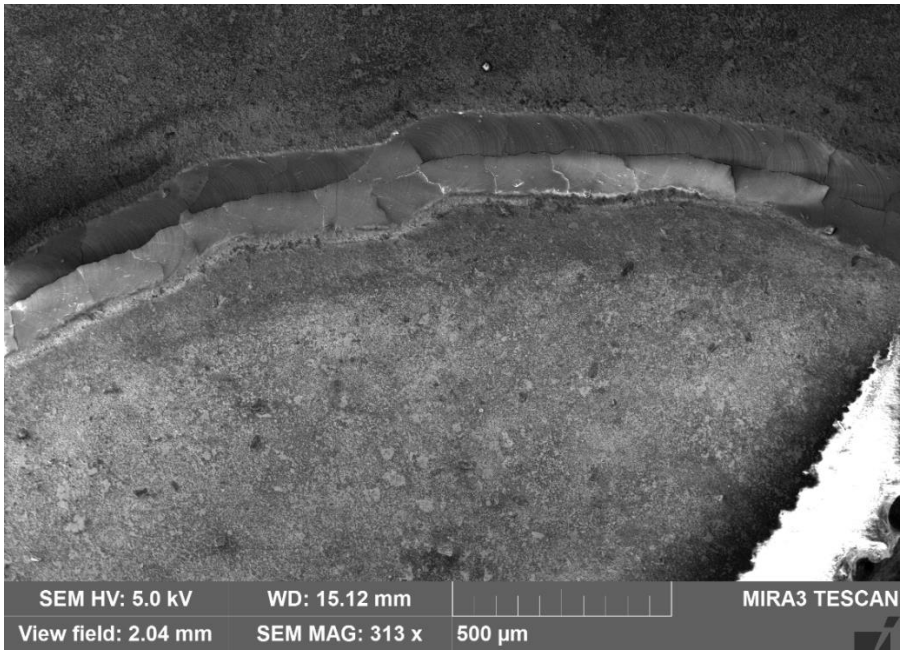

Figure 6.20: SEM image of the semi-circle with d = 4 mm at x313.

In Table 6.8, the resistance value of the untrimmed and trimmed samples are presented and the percentage of the resistance gain was also calculated. The range of the values of *d* tested was from 1 to 5 mm. Once again, the initial resistance value was chosen to be close for the samples. It is shown that the resistance gain for this trim pattern can reach up to 43.89% for the diameter of 5 mm.

Table 6.7: Resistance gain for semi-circle pattern with different values of *d*.

d (mm)	$R_{initial}$ (Ω)	$R_{trimmed}$ (Ω)	Resistance gain (%)	Trimming time (s)
1	78.81	89.96	14.15	1.6
2	78.91	92.45	17.16	3.2
3	78.50	97.5	24.20	4.7
4	77.92	104.56	34.19	6.3
5	78.25	112.6	43.89	8

6.3.5 Elliptical cut

The idea of the elliptical cut was based on a previous study in which a third contact was used to adjust the value of the resistor [9, 11] and it was adjusted to the needs of this study. A schematic approach of the elliptical cut is shown in Figure 6.21. In general, the ellipse is

a curve in a plane surrounding two focal points such that the sum of the distances to the two focal points is constant for every point on the curve. The equation is

$$\frac{x^2}{a^2} + \frac{y^2}{b^2} = 1 \qquad \text{Equation 6-1}$$

in which the horizontal major axis of the ellipse is marked as *a* while the vertical major axis of the ellipse is marked as *b*. The same theory was applied to this design and different values of *a* and *b* were tested to investigate this type of cut. SEM images of the cut are shown in Figure 6.22 (a) and (b).

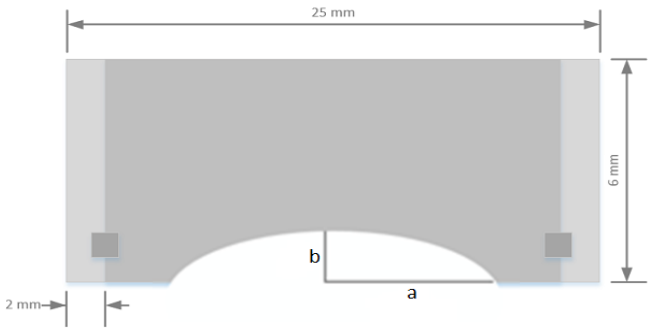

Figure 6.21: Schematic representation of the elliptical cut with variables *a* and *b*.

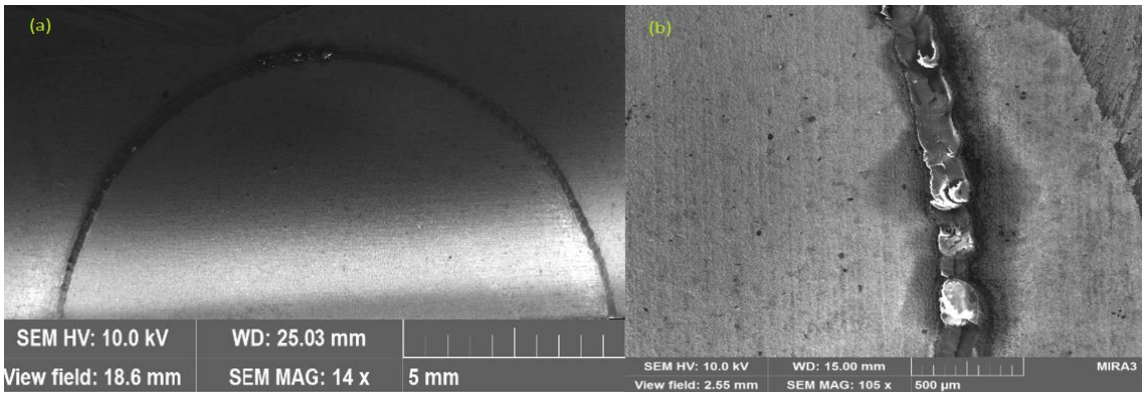

Figure 6.22: SEM image of the elliptical cut with a = 6 mm and b = 3 mm for (a) at x14 and (b) at x105.

In Table 6.8, the change in the resistance value of the elliptical cut is shown and the resistance gain is calculated. The values of *a* tested started from 5 mm up to 7.5 mm while *b* started from 0.3 mm to 2 mm. The elliptical cut shows a unique trend on its resistance gain and it starts from 11.06 % and it can reach up to 31.71% for the case of *a* = 5 mm and *b* from 1 to 5 mm within the fixed area.

Table 6.8: Resistance gain for the elliptical cut for different values of *a* and *b*.

a (mm)	b (mm)	$R_{initial}$ (Ω)	$R_{trimmed}$ (Ω)	Resistance gain (%)	Trimming time (s)
5	1	72.30	80.3	11.06	15
	2		81.2	12.31	15.2
	3		85.32	18.01	16.3
	4		91.05	25.93	17.52
	5		95.23	31.71	19.3
5.5	1	68.25	76.52	12.12	16.3
	2		77.36	13.35	18.5
	3		79.56	16.57	19.2
	4		85.36	25.07	20.3
	5		89.80	31.57	21.4
6	1	78.8	86.95	10.34	19.56
	2		91.36	15.94	20.12
	3		94.65	20.11	20.78
	4		97.35	23.54	21.36
	5		101.2	28.43	21.68
6.5	1	68.52	77.52	13.13	16.35
	2		77.95	13.76	17.56
	3		79.56	16.11	18.95
	4		85.34	24.54	20.3
	5		89.96	31.29	21.5
7	1	69.23	78.65	13.61	15.3
	2		78.95	14.04	17.23
	3		79.47	14.79	18.45
	4		83.26	20.26	19.65
	5		91.20	31.73	20.1
7.5	1	72.56	84.56	16.54	16.35
	2		86.95	19.83	18.74
	3		91.23	25.73	19.89
	4		96.5	32.99	20.13
	5		97.56	34.45	20.65

This type of cut can offer a significant resistance gain which is obviously higher in the case of *a* = 7.5 mm and *b* = 2 mm at the value of 34.45%, since a larger quantity of the film was removed.

6.4 Temperature measurements

The designs that were investigated and presented in the previous sections in relation to their resistance value were also tested in relation to their temperature rise with application of power. This type of test is beneficial for checking the performance of the various trim geometries in high temperatures and how effective these could be when ultimately used as devices within electronic circuits. Four samples were examined for each type of cut so that the repeatability could be measured. The trimmed resistors were connected to a DC regulated power supply (Model 305D) with voltage range of 0-30 V and current from 0-5 A and power was applied to them. The set power values were related to the normalised resistance and the temperature change was measured using a thermal camera (Model: Flir B620). Thermal images were taken each time for different values of power. Four thermal

images for the case of the L-cut are shown in Figure 6.23, for indication of the temperature values with different loads applied to the sample.

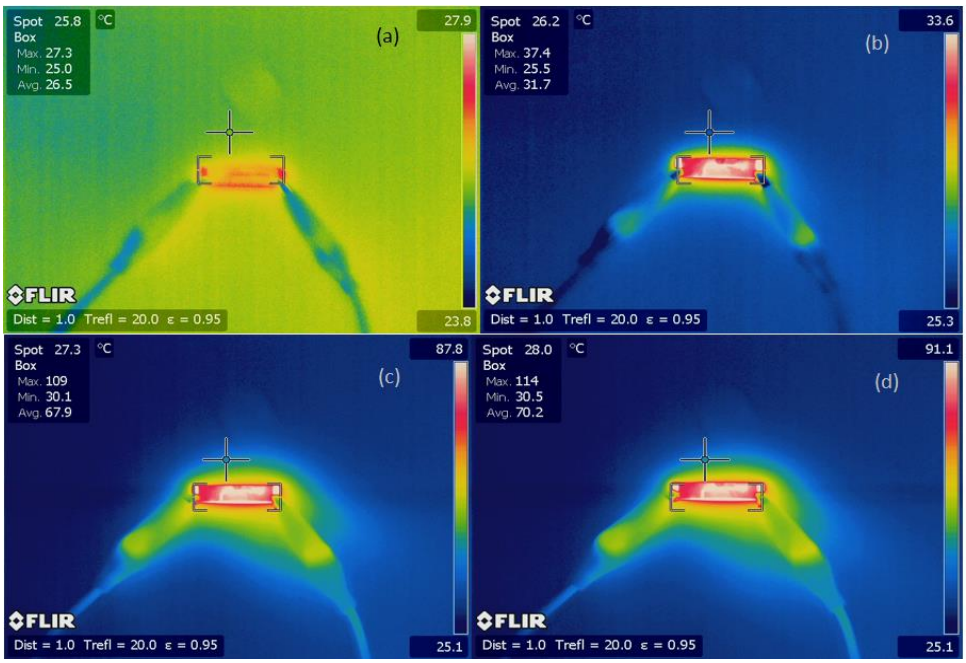

Figure 6.23: Thermal image of the L-cut (a) before applying power, (b) after application of power of 2 W, (c) power of 8 W and (d) power of 12 W.

Based on measurements from the thermal camera for various samples, the temperature change for the L-cut was plotted as shown in Figure 6.24 for trim lengths of x = 7 mm and y = 3 mm. The initial temperature of the resistor is depicted at the starting point before power was applied to it. Then, the temperature starts to rise in steps for all the samples until the final temperature value was close to 80 °C including the difference expressed in the error bars. The trend of the temperature rise is similar for all the samples and the results are repeatable to within ± 8%.

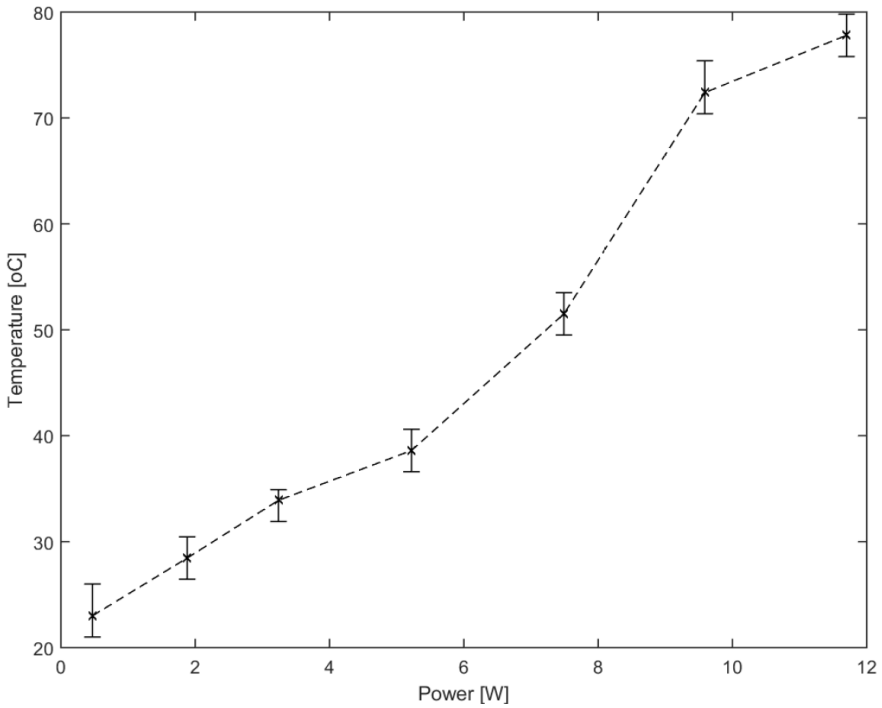

Figure 6.24: Temperature vs. power graph for the case of the L-cut with x = 7 mm and y = 3 mm.

The temperature change in the case of the curved L-cut is presented in Figure 6.25. Four samples were again tested which were trimmed with the same trim lengths of x = 7 mm and y = 3 mm. The starting point of the temperature is close to 28 °C for the lowest point of the power and the highest temperature value is around 83 °C for power of 11.5 W. The trend of the temperature rise is not that close in comparison with the L-cut and the temperature shows a higher increase for the curved L-cut. It is worth mentioning that the starting point is higher than the one for the L-cut. The fluctuations between the samples are represented using error bars and in this case the difference varies from 10 to 15%.

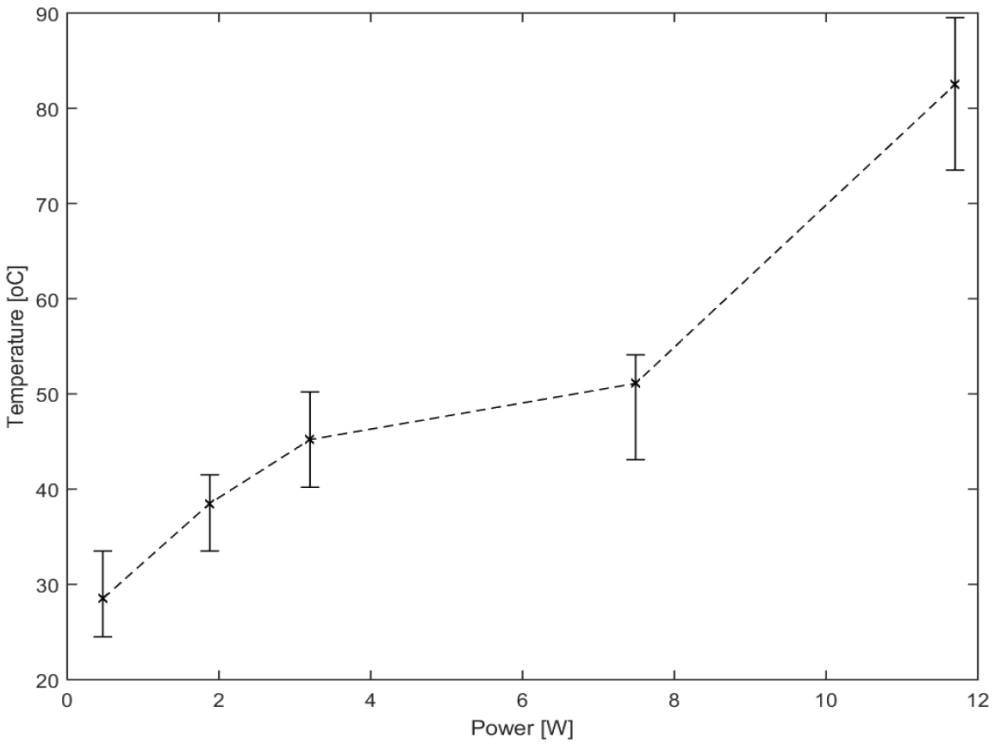

Figure 6.25: Temperature vs. power graph for the case of the curved L-cut with x = 7 mm and y = 3 mm.

As for the angled L-cut, the temperature change of four samples is presented in Figure 6.26, with trim lengths of x = 7 mm and y = 3 mm. As shown, the temperature reaches up to around 68 °C.

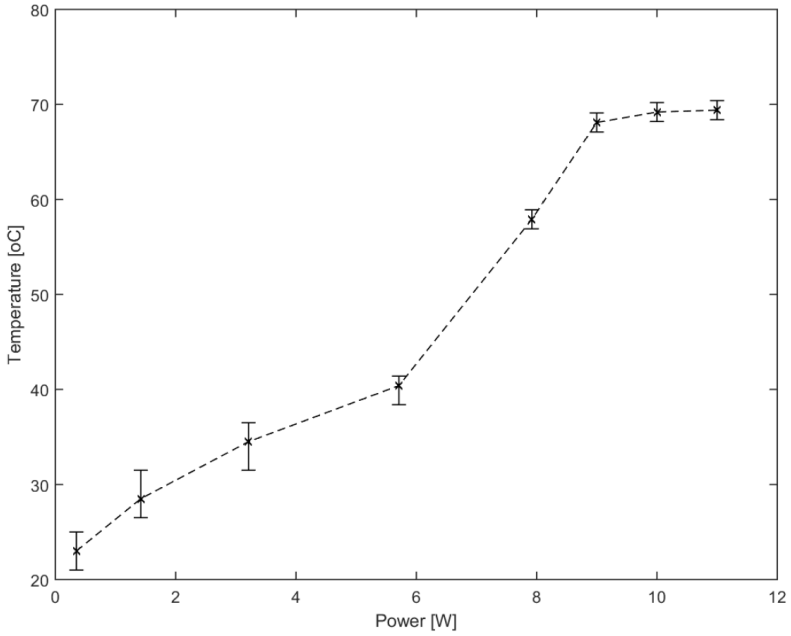

Figure 6.26: Temperature vs. power graph for the case of the angled L-cut with x = 7 mm and y = 3 mm.

The plot contains error bars to show the difference between the samples tested so that the repeatability of the results to be checked. The error is between 10 to 15% which gives confidence for the results of the temperature change.

For the case of the semi-circle, the temperature rise between the samples seem really close, as shown in Figure 6.27 and there are small variations with error of 5 to 15%. The initial temperature is close to 22 °C before power was applied to the resistor and it reached up to around 76 °C for power value of 5.8 W.

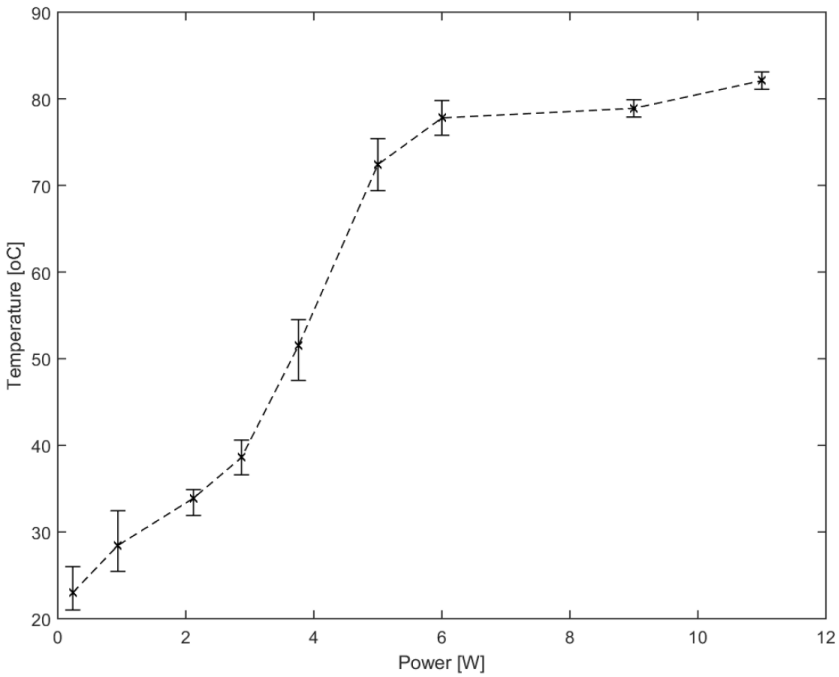

Figure 6.27: Temperature vs. power for the case of the semi-circle pattern with d = 4 mm.

The elliptical cut, as shown in Figure 6.28, also appears to have a similar trend for all the samples tested. The initial value of the temperature before power was applied is close to 28 °C and then it was gradually increased up to the value of 73 °C.

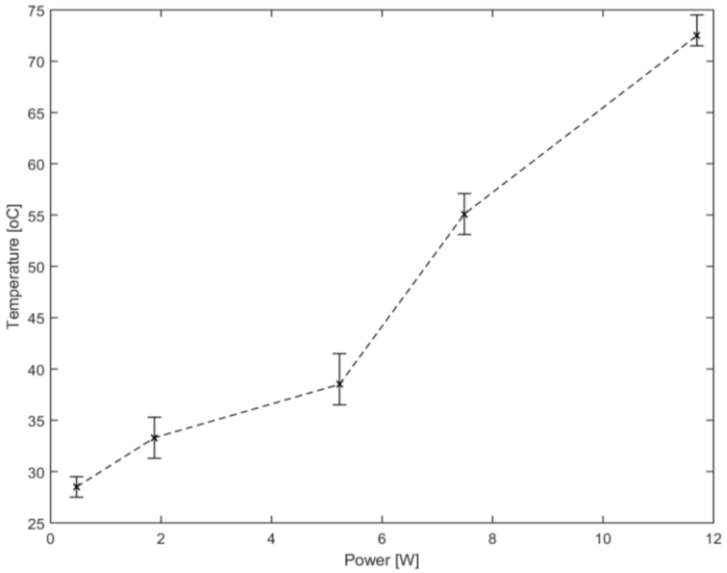

Figure 6.28: Temperature vs. power for the case of the elliptical cut with a = 5 mm and b = 2 mm.

The increase in temperature seems to have a similar trend for semi-circle and elliptical patterns since both patterns offer a very large resistance increase which leads to higher voltage needed to heat up the sample.

6.5 Discussion

In this section, a comparison of the performance of the trim patterns is made based on the results previously presented. The graph in Figure 6.29 includes the resistance change in relation to the trim length for the L-cut, angled-L, curved-L, semi-circle and elliptical cut for k = 2 mm. The trim length refers to the length of the cut, while for the semi-circle and elliptical cut the length was calculated based on the circumference of the shapes. For the semi-circle, the trim length was calculated at 8 mm for the case of d = 5 mm and for the elliptical cut the full trim length was obviously larger than 8 mm for all the cases so it refers to the change up to 8 mm.

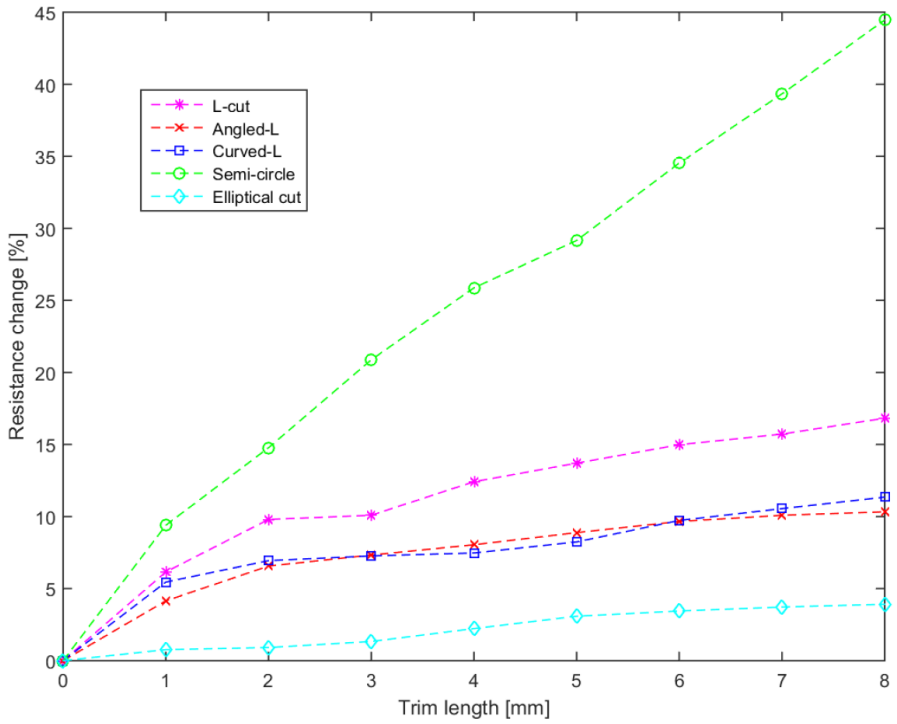

Figure 6.29: Resistance change vs. trim length for all the trim patterns investigated.

As for the L-cut, angled-L and curved-L, the length refers to the sum of the two legs for y = 2 mm and x = 6 mm. It is clearly shown that the semi-circle offers a very large resistance gain which reaches up to 44% for the trim length of 8 mm in relation to the other patterns. The L-cut, as expected, shows a quick increase until 2 mm of the film were removed and then the resistance increase gradually continues up to around 16%. As for the angled L-cut, there is an increase of the resistance which is lower than the one from the L-cut at the value of around 10.5%. The increase in the case of the curved L-cut is a bit higher than the one of the angled L at the final value of 11.3%. The L-cut, angled L and curved L-cut have a similar trend of the rate of the increase of the resistance even though the L-cut offers a larger resistance gain in comparison with the other two variations of L. The elliptical cut appears to have a small resistance gain which is not the case but this was the calculated gain up to the trim length of 8 mm which only covers the 34.88% of the full trim length. Thus, the trim pattern plays an important role in the overall performance of the resistor and especially in the change of the resistance value.

In Figure 6.30, the resistance gain in relation to the trimming time is presented for all the trim patterns for *k* = 2 mm and the same total trim length of 10 mm. The dimensions for the L-cut and curved L-cut were once again for x = 7 mm and y = 3 mm. For the dimensions of the angled L-cut, these were a = 3 mm and y = 7 mm and the trim length of the semi-circle refers to the one of d = 5 mm.

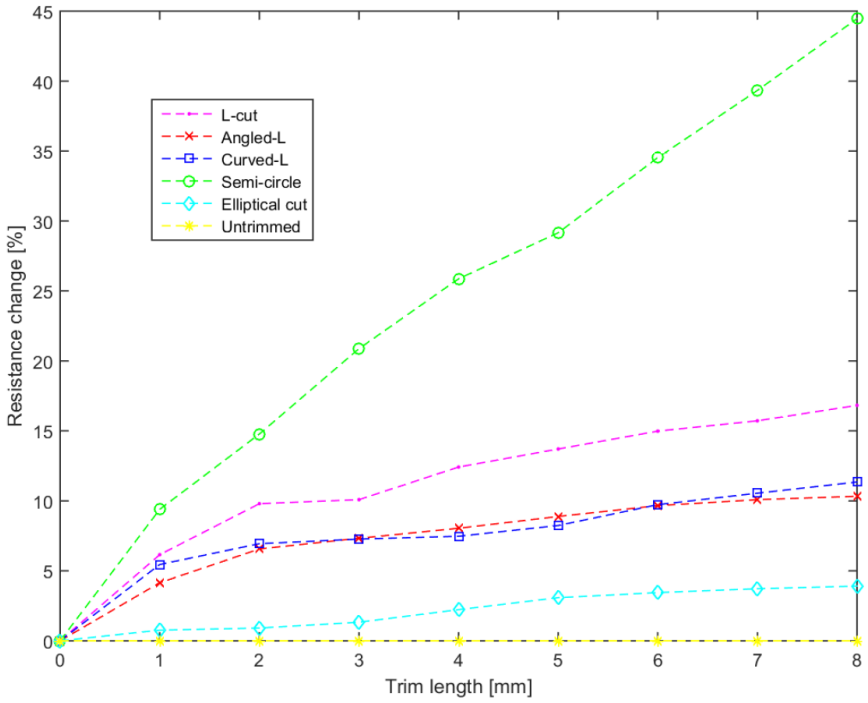

Figure 6.30: Trim gain vs. trimming time for all different geometries.

Once again, the trim gain for the elliptical cut is shown up to the trim length of 8 mm since the total length of the cut was 22.94 mm so that a fair comparison in relation to the trim length of the samples to be made. It is worth noting that only up to the point of trim length of 8 mm is displayed on the graph for a comparison with the other patterns even though it does not depict the total trim gain that this cut can offer which can reach up to around 30%. It is also shown that the semi-circle has the largest trim gain which reaches up to 43%.

The patterns were also compared in relation to the change in their temperature when power was applied to them, see Figure 6.31. The process of the tests and measurements was described in the previous section. The starting point was normalised for a common reference point. The semi-circle pattern is shown to have a large overall increase in the temperature of 140%, which means that it has doubled from its starting point. For the elliptical cut, there is a 98% increase in temperature for power of 6 W. As for the L-cut, angled L and curved L, the trend of the increase in temperature is similar and it reaches up to around 90%. Thus, the semi-circle appears to have the largest increase in temperature change in relation to the rest of the patterns.

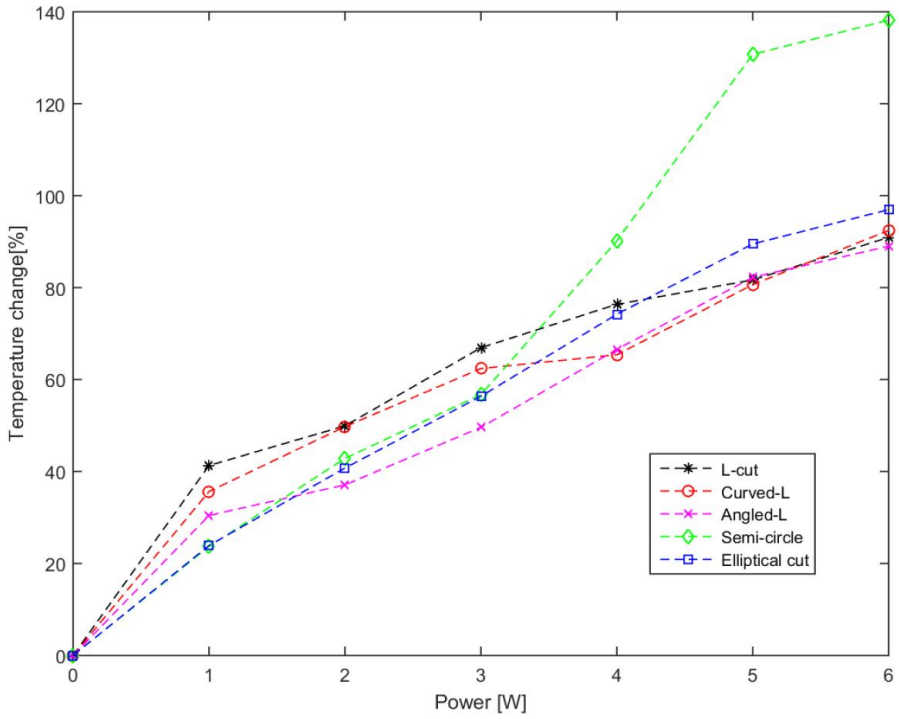

Figure 6.31: Temperature change vs. power for all types of trim patterns.

6.6 Summary

In this chapter, details of the thin film used for the experiments of this study along with a description of how it was manufactured were presented. The common trim pattern of the L-cut as well as novel ones such as the curved L-cut, the angled L-cut, the semi-circle and the elliptical cut were investigated in relation to their resistance gain and temperature rise under load conditions. The results of the resistance change in relation to the trim length were measured and calculated for all the trim patterns and these were compared with the established trim patterns such as the L-cut. The L-cut has proven its popularity since its resistance gain can be easily adjusted to the targeted value and the temperature change was increased up to a certain point. The angled L-cut cannot offer a large increase in resistance but the trimming time needed was less that the other two variations of L. As for the curved L-cut, it had a similar behaviour to that of the L-cut as far as the resistance gain and the change in temperature are concerned. The elliptical cut offers a large resistance gain which is expected since the trim length is by far larger than the other ones due to its geometry. The semi-circle appears to give a large increase in the resistance in a very low trimming time in relation to the other patterns and it is suggested that it can be used for applications where a large resistance value is needed. The value d can be adjusted in relation to the target value of the resistor. The semi-circle and elliptical patterns seem to follow a similar trend in terms of temperature rise, with the semi-circle having the largest change of 140%. However, according to the results, the trimming time for the elliptical cut

was higher than the one for the other patterns since the trim length was larger and it can also be thought that a larger quantity of material was actually removed.

7 Reliability testing and verification of the model

7.1 Introduction

In this chapter, the performance of the thin film resistors with the optimum laser trim patterns was assessed in relation to their reliability, pulse durability and stability for the verification of the model. Reliability refers to the probability that a resistor will perform its desired function and it tends to be generally higher at lower power levels. Resistor tolerance is expressed as the deviations from nominal value in percent and is typically measured at 25 °C. In general, a resistor's value will also change with applied voltage (VCR) and temperature (TCR) [8, 70]. Stability is the change in resistance with time at a specific load or ambient temperature. When these stresses are minimized, the stability of the resistor is better and this is the goal for the manufacturing of thin film resistors.

In general, failure modes on the performance of the thin film resistors include mechanical failures, environmental factors, thermal issues, electrostatic discharge (ESD), overload and surge conditions, load life stability and changes in TCR and PCR [136]. Mechanical failures refer to ongoing vibration which can cause micro-cracking of the resistor material that will lead to change in the resistance value, damage to the resistive element. Common environmental issues such as moisture, contamination and some chemical elements need to be considered since these can affect the performance of the resistor.

It is also important to understand the resistor's heat dissipation properties. The primary heat dissipation mechanism of a low power resistor is by conduction through its component leads or connections, while a high power resistor dissipates heat primarily through radiation. When current passes through a resistor it generates heat and the differential thermal expansions of the different materials comprising the resistor induces relative mechanical changes (stresses) in the resistor [20, 136].

TCR is the best known parameter used to specify a resistor's stability and defines the resistive element's sensitivity to temperature change [20]. PCR quantifies the resistance change due to self-heating when power is applied and is particularly important for resistors used in power applications [136]. Electrostatic discharge (ESD) is another potential problem that can cause unpredictable failure. A resistor that is exposed to an ESD event may fail immediately, or may not operate effectively. As for overload conditions, a continuous overload of a resistor device tends to degrade the insulation resistance and changes the resistor parameters over time. Voltage stresses can cause conduction from normally non-conductive materials in the resistor film leading to deterioration and occasionally failure due to hot spots. It is therefore important to observe the resistor maximum specified voltage [8].

The geometry of a resistor also affects its surge withstand capability. A larger surface area results in a higher film mass and ultimately an improved surge performance. In addition, this increased surface area allows more heat dissipation which is important for power resistor applications. Resistor trimming and the method used for trimming can create weak spots that can cause failure under surge conditions.

In very high-precision resistors, which are designed for critical applications, very accurate and stable resistance values are required. These effects must be taken into account to achieve high stability with changes in load (Joule effect) and ambient temperature. In any material, the internal resistance will change as the temperature changes [20]. This extends to resistors as well. The rate of resistance change based on temperature is expressed using TCR. As previously mentioned, it is indicated in units of ppm/°C and determined from the resistance change from some reference temperature and the change in temperature [8, 70].

Thus, in this chapter, the trim patterns were tested further so that their performance and stability could be assessed in relation to dry heat testing, PCR and TCR.

7.2 Dry heat test

In this section, the process of dry heat testing is analysed. After the film was deposited on the substrate and the thin film resistor was formed, the stability of the resistor was assessed. All the samples before trimming took place were dry heat tested. The resistance value of the resistor was measured after the formation and it is characterised as the initial value. After that the resistors were placed in the glass tube of the furnace (Model: Carbolite Tube Furnace 1200C). Before the tests, the temperature of the furnace at 3 points of the glass tube (centre, left and right) was measured using a thermocouple so that the uniformity of the temperature distribution could be established. In Figure 7.1, the measurements of the temperature in °C are presented in relation to time in minutes. The furnace was switched on and its temperature was set at 220 °C and it was operating for 2 hours. The graph consists of three lines which refer to the different position that the measurements were taken, pointing at the left part, the centre and the right part of the tube of the furnace. As shown, the temperature was gradually increased for the first half an hour and then it reached 220 °C and it was stable after that point. Thus, that gives confidence that the overall temperature distribution is uniform and that this factor was stable for all three positions.

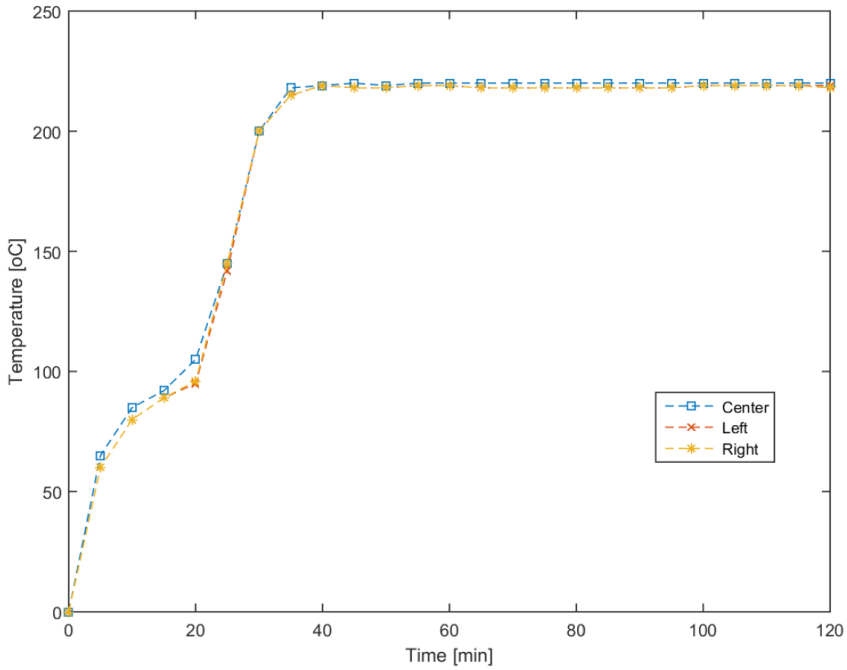

Figure 7.1: Temperature measurements using thermocouple in relation to time to check the temperature distribution.

It is worth mentioning that the samples were placed at the centre of the furnace to make sure that these were treated at the expected temperature and any heat losses to be avoided and the most reliable results achieved.

Since the reliability of the furnace was assessed, the heat treatment of the samples started, which were placed in the centre of the glass tube, as shown in Figure 7.2 and they were sealed using glass ampule connected on both ends (left and right) to the nitrogen (N_2) supply. The two sides had to be firmly sealed and high vacuum grease was used for the connections as well as high temperature polyimide tape to cover the outer part of the connection for additional safety.

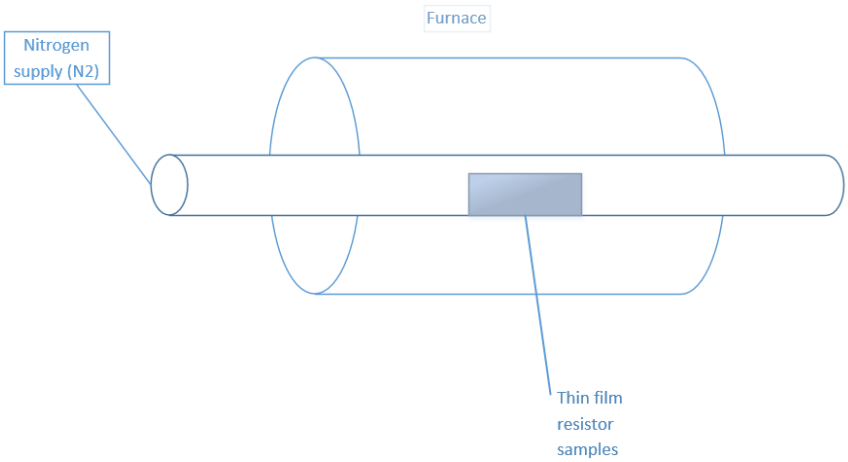

Figure 7.2: Schematic approach showing the position of the samples in the furnace.

For the test with nitrogen, the temperature of the furnace was set at 330 °C and they were treated for 3 hours. After this step was finished, the tube was unsealed left for around 10 minutes and then their resistance value was once again measured and the changes were recorded. It is also worth mentioning that changes in the colour of the thin film were found after the treatment with nitrogen. However, this optical change in colour was uniform throughout the sample and these samples were also checked using spectrophotometry to evaluate if there would be any changes in the behaviour of the film but the change was insignificant, as presented previously in Chapter 6 and the next treatment took place after that step.

Next, the samples were treated in open air and the glass tube was not sealed so that the test could be performed. The temperature of the furnace was set at 240 °C and the samples were treated for 16 hours. After this step, the resistance value of the samples was measured. In Figure 7.3, the percentage of the resistance change is shown in relation to the normalised initial resistance value for 15 samples. The figure refers to the two previously mentioned tests, and one line represents the measurements from the exposure to nitrogen and the other one with the samples left in open air. The line which refers to the initial resistance value which was normalised for common point for the comparisons to be made. After the exposure to nitrogen, the samples appear to have a slight increase in their initial value except for sample 12 which appears to have an increase of more than 5% and sample 14 for which a decrease of 5% was recorded. After the open air treatment, the resistance value appears to be decreased for all the samples in relation to the initial value and the decrease has even reached 14% for the case of sample 12. Thus, it is clear that trimming is required in order the resistance value to be adjusted.

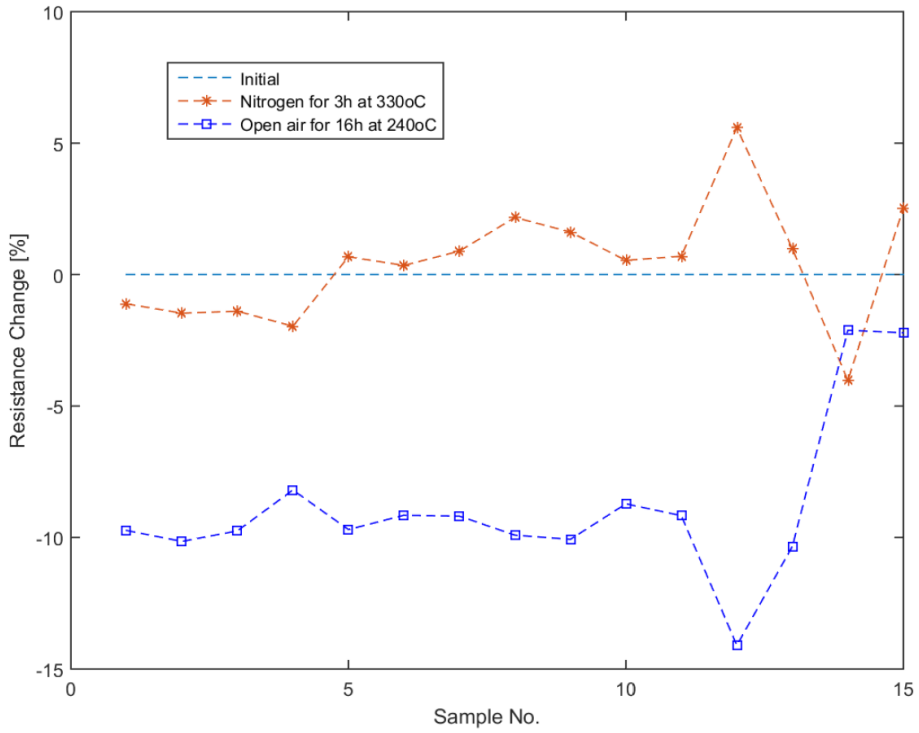

Figure 7.3: Resistance change for 15 samples tested in nitrogen for 3 hours and then in open air for 16 hours.

After the samples were treated with nitrogen and then in open air, these were further tested and were exposed to open air for 7 days for the stability to be checked. The temperature of the furnace was now set at 155 °C and the changes of the resistance value were recorded so that we have the final resistance value.

In Figure 7.4, the percentage of resistance change is shown for 10 samples with normalised initial value. It is clear that most of the samples show a slight increase of the resistance value up to the second day of the test and then it seems that the value is stabilised. The samples S1, S2 and S9 seem to have a large decrease of their resistance value until the second day and then the value becomes stable.

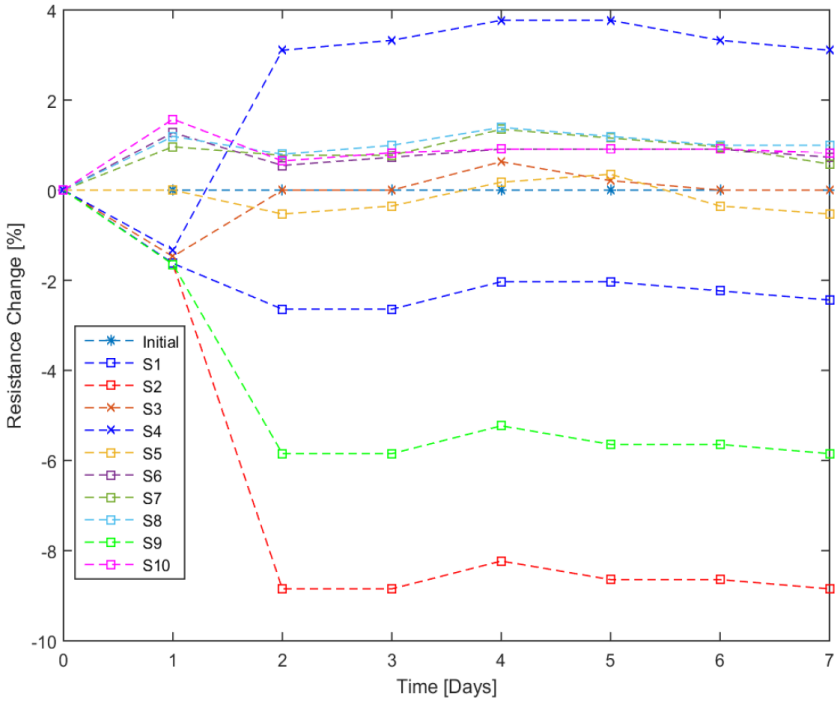

Figure 7.4: Resistance change for 10 samples after dry heat treatment and in open air for 7 days at 155 °C.

Thus, after the results of the 7-day trial, the rest of the batches of the samples were only tested for 2 days, since it gives confidence that the value will be stable after that point. Results for the resistance change for 20 samples for 24 and 48 hours, respectively, are shown in Figure 7.5. The initial resistance value was once again normalised so that there is a common reference point. The trend of the change is similar for most of the samples for both days. It is worth commenting that for this batch of samples the percentage change is quite small with range of 0.05 to 0.35%. The samples that appear to have larger fluctuations are sample number 8, 11, 15 and 20. Sample 8 has an increase in its resistance value of 0.12% while samples 11, 15 and 20 show a decrease up to 0.15%. However, the value in general for all the samples appear to have the same trend and the fluctuations between these 2 days are not that large. Thus, the overall resistance is stable and the samples are ready for laser trimming and further stability tests after the patterns are applied.

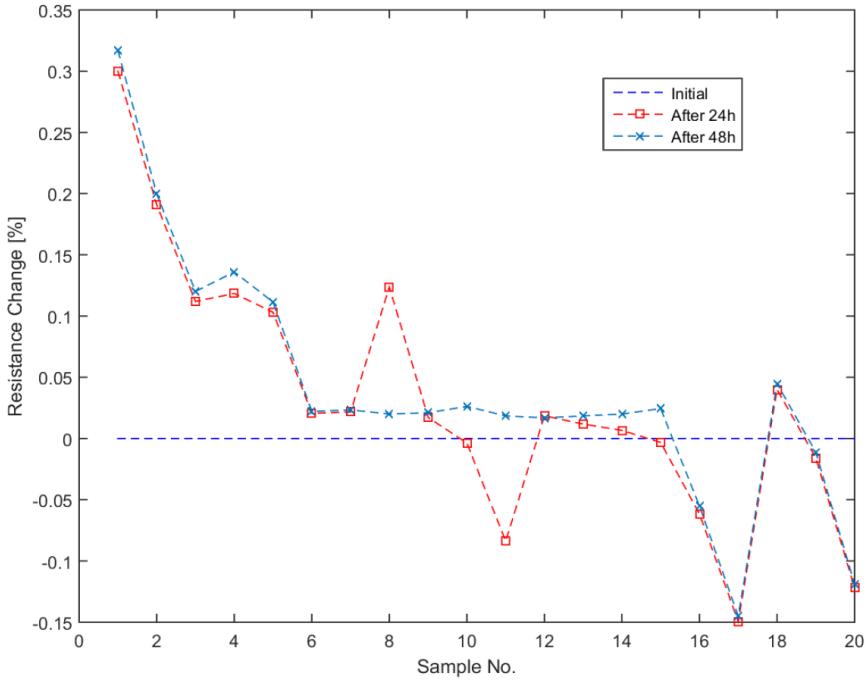

Figure 7.5: Resistance change for 20 dry heat tested samples, left in open air at 155 °C for 24 and 48 hours, respectively.

7.3 Power coefficient of resistance (PCR)

The power coefficient of resistance (PCR) can help to test the stability of the resistor by destabilising thermal shock of suddenly-applied power [136]. The trimmed resistors underwent tests by applying power to them so that the PCR factor to be determined. It is worth commenting that even though PCR is not a well-known factor and not commonly used from manufacturers, it is of great importance since it can show the value of power that a resistor can handle before being damaged or cracked. In general, the PCR is expressed in ppm/W since it is related to the power applied to the resistor [136].

In Figure 7.6, the resistance change is shown in relation to power so that the value of the PCR could be calculated for samples that were trimmed with L-cut, angled L-cut and curved L-cut. The trim length for three designs were 10 mm so that the results were comparable regarding this factor. An increase in the resistance is clearly depicted for all three designs while power was applied to them and as expected the increase of the resistance is higher while higher power was applied to the resistor.

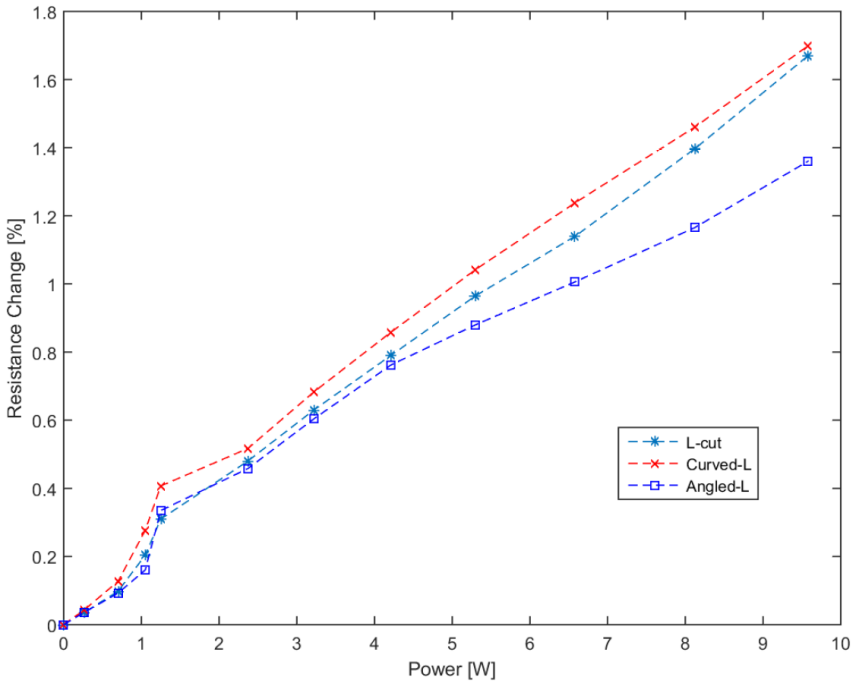

Figure 7.6: PCR based on the resistance change for the L-cut, curved L-cut and angled L-cut.

However, the higher the power, the more changes in colour of the film appeared in the resistor and especially at the part above the x leg of the cut where the current density is higher as generally expected. It is a common fact that the current flows from the contact and it travels through the area above the x-leg until it reached the next contact. When power above 10 W was applied to the resistors, the sample started to show damages and some of them even started to crack.

In Figure 7.7, the resistance change is shown in relation to power for the case of the semi-circle with radius of 4 mm. It is clear that this type of cut gives a larger increase in the resistance as discussed in previous chapters and the power applied to it was adjusted respectively. The error bars represent the resistance change for the 10 reference samples. A sudden increase is happening when power of 0.5 W is applied to the samples and then there is a decrease but overall the change of the resistance value is increased until the highest value of the power is applied to the samples. Once again, the higher the power applied to the samples, the larger the changes in colour and after a certain point damage or small cracks started to appear due to possible thermal shock. As shown in Figure 7.7, the highest power applied to the samples for this case was 10 W.

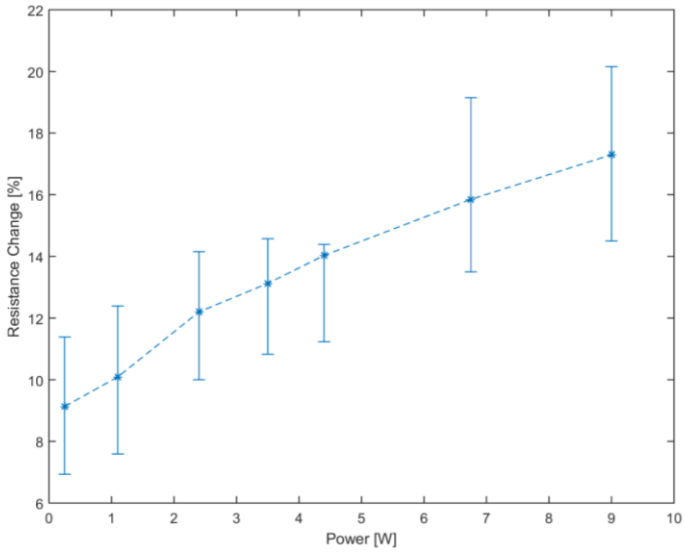

Figure 7.7: PCR for the case of the semi-circle pattern for r = 4 mm based on the change of the resistance for 10 samples.

The case of the elliptical cut with dimensions of a = 5 mm and b = 4 mm before and after application of power is shown in Figure 7.8. It is clear that the cut is uniform and the HAZ around the cut is not visible by human eye at this stage in Figure 7.8 (a). However, in Figure 7.8 (b), the point of the top of the cut in the centre the damage of the film due to the high power applied to it is obvious and this is the high current density area.

Figure 7.8: (a) Thin film resistor trimmed with the elliptical cut before application of power, (b) the resistor after application of higher power value.

The PCR for the case of the elliptical cut is shown in Figure 7.9. The resistance change in relation to the power is presented for the case of the previous mentioned sample trimmed with the elliptical cut. The error bars represent the changes between the samples that were trimmed with the same dimensions. It is shown that there is a small increase on the resistance when the lower power of around 0.4 W is applied to the sample and then the resistance seems to decrease slightly and then increase again.

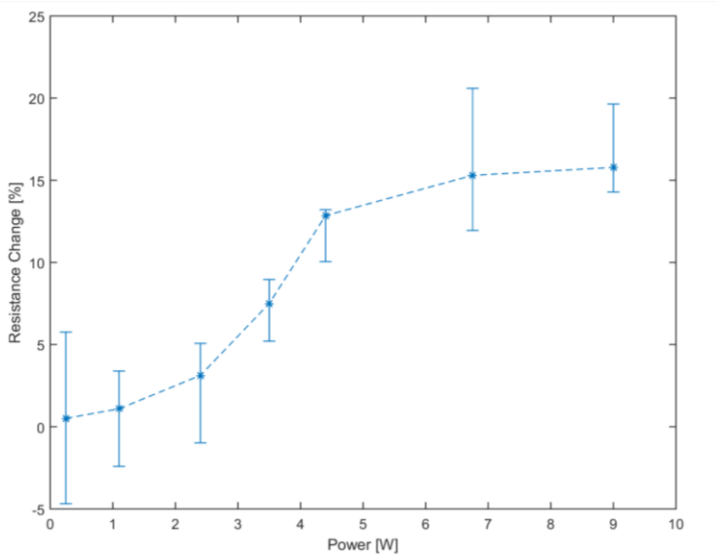

Figure 7.9: PCR for the case of the elliptical cut for a = 5 mm and b = 4 mm based on the resistance change for 10 samples.

Overall, the change in the resistance appears to have a similar trend throughout the measurements showing a small increase until the higher power of 11.5 W was applied to the sample. The trend of the resistance change for the case of the elliptical cut appears to be similar to the semi-circle one, even though in that case the change has shown more fluctuations and also the higher power applied to it was a bit higher due to the fact that there was a higher resistance gain after the trimming.

7.4 Evaluation of the experimental results in relation to simulations

7.4.1 Resistance change

In this section, the experimental and simulation results are evaluated for the different geometries. One comparison refers to the difference in the value of the resistance change based on experimental and simulation results in relation to the trim length. The process of the experiment and simulations were discussed in previous chapters. Thus, in Figure 7.10, the results for the L-cut is shown in relation to the trim length. As shown the length of the cut is 10 mm and it refers to an L-cut with y = 3 mm and x = 7 mm.

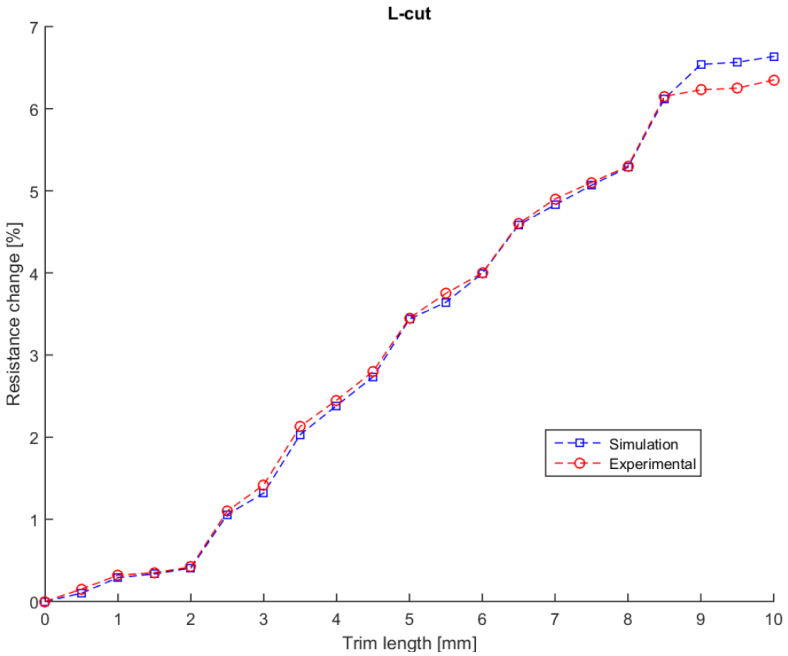

Figure 7.10: Resistance change vs trim length comparing experimental and simulation results for the case of the L-cut.

According to the simulation the resistance change is not that high, even though it is increased as the cut progressed and the trim length was changed. There is an obvious increase in the resistance in general shown in both simulation and experiments but the percentage of the resistance change from the experiments can reach up to 6.8%. It is shown that the results from simulations and the results from experiments are quite close, even identical at some points and they follow the same trend for the case of the L-cut. Some fluctuations appear after the 8 mm between the experimental and simulation results.

As for the angled L-cut, the trend appears to be similar to both experimental and simulation resistance change. In Figure 7.11, the results of the resistance change are presented in relation to the trim length as the previous case of the L-cut. There are small fluctuations which can be defined due to the fact that simulations usually correspond to ideal conditions while the experiments are affected from many external factors such as temperature, equipment fault and clarity of the cut. Also, the experimental value appears to be a bit smaller than the simulation one at 6.5 kΩ and 6.55 kΩ, respectively, but the values are still really close with each other.

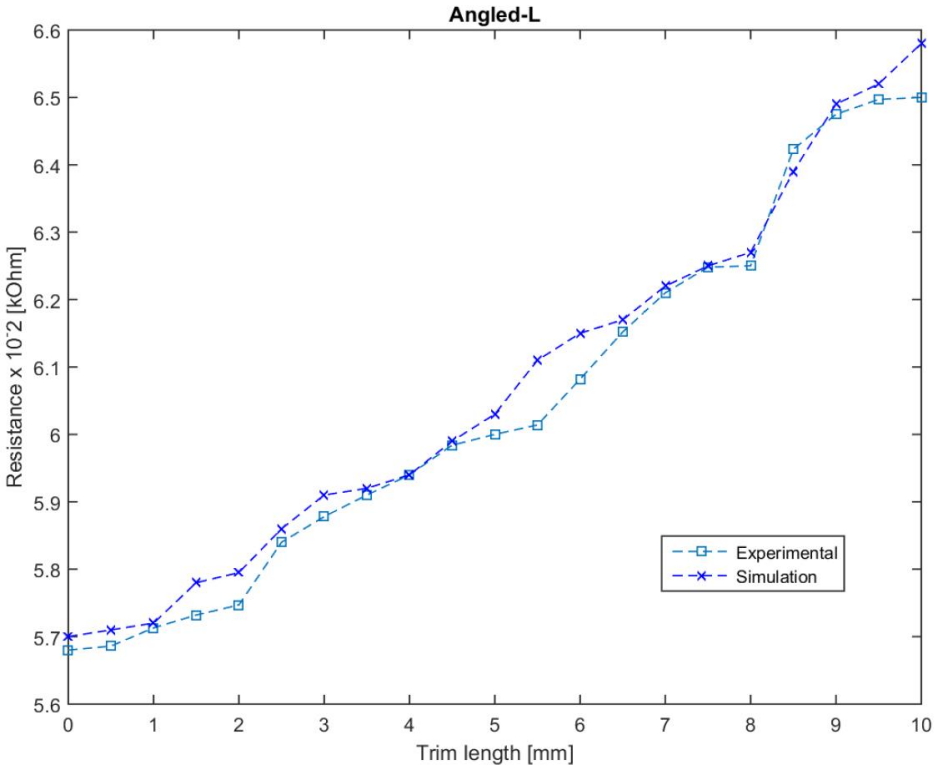

Figure 7.11: Resistance change vs. trim length comparing experimental and simulation results for the case of the angled L-cut.

The curved L-cut, on the other hand, has the same resistance increase in both simulations and experiments until the point in which the curve starts and then the increase is proportional and gradual. It is shown, in Figure 7.12, that it reaches the value of 13 kΩ and 12.3 kΩ for the simulation and experimental result for the higher trim length of 14 mm.

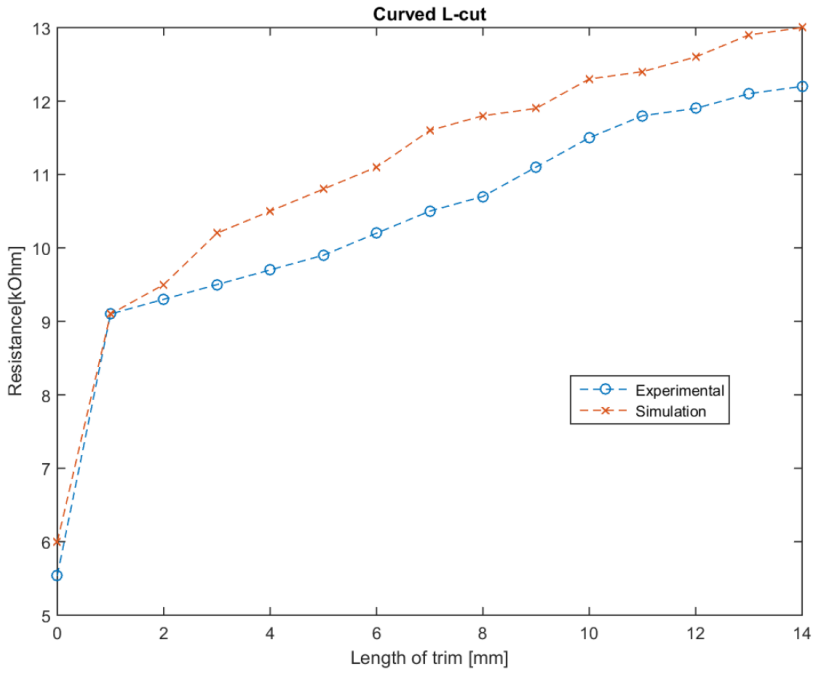

Figure 7.12: Resistance change vs. trim length comparing experimental and simulation results for the case of the curved L-cut.

As for the case of the semi-circle, some fluctuations of the resistance change between experimental and simulation results appear, see Figure 7.13. The change of the resistance value can reach up to 25 % for trim length of 9.42 mm, based on the calculation of the circumference for the experimental results. While the change of the value for the simulation results is around 23% for the same trim length.

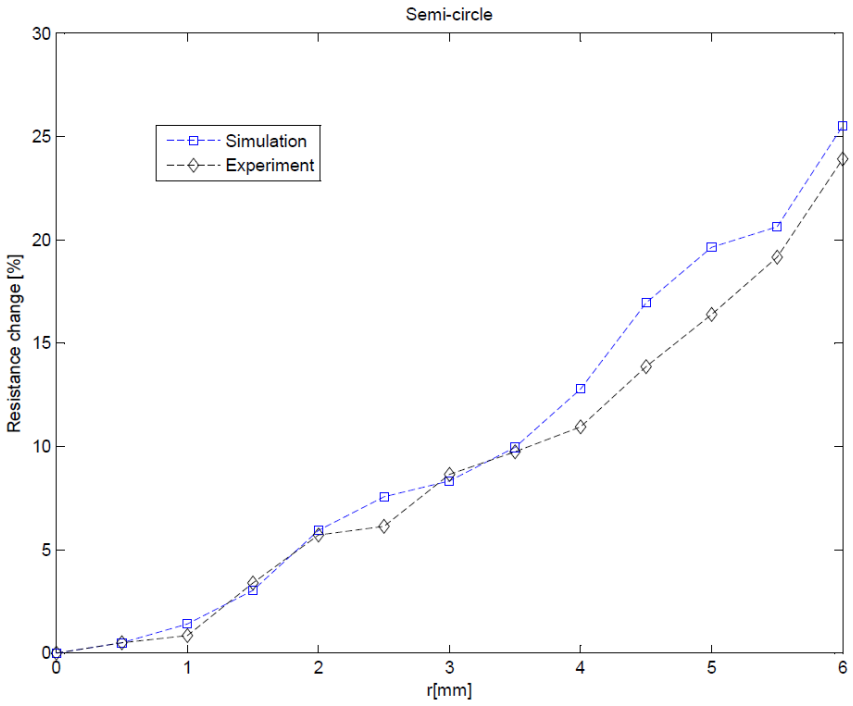

Figure 7.13: Resistance change vs trim length comparing experimental and simulation results for the case of the semi-circle.

7.5 Temperature change

In this section, the temperature change is calculated for the trim patterns that were investigated previously. For the experiments, the temperature was measured in relation to the power applied to the sample each time and the values were recorded. These measurements along with the experimental values that were produced using ANSYS, were plotted and the case of the L-cut is presented in Figure 7.14. It is shown that the temperature can reach up to 90 °C in the simulation results while for the experiments the highest value was 80 °C for a power of 5 W for both cases. The increase of the temperature value is high for both sets of results and the increase is steady.

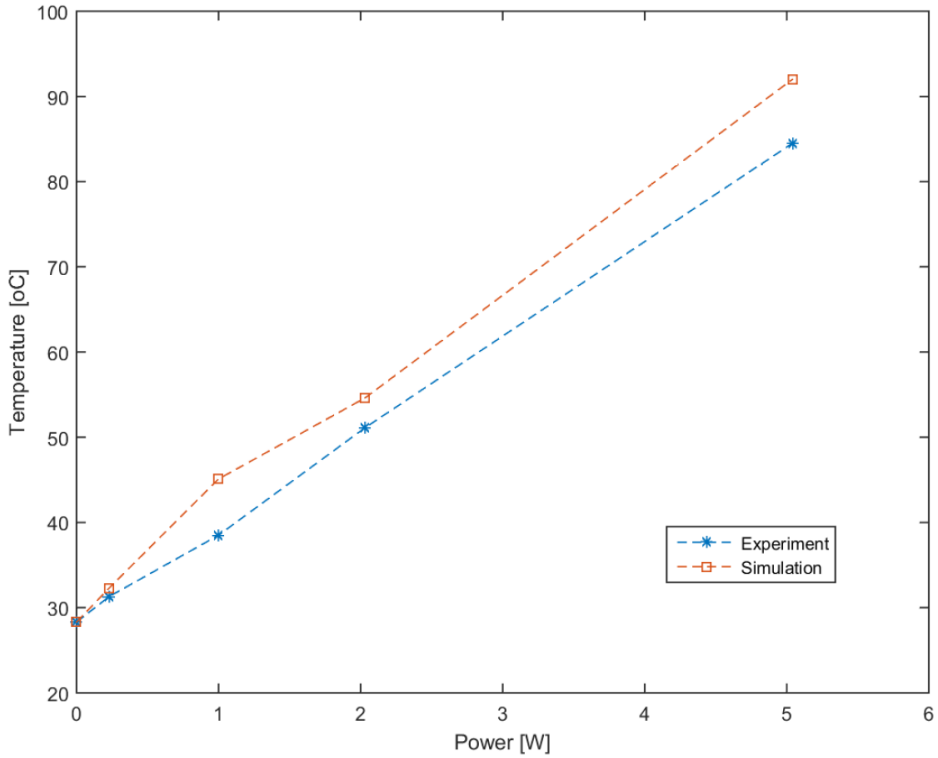

Figure 7.14: Simulation and experimental results for the L-cut.

On the other hand, the temperature of the angled L-cut, as shown in Figure 7.15, was higher for the experimental part rather than the value from the simulations with 69 and 65 °C, respectively. There are a few fluctuations between the two sets of the results but overall the trend is the same regarding the temperature increase.

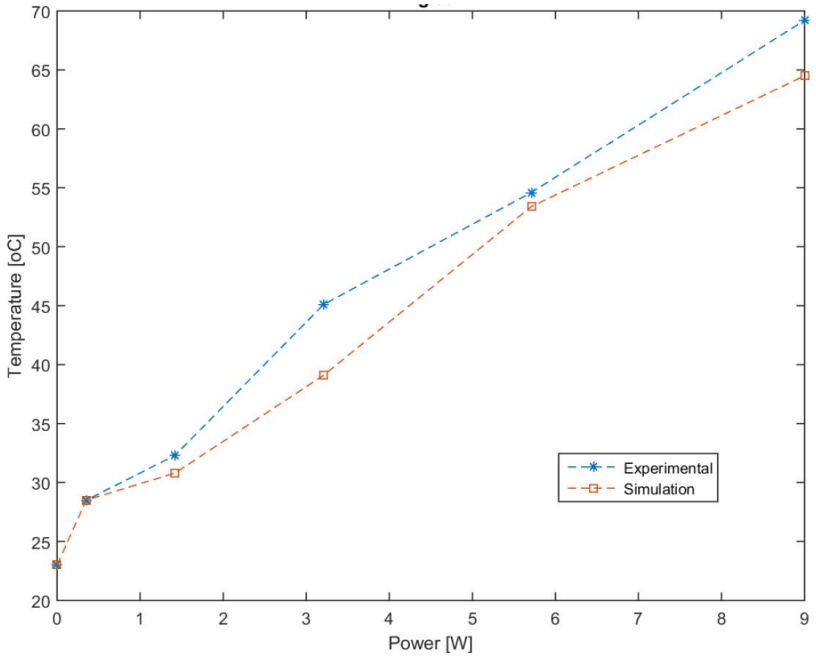

Figure 7.15: Simulation and experimental results for the angled L-cut.

As for the curved L-cut, see Figure 7.16, the temperature of the experimental part was lower than the one from the simulations with 81 and 82 °C, respectively. There are a few fluctuations between the two sets of the results but once again overall the trend is the same even though it seems that it increases faster when a power of 2 W is applied to the sample on the simulation part.

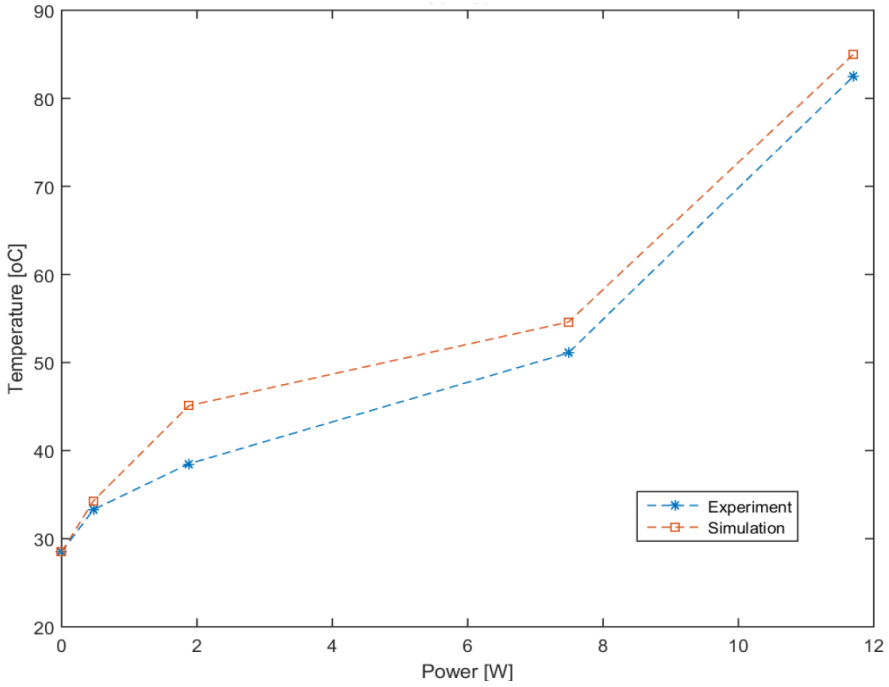

Figure 7.16: Simulation and experimental results for the curved L-cut.

As for the semi-circle, as shown in Figure 7.17, the temperature of the experimental part was higher than the one from the simulations with 78 and 76 °C, respectively. There are a few fluctuations between the two sets of the results but once again overall the trend is the same since the higher the power applied to the sample the higher the increase in temperature.

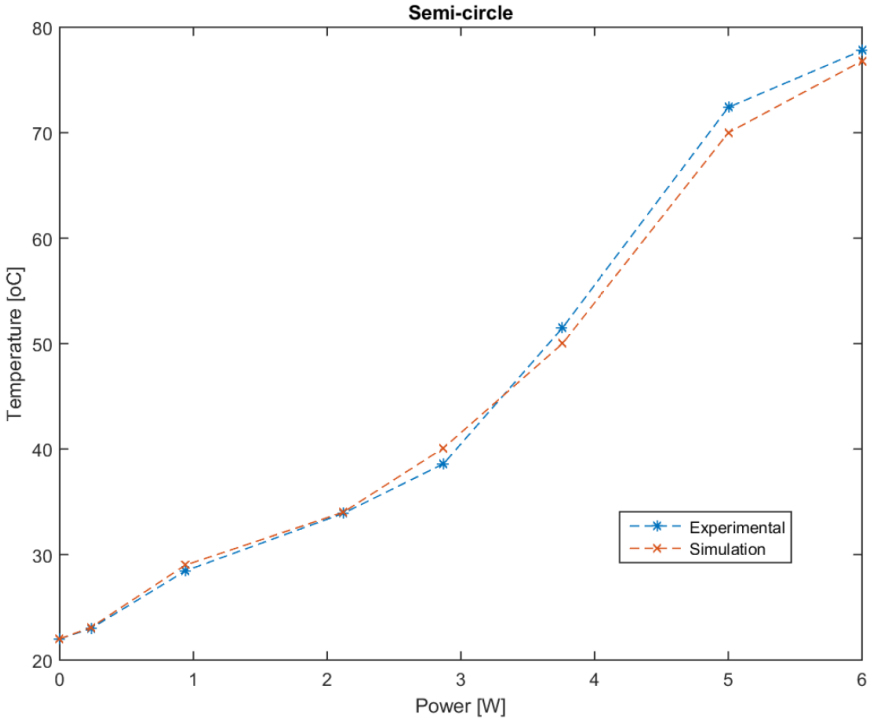

Figure 7.17: Simulation and experimental results for the semi-circle.

7.6 Summary

In this chapter, the verification of the results of the laser trimming was presented. A comparison of the different trim patterns in relation to the resistance change based on experimental and simulation results was investigated. It was shown that both experimental and simulation results were similar for the trim patterns. In addition to this, the temperature measurements in relation to the power applied to the samples with a variety of patterns was also analysed so that the PCR could be determined and clarify the performance of the resistors.

In most cases, the trimming patterns appeared to have similar trends in relation to PCR values and temperature change. The L-cut had the higher change in temperature in comparison with the other cuts while the angled L-cut had the lower increase in temperature which reached up to 65 °C.

8 Conclusions

The research detailed in this thesis has investigated different trim geometries so that the laser trimming method is improved and the patterns were compared in relation to various factors such as the laser trimming time, resistance gain, stability and tolerance accuracy.

In general, laser trimming is an expensive processing step which significantly increases the production costs of integrated circuits from trimming costs. That is the reason why basic and novel geometries were modelled and tested experimentally so that their performance could be assessed. The modelling has shown significant results in relation to the temperature change and the resistance value for the trimming patterns. The numerical simulation was proven very effective and offered reliable results which were extremely close to the experimental ones. An analysis based on the sensitivity of the pattern to the HAZ was also calculated for the basic patterns and the results were a close match to previous studies and reports.

The modelling of the geometries was initially verified experimentally using conductive paper which was used in previous similar studies. Conductive paper proved to be a challenging material regarding its repeatability and overall behaviour. However, it was generally used easily and it offered results fast for the first stages of the verification of the model. Thus, it can be used with confidence in order to emulate resistors and use it for trials with trimming patterns. The experiments were focused on the change of the resistance, TCR and temperature of various common and novel patterns. Thus, it is found that variation in trimming shape and length, has a direct effect on the performance of resistors giving significant increases in the TCR of the resistor. In the case of the trials on the conductive paper, the TCR for the plunge cut reached up to 18.29 ppm/°C and when an additional plunge is added (double plunge), decreased to a value of 14.21 ppm/°C. As for the L-cut, the TCR was found 11.86 ppm/°C and for the scan cut 17.89 ppm/°C. However, for the novel patterns, the TCR for the curved L reached up to 17.22 ppm/°C while the value was found to be lower for the semi-circle at 8.52 ppm/°C. As for the HAZ, it is found that the L-cut has a lower sensitivity to the HAZ, with a value of 10%, in relation to the other patterns.

The processing parameters of the laser cutter which was used, were set after a series of trials so that the optimum settings could be used for the trimming of the films. The laser power, laser speed and frequency were assessed for the materials used for this research. In addition to this, the dimensions of the thin film resistor that was used for the experiments was set at 21 x 6 mm. The samples were also compared based on their reflectance since there has been a variety of batches and thicknesses. The novel patterns and the common pattern of the L-cut were applied to the thin films in a variety of trim lengths and start

positions. Based on both simulation and experimental results the semi-circle has proven to give the largest resistance increase in less time in relation to the others. The L-cut is the most popular cut and this fact was verified from the trials of this study in comparison with the other patterns.

The patterns were also assessed for other factors such as the PCR and laser trimming time. The semi-circle can be used in cases needing a large resistance increase, as the film was cut in less time. It was proven that the trim length is the most important factor that affects the trimming time and resistance gain. It is also shown that the higher the power applied to the resistor, the higher was the temperature increase and the L-cut appeared to have the largest temperature increase. As for the PCR, most of the designs appeared to have a similar trend.

To sum up, the results obtained from modelling were extremely close and could verify reliably the experimental results. The L-cut was proven to be one of the most reliable ones based on its repeatability and resistance gain. The angled L-cut and the curved L-cut even though they are variations of the L-cut are not as good as the common pattern even though their characteristics are similar. As for the elliptical cut, it was shown that it can give a large resistance increase since the length of the trim was longer, hence more laser trimming time was needed. The semi-circle pattern can be thought as an alternative geometry for applications where large resistance increase is needed and its cost is slightly reduced due to less trimming time. It also appears to have a similar behaviour with the other patterns in relation to temperature increase and PCR.

8.1 Financial benefits

This research has not investigated the financial benefits of using the new geometries but it can estimate the advantages they have over the common trim patterns. The novel geometries offer a small reduction of trimming time which eventually lead to financial benefit since the production cost will be reduced at a certain point without the performance of the resistor being affected. For instance, the novel trim patterns and especially the semi-circle one offers a high trim gain in a reduced trimming time.

8.2 Suggestions for future research

This section highlights the potential areas worthy of further consideration.

8.2.1 Optimisation of the prediction algorithm for the HAZ

An algorithm that can predict the exact amount of HAZ surrounding the cut. This study tried to express an estimation of the HAZ based on the sensitivity of the cut. However, an algorithm that can actually predict the area affected by the removal of the film can be beneficial for further optimisation of the performance of the resistor.

8.2.2 Prediction algorithm for the optimum trim pattern

Another algorithm that could be developed would be the one that can predict the optimum trim pattern based on the performance needs. A code that can estimate the best geometry depending on the characteristics and the use of the resistor.

9 References

1. Birkett, M., *OPTIMISATION OF THE PERFORMANCE CHARACTERISTICS OF Cu-Al-Mo THIN FILM RESISTORS*. 2009, Northumbria University. p. 251.
2. Birkett, M. and R. Penlington, *Laser Trimming of CuAlMo Thin-Film Resistors: Effect of Laser Processing Parameters.* Journal of Electronic Materials, 2012. **41**(8): p. 2169-2177.
3. Elshabini-Riad, A.B., Fred, *Thin Film Technology Handbook*. 1998, New York: McGraw-Hill Publishing. 800.
4. Sandborn, P.S., P., *Using embedded resistor emulation and trimming to demonstrate measurement methods and associated engineering model development.* International journal of engineering education, 2006. **22**(1): p. 1-7.
5. Sandborn, P.S., P., *A random trimming approach for obtaining high-precision embedded resistors.* IEEE transactions on advanced packaging, 2008. **31**(1): p. 76-81.
6. Hobbs, P., *Building Electro-Optical Systems: Making it all work*. 2nd ed. 2008. 820.
7. Deluca, P., *A review of thirty-five years of laser trimming with a look to the future.* Proceedings of the IEEE, 2002. **90**(10): p. 1614-1619.
8. Vishay, *Precision Thin Film Technology*. 2015: United States. p. 1-28.
9. Barlage, M., *A stability study of laser patterned thermally stabilized tantalum nitride and tantalum aluminium films.* IEEE Transactions on parts, hybrids and packaging, 1973(PHP-9(2)): p. 123-130.
10. Bos, L., *Performance of thin film chip resistors.* IEEE Transactions on Components, Packaging, and Manufacturing Technology: Part A, 1996. **17**(3): p. 359-365.
11. Bulger, G., *Stability analysis of laser trimmed thin film resistors.* IEEE Transactions on parts, hybrids and packaging, 1975(PHP-11(3)): p. 172-177.
12. Birkett, M.P., R., *Laser Trim Pattern Optimization for CuAlMo Thin-Film Resistors.* IEEE Transactions on Components, Packaging and Manufacturing Technology, 2013. **3**(3): p. 523-529.
13. Kamiński, S.M., Edward;Szymendera,Maciej;Dziedzic,Andrej, *New trim configurations for laser trimmed thick-film resisotrs-Experimental verification.* International Microelectronics and Packaging Society, 2005. **2**(1): p. 1-6.
14. Maissel, L.G., R., *Handbook of Thin Film Technology*. 1970: McGraw-Hill Publications. 18-24.
15. Schimmanz, K.J., S.M., *Film Resistor Design for High Precision Laser Trimming.* Preprint BTU-Cottbus M, 2002: p. 1-13.
16. Ramirez-Angulo, J.G., R., *New laser trimmed film resistor structures for very high stability requirements.* IEEE Transactions on electron devices, 1988. **35**(4): p. 516-518.
17. Nowak, D.M., Edward;Dziedzic,Andrzej;Kita,Jaroslaw, *Fabrication and electrical properties of laser-shaped thick-film and LTCC microresistors* Microelectronics reliability, 2009. **49**: p. 600-606.
18. Nowak, D.D., Andrzej;Hrovat,Marko;Cilensek,Jena. *Miniaturization of thick film resisotrs by laser shaping*. in *33rd International Spring Seminar on Electronics Technology-ISSE 2010*. 2010.
19. Mazda, F.F., *Electronic Engineer's Reference Book*. 6th ed. 1989, Cornwall: Butterworth & Co.
20. Zandman, F., P.R. Simon, and J. Szwarc, *Resistor theory and technology*. 2002: Vishay Intertechnology, Inc.
21. Singh, S.C.Z., H.B.;Guo,C.;Cai,W.P., *Nanomaterials: Processing and Characterisation with Lasers*. 2012, Weinheim,Germany: Wiley-VCH Verlag & Co.
22. Jaeger, R., *Introduction to Microelectronic Fabrication*. 2nd ed. 2002, New Jersey: Prentice Hall.

23. Laboratory, H. *Thin Film Deposition*. 2015 [cited 2017 05/05/2017]; Available from: http://hivatec.ca/consulting-design/thin-film-deposition/.
24. Boo, J.-H., et al., *High-rate deposition of copper thin films using newly designed high-power magnetron sputtering source.* Surface and Coatings Technology, 2004. **188-189**: p. 721-727.
25. Chopra, K.L.K., I., *Thin Film Device Applications*. 1st ed. 1983, Boston,MA: Springer.
26. Qiu, H.W., Fengping; Wu, Ping; Pan, Liqing; Li, Lingyu; Xiong, Liangyon; Tian, Yue, *Effect of deposition rate on structural and electrical properties of Al films deposited on glass by electron beam evaporation.* Thin solid films, 2002. **414**(1): p. 150-153.
27. Chan, K.-Y. and B.-S. Teo, *Sputtering power and deposition pressure effects on the electrical and structural properties of copper thin films.* Journal of Materials Science, 2005. **40**(22): p. 5971-5981.
28. Radhakrishnan, K.G.I., Ng; Gopalakrishnan, R *Reactive sputter deposition and characterization of tantulum nitride thin films.* Materials Science & Engineering B, 1999. **57**(3): p. 224-227.
29. Ramana, C.V., et al., *Growth and surface characterization of sputter-deposited molybdenum oxide thin films.* Applied Surface Science, 2007. **253**(12): p. 5368-5374.
30. Zandman, F.S., Paul-Rene;Szwarc,Joseph, *Resistor Theory and Technology*. 2002: Vishay Intertechnology. 321.
31. Cho, N.-I., et al., *Chemical vapor deposition of copper thin films for multi-level interconnections.* Microelectronic Engineering, 2003. **66**(1-4): p. 415-421.
32. Chou, W.-J., et al., *Optimization of the deposition process of ZrN and TiN thin films on Si(1 0 0) using design of experiment method.* Materials Chemistry and Physics, 2003. **82**(1): p. 228-236.
33. Chowdhury, S., M.T. Laugier, and I.Z. Rahman, *Effects of substrate temperature on bonding structure and mechanical properties of amorphous carbon films.* Thin Solid Films, 2004. **447-448**: p. 174-180.
34. Galdikas, A., *Thin film deposition onto the rough surface phenomenological investigations.* Thin solid films, 2002. **418**(2): p. 112-118.
35. Akiyama, M.H., Tomohiro; Xu, Chao-Nan; Nonaka, Kazuhiro; Watanabe, Tadahiko *Preparation of highly oriented AlN thin films on glass substrates by helicon plasma sputtering and design of experiments.* Thin solid films, 1999. **350**(1): p. 85-90.
36. Akiyama, M.X., Chao-Nan; Nonaka, Kazuhiro; Shobu, Kazuhisa; Watanabe, Tadahiko *Statistical approach for optimizing sputtering conditions of highly oriented aluminium nitride thin films.* Thin solid films, 1998. **315**(1): p. 62-65.
37. Misiano, C. *Thin Film Depositions: the ion-plating technique.* in *HeRe*. 2013. Italy.
38. Robbemond, A.a.T., Barend J *Ion-beam assisted deposition of thin molybdenum films studied by molecular dynamics simulation.* Nuclear Inst. and Methods in Physics Research, 1997. **127**: p. 273-277.
39. Grebe, K.A., I.;Ginzberg,A., *Masking of deposited thin films by means of an aluminum-photoresist composite.* Journal of Vacuum Science and Technology, 1974. **11**(458).
40. Marin, G., *Inclined lithography and photoresist optimization for fabrication of 3D mesh structures*. 2014, Aalto University. p. 80.
41. Wei, A.C. *Composition and photochemical mechanisms of photoresists*. [cited 2017 05/05/2017]; Available from: https://archive.cnx.org/contents/2997481b-ecd7-4e38-9465-677d8adbe0ad@2/composition-and-photochemical-mechanisms-of-photoresists.
42. Adams, T.M. and R.A. Layton, *Introductory MEMS: Fabrication and Applications*. 2008: Springer US.
43. Feng, X., et al., *Thermo-physical properties of thin films composed of anatase TiO2 nanofibers.* Acta Materialia, 2011. **59**(5): p. 1934-1944.
44. Brückner, W. and S. Baunack, *Electrical resistance and mechanical stress in NiCr/Cu/NiCr thin films.* Journal of Applied Physics, 1999. **85**(2): p. 935.

45. Takizawa, Y.S., Katsuo *Corrosion resistant Ni-Cr-Mo alloys in hot concentrated sulphuric acid with active carbon.* Materials Science & Engineering A, 1995. **198**(1): p. 145-152.
46. Thiel, R.a.M., E *TCR control of NiCr Resistors.* IEEE Transactions on Components, Hybrids, and Manufacturing Technology, 1979. **2**(4): p. 467-475.
47. Ishikawa, M.E., Hidehiko; Mikamoto, Naohiro; Nakamura, Tsuneshi; Matsuoka, Masao; Iwakura, Chiaki *Preparation of thin film resistors with low resistivity and low TCR by heat treatment of multilayered Cu/Ni deposits.* Surface & Coatings Technology, 1998. **110**(3): p. 121-127.
48. Keenan, W.F., *Pulsed overload tolerance of SiCr/NiCr and Mo/Si thin film resistors on integrated circuits.* IEEE Transactions on reliability, 1976. **R-25**(4): p. 248-254.
49. Kazi, I.H., et al., *Characterization of sputtered nichrome (Ni–Cr 80/20 wt.%) films for strain gauge applications.* Thin Solid Films, 2006. **515**(4): p. 2602-2606.
50. Petrović, S., et al., *Surface composition and structure of Ni–Cr sputtered coatings exposed in air at room temperature.* Nuclear Instruments and Methods in Physics Research Section B: Beam Interactions with Materials and Atoms, 2007. **256**(1): p. 368-372.
51. Prudenziati, M. and M.L. Gualtieri, *Electrical Properties of Thermally Sprayed Ni- and Ni20Cr-Based Resistors.* Journal of Thermal Spray Technology, 2008. **17**(3): p. 385-394.
52. Kwon, Y., et al., *Structural and surface properties of NiCr thin films prepared by DC magnetron sputtering under variation of annealing conditions.* Microelectronic Engineering, 2005. **82**(3-4): p. 314-320.
53. Privitera, S.L.N., Olivier; Leung,Calvin; Dumont-Girard,Pascale; Cialdella,Bruno;Bongiorno,Corrado;Modica,Roberto, *Morphological and electrical characterization of electrically trimmable thin-film resistors.* IEEE Transactions on electron devices, 2012. **59**(12): p. 3549-3554.
54. Cho, N.-I. and M.C. Kim, *Preparation of Cr–Si multilayer structures for thin film heater applications.* Thin Solid Films, 2005. **475**(1-2): p. 235-238.
55. Kang, S.M., et al., *Control of electrical resistivity of TaN thin films by reactive sputtering for embedded passive resistors.* Thin Solid Films, 2008. **516**(11): p. 3568-3571.
56. Wang, C.M., et al., *Electrical properties of TaN–Cu nanocomposite thin films.* Ceramics International, 2004. **30**(7): p. 1879-1883.
57. Wang, C.M., J.H. Hsieh, and C. Li, *Electrical and piezoresistive properties of TaN–Cu nanocomposite thin films.* Thin Solid Films, 2004. **469-470**: p. 455-459.
58. Waits, R.K., *Silicon-chromium thin-film resistor reliability.* Thin solid films, 1973. **16**(2): p. 237-247.
59. Vinayak, S., et al., *Ni–Cr thin film resistor fabrication for GaAs monolithic microwave integrated circuits.* Thin Solid Films, 2006. **514**(1-2): p. 52-57.
60. Brückner, W.S., J; Baunack, S; Pitschke, W; Knuth, Th *Resistance behaviour and interdiffusion of layered CuNi-NiCr films.* Thin solid films, 1995. **258**(1): p. 236-246.
61. Na, S.-M., et al., *Electrical and structural properties of Ta–N thin film and Ta/Ta–N multilayer for embedded resistor.* Thin Solid Films, 2008. **516**(16): p. 5465-5469.
62. Hoffman, H.a.S., E *Cermet resistors on ceramic substrates.* IEEE Transactions on Components, Hybrids, and Manufacturing Technology, 1981. **4**(4): p. 387-395.
63. Meier, M., et al., *Laser trimming of amorphous Ta42Si13N45 thin films with ultrashort pulses.* Microelectronic Engineering, 2006. **83**(11-12): p. 2234-2237.
64. Chinoy, P. and M. Langlois, *Thin-film embedded resistor and capacitor technologies.* Circuit World, 2004. **30**(1): p. 16-19.
65. Kasap, S.C., P., *Thick Films*, in *Handbook of Electronic and Photonic Materials*, N. White, Editor. 2017, Springer: Cham.
66. Moon, Y.-K., S.-H. Kim, and J.-W. Park, *The influence of substrate temperature on the properties of aluminum-doped zinc oxide thin films deposited by DC magnetron sputtering.* Journal of Materials Science: Materials in Electronics, 2006. **17**(12): p. 973-977.

67. Mishra, S.K., et al., *Effect of pressure and substrate temperature on the deposition of nano-structured silicon–carbon–nitride superhard coatings by magnetron sputtering.* Thin Solid Films, 2007. **515**(11): p. 4738-4744.
68. Palasantzas, G., *Thickness dependant thermal capacitance of thin films with rough boundaries.* Solid State Communications, 2002. **122**(10): p. 523-526.
69. Podda, S.C., G.;Fantini,F.;Vanzi,M., *Failure Analysis of RuO2 Thick Film Chip Resistors.* Microelectronics Reliability, 2004. **44**(9-11): p. 1763-1767.
70. Vishay, *THIN / THICK FILM CHIP RESISTORS*. 2015.
71. Panzini, M.I., *Thick Films: Properties, Technology, and Applications*. 2012: Nova Science Publishers.
72. Horst, S., *LOW COST FABRICATION TECHNIQUES FOR EMBEDDED RESISTORS ON FLEXIBLE ORGANICS AT MILLIMETER WAVE FREQUENCIES*, in *School of Electrical and Computer Engineering*. 2006, Institute of Technology: Georgia
73. Kurihara, Y.T., S; Yamada, K; Kanai, K; Endoh, T *Laser trimming of thick film resistors on aluminum nitride substrates.* IEEE Transactions on Components, Hybrids, and Manufacturing Technology, 1990. **13**(3): p. 596-602.
74. Li, C.-H. and M.-J. Tsai, *3D laser trimming technology for regulating embedded thick-film carbon resistors on a random access memory module.* Journal of Materials Processing Technology, 2009. **209**(4): p. 2057-2067.
75. Kinzel, E., *LASER MICROFABRICATION OF THICK-FILM MICROELECTRONICS*. 2005, Purdue University.
76. Ramirez-Angulo, J.G., R.; Sanchez-Sinencio,E., *Characterisation, evaluation and comparison of laser-trimmed film resistors.* IEEE Journal of solid-state circuits, 1987. **22**(6): p. 1177-1189.
77. Shen, H. and R. Ramanathan, *Fabrication of a low resistivity tantalum nitride thin film.* Microelectronic Engineering, 2006. **83**(2): p. 206-212.
78. Shi, J.R.S., X; Lau, S.P; Sun, Z; Tay, B.K; Tan, H.S *Structural and electrical properties of copper thin films prepared by filitered cathodic vacuum arc technique.* Surface & Coatings Technology, 2001. **138**(2): p. 250-255.
79. Birkett, M., et al., *Structural and electrical properties of CuAlMo thin films prepared by magnetron sputtering.* Thin Solid Films, 2013. **540**: p. 235-241.
80. Chan, K.-Y., T.-Y. Tou, and B.-S. Teo, *Effects of substrate temperature on electrical and structural properties of copper thin films.* Microelectronics Journal, 2006. **37**(9): p. 930-937.
81. Chan, K.-Y., T.-Y. Tou, and B.-S. Teo, *Thickness dependence of the structural and electrical properties of copper films deposited by dc magnetron sputtering technique.* Microelectronics Journal, 2006. **37**(7): p. 608-612.
82. Chemistry, R.S.o., *Anodisation*, in *Royal Society of Chemistry*. 2016, Royal Society of Chemistry.
83. Hess, D.W., *Plasma-assisted oxidation, anodisation, and nitridation of silicon.* IBM Journal of Research and Development, 1999. **43**(1-2): p. 127-145.
84. Seshan, K., *Handbook of Thin Film Deposition*. 2nd ed. 2001. 430.
85. Wang, C.M., et al., *Effects of annealing on the microstructure and electrical properties of TaN-Cu nanocomposite thin films.* Surface and Coatings Technology, 2005. **193**(1-3): p. 173-177.
86. Alaa M. Abd-Elnaiem; A.M. Mebed;A. Gaber2; M.A. , A.-R., *Effect of the Anodization Parameters on the Volume Expansion of Anodized Aluminum Films.* International Journal of ELECTROCHEMICAL SCIENCE, 2013. **8**: p. 10515-10525.
87. Holtje, M., *Apparatus for high speed resistor trimming*. 1974, General Radio Company, Concord, Mass. : United States. p. 1-9.
88. Wang, K.L., P.H.;Lu,D.;Lu,Z;Lennon,A.;. *Stored charge in anodic aluminium oxide passivation layers for silicon solar cells*. in *21st International Photovoltaic Science and Engineering*

Conference. 2011. Fukuoka, Japan: 21st International Photovoltaic Science and Engineering Conference.

89. R.G. Buchheit, R.K.B., M.C. Carroll, R.M. Leard, C. Paglia, and J.L. Searles, *The Electrochemistry of Intermetallic Particles and Localized Corrosion in Al Alloys.* The Journal of The Minerals, Metals & Materials Society (TMS), 2001. **53**(7): p. 29-33.

90. Lins, S., J., *PRECISION ELECTRICAL COMPONENT*

ADJUSTMENT METHOD 1968, Sperry Rand Corporation: United States. p. 1-10.

91. Xin, X.L., B., *High Precision Low Temperature Coefficient Current Reference*

with Resistor Compensation in *The 2nd International Conference on Computer Application and System Modeling*. 2012: Paris,France. p. 1-5.

92. Babcock, J.A.P., S.J., *Precision Electrical Trimming of Very Low TCR*

Poly-SiGe Resistors. IEEE ELECTRON DEVICE LETTERS, 2000. **21**(6): p. 283-286.

93. Feldbaumer, D.W.B., J.A; Mercier, V.M; Chun, C.K.Y *Pulse Current Trimming of Polysilicon Resistors.* IEEE Transactions on Electron Devices, 1995. **42**(4): p. 689-696.

94. Boella, G. and F. Galliana, *Analysis of the voltage coefficient of high value standard resistors.* Measurement, 2008. **41**(1): p. 1-9.

95. Dziedzic, A.K., Jaroslaw;Machb,Pavel, *Voltage nonlinearity of carbon blackpolyesterimide thick resistive films.* Vacuum, 1998. **50**(1-2): p. 125-130.

96. Gravano, S., et al., *Monte Carlo simulation of current–voltage characteristics in metal–insulator–metal thin film structures.* Thin Solid Films, 2003. **433**(1-2): p. 321-325.

97. Grimaldi, C.M., T.;Ryser,P.;Strassler,S., *A random resistor network model of voltage trimming.* Journal of Physics D: Applied physics, 2004. **37**: p. 2170-2174.

98. Stanimirović, I., M.M. Jevtić, and Z. Stanimirović, *Multiple high-voltage pulse stressing of conventional thick-film resistors.* Microelectronics Reliability, 2007. **47**(12): p. 2242-2248.

99. Gofuku, E.O., Toshio;Kohara,Masanobu;Nunoshita,Masahiro, *Resistance adjustment with short pulse Nd:YAG laser for ruo2 based thick-film resistors based in polyamide film*IEEE Transactions on Components, Hybrids, and Manufacturing Technology, 1993. **16**(6): p. 592-597.

100. Hänel, J.K., Bernd; Bleul, Karsten; Kaufmann, Christian; Bonitz, Jens *Laser Trimming of Micro Mirror Devices: Ultrashort UV-Laserpulses Allow Ultra-precise Processing.* Laser Technik Journal, 2008. **5**(1): p. 36-39.

101. Heinrich, A., et al., *Influence of oxygen pressure, temperature and substrate/target distance on Cu2Ta4O12 thin films prepared by pulsed-laser deposition.* Thin Solid Films, 2005. **479**(1-2): p. 12-16.

102. Jones, J.G., et al., *Plasma diagnostics of hybrid magnetron sputtering and pulsed laser deposition.* Surface and Coatings Technology, 2006. **201**(7): p. 4040-4045.

103. Tobita, T.a.T., H *New trimming technology of a thick film resistor by the pulse voltage method.* IEEE Transactions on Components, Hybrids, and Manufacturing Technology, 1991. **14**(3): p. 613-617.

104. Zhang, D.M., et al., *Influence of kinetic energy and substrate temperature on thin film growth in pulsed laser deposition.* Surface and Coatings Technology, 2006. **200**(12-13): p. 4027-4031.

105. Zhao, J.-L., et al., *Structural, optical and electrical properties of ZnO films grown by pulsed laser deposition (PLD).* Journal of Crystal Growth, 2005. **276**(3-4): p. 507-512.

106. Maluf, N., *An introduction to microelectrochemical systems engineering*. 2000: Artech House. 1-277.

107. Faith, T.J., J *Fluid abrasive trimming of thin-film resistors.* IEEE Transactions on Parts, Hybrids, and Packaging, 1976. **12**(2): p. 133-138.

108. Licari, J.J.H., L.A., *Handbook of polymer coatings for electronics: Chemistry, Technology and Applications*. 2nd ed., New Jersey,USA: Noyes Publications.
109. Poulsen, R.G., *Plasma etching in integrated circuit manufacture-A review.* Journal of vacuum science and technology, 1998. **14**(1).
110. Boulais, E.F., Julie;Chateauneuf,Alexandre;Savaria,Yvon, *Laser-Induced Resistance fine tuning of integrated polysilicon thin film resisotrs.* IEEE Transactions on electron devices, 2011. **58**(2): p. 572-575.
111. Schmidt, H.E.a.C., Bruce L *Predicting the effect of high speed laser trimming on resistor stability*. in *Electronic Components and Technology Conference*. 1989. Houston, TX IEEE.
112. Licari, J.J.H., L.A., *Hybrid Microcircuit technology handbook: Materials,Processes,Design, Testing and Production* 1998, New jersey: Noyes Publications.
113. IPCI. *Schematic structure of a laser trimming system*. 2015 [cited 2016 02/03/2016]; Available from: http://81.161.252.57/ipci/courses/thickfilm/index_33.htm.
114. Antonov, Y.N., *Use of laser trimming for the development of a project for accuracy-normalization of the resistance of resistors in hybrid integrated circuits.* Journal of Communications Technology and Electronics, 2006. **51**(12): p. 1351-1355.
115. Dow, R.M., M; Richardson, T; Swenson, E *Reducing post trim drift of thin film resistors by optimising yag laser output characteristics.* IEEE Transactions on Components, Hybrids, and Manufacturing Technology, 1978. **1**(4): p. 392-397.
116. Fehlhaber, P., *Laser trimming of silicon-chromium thin film resistors*, in *Solid state technology*. 1971. p. 33-36.
117. Gleine, W.M., J *Laser trimming of SiON components for integrated optics.* Journal of Lightwave Technology, 1991. **9**(11): p. 1626-1629.
118. Shyha, I., *An Investigation into CO2 Laser Trimming of CFRP and GFRP Composites.* Procedia Engineering, 2013. **63**: p. 931-937.
119. Papp, G., *Simulation of laser trimming of film resistors.* Periodica Polytechnica ser. el. eng., 1993. **37**(1): p. 43-52.
120. Kestenbaum, A.a.B., T *Photoexcitation Effects During Laser Trimming of Thin-Film Resistors on Silicon.* IEEE Transactions on Components, Hybrids, and Manufacturing Technology, 1980. **3**(1): p. 166-171.
121. Fjeldsted, K.G., L., *Optimal designs for embedded passives laser trim.* Circuitree, 2004. **17**: p. 10-14.
122. Shier, J., *A finite mesh technique for laser trimming of thin film resistors.* IEEE Journal of solid-state circuits, 1988. **23**(4): p. 1005-1009.
123. Manolescu, A.M., Anca Manuela. *Laser trimming modeling of thin film integrated resistors*. in *International semiconductor conference*. 2007.
124. Meunier, M.G., Y.;Savaria,Y.;Lacourse,A.;Cadotte,M., *A novel laser trimming technique for microelectronics.* Applied surface science, 2002. **186**(1): p. 52-56.
125. Meunier, M.M., M; Gagnon, Y; Lacourse, A; Ducharme, M; Rioux, S; Savaria, Y; Savaria, Y, *Precision resistor laser trimming for analog microelectronics*, in *Conference on Lasers and Electro-Optics (CLEO)*. 2007, IEEE: Baltimore, MD p. 1.
126. Huang, Y.C., R.F; Smith, W.F *The reliability study of laser trimmed resistor components*. in *41st Electronic Components & Technology Conference*. 1991. Atlanta, GA IEEE.
127. Liou, B.W., *Use of laser trimming for the fabrication of high precise n-p compensation-doped polycrystalline silicon thin film resistors.* Journal of computational and theoretical nanoscience, 2011. **8**(11): p. 2291-2298.
128. Wang, Z.Y., Xiaodong;Sun,Yuan;Zhao,Xiaobing. *The influence of laser spot on resistance of chip resistors*. in *2010 Symposium of Photonics and Optoelectronics*. 2010.
129. BWTEK. *Spectrometer knowledge*. 2017 [cited 2017 03/06/2017]; Available from: http://bwtek.com/spectrometer-introduction/.
130. Shimadzu. *UV-Vis Spectrophotometers*. 2016; Available from: https://www.ssi.shimadzu.com/products/productgroup.cfm?subcatlink=uvvisspectro.

131. Hall, P., *Resistance calculations for thin film rectangles.* Thin solid films, 1997. **300**: p. 256-264.
132. Yan, Y., *High quality laser machining of alumina ceramics*, in *Faculty of Engineering and Physical Sciences*. 2012, The University of Manchester. p. 256.
133. Conradt, R.M., L., *Thick-film laser trimming principles, techniques and recommendations.* Electrocomponent science and technology, 1981. **9**: p. 9-14.
134. Ready, J., *Industrial applications of lasers* 1997, Minessota: Academic Press.
135. Schuoker, D., *High power lasers in production engineering*. 1999, Austria: Imperial College Press & World Scientific Ltd.
136. Zandman, F. *How to select resistors and avoid unforessen stress factors*. 2010 [cited 2015 10/04/2015]; Available from: http://www.vishaypg.com/docs/63501/how_to.pdf.

10 Appendix

Published material

Proceedings of the 13th International Conference on Manufacturing Research (ICMR2015)

A NOVEL METHOD OF COMPARING LASER TRIM PATTERN GEOMETRIES OF THIN FILM RESISTORS

Maria Alafogianni
Department of Mechanical & Construction Engineering
Northumbria University
Newcastle Upon Tyne
NE1 8ST, UK
maria.alafogianni@northumbria.ac.uk

Martin Birkett
Department of Mechanical & Construction Engineering
Northumbria University
Newcastle Upon Tyne
NE1 8ST, UK
martin.birkett@northumbria.ac.uk

Roger Penlington
Department of Mechanical & Construction Engineering
Northumbria University
Newcastle Upon Tyne
NE1 8ST, UK
roger.penlington@northumbria.ac.uk

ABSTRACT

This paper studies the effects of varying laser trimming geometries on key performance parameters of bar-shaped thin film resistors. Several popular trim patterns including the plunge cut, L-cut and serpentine cut were modelled and their effect on heat-affected zone (HAZ) sensitivity and temperature coefficient of resistance (TCR) were investigated. It is found that variation in resistor dimensions and trim length in the trimming algorithm can give significant increases in the TCR of the thin films with results of 220-250 ppm/°C for the serpentine cut, 220-320 ppm/°C for the plunge cut and 250-290 ppm/°C for the L-cut. It is also shown that the serpentine cut is the most sensitive to variation in the dimensions of the HAZ with a sensitivity value of 12% when compared to the L-cut and plunge cut which produced values of 10% and 11% respectively. In addition to results for the TCR and HAZ, a novel method of predicting the optimum trim pattern to minimize the final resistance value tolerance of the thin film is proposed.

Keywords: Laser trimming, thin film resistors, optimization.

1 INTRODUCTION

Resistors are normally fabricated to lower resistance values than required and then adjusted towards target value by trimming away sections of the film material [1]. Thus, laser trimming can be thought as an essential process in the manufacture of precision thin film resistors with tolerances better than ±10%.There is a variety of trim patterns that can be used for the adjustment of bar-shaped thin film resistors such as the plunge-cut, L-cut, shadow cut, double plunge cut, scan cut and serpentine cut, as shown in Figure 1[2].

The plunge cut is simple and economical and it consists of a single kerf orthogonal to the current flow but its tolerance accuracy is limited. The L-cut, in which a cut perpendicular to the current flow in the resistor quickly increases the resistance close to the target value and then the direction of the trim changes to parallel to the current flow in order to fine trim to the desired value. The L-cut is the most frequently used method due to its stability and tolerance accuracy. As for the shadow cut, an additional plunge is added to the side of an L-cut and the double cut is achieved by trimming straight into the material parallel to the first plunge. Both patterns can be used in order to achieve tighter tolerances but are more expensive due to the additional trimming time required. The scan cut is mostly used in high-frequency applications but it is very time consuming and thus not cost-effective for general use. Another trimming pattern is the serpentine cut that consists of multiple cuts in areas

of high current density in order to give large increases in resistance value and improvements in tolerance accuracy. However, this type of cut appears to have stability issues.

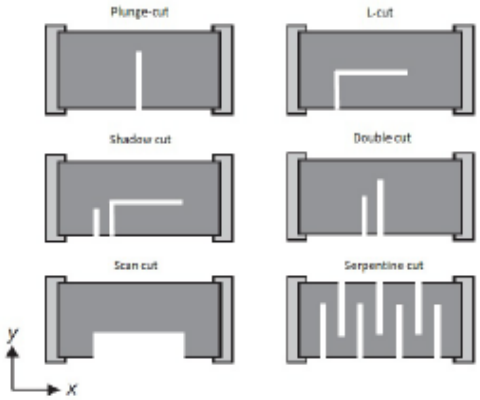

Figure 1: Resistor trimming patterns [2].

Previous studies on modelling of trimmed resistors include numerical trim simulations using computer aided design, finite difference method and boundary element method in order to design and predict trimmed resistors[8-9],[12]. In addition to this, models have been demonstrated for predicting the performance of laser trimmed resistors concerning the HAZ, which is an unstable zone of material adjacent to each cut path that has been significantly heated but not vaporized by the laser due to the non-uniform energy distribution in the beam which is expressed as a Gaussian distribution [10-11], see Figure 2.

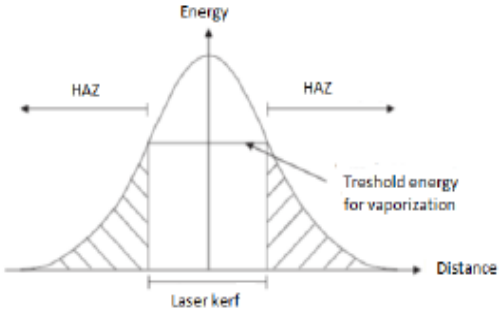

Figure 2: Laser beam profile as a Gaussian distribution [2,10-11].

Another important parameter that can change depending on the resistor geometry is the temperature coefficient of resistance (TCR) which is used to specify the stability and the sensitivity of the material with change in temperature [11].

In this paper, the trim patterns chosen for comparison on the numerical simulation model were the plunge-cut, the L-cut and the serpentine cut. The determination of the resistance value as well as the temperature effects were considered for the characterisation of the trim structures.. Thus, the effect of these three trim patterns on the HAZ and the TCR of the thin film resistors were investigated.

2 MODEL OF RESISTOR TRIMMING

A numerical simulation using MATLAB that allows variation in trimming patterns taking into account the HAZ around the trim was implemented in this study. It is assumed that the resistor is uniform in the third dimension and with these limits becomes a two-dimensional problem. Furthermore, the flow of the current is assumed to be uniform across the resistor. The model is based on the summation of resistors in series as in the following equation:

$$R = R_1 + R_2 + R_3 \quad (1)$$

However, as the model consists of various parameters; certain variables should be taken into account, such as the dimensions of the resistor and the location and the length of the trim. It is also assumed that the laser trim has infinite precision at the trim time and temperature. Thus, Equation (1) can be further refined as follows:

$$R_t = R\left(\frac{x_1}{W}\right) + R\left(\frac{x_2}{W-D}\right) + R\left(\frac{x_3}{W}\right) \quad (2)$$

Where R is the sheet resistance, W is the width of the resistor, D is the length of the trim and x_1,x_2 and x_3 are presented for the plunge cut in Figure 3 [12-13]. It is worth commenting that Equation (2) under predicts the resistance value and needs to be expanded as follows:

$$R = R\frac{x_1}{2W} + R\sum_{i=1}^{n}\left[\frac{\frac{x_1}{2n}}{W-\left(\frac{D}{n}\right)\left(\frac{2i-1}{2}\right)}\right] + R\left(\frac{x_2}{W-D}\right) + R\sum_{j=1}^{m}\left[\frac{\frac{x_3}{2m}}{W-\left(\frac{D}{m}\right)\left(\frac{2j-1}{2}\right)}\right] + R\frac{x_3}{2W} \quad (3)$$

Where n and m are the number of rectangles on the left and right side of the resistor respectively. As a consequence, an advanced model can be expressed by the following equation:

$$R = R\int_0^{x1}\frac{dx}{W-\frac{D}{x1}x} + R\left(\frac{x2}{W-D}\right) + R\int_0^{x3}\frac{dx}{W-\frac{D}{x3}x} = R\left[\left(\frac{x_1+x_3}{D}\right)\ln\left(\frac{W}{W-D}\right) + \left(\frac{x_2}{W-D}\right)\right] \quad (4)$$

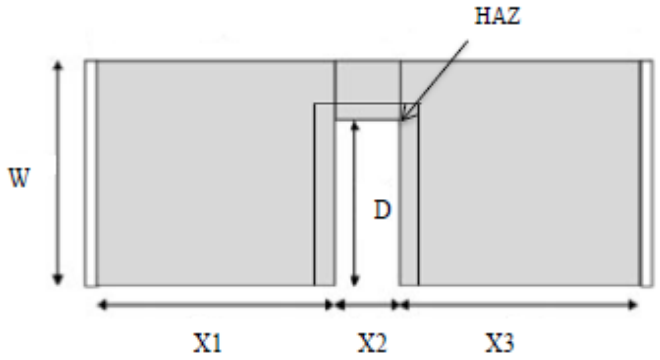

Figure 3: Presentation of the variables used for modelling the plunge cut [12].

The TCR is determined as follows:

$$TCR = \frac{R_2-R_1}{R_1(T_2-T_1)} \times 10^{-6} \quad (5)$$

Where R_2 is the resistance value at operating temperature, R_1 is the resistance value at room temperature, T_2 is the operating temperature and T_1 is the room temperature. Moreover, the change of the resistance value due to the effect of the TCR is given below:

$$R_{delta} = R_{nominal} \times T_{delta} \times TCR \quad (6)$$

Where $R_{nominal}$ is the initial resistance value, T_{delta} is the increase or decrease of the temperature and TCR is the temperature coefficient of resistance.

The sensitivity of the HAZ is defined as the fraction of the total power that is dissipated in the HAZ

and is given below:

$$S_{HAZ} = \frac{P_{HAZ}}{P_S} \tag{7}$$

Where P_{HAZ} is the power dissipated in the HAZ and Ps is the total power [9-13].

A similar approach to the one above for the plunge cut was followed for the serpentine-cut in order to calculate the resistance, TCR and the HAZ. As for the L-cut, it is shown in Figure 4 that the total resistance is the parallel-series combination of R_1, R_2 and R_3 and the following equation was used:

$$R = \frac{R_1 \times R_2}{R_1 + R_2} + R_3 \tag{8}$$

Where R_1 and R_2 are two resistors in parallel and R_2 is affected by the trimming due to the fact that it contains the HAZ. R_3 is in series with the parallel combination of R_1 and R_2 and is the area that is not affected by the laser trimming [14].

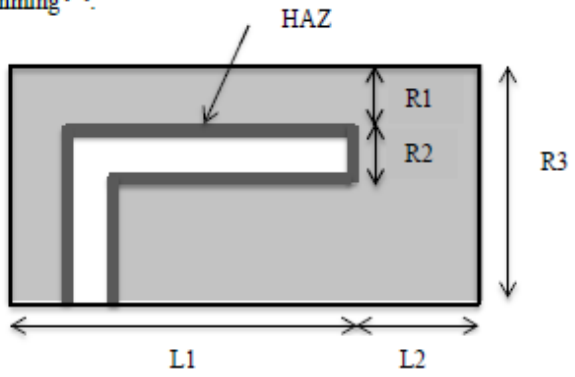

Figure 4: Presentation of the variables used for modelling the L-cut [14].

3 RESULTS AND DISCUSSION

The type of resistors that were investigated in this study were bar thin films with a range of resistance values from 50 to 200 Ω. It is assumed that the type of material used and the resistance value are the same for all the different trim pattern designs that were compared. The serpentine cut was modelled to consist of 5 plunges in areas of high current density. In addition to this, the TCR and the sensitivity to the HAZ were calculated taking into account the trim length and the location of the trim. The model proposed for the calculation of the resistance value assumes a uniform current flow across the resistor. The *n* and *m* rectangles are the numbers of rectangles on the resistor and their values can range from 5 to 25. The sheet resistance was set to 25 Ω/square for the calculations and the value of the room temperature was set at 20°C.

Some indicative dimensions of the resistor that was used during the modelling are shown in Table 1. It is shown that the indicative length varies between 5.1 and 16.3 mm while the width of the resistor is between 2.5 and 8.1mm.

Table 1: Resistor dimensions.

Length (mm)	Width (mm)
5.1	2.5
7.5	3.7
8.5	4.2
10.2	5.0
16.3	8.1

The value of the trim length which, is the number of squares of material removed, varies from 0 to 10 mm for the plunge and serpentine cut and from 0 to 25 mm for the L-cut. Both plunge cut and serpentine cut have the ability to approach a resistance value of 100 Ω with the minimum of trim length. The TCR depends on the resistance value and the changes in temperature. Figure 5 shows the results for TCR versus trim length for the three different cuts when trimmed to the same target resistance values. The values of TCR vary between 220 and 320 ppm/ $^{\circ}$C for the plunge cut and between 220 and 250 ppm/$^{\circ}$C for the serpentine cut. As for the L-cut, the value of the TCR is between 250 and 290 ppm/$^{\circ}$C for the trim length from 0 to 10mm.Thus, it is shown that the trim length can change the TCR.

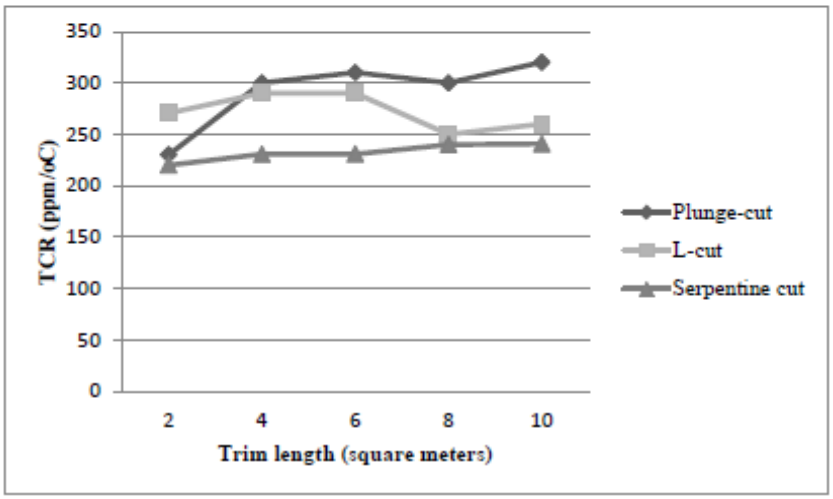

Figure 5: Modelling results for TCR per length of the trim for the plunge-cut, L-cut and serpentine cut.

In addition to the results for TCR, the sensitivity of the HAZ on the three trim patterns was calculated. As shown in Table 2, the sensitivity of HAZ is related to the P_{max} density. It was found that the sensitivity of the HAZ in serpentine cut has the greatest change in the resistance value at an average of 12% due to the fact that P_{max} is increased. It is also shown that the sensitivity of the plunge cut is 11% while for the L-cut is 10%.

Table 2: Average of HAZ sensitivity and P_{max} density for different trim patterns.

Type of cut	S_{HAZ}	P_{max} (%)
Plunge cut	0.11	1.29
L-cut	0.10	0.82
Serpentine cut	0.12	2.17

It is reasonable to suppose that sensitivity of the HAZ of the serpentine cut is the highest due to the large trim length that causes the increased amount of heat affected zone surrounding it and suggests that the use of the serpentine cut may lead to problems in the stability of the resistor. It is also worth noting that the L-cut has a reduced sensitivity of HAZ and this could be the reason why it is currently the most frequently employed trim pattern for the adjustment of thin film resistors.

4 CONCLUSION

This paper has demonstrated the importance of appropriate laser trim pattern design and the effect on the sensitivity of the HAZ and the TCR of the thin film resistor material. Through investigation of the chosen trim patterns, it was possible to model these geometries and compare them in relation to the above factors. The trim length, the dimensions of the resistor and the type of cut play an important

role in the fabrication of bar thin film resistors due to their effects on the HAZ and the final resistance value. It was also found that the TCR can slightly change in comparison with the trim length of each type of cut. The sensitivity of the HAZ, as a value, was proven to be useful in order to characterize and compare the given trim pattern designs and it was shown that the serpentine cut has a great sensitivity on the HAZ especially in comparison with the plunge and L-cut patterns. In addition to this, the serpentine cut has the greatest change in the resistance value at around 12%. Future research will focus on the possibility of further development of the prediction and optimisation of the resistor design process by designing trim strategies that will have a significant impact on the manufacture of thin film resistors.

REFERENCES

[1].Fjeldsted, K. & Gottfried, L., 2004. Optimal designs for embedded passives laser trim. *Circuitree,* Volume 17, pp. 10-14.

[2].Birkett, M. & Penlington, R., 2013. Laser trim pattern optimisation for CuAlMo thin film resistors. *IEEE Transactions on components,packaging and manufacturing technology,* 3(3), pp. 523-529.

[3].Deluca, P., 2002. A review of thirty-five years of laser trimming with a look to the future. *Proceedings of the IEEE,* 90(10), pp. 1614-1619.

[4].Elshabini-Riad, A. & Bhutta, I., 1993. Lightly trimming the hybrids. *Circuits and devices,* pp. 30-34.

[5].Albin, A. & Swerson, E., 1971. Laser resistance trimming from the measurement point of view. *IEEE Transactions on parts,hybrids and packaging,* pp. 14-19.

[6].Manolescu, A. & Manolescu, A., 2007. *Laser trimming modelling of thin film integrated resistors.* Sinaia, Semiconductor Conference, pp. 473-476.

[7].Shier, J., 1988. A finite mesh technique for laser trimming of thin film resistors. *IEEE Journal of solid-state circuits,* 23(4), pp. 1005-1009.

[8].Schimmanz, K. & Jacobsen, S., 2001. Film resistor design for high precision laser trimming. *IEEE Transactions on Computer-Aided Design of Integrated Circuits & Systems,* pp. 1-13.

[9].Papp, G., 1993. Simulation of laser trimming of film resistors. *Periodica Polytechnica,* 37(1), pp. 43-52.

[10].Ramirez-Angulo, J. & Geiger, R., 1988. New laser trimmed film resistor structures for very high stability requirements. *IEEE Transactions on electron devices,* 35(4), pp. 516-518.

[11].Ramirez-Angulo, J., Geiger, R. & Sanchez-Sinencio, E., 1987. Characterisation, evaluation and comparison of laser trimmed film resistors. *IEEE Journal of solid-state circuits,* SC-22(6), pp. 1177-1189.

[12].Sandborn, P. & Sandborn, P., 2006. Using embedded resisotr emulation and trimming to demonstrate measurement methods and associated engineering model development. *International journal of engineering education,* 22(1), pp. 1-7.

[13].Sandborn, P. & Sandborn, P., 2008. A random trimming approach for obtaining high-precision embedded resistors. *IEEE Transactions on Advanced Packaging,* 31(1), pp. 76-81.

[14].Bulger, G., 1975. Stability analysis of laser trimmed thin film resistors. *IEEE Transactions on parts, hybrids and packaging,* PHP-11(3), pp. 172-177.

Resistor trimming geometry; past, present and future

M Alafogianni[1], R Penlington[1], M Birkett[1],

[1]Faculty or Engineering and Environment
Northumbria University, Newcatle upon Tyne, NE1 8ST, UK

E-mail: maria.alafogianni@northumbria.ac.uk

Abstract. This paper explores the key developments in thin film resistive trimming geometry for use in the fabrication of discrete precision resistors. Firstly an introduction to the laser trimming process is given with respect to well established trim geometries such as the plunge, 'L' and serpentine cuts. The effect of these trim patterns on key electrical properties of resistance tolerance and temperature co-efficient of resistance (TCR) of the thin films is then discussed before the performance of more recent geometries such as the three-contact and random trim approaches are reviewed. In addition to the properties of the standard trim patterns, the concept of the heat affected zone (HAZ) and ablation energy and the effect of introducing a 'fine' trim in areas of low current density to improve device performance are also studied. It is shown how trimming geometry and laser parameters can be systematically controlled to produce thin film resistors of the required properties for varying applications such as high precision, long term stability and high power pulse performance.

Introduction

For thin film resistors it is generally impossible to deposit batches of product with resistance tolerances better than about ±10% [1-3]. This is due to problems in attaining uniform sheet resistance, but mainly due to dimensional variation of the individual resistor elements in the batch, a problem which is amplified as the resistor size decreases [3, 4].

Thus, it is normal to fabricate the resistor film to a lower resistance value than required and then adjust it by removing or 'trimming' away sections of the film material to increase the resistance to its target value in order precision of less than 10% to be succeeded [5, 6].

There are many different trimming methods which can be used to adjust the value of the resistor such as anodisation, heat trimming, electrical trimming, mechanical trimming, chemical trimming and laser trimming [1, 2]. However, laser trimming is by far the most effective and popular method and is still a subject of continuing theoretical and experimental research and optimisation [7-24].

This paper discusses the laser trimming process of thin film resistors with regard to both conventional and well established trim patterns and the influence of their geometry on key electrical performance properties such as resistor tolerance and temperature co-efficient of resistance (TCR). The concept of the heat affected zone (HAZ) bordering the kerf is also introduced and some recent trim patterns design to reduce its effects are discussed.

Laser trimming

2.1. Laser trimming process

The laser uses a light beam of a few μm in diameter to remove the resistive film from the ceramic substrate in a very short time period of less than 1 ms. The high intensity light pulse is then absorbed by the material causing it to heat and vaporise. This process depends on the intensity of the laser pulse, or the power level, the focus of the pulse as well as the properties of the material being ablated [1].

The laser beam is scanned across the resistor to produce a continuous kerf, changing the resistance value of the film as it progresses. The accuracy of the adjustment of the resistance value is dependent on the properties of the laser beam itself, the shape of the cut and also the speed at which the measurement system can switch the laser beam off between pulses once the target resistance value is reached [1, 12-13].

There are two main types of laser used for the adjustment of resistive films; the pulsed carbon dioxide (CO2) and the neodymium: yttrium-aluminium-garnet (Nd: YAG) laser. As for the CO2, it has a long pulse width with high energy per pulse, which causes vaporisation of the film [1]. However, the long pulse width can also cause damage to the substrate and the material at the edge of

the kerf, the heat affected zone (HAZ) [17]. On the other hand, the YAG laser uses an acousto-optic Q-switch for a two way optical switching of the laser beam. This system is able to produce short pulses of high peak power at a wavelength of 1064nm, to rapidly vaporise the film, whilst minimizing heat flow and damage to the material surrounding the kerf [1]. Additional reductions in the HAZ can be succeeded by lasers operating in the green region of the visible spectrum due to the decrease in laser spot size resulting from the shorter wavelength of 532nm [14].

2.2. Conventional trimming geometries

There are various different laser trim patterns which can be used for the adjustment of surface mount bar shape resistors as shown in Figure 1. The influence of the width and length of the cutting line, the number of cuts is really important concerning the device geometry [25]. The plunge cut (Figure 1a) is the simplest and economical cut consisting of a single kerf orthogonal to the current flow through the resistive element but its overall tolerance accuracy can be less than other methods [5,15-16].

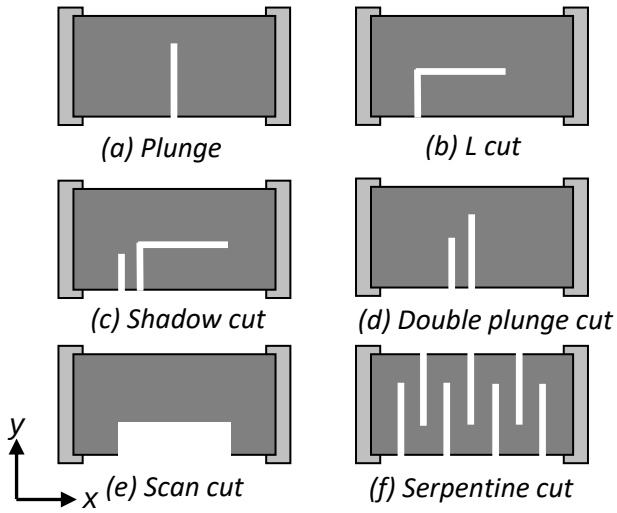

Figure 1. Commonly used laser trim kerf shapes [15]

The 'L' cut (Figure 1b) is perhaps the most frequently employed method due to its superior stability and tolerance accuracy. With this type of cut the resistance increases rapidly as the kerf is cut perpendicular to the current flow (y direction), which is called transverse cutting. Then, more gradually when it turns through 90º and cuts parallel to the current flow (x direction), which is called longitudinal cutting, until target value is reached i.e. in an area of equal current density, see Figure 2. [26, 27]

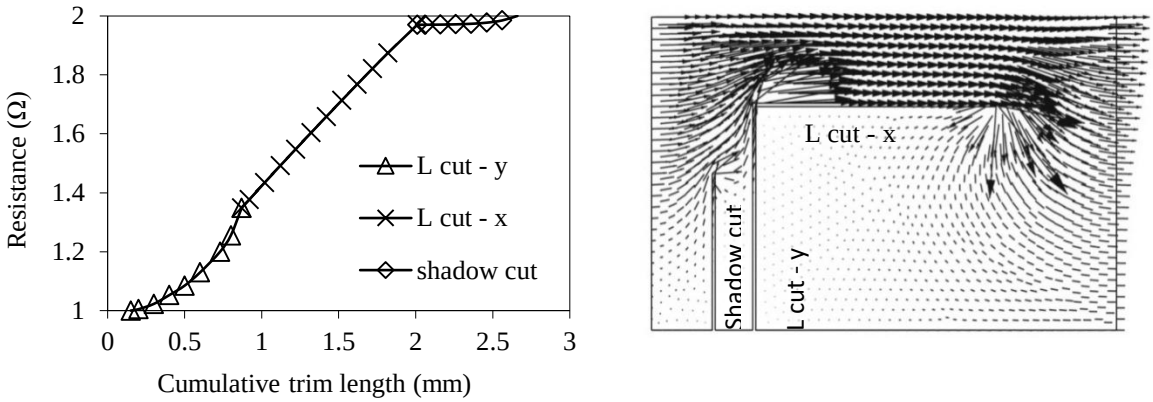

Figure 2. Typical plots of resistance increase with kerf length and correspondingmodel of current density for the 'L' cut and shadow cut [15].

The stability of the resistor can be maximised according to the variations on the x and y lengths. It is worth noting that when the y leg is as short as possible leaving maximum resistor line width remaining, the optimum performance is achieved. However, the trim time is increased and there is also the risk of trimming into the resistor termination with the extended x leg. Thus, with the 'L' cut, there is the opportunity to find a balance between trim speed and tolerance and stability accuracy but it is slightly more expensive than the plunge cut due to the additional time required to perform this cut [12-13, 23].

A shadow cut (Figure 1c) consists of an additional plunge to the side of an 'L' cut or plunge cut (double plunge (Figure 1d)). As a result, tighter resistance tolerances can be achieved as the kerf is cut in an area of low current density in the 'shadow' of the first cut, see Figure 3. The additional trimming time needed makes this type of cut quite expensive [5, 15].

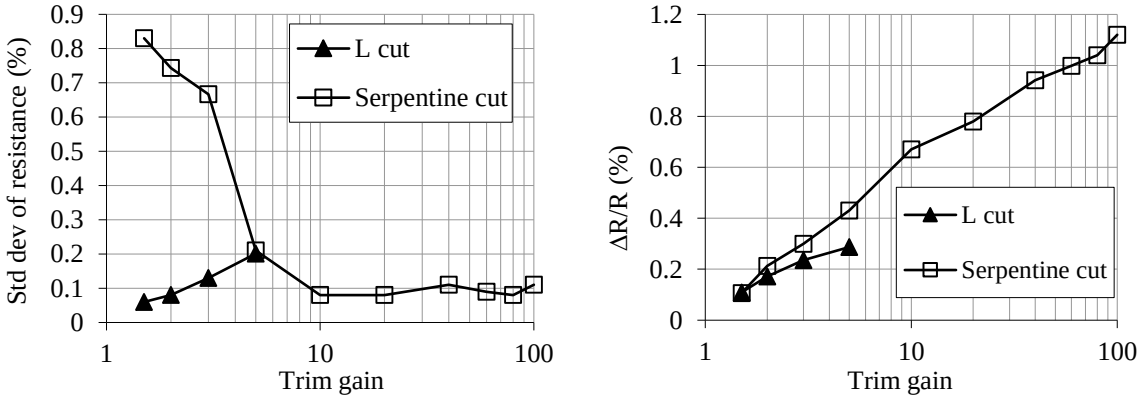

Figure 3. Variation in standard deviation of resistance and resistance stability with increasing trim gain for CuAlMo TFR's trimmed with both 'L' cut and serpentine cut [15].

A serpentine cut (Figure 1e) consists of multiple cuts made in areas of high current density which effectively increase the geometric length of the resistor and thus its resistance value. It has the ability to give a large resistance gain. As a result, the tolerance accuracy of the resistor is improved as shown in Figure 4. This type of cut can be employed when the pre-value resistance is much lower than the target value. However, a long trim length can lead to stability problems due to the large amount of HAZ surrounding it. In addition to this, when the resistance gain is very large, the TCR increases and causes instabilities due to the amount of material which has been raised to temperatures in excess of the zero TCR heat treatment temperature without being vaporised. [28, 29]

However, a solution to this issue would be a two stage serpentine trim to be employed when precision thin film resistors are required. During the first trim stage, the majority of the trimming is performed in order the resistor to be adjusted to around -1% from its target value. Then, the device is stabilised, typically overnight at around 200ºC to relieve stresses built up in the HAZ [15]. Predicting the resistance change that occurs during this stabilisation operation is not possible. As a consequence, the second stage of the process, which is called fine trim, is required for the accurate adjustment of the resistor to target value. It usually consists of one or two plunges in the shadow of the first serpentine as shown in Figure 4. However, this type of cut can be very time consuming and expensive, but the increasing availability of auto substrate handling equipment can help reducing the labour cost involved [15, 16].

The scan cut (Figure 1f) is the most commonly used due to its stability [28] and especially when the device is required for high frequency applications to minimise creation of capacitive reactance components of an RC circuit. It also finds use in high voltage situations as the likelihood of voltage breakdown across the trim kerf is greatly reduced. This type of cut is very time consuming to perform and is not cost effective for general use [15, 28].

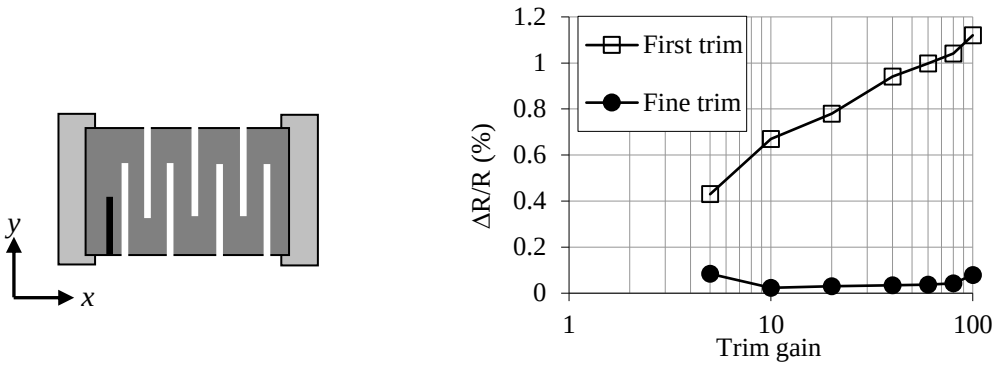

Figure 4. Two stage serpentine trim pattern and corresponding variation in resistance stability with increasing trim gain for CuAlMo TFR's trimmed with both first and fine trims [15].

2.3. The heat affected zone (HAZ)

A major cause of post-trim drift in laser trimmed resistors is due to the HAZ bordering the kerf [15, 29] and it would be beneficial to consider this area in more detail. It is worth commenting that the energy profile of the beam has a Gaussian distribution due to the fact that a Q-switched YAG laser is adjusted to operate in single traverse electromagnetic (TEM_{00}) mode. This profile can be translated into a Gaussian temperature profile as far as the thin films are concerned and it is shown in Figure 5.

It is noted that the central part of the profile has sufficient intensity to cause vaporisation of the thin film. As for the areas of film adjacent to the kerf, the energy absorbed from the laser beam is less than the threshold required for vaporisation. Thus, this region of the film becomes a heat affected zone and can considerably cause more changes and variations in the resistance than areas of film that are not irradiated by the laser beam [20, 21].

This aging effect is caused due to the fact that the film which was stabilised prior to the adjustment process and it has now been re-exposed along the edges of the laser kerf. The changes in the resistance are related to changes in the structural properties of the film material because of the rapid heating and cooling during the trimming process such as the sheet resistance and TCR [29-31].

It is worthwhile thinking that the length of the kerf and the effect of the HAZ in the trimmed resistors are important parameters that can determine the overall stability of the resistor [22]. These parameters can be optimised by varying the shape of the continuous trim and the properties of the laser beam itself.

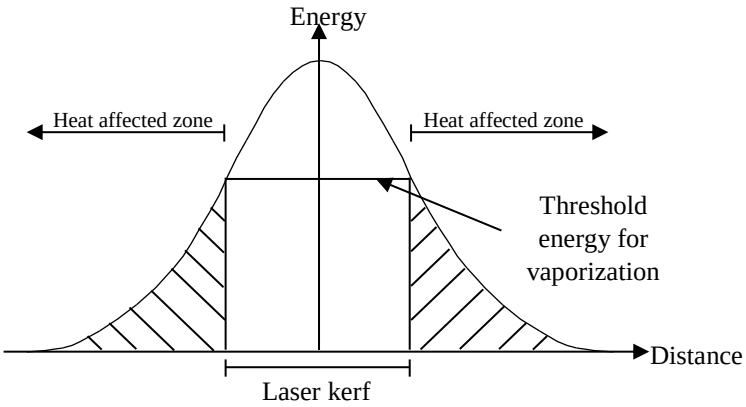

Figure 5. The fundamental mode laser beam profile as a Gaussian distribution [15, 29-31].

2.4. Alternative trimming geometries

An alternative trimming method in order to avoid the issues associated with the HAZ is link cutting [13]. This process can be applied by opening up shorting bars in loop and ladder type patterns to increase the resistance in discrete steps. Once the trimming bars are opened the current is redirected around the new longer path and any current crowding in the trimmed area or HAZ is eliminated. Although this method can provide a solution to the issues caused by the aging effects, a greater chip

area is required compared to the conventional bar design. Moreover, as the resistance is adjusted in discrete steps a very large number of links may be required [13].

However, there have been methods applying the link cutting approach to bar resistors. The Swiss cheese pattern can be thought as the most popular cut using the benefits of the link cutting approach. This method forces current crowding only in non-heat affected areas [29-31].

Another study proposed a type of laser trimming performing an L-cut in a 'top hat' shape thin film resistor, avoiding excessive crowding of the current lines after trimming [27]. A more recent study has focused on the effect of replacing the two contact bar resistor with a three contact distributed structure and then trimming the resistor by narrow cuts in a variety of shapes around the additional contact and it can be shown in Figure 6(a) [17]. In addition to this, another approach proposed for designing resistors was the random trimming. This method is performed by cutting a hole in a random point that was combined with a single plunge cut as shown in Figure 6(b). First, the single plunge is applied in order to offer rough adjustment and wide trim range fast and then random trim spots and voids helped to get closer to the target resistance [5].

Both of these methods have shown encouraging results and it was found that the resistance could be increased more controllably than an L-cut [5,6], but the additional trimming time and materials required were negative factors concerning satisfying improvements in the production of thin film resistors.

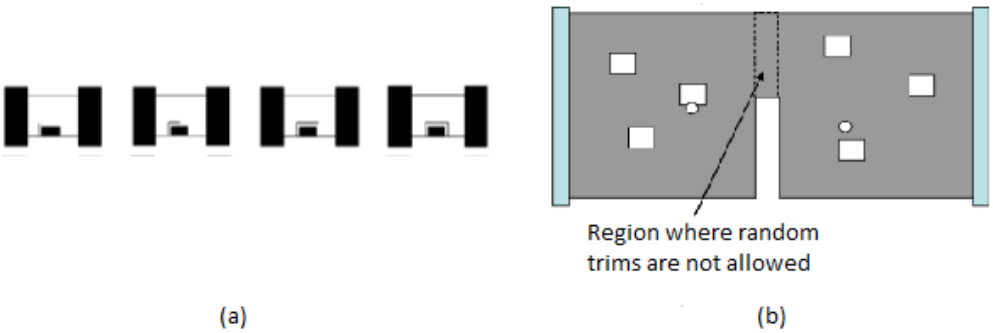

Figure 6. (a) Illustration of laser cut length used in three-contact resistors with rectangular additional contact [17], (b) Random trimming with single plunge cut [5].

Conclusions

This paper introduced the laser trimming process which can be thought as the most precise and reliable method in order to adjust the resistance value of bar-shaped thin film resistors. The advantages and disadvantages of common trim patterns were discussed and the effect of the HAZ on the performance of the resistors was also introduced. It is worth noting that trimming geometries play an important role on the characteristics of the resistors such as stability and tolerance accuracy. Moreover, trim pattern design has an effect on the resistance distribution and long term resistance performance of thin film resistors. It was also noted that the L-cut is the most commonly used trim pattern due to its expected tolerance which is less than 1% as well as its stability.

In addition to this, recent studies have focused on alternative trimming geometries and were presented in this paper such as the three-contact geometry and the random trim approach besides their positive results. However, these approaches, besides their promising results, did not appear to fulfil the improvements in the resistor performance reported due to the additional trimming time and materials needed. Therefore computer modelling of laser trim patterns could help in predicting and optimizing the resistor design process by designing new trim strategies. Within these limits, the maximum trim speed, overall performance and quality characteristics could be achieved. Thus, further research could focus on the possibility of improving the trimmed structures taking into account the factors that affect the performance of the resistors such as TCR and HAZ.

References

[1] Elshabini-Riad A and Barlow F 1998 *Thin Film Technology Handbook* (New York: McGraw-Hill) chapter 3 pp1-19

[2] Elshabini-Riad A and Bhutta I 1993 Lightly trimming the hybrids *Circuits and Devices* 30-4

[3] Fjeldsted K and Gottfried L 2004 Optimal designs for embedded passives laser trim *Circuitree* **7** 10-4

Effects of varying laser trimming geometries on thin film resistors

Maria Alafogianni[1]*,Martin Birkett[1],Roger Penlington[1]

[1]Northumbria University, Faculty of Engineering and Environment, Newcastle Upon Tyne, NE1 8ST, United Kingdom

Abstract

Purpose - This paper studies the effects of varying laser trim patterns on several performance parameters of thin film resistors such as the temperature coefficient of resistance (TCR) and target resistance value.

Design/methodology/approach - The benefits and limitations of basic trim patterns are taken into consideration and the plunge cut, double plunge cut and the curved L-cut were selected to be modelled and tested experimentally. A computer simulation of the laser trim patterns has been developed for the modelling process of the resistors. The influence of the trim length and resistor dimensions on the TCR performance and resistance value of the resistors is investigated.

Findings - It is found that variation in trim length, with the range of 5 up to 15mm, can give significant increases in the TCR of the thin films. Thus, for the plunge cut can reach up to 11.51ppm/^{o}C, for the double plunge cut is 14.34 ppm/^{o}C and for the curved L-cut up to 5.11 ppm/^{o}C.

Originality/value – Research on the effects of various laser trimming geometries on the TCR and target resistance accuracy is limited, especially for patterns such as the curved L-cut, which is investigated in this paper.

Keywords Laser trimming process, optimization, thin film resistor.

Paper type Research Paper

*Contact:maria.alafogianni@northumbria.ac.uk

1. Introduction

Nowadays, there is a high demand for cost-effective electronic devices with tolerances better than ±10%. Thin film resistors with such accuracy and low resistivity are required especially in portable devices in order to reduce energy consumption [1-4].Laser trimming is the most popular trimming method for the manufacture of thin and thick film resistors [1-2]. In general, resistors are fabricated to lower resistance values than needed and then the target value is increased by trimming away sections of the material.

There is a variety of different trim patterns, as presented in Figure 1, that are commonly used in the manufacture of thin film resistors such as the plunge cut, L-cut, double plunge cut, serpentine cut and scan cut.

The plunge cut is simple and economical and it consists of a single kerf orthogonal to the current flow but its tolerance accuracy is limited.

Figure 1 Basic resistor trimming patterns [2].

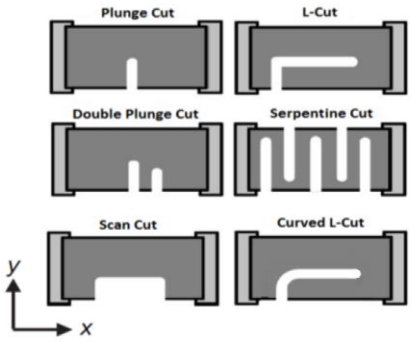

The L-cut consists of a cut perpendicular to the current flow in the resistor which quickly increases the resistance close to the target value and then the direction of the trim changes to parallel to the current flow in order to fine trim to the desired value. It is commonly used due to its stability and tolerance accuracy. As for the double plunge cut, an additional plunge is added to the side of the plunge cut. This method allows even tighter resistance tolerances to be achieved due to the fact that the kerf is cut in an area of low current density but it is more expensive because of the additional trimming time needed. The scan cut is mostly used in high frequency applications but it is very time consuming and thus not cost-effective for general use. Another trimming pattern is the serpentine cut that consists of multiple cuts in areas of high current density in order to give large increases in resistance value and improvements in tolerance accuracy but it appears to have stability issues.

However, the performance of these patterns can be optimised in order to achieve tolerance of 1% and better stability. Thus, further study of specialized cuts like the curved L-cut is needed [2-5].

Previous studies on modelling of trimmed resistors include numerical trim simulations using computer aided design, finite difference method and boundary element method in order to design and predict trimmed resistors [7-18].

In this paper, a simulation model is described and is verified experimentally by trimming resistive paper. The model can make comparisons between the selected trim patterns investigating the effect of the trim length, resistor dimensions and TCR.

2. Resistor Trim Modelling

2.1 Simulation of resistor trimming

For the modelling procedure, a numerical simulation is proposed in which different trim patterns can be modelled and analyzed. The resistance value R is given by:

$$R = \frac{\rho L}{A} = \frac{\rho L}{TW} = \frac{\rho}{T}\left(\frac{L}{W}\right) = R_{\square}\left(\frac{L}{W}\right) \qquad (1)$$

Where; ρ is the bulk resistivity, A is the cross-sectional area of the resistor, $R_{\square}$ is the sheet resistance, and L, W and T are the length, width and thickness of the resistor respectively.

For the plunge cut, see Figure 2, the formulations are given by equations 2 and 3.

$$R = R_1 + R_2 + R_3 \qquad (2)$$

$$R = r\sum_{i=1}^{n}\left[\frac{\frac{x_1}{n}}{W-\left(\frac{D}{n}\right)\left(\frac{2i-1}{2}\right)}\right] + r\left(\frac{x_2}{W-D}\right) + r\sum_{i=1}^{m}\left[\frac{\frac{x_3}{m}}{W-\left(\frac{D}{m}\right)\left(\frac{2i-1}{2}\right)}\right] \qquad (3)$$

Where; n and m are the number of rectangles on either side of the trim and r is a specified value which depends on the normalised resistance value, L and W [7-13].

The TCR is determined as follows:

$$TCR = \frac{R_{T2}-R_{T1}}{R_{T1}(T2-T1)} \times 10^{-6} \qquad (4)$$

Where; R_{T1} is the resistance value at room temperature, T_1, and R_{T2} is the resistance value at operating temperature, T_2.

Figure 2 Model for the plunge cut [6],[7].

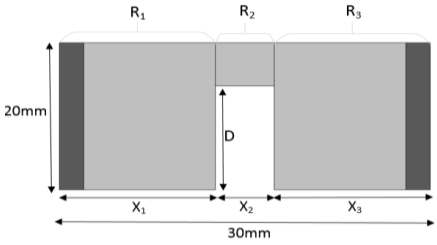

Moreover, the change of the resistance value due to the effect of the TCR is given by:

$R_{delta}=R_{nominal}\times T_{delta}\times TCR$ *(5)*

Where $R_{nominal}$ is the initial resistance value, T_{delta} is the increase or decrease of the temperature and *TCR* is the temperature coefficient of resistance.

A similar approach to the one above for the plunge cut was followed for the double plunge cut in order to calculate the resistance and TCR.

As for the L-cut, it is shown in Figure 3 that the total resistance is the parallel-series combination of R_1, R_2 and R_3 and the following equation was used:

$R = \frac{R_1 \times R_2}{R_1 + R_2} + R_3$ *(6)*

Where; R_1 and R_2 are two resistors in parallel and R_2 is affected by the trimming due to the fact that it contains the HAZ. R_3 is in series with the parallel combination of R_1 and R_2 and is the area that is not affected by the laser trimming [11-15].

Figure 3 Model for the curved L-cut.

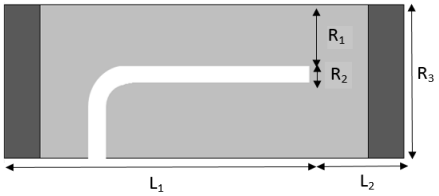

2.2 Experimental analysis

The experimental procedure concerns tests with the use of resistive paper (PASCO Scientific PK-9025) with resistivity of approximately 5000 Ω/□. The resistance value of the paper was found to vary slightly from sheet to sheet and normalization of the measurements was needed. To normalize the various sheets 10 initial measurements from each sheet were taken before trimming and then the measurements were averaged.

For a constant ratio ($\frac{L}{W}$), resistors of varying sizes can have similar resistance characteristics. Thus, the desired shape of the resistive paper is a rectangle with dimensions 30mm x 20mm. These dimensions were chosen for the experiments in order to depict the change in temperature effectively.

Then, five samples of each of the selected trim patterns were created using an Epilog Laser Mini Model 8000. Carbon ink contacts were added to the two ends of the resistor and alligator clips were then connected to measure the resistance value at room temperature. It was found that with the addition of the contacts the measurement error can be significantly reduced. The temperature change was also measured each time with the use of a thermal camera (Model: FLIR B620) when a potential of 10V was applied across the resistor element. Thus, the TCR can be found from the resistance measurement at different temperatures.

3. Results and discussion

The room temperature for the modelling and experiments was set at 23ºC. The width of the trim of the samples was 3mm for the plunge and double plunge cut and 5mm for the curved L-cut. Some indicative results for the TCR of different samples with various trim lengths are shown in Table 1.

Table 1 Experimental results for Temperature and TCR.

Type of cut	Trim length (mm)	Temperature (ºC)	TCR (ppm/ºC)
Plunge cut	5	30	2.6
	10	33.8	10.81
	15	34.5	11.51
	5	24.3	12.14
	10		
	5	26.3	12.74

Double Plunge cut	15		
	10	27	14.34
	15		
Curved L-cut	3	25.7	4.10
	5	27.5	4.91
	10	28.1	5.11

It is worth commenting that the resistor with the plunge cut appears to have a significant rise in temperature when voltage is applied to it. Thus, for trim length of 5mm the temperature reaches up to 30ºC while for the trim length of 10mm and 15mm, the values of temperature are 33.8ºC and 34.5ºC respectively.

For the double plunge cut, the temperature for trim length of 5mm and 10mm is 24.3ºC. For the cuts of 5mm and 15mm as well as 10mm and 15mm, the values of temperature are 26.3 ºC and 27 ºC respectively. As for the curved L-cut, the temperature is 25.7ºC, 27.5ºC and 28.1ºC for trim lengths of 3mm, 5mm and 10mm, respectively.

It is also shown that the TCR varies in relation to the trim geometry and length. For the plunge cut, the TCR can reach 11.51 ppm/ºC and 14.34 ppm/ºC for the double plunge cut. As for the curved L-cut, the value of TCR is lower in comparison with the plunge and double plunge cut, with values of 5.11 ppm/ºC.

The change in the resistance value for the trim length with range of 0-14mm from simulations in comparison with the experiments for the plunge cut, double plunge and the curved L-cut are shown in Figure 4.

It is shown that the results from the simulations are close to those obtained from the experiments for all three patterns. The normalised resistance value before trimming is 5.25 kΩ for all the samples and the highest resistance value for trim length of 14mm is around 15kΩ for plunge and double plunge cut and around 12kΩ for the curved L-cut.

The progression that the resistance makes as the trim length is increased is clearly depicted at the plots. It is worth commenting that the resistance value in the plunge cut increases faster and less trimming time is needed to perform this cut than the other two patterns. Furthermore, for the double plunge cut, it is shown that the resistance value increases fast for the first plunge and then for the second cut (shadow) the increase is slower. This cut seems to be a good option but the additional trimming time needed, increases the production costs.

As for the curved L-cut, the resistors were trimmed so that the trim changed direction after 10mm. In the plot, the change of direction of the cut is shown when the slope of the line changes. As for the highest trimmed value for this pattern was 12.2 kΩ for trim length of 14mm. It is worth noting that once again the resistance value increases fast until the point in which the cut changes direction after 10mm. As a result, this type of cut can be considered to be the most accurate pattern in comparison with the other ones.

Figure 4 Resistance value change in plunge (a), double plunge (b) and curved L-cut (c).

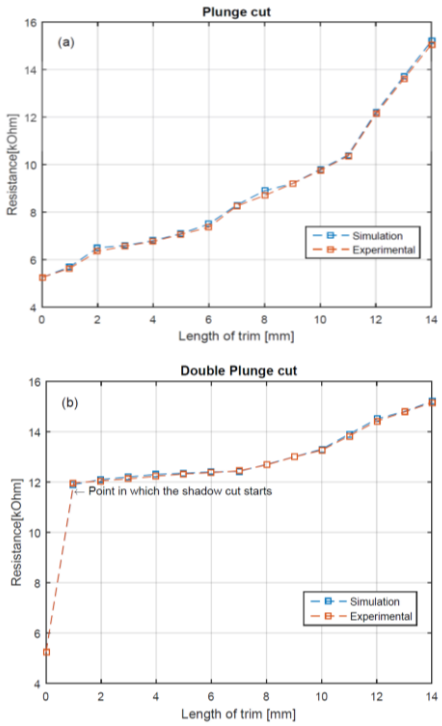

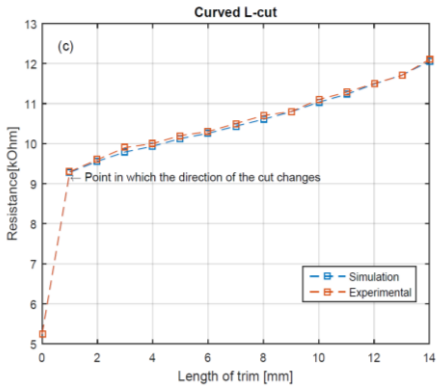

4. Conclusion

This paper describes the development of the model of laser trim patterns and it is also verified experimentally. The importance of appropriate laser trim pattern design and the effect of trim length and TCR of the thin film resistor material was demonstrated. It is found that variation in resistor dimensions, trim length and type of cut play an important role in the fabrication of thin film resistors due to their effect in the final resistance value.

In addition to this, significant increases in the TCR were shown especially for the plunge and double plunge cut. Trimming patterns affect the resistance value, as the plunge cut shows a rate of resistance increase in relation to the double plunge cut. Thus, both trim patterns can produce a high target resistance fast. As for the curved L-cut, it is shown to have different characteristics as far as the rate of increase in the resistance value is concerned which is slower than the other patterns. Thus, it can be thought as a potential method to control the rate of change of resistance and it can lead to more accurate results.

5. References

[1].Fjeldsted, K. &. G. L., (2004), Optimal designs for embedded passives laser trim''. *Circuitree,*17, pp. 10-14.

[2].Birkett, M. & Penlington, R., (2013),''Laser trim pattern optimisation for CuAlMo thin film resistors''. *IEEE Transactions on components,packaging and manufacturing technology,* 3(3), pp. 523-529.

[3].Deluca, P., (2002), ''A review of thirty-five years of laser trimming with a look to the future''. *Proceedings of the IEEE,* 90(10), pp. 1614-1619.

[4].Elshabini-Riad, A. & Bhutta, I., (1993), ''Lightly trimming the hybrids''. *Circuits and devices,* pp. 30-34.

[5].Albin, A. & Swerson, E., (1971), "Laser resistance trimming from the measurement point of view". *IEEE Transactions on parts,hybrids and packaging,* pp. 14-19.

[6].Sandborn, P. & Sandborn, P., (2006), "Using embedded resisotr emulation and trimming to demonstrate measurement methods and associated engineering model development". *International journal of engineering education,* 22(1), pp. 1-7.

[7].Sandborn, P. & Sandborn, P., (2008), "A random trimming approach for obtaining high-precision embedded resistors". *IEEE Transactions on Advanced Packaging,* 31(1), pp. 76-81.

[8].Ramirez-Angulo,J. *et al.*,(1987), Characterization,Evaluation and Comparison of Laser-Trimmed Film Resistors. *IEEE Journal of Solid-State Circuits,* SC-22(6), pp. 1177-1189.

[9].Ramirez-Angulo, J. & Geiger, R., (1988), "New laser trimmed film resistor structures for very high stability requirements". *IEEE Transactions on electron devices,* 35(4), pp. 516-518.

[10].Papp, G., (1993), "Simulation of laser trimming of film resistors". *Periodica Polytechnica,* 37(1), pp. 43-52.

[11].Schimmanz, K. & Jacobsen, S., (2001), "Film resistor design for high precision laser trimming". *IEEE Transactions on Computer-Aided Design of Integrated Circuits & Systems,* pp. 1-13.

[12].Shier, J., (1988), "A finite mesh technique for laser trimming of thin film resistors". *IEEE Journal of solid-state circuits,* 23(4), pp. 1005-1009.

[13].Bulger, G., (1975), "Stability analysis of laser trimmed thin film resistors". *IEEE Transactions on parts, hybrids and packaging,* PHP-11(3), pp. 172-177.

[14].Barlage, M., (1973), "A stability study of laser patterned thermally stabilised tantalum nitride and tantalum aluminium films". *IEEE Transactions on parts, hybrids and packaging,* PHP-9(2), pp. 123-130.

[15].Meier, M., (2006), Laser trimming of amorphous Ta42Si13N45 thin films with ultrashort pulses. *Microelectronic Engineering,* 83, pp. 2234-2237.

[16].Nowak, D., *et al.*, (2009), Fabrication and electrical properties of laser-shaped thick-film and LTCC microresistors. *Microelectronics Reliability,*49, pp. 600-606.

[17].Wronski, M. *et al*., (2005), New trim configurations for laser trimmed thick-film resistors-theoretical analysis, numerical simulation and experimental verification. *Microelectronics Reliability*, Issue 45, pp. 1941-1948.

[18].Dziedzic, A. *et al.*, (2006), "Advanced electrical and stability characterization of untrimmed and variously trimmed thick-film and LTCC resistors". *Microelectronics Reliability*, 46, pp. 352-359.